Analysis of soluble ions from dust and sea salt over the last glacial cycle in polar deep ice cores

Marie-Louise Siggaard-Andersen

PhD Thesis

Alfred Wegener Institute fûr Polar- und Meeresforschung, Fachbereich Geosystem
Columbus Strasse, 27568 Bremerhaven, Germany

Submitted October 2004 to University of Bremen, Fachbereich 5 - Geowissenschaften
Klagenfurter Strasse, 28359, Bremen, Germany

Analysis of soluble ions from dust and sea salt over the last glacial cycle in polar deep ice cores

Dissertation
zur Erlangung des
Doktorgrades der Naturwissenschaften

im Fachbereich 5
der Universität Bremen

vorgelegt von

Marie-Louise Siggaard-Andersen
Bremen

2005

Tag des Kolloquiums: 2005-05-18

Gutachter:
1. Prof. Dr. Heinz Miller
2. Prof. Thilo von Dobeneck

Prüfer:
1. Prof. Bleil
2. Dr. Hubertus Fischer

Abstract

The Greenland and Antarctic ice sheets contain trace amounts of dust and sea salt aerosols that have been wind transported over long distances before they were deposited onto the ice. Concentrations of chemical impurities measured in Greenland and Antarctic ice cores reflect past atmospheric contents of aerosols. Over the last glacial cycle, ice core concentrations vary up to two orders of magnitudes for mineral dust species and one order of magnitude for sea salt species, indicating large variations in conditions for aerosol emission and transport.
In this thesis a Greenland ice core record of soluble ions derived from dust and sea salt over the last glacial period from the NorthGRIP ice core is presented. A statistical method used to analyse variations in ice core concentrations of soluble dust and sea salt species and a physical interpretation of the statistical parameters in terms of large scale transport properties is introduced.

As a new component in ice core records, lithium is introduced in the analyses. A paper presenting the lithium measuring technique and exemplary lithium ice core data is included in this thesis. The geochemical properties of lithium suggest that lithium, like calcium, is leached from dust minerals. Analyses of NorthGRIP and DomeC ice core records of soluble dust species show that while soluble calcium can be used as an indicator of quantities of mineral dust, lithium is to a higher extend indicating mineral characteristics and weathering processes in the dust source areas.

The thesis is build up of relatively independent chapters. The first chapter (Chapter 1) is a very brief introduction to quaternary climates.
The following chapter (Chapter 2) is introducing and discussing aspects of dust and sea salt aerosol cycles that are relevant for the remaining chapters and provide the background for the following discussions in the thesis. This second chapter conclude that the Greenland ice core concentrations of dust and sea salt are resulting from the high variability of the upper level wind patterns, and therefore mainly reflect large scale patterns and strength of the upper level winds in the northern hemisphere.
The following three chapters (Chapter 3-5) are concerning the measuring technique of lithium and new findings from the NorthGRIP and the DomeC ice cores based on lithium records. A lithium anomaly appearing in the NorthGRIP ice core around the Holocene 8.2 ka BP cold event provides evidence that major changes in the water-balance in the Qaidam basin, located north of the Tibetan plateau, occurred rapidly, and indicates a coupling between Asian monsoonal circulation and North Atlantic climate. An analysis of the chemistry of dust species, including lithium, in the DomeC ice core showed different characteristics of the dust material for the Holocene and for the last glacial, suggesting different dust sources during the Holocene and during the late Pleistocene.

In Chapter 6 a statistical analysis of the NorthGRIP ice core record of soluble ions is presented and a physical interpretation of the statistical parameters is introduced. The analysis leads to a discussion of large-scale patterns of atmospheric circulation and

cycles of mineral dust and sea salt aerosol in the northern hemisphere during the last glacial period.

A paper by NorthGRIP members (2004), presenting the NorthGRIP isotope curve back into the last interglacial, is included in the thesis (Chapter 7). That paper suggests a different atmospheric circulation during the last glacial period than at present with a regional effect in precipitation, where the NorthGRIP isotope record is more influenced by precipitation from a northerly transport path than the GRIP isotope record.

The following chapter (Chapter 8) describes an analysis of long term trends in the NorthGRIP chemical record suggesting the occurrence of two distinct configurations of northern hemispheric atmospheric circulations during the early part of the last glacial period. One configuration that characterises most of the glacial period, has a possible transport pathway north of the Laurentide ice sheet. The other configuration that characterises only certain time-periods during the early part of the last glacial period, shows weaker conditions for transport, with a possible pathway south of the Laurentide ice sheet. The atmospheric circulation seems to have shifted rapidly between these two configurations during stage 5 on a timescale different from that of the D/O events. These results suggest that the large-scale atmospheric patterns are relatively resistant to the climate changes during the D/O events, but have however, the capability to reorganize rapidly.

Acknowledgements

This PhD thesis is submitted to the [1]University of Bremen, Germany. The PhD work was performed at [2]Alfred Wegener Institute (AWI) in Bremerhaven, Germany under supervision of Prof. Dr. Heinz Miller and Dr. Hubertus Fischer.

Prior to my PhD work in Germany, I was employed at the University of Copenhagen, Denmark as a scientific assistant performing chemical analyses of ice cores from NorthGRIP and EPICA DomeC. During this time I was introduced to the field of glaciochemistry by Dr. Henrik Brink Clausen.

I want to thank Prof. Dr. Dorthe Dahl Jensen, Niels Gundestrup and Prof. Dr. Heinz Miller for giving me the opportunity to participate in fieldwork at NorthGRIP. Here I have met many nice people and made great experiences working with ice cores in the Arctic environment.

The results of this thesis could not have been reached without input from Aksel Walløe Hansen, Claus Hammer, Peter Ditlevsen, Pierre Biscaye, and Sigfus Johnsen.
I will also acknowledge helpful comments to this manuscript from Anders Svensson, Chris Zweick, Katrine Krogh Andersen, Matthias Bigler, Ole Siggaard-Andersen, Paolo Gabrielli, Sepp Kipfstuhl, and Urs Ruth.
I want to give a very special thanks to Dr. Hubertus Fischer for reading my manuscripts, at any stage in the writing process, in detail for commenting and discussions.

During my stay in Germany my colleges were also my closest friends and I have spent many cheerful moments together with all those guys. Here I will mention Professor Fernando Valero-Delgado and Paul Juckschat, for beeing always in a good mood. I will also mention Dr. Hans Oerther for his support filling out formulars and checking my german.

Til sidst vil jeg takke Niels Agersnap Larsen, mine forældre Mette og Ole Siggaard-Andersen, min bror Jens Siggaard-Andersen, samt resten af min familie for moralsk opbakning og støtte under hele PhD forløbet.

1) Universität Bremen Fachbereich 05, Geowissenschaften, Klagenfurter Straße 2, 28359 Bremen, Germany.
2) Stiftung Alfred-Wegener-Institut für Polar- und Meeresforschung in der Helmholtz-Gemeinschaft, Columbusstrasse, 27568 Bremerhaven, Deutschland. Fachbereich Geosystem, Section für Lithosphäre und polare Eisschilde.

Contents

1: Introduction

1.1 Global ice sheets during past and present

During the last 2-3 million years the climate of the Earth has experienced long periods of extended glaciations separated by relatively short interglacials of distinctly less glaciation. Marine sediment cores and polar ice cores have provided important knowledge of these climate variations. Those archives record the climatic influences on physical or biological factors acting on the sedimentary system or organisms deposited within.

Formation of permanent glaciers and ice sheets on Earth causes an isotope fractionation of the global water reservoir where ice in glaciers and ice-sheets is depleted in the isotopes, ^{18}O and ^{2}H (deuterium), i.e. it is isotopic lighter than ocean water. The isotope composition of the isotopic heavier ocean water therefore reflects the global ice volume.

Evidence for existence of permanent ice on Earth is found from zoo-plankton living in deep oceans (benthic foraminifera). Their calcareous ($CaCO_3$) shells are deposited on the sea-floor where they build up an archive of past ocean oxygen isotope composition.

Further evidence for the existence and change of ice sheets can be retrieved from ice rafted debris (IRD) that is crustal material deposited on the ocean floor after being transported over open water in ice bergs.

Major changes in the global climate during the last 65 million years based on more than 40 deep-sea sediment cores are shown in Figure (1.1) (from Zachos et al., 2001). The $\delta^{18}O$ curve is obtained from analysis of benthic foraminifera and represents partly deep-ocean temperatures and partly global ice volume. The $\delta^{13}C$ curve reflects primarily changes in ocean circulation. The rapid step in the $\delta^{18}O$ curve around 34 million years ago indicates the formation of permanent ice sheets in Antarctica. The opposite step 26-27 million years ago reflects partly an increase in ocean temperatures and partly a reduction in Antarctic ice extent. The formation of the present day East Antarctic ice sheet is indicated by the rapid increase in deep-sea $\delta^{18}O$ beginning around 14 million years ago, whereas the formation of the West Antarctic ice sheet is seen as a gradual increase in $\delta^{18}O$ 10-6 million years ago. In the northern hemisphere glaciations intensified between 3 million and 2.5 million years ago (Shackleton, 1997).

Changes in climate on time scales of 10^7 years are induced by plate tectonic processes. Some tectonic processes that occurred synchronously with major changes in glaciations are indicated in Figure (1.1). Highly debated, Antarctic glaciations could be related to the opening of the Tasmanian-Antarctic passage leading to an isolated Southern Ocean (e.g. DeConto and Pollard, 2003) whereas northern hemispheric glaciations could be related to the closing of the Panama sea-way (Haug and Tiedemann, 1998) or an uplift of the Tibetan Plateau (An et al., 2001).

On shorter time scales, climate variations are driven by the cycling properties of Earth's orbital parameters; eccentricity with a periodicity of 100 and 400 ka, obliquity with a periodicity of 41 ka, and precession with a periodicity of 19 and 23 ka. The cycling in Earth's climate is often referred to as Milankowitch-cycles after Milutin Milankowitch who in 1941 described the connection between global glacier extent and seasonality of insolation at 65ºN. The sensitivity of the global ice volume to the northern hemisphere insolation is a consequence of a non-homogeneous distribution of continents and oceans

and of ocean circulation. Due to the large continental coverage and the meridional ocean circulation in the North Atlantic, the northern hemisphere responds strongly to changes in insolation.

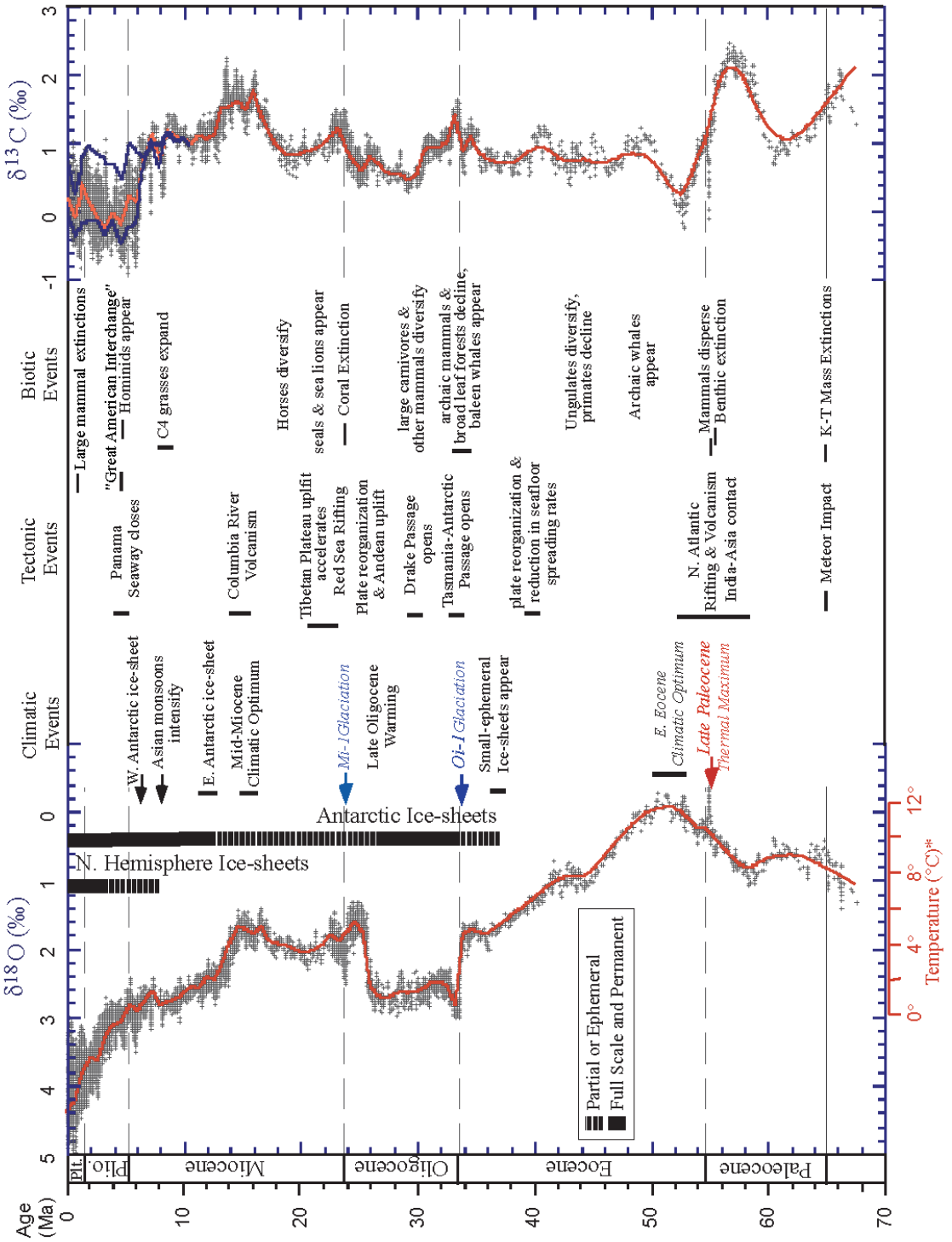

Figure 1.1: *Climate development over the last 65 million years from more than 40 marine sediment cores (from Zachos et al., 2001).*

The obliquity (tilt of Earth's axis relative to the orbit plane), determining the strength of seasonal variations, has the dominant influence on timings of major changes in ice volume. The Pliocene/Pleistocene boundary 1.77 million years BP is characterised by the onset of regular 41 ka cycles in marine sediment records (Shackleton, 1997). Later in the Pleistocene, the influence of precession (direction of tilt in the orbit plane), and eccentricity (shape of Earth's orbit) on climate became larger and resulted in a 100 ka cyclic behaviour of the climate system.
The SPECMAP time scale is a well-established chronology obtained by tuning changes in a stacked marine sediment record to changes in northern hemisphere insolation (Imbrie et al., 1993). The alternating climate conditions recorded in marine sediment cores such as the SPECMAP record are classified as Marine Isotope Stages (MIS) numbered from the top of the cores (Martinson et al., 1987). Marine Isotope Stages are roughly marked on Figure 1.2. For higher resolution records these stages are further divided into sub-stages e.g. 5a-5e.
The so-called "100 ka" climate cycle of the late Pleistocene is characterised by interchanging long time periods of high degree of glaciations and relatively short interglacials, with less glaciations. The last glacial cycle refers to the time period from the last interglacial, MIS5e, around 120 ka BP and up to present. The current climate period, MIS1 or the Holocene, began approximately 11.5 ka BP.

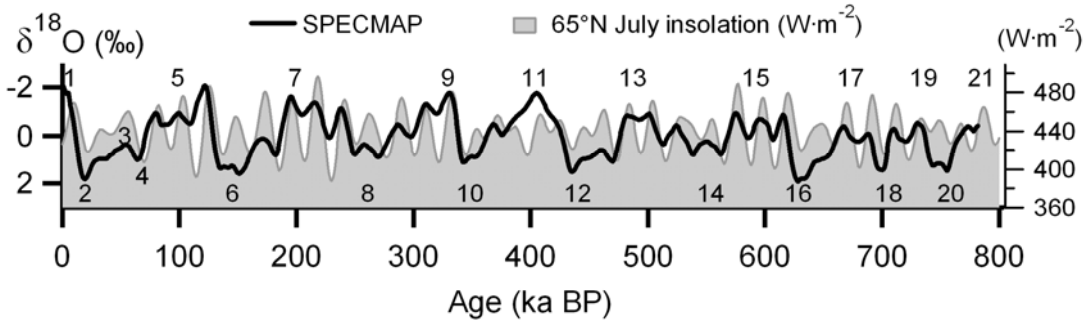

Figure 1.2: *Insolation at 65ºN (Berger, 1992) versus the SPECMAP record (Imbrie and Duffy, 1990), which is a normalized stacked $\delta^{18}O$ series from planktonic foraminifera (reflecting ocean surface temperatures). The marine isotope stages (MIS) are roughly indicated.*

At present, permanent ice sheets and glaciers contain 2.2% of the global water reservoirs. The Antarctic ice sheet, with a 10 times larger volume than the Greenland ice sheet, constitutes the majority of the global ice volume. During the Last Glacial Maximum (LGM), approximately 21 ka BP, about 6-7% of the global water reservoir was held in ice sheets and glaciers. The Antarctic and the Greenland ice sheets have decreased only little since the last glacial, but in the northern hemisphere huge glaciers located in North America and in Eurasia have melted away. The Scandinavian ice sheet was larger than the Greenland ice sheet and the Laurentide ice sheet in North America was as large as the present day Antarctic ice sheet.
Landscapes together with terrestrial and marine sediment records provide evidence for the extent of continental ice sheets and sea ice during past glacial and interglacial

periods. Further knowledge on the extent of past ice sheets and sea ice is obtained from ice sheet modelling and from General Circulation Model (GCM) simulations.
During the LGM the combined ice volume of northern hemispheric ice sheets was exceeding the present Antarctic ice sheet almost by a factor of two (Bintanja et al., 2002) and consequently the global sea level was 120 m lower than today (Bard et al., 1990) and large continental shelves were exposed.
Figure 1.3 shows a reconstruction of the global water reservoir for the present and for the LGM (from Huybrechts and Zweck, 2004).

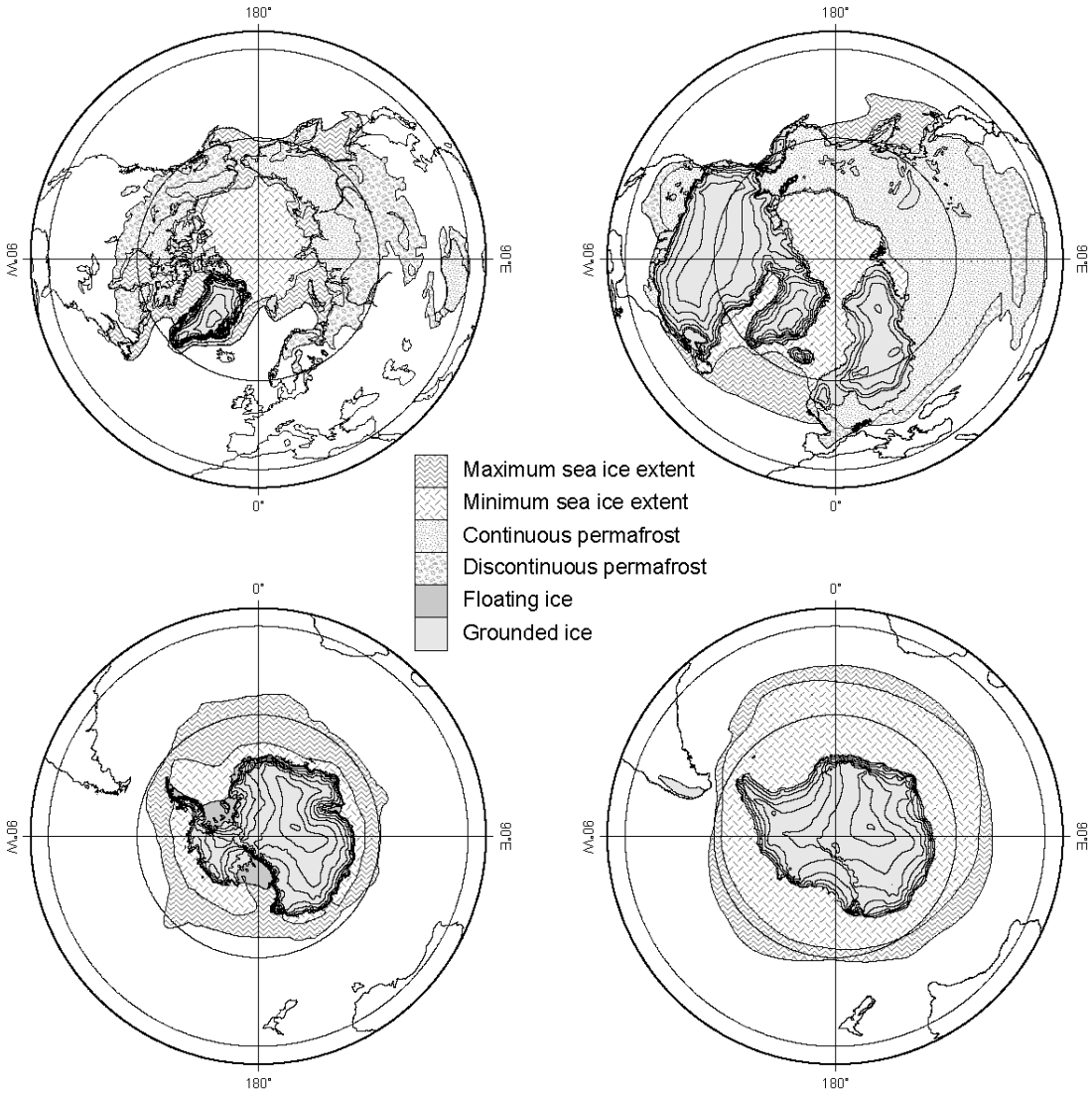

Figure 1.3: *Ice sheets, seasonal sea ice extent and continents for present (left) and for LGM (right) for the northern (top) and the southern (bottom) hemispheres. Contour-lines on the ice sheets correspond to 500 m height intervals. (Data compiled by Huybrechts and Zweck (2004)).*

1.2 Climate history from deep polar ice cores

While volume and coverage of ice sheets is closely coupled to climate (e.g. through the albedo and the atmospheric and ocean circulation), ice sheets also serve as climate archives. High altitude ice sheets are built up of single snow fall events deposited layer by layer, and kept frozen. The fraction of heavy isotopes in precipitation depends on the temperature history of the water vapour. Therefore, the snow layers in an ice sheet record and preserve information about circulation and temperature. Due to a higher sedimentation rate, polar ice core records have in general higher resolution and resolve more details in the climate history than marine sediment cores.
Together with snow precipitation, various types of aerosols, which are wind-blown continental and marine material and aerosols produced in the atmosphere, are deposited within the ice. Ice sheets therefore also contain an archive of aerosols. Furthermore, in the process of compaction from snow to ice, air bubbles are captured within the ice. This process creates a unique archive of paleo-atmospheric composition such as the concentration of greenhouse gasses.
The ice inside an ice sheet is under pressure from the overlying ice mass and is therefore constantly moving towards the edges. For steady-state conditions the supply of ice from a new layer of snow on top of an ice sheet is balanced by melting or ice berg calving at the edges. The deepest part of an ice sheet might in principle contain precipitation that reaches back to the time when the ice sheet was building up, but thinning and disturbances of the stratigraphy by the dynamical processes is likely to have disturbed the layer structure of the deepest ice. The temperature in an ice sheet is very insensitive to the surrounding temperatures due to the poor heat conducting properties of ice. Geothermal heat-flux from underneath the ice sheet heats up the basal ice, but is balanced by the dynamical processes in the ice sheet. At some locations however the geothermal heat-flux may cause melting of the ice sheet at the bottom and thereby limiting the age of the oldest ice.

Precise dating of the Greenland and Antarctic ice core records is essential for inter-comparisons and for the understanding of the dynamical processes involved in rapid climatic changes, and is a topic of major interest. Ice cores have been dated through synchronisation of ice core records with the deep-sea SPECMAP chronology (e.g. Petit et al., 1990) or with insolation changes assuming a non-linear character of the climate system (Parrenin et al., 2001), but dating by ice sheet modelling is more commonly used (e.g. Johnsen and Dansgaard, 1992; Petit et al., 1999; Schwander et al., 2001). Known volcanic eruptions, stratospheric radio nuclides varying in parallel to large solar out-burst, and nuclear bomb testing, are identified in the ice cores and provide accurate time markers (Hammer et al., 1978; Hammer, 1980; Clausen et al., 1997; Schwander et al., 2001). Annual layer counting is used whenever ice core records in annual resolution are available (Hammer et al., 1978; Dansgaard et al., 1993; Meese et al., 1997). Annual layer counting using high resolution chemical records and visual stratigraphy is currently processed on the NorthGRIP ice core in order to obtain an accurate north hemispheric chronology for the last glacial cycle (Copenhagen Dating Initiative members, 2002).

Greenland ice cores: In central Greenland the ice sheet is approximately 3 km thick. The two Greenland Summit ice cores from the Greenland Ice core Project (GRIP) and

from the Greenland Ice Sheet Project-2 (GISP2) reach possibly more than 250 ka back in time (Dansgaard et al., 1993) but show strongly diverging records in their deepest parts. Evidence from gas contents and compositions in the GRIP ice core suggested that this ice core has a preserved stratigraphy reaching back to substage 5d approximately 115 ka BP, while the stratigraphy in the deepest 250 m of the core is likely to be affected by large-scale disturbances (Johnsen et al., 1997). The divergence in the two records has put focus on the climate of the last inter glacial, the Eemian, approximately 115-130 ka BP. In 1996 the NorthGRIP deep drilling programme started with the main goal of obtaining an undisturbed high-resolution record of the Eemian climate period, (Dahl-Jensen et al., 2002). The drilling reached the bottom in 2003, with an undisturbed record reaching back into the Eemian period (NorthGRIP members, 2004). Water recovered at the bedrock indicated that bottom melting occurs at NorthGRIP and is preventing shear stress disturbance of the stratigraphy (NorthGRIP members, 2004).

Antarctic ice cores: The Antarctic ice sheets has a thickness of up to 4 km and due to a much lower snow accumulation rate it has a preserved stratigraphy reaching much longer back in time than the Greenland ice sheet.
The 3310 m long Vostok ice core is dated back to 420 ka BP (Petit, 1999), while the Dome Fuji ice core is dated back to 340 ka BP (Watanabe et al., 2003), and the EPICA Dome Concordia (EDC) ice core, which today is the longest ice core record, is dated back to 740 ka BP at a depth of 3139 m (EPICA community members, 2004). The EDC drilling is not finished, which means that even older ice is going to be recovered.

1.3 Millennial scale climate variations

Dansgaard-Oeschger events: Greenland ice core records have revealed evidence for millennial scale interruptions of the cold glacial climate by distinctly warmer interstadials, the so called Dansgaard/Oeschger (D/O) events. In the GRIP ice core 24 such events were identified. Interstadials are numbered GIS-n (Greenland InterStadials) with n=1, 2 … from the top (Dansgaard et al., 1993) (see Figure 1.5). The preceding stadials (Greenland Stadials) are numbered GS-(n+1) (Walker et al., 1999). The new NorthGRIP ice core has revealed one more D/O event, GIS-25, and one more stadial, GS-26, early in the last glacial period (NorthGRIP members, 2004).
D/O events are characteristic for rapid warming, within a few decades, associated with enhanced thermohaline circulation (THC) in the North Atlantic (see Figure 1.4) and simultaneous retreat of continental glaciers. D/O events are also observed in many marine and terrestrial records (e.g. Voelker et al., 2002) indicating that major environmental changes occurred in the northern hemisphere during these events.

Heinrich events: Another type of millennial scale climate events, the so called Heinrich events, are observed in North Atlantic sediment cores as distinct layers of ice rafted debris (IRD). IRD-layers in marine sediments are evidence for events of massive ice berg discharge into the North Atlantic. During the most prominent Heinrich events (H1-H6), which occurred approximately every 10 ka during MIS2, MIS3, and MIS4 (Bond et al., 1992), icebergs were discharged synchronously from all ice sheets surrounding the North Atlantic. During these events up to 10 % of the Laurentide ice sheet slid into

the North Atlantic and resulted in a break down of the thermohaline circulation (see Figure 1.4).
Heinrich events only occurred during cold stadial conditions, and are believed to have happened when the height of the ice sheets reached a certain threshold, where the pressure melting point for the basal ice coincided with the basal temperatures. It has been suggested that sea level change caused by a spontaneous ice berg discharge could generate a chain reaction of ice berg discharge around the North Atlantic (Bond and Lotti, 1995).

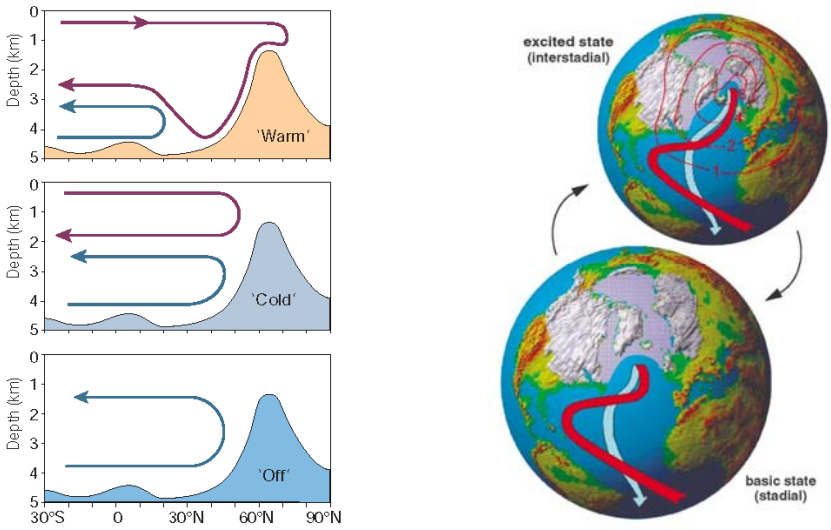

Figure 1.4: *Left: three modes of THC in the North Atlantic; the interstadial, the stadial and the Heinrich mode respectively (from Rahmstorf, 2002). In the interstadial mode the overturning of warm salty water takes place in the Nordic Seas. During an interstadial the mode slowly weakens until a rapid shift into the stadial mode occurs. In the Heinrich mode the massive iceberg discharge breaks down the THC and causes cooling at low latitudes. Right: the stable stadial mode and the unstable interstadial mode (from Ganopolski and Rahmstorf, 2002).*

The forcing of Heinrich and D/O events is not yet understood and is a topic of major interest. Since Heinrich events are succeeded by warm interstadials (e.g H4 by GIS-8 and H5 by GIS-12) followed by gradually weaker and shorter interstadials, it has been suggested that the two types of events are connected through a combination of ice sheet dynamics, releasing huge amounts of ice into the North Atlantic, and ocean thermohaline circulation (Bond et al., 1993). Later Bond et al. (1997) has suggested a 1470 years cyclic pacing of the Heinrich and D/O events but without evidence for such a cycling in the dynamic system or in the solar output. However a similar cyclic property of ice berg discharge through-out the Holocene correlating with production rates of cosmogenic nuclides has suggested a pacing by solar output (Bond et al., 2001).
Stochastic resonance behaviour of the timing of the D/O events has been suggested (Alley et al., 2001; Ganopolski and Rahmstorf, 2001; Ganopolski and Rahmstorf, 2002) and forced model studies of Ganopolski and Rahmstorf (2001) were able to reproduce rapid climate variations for glacial conditions; however, they do not provide a convincing trigger for either D/O or Heinrich events. One step closer to an

understanding of the dynamical processes acting during abrupt glacial climate events could be obtained by Knutti et al. (2004), who, using a coupled climate model, demonstrated that temperature and sea level variations during the last glacial period largely can be explained by combined oceanic heat and freshwater anomalies, but the forcing of these changes in ocean circulation still needs to be determined.

Antarctic counterparts: While D/O and Heinrich events are northern hemisphere phenomena, climate instability during the last glacial is also observed in Antarctic ice cores. Antarctic warming events, A1-A7 occur asynchronously with the very warm D/O events in the North (Blunier et al., 1998) (see Figure 1.5).
A detailed synchronisation of Greenland and Antarctic ice core records using the methane content, which represents a global signal, has shown that every D/O event have an asynchronous Antarctic counterpart (Blunier and Brook., 2001). They suggest a persistent see saw mechanism driven by the northern hemisphere during the last glacial period. This idea has further been developed by Stocker and Johnsen (2002) implying a Southern Ocean heat reservoir which is either drained or filled by varying heat export into the North Atlantic. This see saw concept was extended in the coupled ocean-atmosphere-sea ice general circulation model used by Knutti et al. (2004).

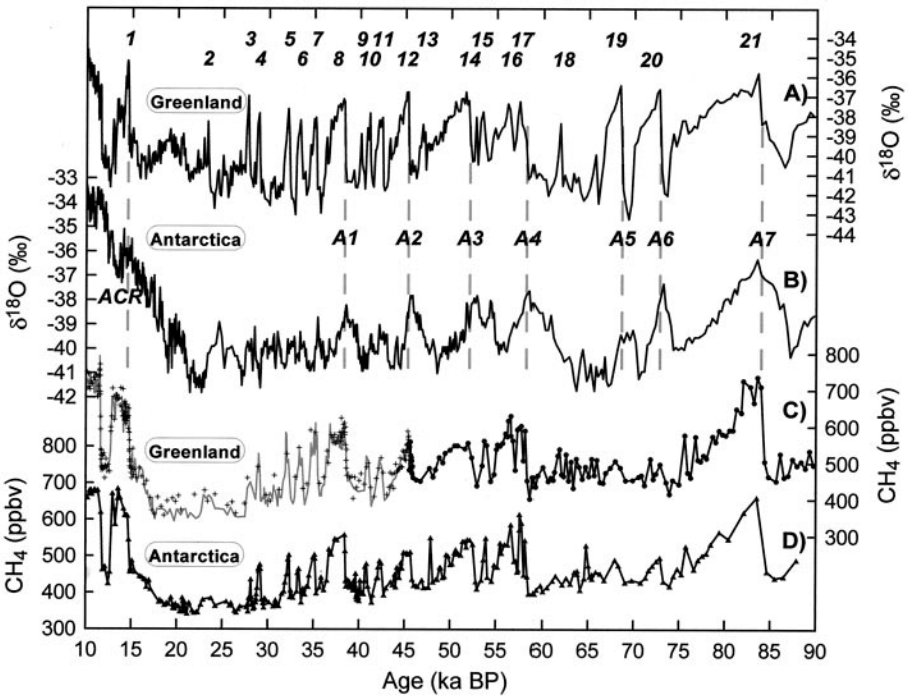

Figure 1.5: *Synchronization of isotope records from GISP2 and Byrd using methane records from GRIP/GISP2 and Byrd respectively (from Blunier and Brook, 2001)*

1.4 Ice core records of chemical impurities

Ice core concentrations of dust and sea salt show much stronger variations with climatic changes than isotope records (De Angelis et al., 1997; Fuhrer et al., 1999; Petit et al., 1999). Furthermore, high frequency variations, such as annual signals, are generally better resolved in the chemical records than in the isotope records; mainly because isotopes are subject to diffusion processes in the firn snow and ice (Hammer et al., 1978).

Over time there has been an increasing interest in detailed chemical analyses of deep polar ice cores. Techniques for micro analyses of dust particles and continuous flow-analysis have been currently developed and improved for that purpose. For the recently recovered Greenland NorthGRIP deep ice core and for the current Antarctic EPICA deep ice core drillings at Dome Concordia and in Dronning Maud Land, chemical analyses have been strongly intensified compared to previous deep ice cores (Dahl-Jensen et al., 2002; Miller and EPICA members, 2002).

In this thesis chemical impurities derived from mineral dust and sea salt aerosol in polar ice cores are studied. Ice core records of soluble lithium are presented and discussed in relation to source characteristics of the mineral dust. A statistical analysis of soluble ions in the NorthGRIP ice core is presented and discussed in relation to north hemispheric large-scale transport patterns for mineral dust and sea salt aerosol.

1.5 References

Alley, R. B., P. A. Mayewski, et al. (1997). "Holocene climatic instability: a prominent widespread event 8200 yr ago." Geology **25**(6): 483-486.

An, Z., J. E. Kutzbach, et al. (2001). "Evolution of Asian monsoons and phased uplift of the Himalaya-Tibetan plateau since Late Miocene times." Nature **411**: 62-66.

Bard, E., B. Hamelin, et al. (1990). "U-Th ages obtained by mass spectrometry in corals from Barbados: sea level during the past 130,000 years." Nature **346**(6283): 456-458.

Berger, A. (1992). "Orbital Variations and Insolation Database. IGBP PAGES/WDCA Data Contribution Series #: 92-007. NOAA/NGDC Paleoclimatology Program, Boulder CO, USA."

Bintanja, R., R. S. W. van de Wal, et al. (2002). "Global ice volume variations through the last glacial cycle simulated by a 3-D ice-dynamical model." Quaternary International **95-96**: 11-23.

Blunier, T. and E. J. Brook (2001). "Timing of millennial-scale climate change in Antarctica and Greenland during the last glacial period." Science **291**: 109-112.

Blunier, T., J. Chappellaz, et al. (1998). "Asynchrony of Antarctic and Greenland climate change during the last glacial period." Nature **394**: 739-743.

Bond, G., W. Broecker, et al. (1993). "Correlations between climate records from North Atlantic sediments and Greenland ice." Nature **365**(6442): 143-147.

Bond, G., H. Heinrich, et al. (1992). "Evidence for massive discharges of icebergs into the North Atlantic ocean during the last glacial period." Nature **360**: 245-249.

Bond, G., B. Kromer, et al. (2001). "Persistent solar influence on north Atlantic climate during the Holocene." Science **294**: 2130-2136.

Bond, G., W. Showers, et al. (1997). "A pervasive millennial-scale cycle in North Atlantic Holocene and glacial climates." Science **278**: 1257-1266.

Bond, G. C. and R. Lotti (1995). "Iceberg discharges into the North Atlantic on millennial time scales during the last glaciation." Science **267**: 1005-1010.

Copenhagen Dating Initiative members (2002). "Glaciologi-Dateringsinitiativet." http://www.glaciology.gfy.ku.dk.

Dansgaard, W., S. J. Johnsen, et al. (1993). "Evidence for general instability of past climate from a 250-kyr ice-core record." Nature **364**(6434): 218-220.
De Angelis, M., J. P. Steffensen, et al. (1997). "Primary aerosol (sea salt and soil dust) deposited in Greenland ice during the last climatic cycle: Comparison with east Antarctic records." Journal of Geophysical Research **102**(C12): 26681-26698.
DeConto, R. M. and D. Pollard (2003). "Rapid Cenozoic glaciation of Antarctica induced by declining atmospheric CO_2." Nature **421**(6920): 245-249.
EPICA community members (2004). "Eight glacial cycles from an Antarctic ice core." Nature **429**(6692): 623-628.
Ganopolski, A. and S. Rahmstorf (2000). "Rapid changes of glacial climate simulated in a coupled climate model." Nature **409**: 153-158.
Ganopolski, A. and S. Rahmstorf (2002). "Abrupt glacial climate changes due to stochastic resonance." Physical Review Letters **88**(3): 038501.
Hammer, C. U. (1980). "Acidity of polar ice cores in relation to absolute dating, past volcanism, and radio-echoes." Journal of Glaciology **25**(93): 359-372.
Hammer, C. U., H. B. Clausen, et al. (1978). "Dating of Greenland ice cores by flow models, isotopes, volcanic debris, and continental dust." Journal of Glaciology **20**(82): 3-26.
Haug, G. H. and R. Tiedemann (1998). "Effect of the formation of the Isthmus of Panama on Atlantic Ocean thermohaline circulation." Nature **393**: 673-676.
Huybrechts, P. and C. Zweck (in preparation). The cryosphere. Encyclopaedia of Paleoclimate.
Imbrie, J. and A. Duffy et al "SPECMAP Archive #1, U.S. National Geophysical Data Center (NGDC), avaiable at: http://www.ngdc.noaa.gov/mgg/geology/data/specmap."
Imbrie, J., A. Berger, et al. (1993). Role of orbital forcing: A two-million-year perspective. Global Changes in the Perspective of the Past. J. A. Eddy and H. Oeschger, John Wiley & Sons Ltd.**:** 263-277.
Johnsen, S. J. and W. Dansgaard (1992). On flow model dating of stable isotope records from Greenland ice cores. The Last Deglaciation: Absolute and Radiocarbon Chronologies. E. Bard and W. S. Broecker. New York, Springer-Verlag. **2:** 13-24.
Knutti, R., J. Fllückiger, et al. (2004). "Strong hemispheric coupling of glacial climate through freshwater discharge and ocean circulation." Nature **430**: 851-856.
Martinson, D. G., N. G. Pisias, et al. (1987). "Age dating and the orbital theory of the ice ages: development of a high-resolution 0 to 300.000 year chronostratigraphy." Quaternary Research **27**: 1-29.
Meese, D. A., A. J. Gow, et al. (1997). "The Greenland Ice Sheet Project 2 depth-age scale: Methods and results." Journal of Geophysical Research **102**(C12): 26411-26423.
Miller, H. and E. members (2002). "EPICA Annual Report 05/2001-04/2002."
North Greenland Ice-Core Project (NorthGRIP) Members (in press, 2004). "High resolution Climate Record of the Northern Hemisphere reaching into the last Glacial Interglacial Period." Nature.
Parrenin, F., J. Jouzel, et al. (2001). "Dating the Vostok ice core by an inverse method." Journal of Geophysical Research **106**(D23): 31837-31851.
Petit, J. R., J. Jouzel, et al. (1999). "Climate and atmospheric history of the past 420,000 years from the Vostok ice core, Antarctica." Nature **399**: 429-436.
Petit, J. R., L. Mounier, et al. (1990). "Palaeoclimatological and chronological implications of the Vostok core dust record." Nature **343**: 56-58.
Rahmstorf, S. (2002). "Ocean circulation and climate during the past 120,000 years." Nature **419**(6903): 207-214.
Shackleton, N. J. (1997). "The deep-sea sediment record and the Pliocene-pleistocene boundary." Quaternary International **40**(1): 33-35.
Voelker, A. H. L. and workshop participants (2002). "Global distribution of centennial-scale records for Marine Isotope Stage (MIS) 3: A database." Quaternary Science Reviews **21**: 1185-1212.
Walker, M. J. C., S. Björck, et al. (1999). "Isotopic "events" in the GRIP ice core: a stratotype for the Late Pleistocene." Quaternary Science Reviews **18**: 1143-1150.
Watanabe, O., J. Jouzel, et al. (2003). "Homogeneous climate variability across East Antarctica over the past three glacial cycles." Nature **422**: 509-512.
Zachos, J., M. Pagani, et al. (2001). "Trends, rhythms, and aberrations in global climate 65 Ma to present." Science **292**(5517): 686-693.

2: The global cycles of dust and sea salt inferred from Greenland ice cores and from climate models

2.1 Introduction

Concentrations of dust and sea salt in central Greenland ice cores show strong seasonal variations both for present day conditions and for the last glacial. At present the main fraction of dust and sea salt is deposited during the winter/spring season with the seasonal sea salt peak slightly preceding the seasonal dust peak (Steffensen, 1988; Ruth et al., 2002). On longer terms major changes in dust and sea salt concentrations occur simultaneously with major changes in the isotope records indicating that the strengths of source emission and transport of those impurities to the ice strongly depends on climate conditions (Dansgaard et al., 1984; Legrand and Delmas, 1988; Petit et al., 1990).
In Greenland ice cores dust concentrations are up to 100 times higher and sea salt concentrations are up to 10 times higher for the Last Glacial Maximum (LGM) than for present day condition (De Angelis et al., 1997; Steffensen, 1997; Ruth et al., 2003). The very elevated dust concentrations for the LGM has been attributed to a combination of different effects of climate conditions: More arid surface conditions and more intensive wind systems in the source areas (De Angelis et al., 1997; Fuhrer et al., 1999; Ruth et al., 2003) as well as extended source areas due to a lower sea level and to a southward movement of the polar front (De Angelis et al., 1997), stronger atmospheric circulation (Mayewski et al., 1997), and longer aerosol life-times due to a weaker hydrological cycle (Hansson, 1995).
It is believed that aerosol dust affects the climate in several ways through influences on the global radiative balance, on atmospheric chemistry, and on the biogeochemical cycling (Prospero et al., 1983; Derbyshire, 2003; Tegen, 2003). Therefore the global dust cycle has certain relevance in climate model predictions. Satellite observations can be used for validation of large-scale dust patterns in present day dust cycle models (Prospero et al., 2002; Gong et al., 2003; Tegen, 2003), but dust records from polar ice cores are considered to be of unique importance for validations of global dust cycle models for both past and present climate conditions (Kohfeld et al., 2001). Aerosol dust has been subject to much larger attention than sea salt aerosol partly because of its coupling to climate conditions and partly because dust records are available from many different locations world-wide (Kohfeld et al., 2001). However because ice cores provide dust and sea salt records in parallel, climate influences on these two different particulate aerosol species can be jointly investigated. Rapid climate changes at glacial/interglacial transitions and during Dansgaard/Oeschger (D/O) events, generally occur more abrupt in the records of dust and sea salt than in isotope records (Dansgaard et al., 1989; Fuhrer et al., 1999). Those records are therefore important for understanding the changes in climate dynamical processes associated with rapid climate changes.

2.2 Atmospheric dust

Aerosol dust consists of fine mineral particles that are suspended into the atmosphere during strong surface winds. Enormous amounts of mineral dust are loaded into the atmosphere. It is estimated that globally 10^{11} kg·a^{-1} of mineral dust particles (< 5 μm) are emitted (Prospero et al., 1983).
There is a large geographical variation in the distribution of dust sources. On a global scale the dominant dust sources are located on the northern Hemisphere, mainly in North Africa, the Middle East, Central Asia, and the Indian subcontinent (Prospero et al., 2002) (see Figure 2.1).

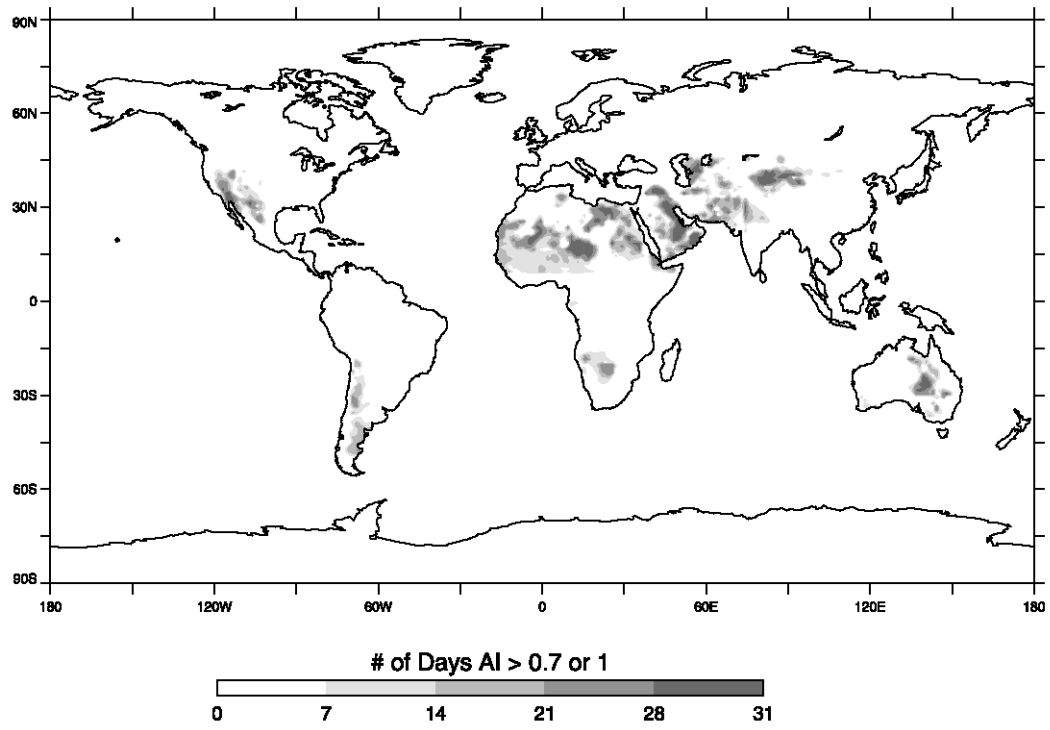

Figure 2.1: *The global distribution of dust sources identified with the TOMS (Total Ozone Mapping Spectrometer) instrument on the nimbus 7 satellite measuring back-scattered UV radiance (indicated by an Aerosol Index (AI)) (from Prospero, 2002).*

Aerosol dust is mainly deposited down-wind from the source areas, but dust that is lifted up into the mid and upper troposphere may be long-range transported over thousands of km by upper level winds. Trace amounts of this dust reaches as far as to the remote areas of the Greenland and Antarctic ice sheets.
Although physical processes governing dust mobilizations and transport are considered well understood they might be oversimplified in models (Tegen, 2003). Modellers have had large difficulties in obtaining ice core levels of dust and sea salt concentrations in simulations based on present day's knowledge about emission/deposition processes and wind circulation. These difficulties are concerning both present day's and LGM conditions as well as the LGM/present day relative change (Reader and McFarlane, 2003; Tegen, 2003; Werner et al., 2003).

The dust found in Greenland ice cores consists of very fine particles – around 2 μm in diameter. In the source area such fine particles are mobilized through the process of saltation, i.e. through impact from larger particles typically in the range of 60 μm – 100 μm, which are again mobilized when surface wind speeds exceed a certain threshold (Gillette, 1980; Genthon, 1992a; Pye, 1995). Soil moisture has a limiting effect on dust emissions, and fine particles are more sensitive to soil moisture than larger particles because of their relatively larger surfaces. Another effect of moisture is chemical weathering, which among other factors leaches salts from the rocks. In dry periods salts can form a resistant crust on the soil surface (Gillette et al., 1982). In models dust and sea salt emission fluxes are estimated on the basis of parameterizations of lift from the ground (horizontal flux) and mixing with the atmosphere (vertical flux) (e.g. Genthon 1992a). The horizontal particle flux is calculated on the basis of surface windspeeds to the third or fourth power and on parameterizations of soil-surface properties, which include particle sizes, soil moisture, surface roughness, and vegetation cover. The vertical particle flux is determined using an emission factor (Genthon, 1992a; Tegen, 2003).

Silt-sized particles are formed during processes of chemical and physical weathering and glacial crushing and grinding (Pye, 1995). Topographic depressions, acting as reservoirs for these particles, are preferential dust source areas (Tegen et al. 2002; Sun, 2002). Satellite observations have shown that dust plumes are often generated at alluvial fans or along lake shore-lines (Prospero et al., 2002; Sun, 2002). Although soil moisture is a limiting factor in dust emission processes especially for the fine particle fraction, the action of water might be of major importance in the production of the fine particles (Prospero et al, 2002), explaining why semi-arid areas often are greater dust sources than hyper-arid areas (Arnold et al., 1998).

2.3 East Asian dust sources

As indicated in Figure 2.1 dust sources in North Africa and in the Middle East are delivering the major amounts of dust to the atmosphere at present. However, the large desert areas in Central Asia are important dust source areas for the Eastern Asia and North Pacific. Large amounts of dust from Chinese deserts are deposited down-wind onto Chinese loess deposits, which are highly investigated for interpretations of paleo-climate records from the loess strata (Derbyshire, 1995; Zhang et al., 1999; Porter, 2001). Asian dust source areas are exceptional in the sense that they are located remote from major Quaternary ice sheets (Derbyshire, 2003). Particles generated at piedmont alluvial fans up wind from the western part of the Chinese loess plateau are potentially important sources to Quaternary loess in North China (Derbyshire et al., 1998; Sun, 2002).
Investigations of Chinese loess deposits are important for a better understanding of processes influencing the global dust fluxes (Derbyshire et al., 1998) and they also provide important information for the understanding of Greenland ice core dust records.

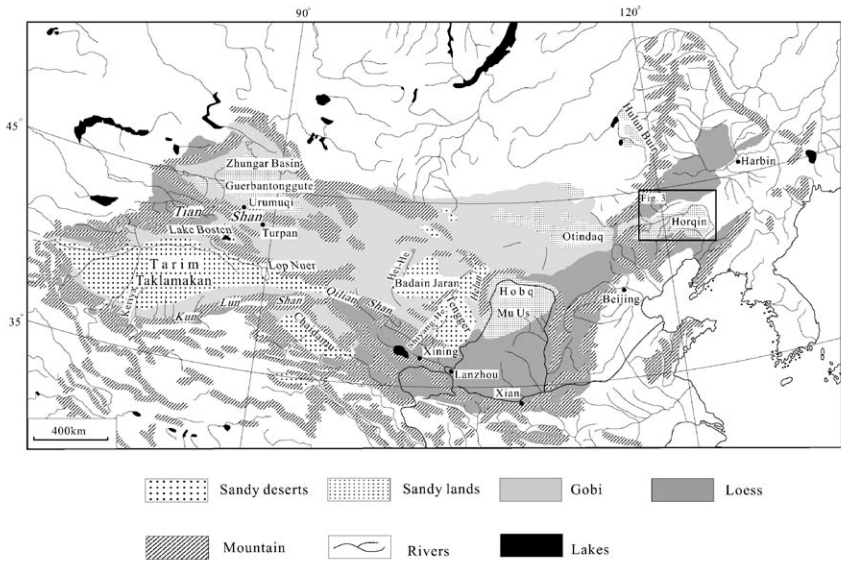

Figure 2.2: *Chinese deserts and loess deposits (from Yang et al., 2004).*

Isotopic composition of Sr and Nd (strontium and neodymium) together with mineral characteristics of Greenland ice core dust material has been applied to show that the most important source region for dust deposited onto the Greenland ice sheet during the last glacial period is located in the eastern Asian desert areas (Biscaye et al., 1997; Svensson et al., 2000). Recent and more detailed analyses of present day's dust deposited at NorthGRIP show that this material mainly origins from the Taklamakan desert north of the Tibetan plateau (see Figure 2.2) (Bory et al., 2003).

The wind system in Eastern Asia is very complex and shows strong seasonality. During winter, cold and dry westerly and north westerly winds associated with the Siberian high pressure system governs almost the whole of western and central China (Asian winter monsoon). During summer, radiative heating of air generates low air pressures over the southern Asian continent. Moist and warm marine air masses from the Pacific and from the Indian Ocean are brought to eastern China (East Asian summer monsoon) and to southern Tibet and southern China (Indian summer monsoon), respectively. Another monsoon system, the Tibetan Plateau monsoon, modifies the strength of the surrounding monsoons (e.g. Yu et al., 2001). The Tibetan Plateau, which has an average elevation of more than 4000 m above sea level, also influences upper level atmospheric circulation.
The areas north of the Tibetan plateau and in the northern China are today arid areas, while areas in eastern China are relatively wet. However, due to changes in strength of the monsoon circulations and changes in the precipitation/evaporation balance, the water balance in Chinese regions has been much different during glacial times. During the LGM, large freshwater lakes occupied the basins in the western Chinese desert area that today are salt lakes or playas, whereas eastern Chinese areas were much dryer than today (Yu et al., 2001).

In the literature, processes for dust deposited regionally in China and processes for long-range transported dusts are treated distinctly (Pye, 1995; Zhang et al., 1999; An, 2000; Sun, 2002) (see Figure 2.3). Dust mobilized during north westerly winds in the lower

troposphere during the Asian winter monsoon season is mainly deposited down-wind onto Chinese loess deposits. In contrast long-range transported dust from China is associated with the occurrence of desert dust storms during the spring season (Zhang et al., 1999; Sun, 2002) (see Figure 2.4). The spring peak observed in Greenland ice core dust records is likely to be associated with the dust storm season in western China (De Angelis et al., 1997; Bory et al., 2003), whereas deserts located in the Inner Mongolia contributes to a year around background dust deposition in Greenland (Bory et al., 2003).

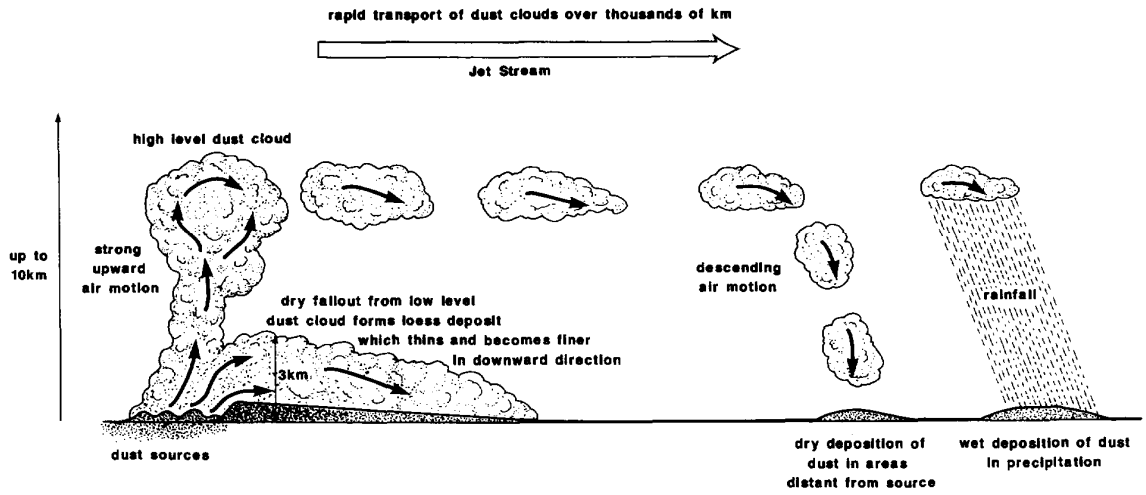

Figure 2.3: *Schematic representation of two contrasting modes of aeolian dust transport and deposition proposed for dust flux from the deserts of northwest China to the Loess Plateau and North Pacific Ocean during the Quaternary (from Pye and Zhou, 1989).*

The dust storms are generated by strong winds from outbreaks of cold air from the north, which combined with arid conditions during the spring season, provide the conditions for uplift of dust to the mid and upper troposphere (Sun et al., 2001). The dust storm season lasts three months from March to May with the major occurrence of dust storms in April (Sun et al., 2001).

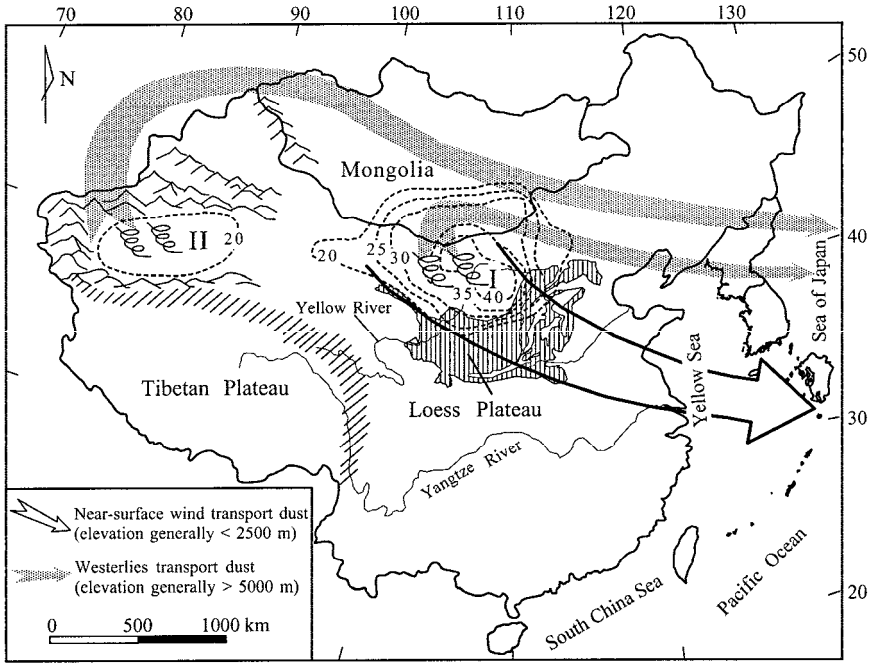

Figure 2.4: *Map showing the pathways of dust entrained from the two dominant dust source regions of China. Dashed contour lines indicate the number of dust storm events during the spring season of 1960–1999. Area I is the Gobi desert in southern Mongolia as well as the adjoining gobi and sand deserts in China; Area II is the Taklimakan Desert (From Sun, 2002).*

The Mongolian Gobi desert has the highest frequency of dust storms (Sun et al., 2001); however satellite observations show stronger persistent seasonal dust activity in the Tarim pendi (basin) ranging from February to September (Prospero et al., 2002). The topographic conditions around the Tarim pendi north of the Tibetan plateau result in particularly strong air dynamics in the Taklamakan desert where dust is lifted up to an altitude of 5000-8000 m (corresponding to 600—350 hPa), whereas dust from the Mongolian Gobi desert is lifted up to an altitude of only 3000 m. (Zhang et al., 1999; Sun et al., 2001). Dust plumes from the Tarim pendi are therefore more likely to be long-range transported as far as to Greenland than dust from the Mongolian Gobi desert (Bory et al., 2003).

2.4 Long-range transport patterns for Chinese dust

The polar jet stream is a strong high altitude east-ward wind near 60ºN that results from strong temperature gradients between cold and dry polar air masses and warm and moist air masses from lower latitudes. Around 30ºN another and weaker subtropical jet stream is flowing. The polar and subtropical jet streams are not always well defined and sometimes they fail to be continuous. Together they form a global wave that is associated with the westerlies and with strong meteorological dynamics at the surface. Examples of the coupling between upper level wind patterns and surface winds are the cold outbreaks of the polar jet stream that generate the Asian dust storms. The jet stream

patterns therefore indicate geographical locations of favourable conditions both for aerosol uplift and for long-range transport. The jet stream patterns show large day-to-day variations but have a pronounced seasonality with the southern most positions during winter.
Transport pathways of dust plumes generated during dust storms in China have been followed by satellites. Large plumes from both the Tarim pendi and the Mongolian Gobi deserts are transported with the westerlies across the Pacific Ocean and reach the west coast of North America approximately in one week (e.g. Husar et al., 2001). Observations over the North Pacific Ocean show that this is a general transport pattern of dust plumes. There is a seasonal variation with the highest dust concentrations appearing from February until June (Prospero et al., 1989).
Figure 2.5 shows 300 mbar geo-potential heights for both for the monthly mean and for a single day of April 2003. Average geo-potential heights do not indicate a persistent pathway for upper level winds across Greenland during the spring season. The monthly mean wind pattern for April suggests a more southerly path way over the North Atlantic to Europe. The possibility of such a transport path is confirmed through the finding of Chinese dust in glaciers in the Alps (Grousset et al., 2003). However, variations of the geopotential height patterns are relatively large especially in the Arctic. Because these variations occurs with a high frequency, long-range transport of dust from Chinese deserts to the Greenland ice sheet with the westerlies over North America and north to Greenland is a possible pathway. Dust from a dust storm can reside in the atmosphere over several weeks and may take a full turn around the North Hemisphere before it eventually is lead over Greenland.

While upper-level wind patterns provide a picture of large-scale patterns of long-range transport pathways, back trajectories give a complementary picture of transport paths for air masses reaching a specific destination. Back-trajectory analyses are used for determinations of source areas and transport pathways. From a statistical analysis of ten-thousands of back trajectories over 44 years to Greenland Summit, Kahl et al. (1997) has determined four dominant trajectory components for different seasons and altitudes. However, as pointed out by Kahl et al. (1997) these components are not resolving the large inter-annual (as well as high frequency) variations in large-scale transport patterns. Further more the studied trajectories are not necessarily associated with aerosol depositions or precipitation since aerosols and moisture are not necessarily transported along a typical wind direction. Therefore, only trajectory studies in association with events of precipitation or depositions of dust and sea salt aerosol are meaningful for evaluations of source areas and transport paths for aerosol and precipitation in Greenland.

Considering back trajectory analyses from Greenland Summit by Kahl et al., (1997), Bory et al. (2003) suggest a more northern transport path for dust reaching Greenland than dust reaching the west coast of America as a vertical effect in the dust transport pathways. However, present day transport pathways over the Canadian Arctic during winter/spring are very unlikely because of the Canadian vortex that leads air masses south over North America.

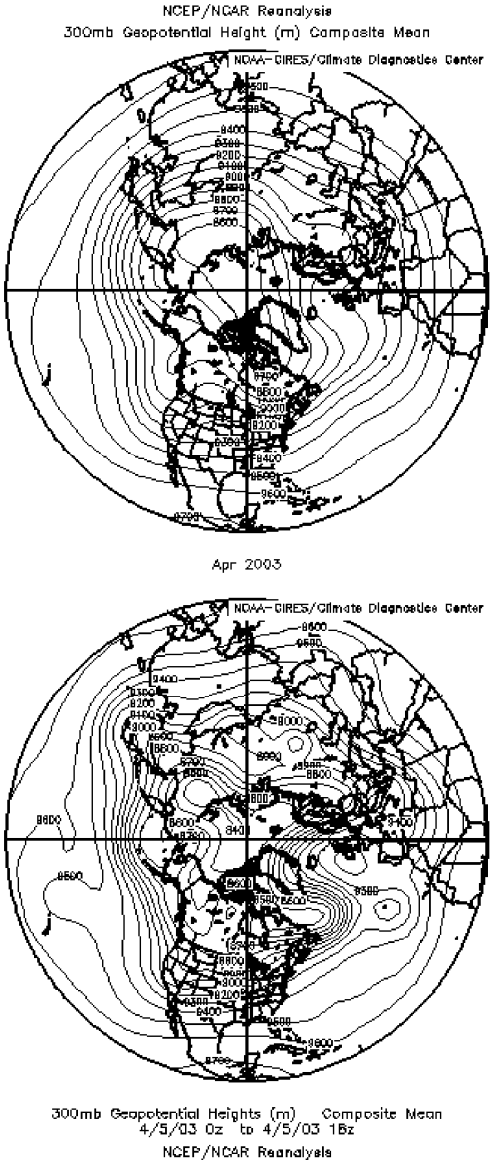

Figure 2.5: *300 hPa geo potential heights monthly mean for April 2003 (top) and for a single day in April 2003 (bottom). The contour lines, corresponding to 100 m height intervals, reflect the average high altitude wind patterns and the spacing indicates wind speeds. The mean April 2003 pattern shows that contour lines going out from central Asia are crossing Southern North America and South Europe/North Africa. During a single day the contour line is going north over the North Atlantic and crossing Greenland. (Provided by the NOAA-CIRES Climate Diagnostics Center, Boulder Colorado from their Web site at http://www.cdc.noaa.gov/cgi-bin/db_search/SearchMenus.pl).*

2.5 Sea salt aerosol emission and transport

Sea salt aerosol results from evaporation of sea spray produced by bubble bursting or during wind induced wave breaking. The global emission of sea salt particles < 5 μm is similar to that of dust, 10^{11} kg·a^{-1} (Prospero et al., 1983). Emission of sea salt depends like dust on surface wind speeds and we may consider all ocean surfaces as potential source regions. The horizontal sea salt flux is modelled exponentially from surface wind speed (Erickson et al., 1986; Genthon, 1992b; Reader and McFarlane, 2003).
Recently salt brines formed on top of sea ice during its formation have been established as an alternative source to sea salt aerosol (Wagenbach et al., 1998). In the coastal areas of Antarctica local sea ice brines are considered to be the major source to sea salt aerosol (Rankin et al., 2002). Sea ice has also been proposed as the major source to sea salt in inland Antarctica (Wolff et al., 2003). But until now no data are available on the contribution from sea ice to sea salt aerosol, especially as compared to the open ocean, and generally sea salt deposited onto the inland Antarctica and Greenland ice sheets are considered as long-range transported sea salt aerosol reflecting storminess over open ocean and conditions for transport (Legrand and Delmas, 1988; Mayewski et al., 1997; De Angelis et al., 1997; Petit et al., 1999; Stenni et al., 2001).

Present day large-scale transport properties of sea salt generated over open ocean can be described in a way similar to that for mineral dust, where conditions both for uplift and long-range transport are associated with upper level wind patterns. Strong winds both at the surface and at high altitudes will favour both uplift and long-range transport. From this point of view ocean surfaces both in the North Pacific and in the North Atlantic are possible source areas for sea salt deposited in Greenland. During winter wind speeds both at the surface and at the upper-level are much stronger than during summer (see Figure 2.6), consistent with the appearance of sea salt as a winter peak in ice core records (Steffensen, 1988).
For example, on the January 2003 plots average surface wind speeds are up to 15 m·s^{-1} in the North Pacific and average upper-level wind speeds over this area is around 50 m·s^{-1}, whereas on the July 2003 plots surface wind speeds are < 10 m·s^{-1} and over areas of highest surface wind speeds upper-level winds are not stronger than 20 m·s^{-1}.

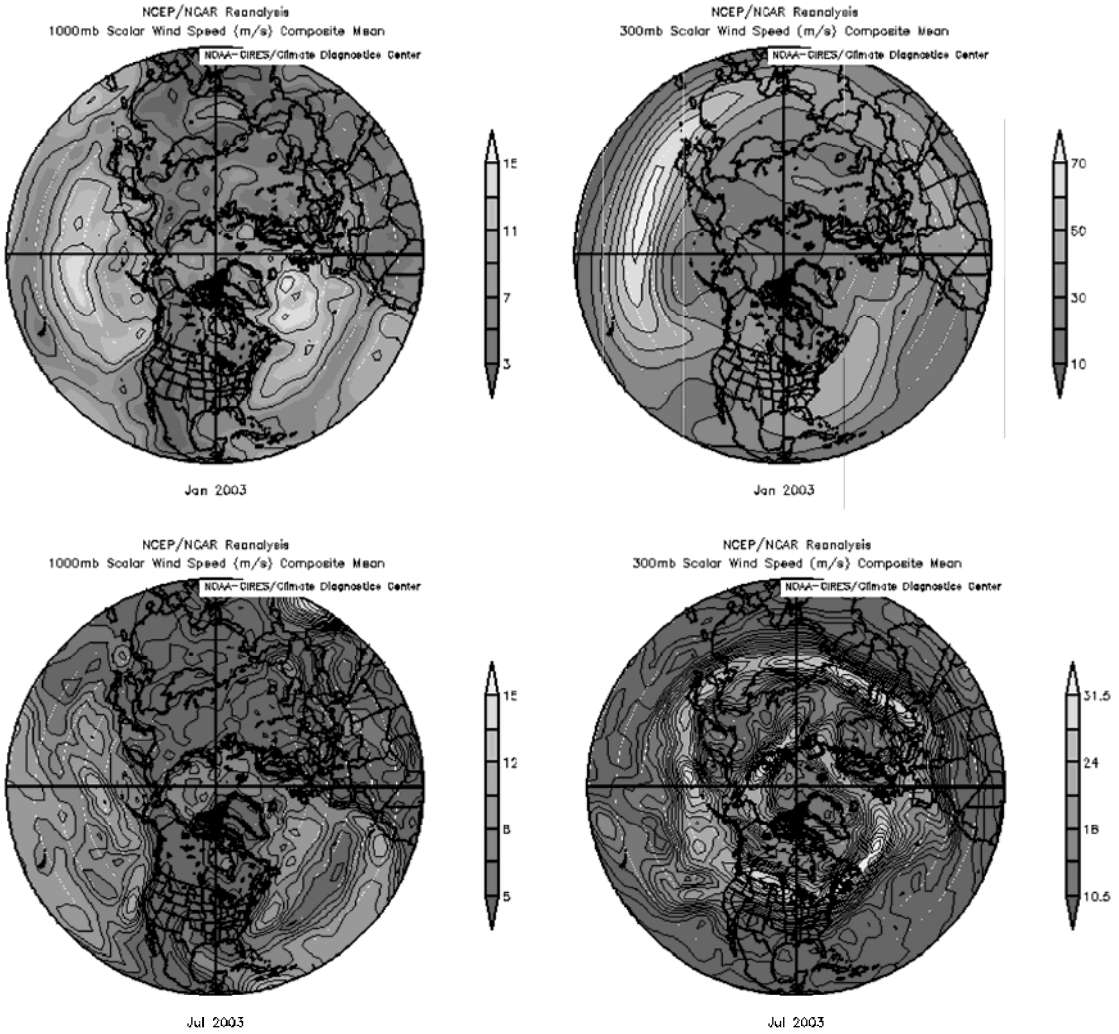

Figure 2.6: *Average wind speeds at 1000 hPa and 300 hPa for January 2003 (upper pictures) and July 2003 (lower pictures). Note that the scales are different on the different pictures. (Provided by the NOAA-CIRES Climate Diagnostics Center, Boulder Colorado from their Web site at http://www.cdc.noaa.gov)*

2.6 Aerosol deposition processes

Deposition of dust and sea salt suspended in the air occurs by different processes during dry and wet conditions. Dry deposition occurs through sedimentation by gravity or turbulent air-to-surface contact (Genthon, 1992a). High surface winds and rough surfaces favour dry deposition. Wet deposition is removal of aerosol by precipitation and involves two different processes, nucleation scavenging and collision scavenging.
In nucleation scavenging aerosols are involved in cloud formation dependent on the phase of precipitation (ice crystals, snowflakes or water droplets) and on the hygroscopic properties of the aerosol (e.g. Seinfeld and Pandis, 1997). Different aerosol types can have different hygroscopic properties and thereby different nucleation scavenging rates.
In collision scavenging, precipitation collides with aerosols while falling through the air in and below the cloud. Collision scavenging rates are strongly dependent on the sizes both of the droplets and of the aerosols. The collision removal efficiency is lowest for particles around 1-2 μm in diameters (e.g. Seinfeld and Pandis, 1997).

Mass flux of aerosol onto the surface due to dry deposition (J_{dry}, mass per area and time) equals the apparent falling velocity of aerosol particles (v_{dry}, length divided by time) times the mass concentration of aerosol particles in the air (C_{air}, mass per volume): $J_{dry} = v_{dry} \cdot C_{air}$. The dry deposition velocity, v_{dry}, depends both on gravitational settling and of turbulent contact with the surface (Genthon, 1992a) and is often given in $cm \cdot s^{-1}$ (e.g. Davidson et al., 1996).
The wet deposition flux onto the surface (J_{wet}) equals the precipitation flux (J_P, mass per area and time) times the mass fraction of aerosol particles in the precipitation (w_P, mass divided by mass): $J_{wet} = J_P \cdot w_P$ where w_P equals the mass concentration of aerosol in the precipitation divided by the mass density of the precipitation (ρ_P, close to 1.00 $g \cdot cm^{-3}$): $w_P = C_P / \rho_P$.
The 'scavenging ratio' ($R_{P/air}$) is the mass concentration of aerosol in the precipitate divided by the mass concentration of aerosol in the air: $R_{P/air} = C_P / C_{air}$. Due to the complexity of the scavenging mechanism, wet deposition rates are hard to quantify (e.g. Prospero, 1983). Modellers typically use a 'scavenging ratio' around 1000 (e.g. Tegen et al., 2002).

The decrease in mass concentration of aerosol in the air due to dry and wet depositions is described by the decremence rates, Λ_{wet} and Λ_{dry} (unit s^{-1} or h^{-1}) that are defined by, $\Lambda_{dry} = (\partial \ln C_{air} / \partial t)_{dry}$ and $\Lambda_{wet} = (\partial \ln C_{air} / \partial t)_{wet}$. The wet decremence rate may also be expressed in terms the scavenging coefficient, α_{wet} (unit $m^2 \cdot kg^{-1}$) and the precipitation flux: $\Lambda_{wet} = \alpha_{wet} \cdot J_P$ (Genthon, 1992a; Seinfeld and Pandis, 1997).
The aerosol concentration in a moving air parcel is decreasing with time due to depositions of aerosol. Disregarding other factors acting on atmospheric aerosol concentrations, such as mixing of air masses, the rate of change in aerosol concentration can be described in terms of the atmospheric lifetime, τ: $\partial C_{air}/\partial t = -(1 / \tau) \cdot C_{air}$, where $\tau = 1 / (\Lambda_{dry} + \Lambda_{wet})$.

Implications for aerosol characteristics: Both dry and wet deposition processes result in a modification over time of size and mineral characteristics of aerosol in a moving air parcel.
Aerosol deposited regionally downwind from the source region is mainly transported and deposited under dry conditions, where coarse particles will settle out of the atmosphere faster than fine particles due to an r^2 dependency of sedimentation rates. This size modification has been applied to interpretations of Chinese loess strata where grain sizes have been used to indicate past transport distances and wind-strengths, reflecting strengths of the winter monsoon, whereas clay-mineralogy has been used to indicate chemical alternation processes in humid environments, reflecting the strength of the summer monsoon (An, 2000; Porter, 2001). Arnold et al. (1998) points out that also transport time might have an effect on the clay mineralogy in loess strata because clay minerals dominate the very fine fraction in aerosol dust while primary minerals, like quartz and feldspars, dominate the coarse fraction.
Long-range transported aerosols are subject to wet-deposition processes (Tegen, 2003). Due to little precipitation in Arctic regions aerosol life-times in those regions can be one order of magnitude longer than in regions at mid latitudes. Aerosol life-times for long-range transported aerosol depend both on amounts and on properties of the precipitation and of hygroscopic properties and of aerosol sizes as well (e.g. Jaffrezo et al., 1993). Particles with sizes around 1-2 μm in diameter have a much longer life-time than both smaller and larger particles. However, parameterization of wet deposition in dust cycle models do not take nucleation scavenging processes and the size dependency of collision scavenging into account. This simplification increases the uncertainty of model predictions of dust in remote regions (Tegen, 2003).

It has been debated whether size distributions of long-range transported dust reach an equilibrium size distribution after a few thousand kilometres (Arnold et al., 1998). Dust size characteristics observed in Greenland ice cores are close to the preferred size distribution for collision scavenging processes and show only little variation (Steffensen, 1997; Ruth et al., 2003). However a systematic change of size mode observed in the GRIP ice core (Steffensen, 1997) and in the continuous record of dust from the NorthGRIP ice core has indicated that transport times have an influence on size characteristics of the long-range transported dust deposited in Greenland (Ruth et al., 2003).

Air concentrations of aerosols inferred from ice cores: The flux of aerosol deposition on the ice (J_{ice}, mass per area per time) is the sum of dry deposition and wet deposition:

$$J_{ice} = J_{dry} + J_{wet} = \nu_{dry} \cdot C_{air} + R_{P/air} \cdot C_{air} \cdot Acc.$$

ν_{dry}, C_{air}, and $R_{P/air}$ have been described in the preceding section. $Acc = (J_P / \rho_P)$ is the snow accumulation rate (volume per area and time in 'water equivalents' or in 'ice equivalents', i.e. height per time). Ice core concentrations of aerosol species are related to the fluxes by

$$C_{ice} = J_{ice} \cdot Acc^{-1}$$

Ice core concentrations of aerosol species reflect the aerosol contents in the air mass, but depend on the deposition process and on the accumulation rate. Often the aerosol deposition fluxes onto the ice are used instead of concentrations, but also fluxes depend on the deposition process and accumulation rate as well.

Hilamo et al., (1993), analysed dry deposition at Dye 3 and found that dry deposition of particles in the coarse mode (1-5μm diameter) was not negligible. Davidson et al., (1996), quantified wet and dry depositions rates at Summit Greenland for present day and found that wet deposition were dominant but a significant amount of aerosol was deposited through dry deposition. Although wet and dry deposition rates of aerosol can be quantified, the strong seasonality in deposition of various species adds an uncertainty to the estimation of past air concentrations.
Alley et al., (1995), estimated relative changes in concentrations in the air for the Younger-Dryas/Pre-Boreal transition based on a simple model interpolating between flux-estimates and ice core concentrations in the GISP2 ice core and found that relative variations in ice core concentrations provide fairly good estimates of variations in air concentrations, whereas variations in fluxes largely underestimates variations in air concentrations.
Meeker et al., (1997), did a detailed variance analysis on chemical species and accumulation in the GISP2 ice core over the last 17 ka and found that dry depositions are negligible compared to wet depositions.
De Angelis et al. (1997) found that fluxes of dust and sea salt for both for Greenland and Antarctica were proportional to $C_{air} \cdot (Acc + K)$ where K is an empirical constant of 5 $cm \cdot a^{-1}$. Using this proportionality for central Greenland, where the accumulation rate at present is about 20 $cm \cdot a^{-1}$ versus about 5 $cm \cdot a^{-1}$ during LGM, we estimate the C_{ice} / C_{air} ratio to be 60 % higher for LGM than for present. Compared to changes in concentrations of impurities of one to two orders of magnitudes, changes in accumulation rates have a minimal effect on ice core concentrations.

2.7 The global cycles of dust and sea salt predicted by models

Predictions of dust emission fluxes are considered to be the greatest uncertainty in models of the global dust cycle (Tegen, 2003). Recent model simulations of the global dust cycle for past and present climate conditions show that the vegetation cover may have a major influence on dust emission.
Mahowald et al. (1999) simulated the current and the Last Glacial Maximum (LGM) dust cycle including a model for global vegetation cover and obtained realistic dust deposition fluxes. However, their extended source areas for glacial conditions were somewhat unrealistically large.
Tegen et al. (2002) took seasonal variation in vegetation cover and variations in vegetation types into account and showed that seasonal variation in vegetation is important in capturing the spring dust emission events from central Asia. Further, they considered topographic lows, depositing the fine grained rock material produced during glacial and fluvial erosion, as preferential dust source areas. Their present day source model was consistent with source areas observed by TOMS satellite observations. Their simulations indicated that dry lake beds make substantial contributions to global dust emissions as they constitute the known hot-spots of dust emission. They achieved realistic simulations of the modern dust cycle, although they underestimated dust deposition in the North Pacific due to an underestimation of wind speeds.
The model of Tegen et al. (2002) was extended by Werner et al. (2002) who simulated the current and the LGM dust cycles taking a seasonal cycle in both vegetation and precipitation into account. They simulated a factor of 2.2 higher global dust emission

during the LGM than today, of which 25% was due to lower sea level, and 65% was explained by higher surface wind speeds, and only 10% was caused by expansion of dust source areas by sparser vegetation. In Asia 88% of the increase in dust emissions was due to higher wind speeds. Over the North Pacific dust deposition was a factor of 5 higher due to stronger transport winds. Further, Werner et al. (2002) found that the dust season was longer during the LGM and the seasonal maximum was shifted from spring to July-August. They obtained realistic seasonal variations in ice core dust concentrations for LGM mainly due to an effect of seasonal variations in local precipitation affecting the balance of dry and wet deposition and less to an effect of seasonality of the dust cycle. They explain the large LGM/present day difference in dust concentrations as being mainly an effect of changes in local precipitation.
Zou and Zhai (2004) compared recent changes in vegetation with changing occurrence of Chinese dust storms and found that the effect of prior summer vegetation on the variation of spring dust storms is particularly evident in the central and eastern part of northern China. However in the north western Chinese desert areas vegetation is too sparse to have a major influence on the occurrence of dust storms. In summary, vegetation might be important for the global dust emission, but the effect from vegetation simulated in dust cycle models cannot be verified from Greenland ice core dust records because these are not influenced significantly by changes in vegetation.

While modellers have focused on influences on dust emission by vegetation, the emission factor also depends strongly on soil type (Tegen et al., 2002). One limitation in many dust cycle models is a simplification of wet deposition by using only a single scavenging coefficient. Another limitation in dust cycle models is that they account for transport modifications of the size distribution by tuning the size distribution of the emitted dust (Mahowald et al., 1999). Gong et al. (2003) inferred the soil grain size distribution, for accurate simulations of spatial and temporal distributions of dust storm events. They simulated April 2001 Chinese dust storm emissions and long-range transport to North Pacific and North America. Their simulations of dust emission yields reasonable spatial and temporal distributions compared with observations. Further Gong et al. (2003) simulate spatial and temporal properties of the long range transport that correlate reasonably well with observations. Their simulation of the long-range transport of the dust plumes showed that the vertical atmospheric distribution peak altitude was 4000-5000 m over the North Pacific and 5000-7000 m at the North American coast. As the dust moved across the North Pacific concentrations were reduced considerably due to wet and dry depositions, affecting dust at lower altitudes more than dust at high altitudes.

An attempt to model ice core sea salt concentrations for present and LGM conditions was made by Reader and McFarlane (2003). Their simulated deposition rates in Greenland of sea salt from open oceans were much lower than observed. Further they simulated a tenfold lower concentrations for LGM than for the present which is in contrast to the observed almost tenfold higher concentration during LGM. Considering sea ice brines as a possible source to sea salt aerosol, and assuming that 1-2 % of the global sea salt aerosol comes from sea ice, they simulated a 4-5 fold higher concentrations for LGM than for the present – a result that matches observations better, although it is very sensitive to parameterizations of wet depositions and precipitation. The source parameterization of Reader and McFarlane (2003) is based on sea ice

coverage and not on formation of sea ice and is therefore unrealistic because salt brines only exist on top of freshly formed sea ice (Wagenbach et al., 1998). Furthermore their chosen parameterization of wet deposition for LGM might not be realistic but it was necessary for achievement of realistic ice core concentrations. Readers and McFarlane (2003), conclude that the discrepancies between their results of ice core concentrations and measured data both for sea salt and dust are likely to be due to underestimations of LGM wind extremes and errors in transport patterns.

2.8 Atmospheric circulation during the last glacial period

During the last glacial period large continental ice sheets, extended mountain glaciers, and a decreased sea level resulted in markedly different topographic conditions, which not only have set the physical boundaries for the atmosphere, also height and albedo effects from glaciers and ice sheets influenced air pressures and temperatures. Furthermore during the last glacial sea surface temperatures and sea ice extent were much different from today. Due to these different conditions a strong modification of the glacial jet stream patterns should be expected.

Major efforts have been made in computer simulations of atmospheric circulation for the climate conditions of both present day and LGM. Simulations of past climate conditions mainly serve the purpose of evaluating numerical models. The global and regional climate conditions of the LGM represent the largest difference in recent time from present day conditions and therefore represent an extreme challenge for climate models. Although it is not their major goal, the model simulations provide results that are useful for analyses and interpretations of paleoclimatic data.
General Circulation Models (GCM) simulate influences of various forcing on global climate conditions. Such forcing includes insolation and radiation balance, which depends on surface and cloud albedo and on the atmospheric content of greenhouse gases. These simulations are limited by computer capacity and performance and therefore often GCM's have been restricted to simulate only a subsystem within the global climate system using prescribed boundary conditions. The atmosphere responds fast to climate change and is therefore the climate subsystem that is most suitable for computer simulations (Hewitt et al., 2001).
For atmospheric GCM simulations of the LGM, the boundary conditions are obtained from paleoclimate reconstructions, such as sea surface temperature reconstruction from the CLIMAP members (1981) and the ice sheet topography reconstruction of Peltier (1994). One major limitation in the GCM's is the spatial resolution in the models, but uncertainties in the boundary conditions add large uncertainties to the model output. The Paleoclimate Modelling Intercomparison Project (PMIP) has evaluated and compared atmospheric GCM's using the same boundary conditions in all models in order to determine which results are model dependent (Joussaume and Taylor, 2001).
Atmospheric coupled GCM simulations have reached very different conclusions about LGM large scale wind patterns. In general, atmospheric GCM's obtain for LGM a strengthening of the jet stream, due to increased surface temperature gradients, and a southward displacement over North America, due to the Laurentide ice sheet (e.g. Bartlein et al., 1998). Simulations using the first version of Climate Community Models (CCM0), suggested a split jet stream pattern over North America, which during winter

brought cold air to the North Atlantic via the corridor between the Laurentide and the Greenland ice sheets (Kutzbach and Wright, 1986). During winter the strongest jet stream was found in the North Atlantic, whereas during summer a very strong jet stream was found along the southern branch over North America. The CCM0 has been followed by the more advanced versions CCM1, CCM2, CCM3, that include more details in the climate system, better climate models, higher spatial resolution, improved boundary conditions, and better resolution in time. The later CCM versions used lower reconstructions of the Laurentide and the Scandinavian ice sheets than the CCM0 and therefore their simulations did not support a split jet stream during the LGM.

According to the discussions in the previous sections about transport of dust and sea salt to the Greenland ice sheet, a more southerly migrating jet stream would result in less favourable conditions for dust and sea salt aerosol reaching Greenland. This is not consistent with Greenland ice core records that indicate much higher concentrations of dust and sea salt aerosol for the last glacial period than at present. New results from the NorthGRIP ice core (NorthGRIP members, 2004) suggest a regional effect in precipitation during the last glacial period, where the NorthGRIP ice core represents a more northerly pathway for the moisture than the GRIP ice core, with a possible source in the North Pacific.

A very resent simulation using a regional meso-scale model (polar MM5), with boundary conditions generated from a CCM3 simulation, suggests a strong seasonality in the jet stream with a split winter configuration over the Laurentide ice sheet (Bromwich et al., 2004) (see Figure 2.7). In this simulation the winter configuration is characteristic for a strong northern branch of the jet stream and a weaker southern branch. During spring the northern branch intensifies and then fades out during summer while the southern branch moves slightly north. In this winter configuration the polar vortex is moved to the east of Greenland, and is therefore not limiting the northern transport to Greenland.

A strong jet stream north of the Laurentide ice sheet during winter could effectively have transported dust from Western China and sea salt from the North Pacific to Greenland resulting in much higher ice core concentrations for LGM than for the present.

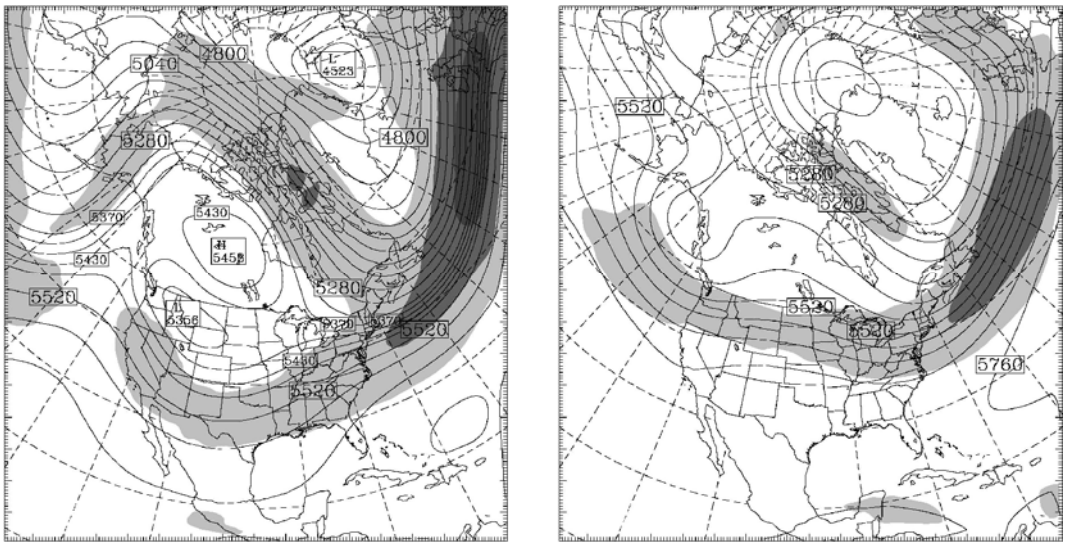

Figure 2.7: *Polar MM5 LGM January (left) and July (right) monthly mean 500 hPa geo-potential height and wind speed. The contour intervals are 60 m (from Bromwich et al., 2004). During spring the northern branch of the jet stream intensifies before it fades out and turns into the summer configuration.*

2.9 Summary

Dust deposited onto the Greenland ice sheet during the last glacial period and at present is most likely from sources located in the East Asian desert areas. The spring peak observed in Greenland ice core dust records is associated with the Chinese dust storm season both at present and during the last glacial. During LGM the dust storm season might have been longer and a stronger jet stream could have generated dust storms more frequently. Results from dust model simulations suggest that dust emission from Chinese deserts mainly is influenced by surface winds. Furthermore, correlations of dust storms in the western Chinese desert areas with vegetation cover shows that dust emissions in these areas are not influenced by vegetation cover.

Upper level wind patterns indicate conditions for emission and uplift at the surface as well as conditions for long-range transport. The key to understand the large-scale patterns of the long-range transport of dust and sea salt aerosol to Greenland is a consideration of the large variations in upper level wind patterns. Because of the high frequency of those variations a persistent seasonal pattern appears in Greenland ice core records of mineral dust and sea salt. Greenland ice core records of dust and sea salt therefore reflect large-scale patterns of upper level winds in the northern hemisphere.
Upper level present day wind patterns suggest a common transport path for dust and sea salt over the North Pacific and North America and then north wards in the North Atlantic, with possible source areas for sea salt both in the North Pacific and in the North Atlantic. The different seasonality of dust and sea salt observed in Greenland is likely to be an effect of soil moisture that inhibits dust emissions during winter.

Global dust cycle models have had difficulties obtaining realistic simulations of dust depositions in Greenland at present. Ignoring modifications of particle size distributions during wet depositions and a bad parameterization of grain size properties in source regions could be the simplifications that cause the large uncertainty in model simulation of the global dust cycle. Furthermore the parameterizations of the wet deposition themselves might also be a source for uncertainty in model predictions. Simulations of the LGM dust cycle could be further limited by uncertainties in the reconstruction of transport pathways and wind speeds.

2.10 References

Alley, R., R. C. Finkel, et al. (1995). "Changes in continental and sea-salt atmospheric loadings in central Greenland during the most recent deglaciation: Model-based estimates." Journal of Glaciology **41**(139): 503-514.

An, Z. (2000). "The history and variability of the East Asian paleomonsoon climate." Quaternary Science Reviews **19**: 171-187.

Arnold, E., J. Merrill, et al. (1998). "The effect of source area and atmospheric transport on mineral aerosol collected over the North Pacific Ocean." Global and Planetary Change **18**(3-4): 137-159.

Bartlein, P. J., K. H. Anderson, et al. (1998). "Paleoclimate simulations for North America over the past 21,000 years: Features of the simulated climate and comparisons with paleoenvironmental data." Quaternary Science Reviews **17**(6-7): 549-585.

Biscaye, P. E., F. E. Grousset, et al. (1997). "Asian provenance of glacial dust (stage 2) in the Greenland Ice Sheet Project 2 Ice Core, Summit, Greenland." Journal of Geophysical Research **102**(C12): 26765-26781.

Bory, A. J.-M., P. E. Biscaye, et al. (2003). "Two distinct seasonal Asian source regions for mineral dust deposited in Greenland (NorthGRIP)." Geophysical Research Letters **30**(4): doi:10.1029/2002GL016446.

Bory, A. J.-M., P. E. Biscaye, et al. (2002). "Seasonal variability in the origin of recent atmospheric mineral dust at NorthGRIP, Greenland." Earth and Planetary Science Letters **196**(No. 3-4): 123-134.

Bromwich, D. H., E. R. Toracinta, et al. (2004). "Polar MM5 simulations of the winter climate of the Laurentide Ice Sheet at the LGM." Journal of Climate **17**: 3415-3433.

CLIMAP Members (1981). "Seasonal reconstructions of the Earth's surface at the last glacial maximum." Geological Society of America Map and Chart Series, MC-36. Geological Society of America, Boulder, Colorado.

Dansgaard, W., S. J. Johnsen, et al. (1984). North Atlantic climatic oscillations revealed by deep Greenland Ice Cores. Climatic Processes and Climate Sensitivity. J. E. Hansen and T. Takahashi. Washington D.C., American Geophysical Union (AGU). Maurice Ewing **5:** 288-298.

Dansgaard, W., J. W. C. White, et al. (1989). "The abrupt termination of the Younger Dryas climate event." Nature **339**(6225): 532-534.

Davidson, C. I., M. H. Bergin, et al. (1996). The deposition of particles and gases to ice sheets. Chemical Exchange Between the Atmosphere and Polar Snow. E. W. Wolff and R. C. Bales. New York, Springer-Verlag. **43:** 275-306.

De Angelis, M., J. P. Steffensen, et al. (1997). "Primary aerosol (sea salt and soil dust) deposited in Greenland ice during the last climatic cycle: Comparison with east Antarctic records." Journal of Geophysical Research **102**(C12): 26681-26698.

Derbyshire, E. (1995). "Aeolian sediments in the quaternary record: an introduction." Quaternary Science Reviews **14**(7-8): 641-643.

Derbyshire, E. (2003). "Loess, and the dust indicators and records of terrestrial and marine palaeoenvironments (DIRTMAP) database." Quaternary Science Reviews **22**: 1813-1819.

Derbyshire, E., X. M. Meng, et al. (1998). "Provenance, transport and characteristics of modern aeolian dust in western Gansu Province, China, and interpretation of the Quaternary loess record." Journal of Arid Environments **39**: 497-516.

Erickson, D. J., J. T. Merrill, et al. (1986). "Seasonal estimates of global atmospheric sea-salt distributions." Journal of Geophysical Research **91**(D1): 1067-1072.

Fuhrer, K., E. W. Wolff, et al. (1999). "Timescales for dust variability in the Greenland Ice Core Project (GRIP) ice core in the last 100,000 years." Journal of Geophysical Research **104**(D24): 31043-31052.

Genthon, C. (1992a). Simulations of the long-range transport of desert dust and sea-salt in a general circulation model. Precipitation scavenging and atmosphere-surface exchange. S. E. Schwartz and W. G. N. Slinn. Washington, Hemisphere Publishing Corporation. **3:** 1783-1794.

Genthon, C. (1992b). "Simulations of desert dust and sea-salt aerosols in Antarctica with a general circulation model of the atmosphere." Tellus **44B**: 371-389.

Gillette, D. (1980). "Major contributions of natural primary continental aerosols: Source mechanisms." Annals New York Academy of Sciences **338**: 348-358.

Gillette, D. A., J. Adams, et al. (1982). "Treshold friction velocities and rupture moduli for crusted desert soils for the input of soil particles into the air." Journal of Geophysical Research **87**(C11): 9003-9015.

Gong, S. L., X.Y. Zhang, T.L. Zhao, I.G. McKendry, D.A. Jaffe, and N.M. Lu, (2003). "Characterization of soil dust distributions in China and its transport during 2001 ACE-ASIA 2. Model simulation and validation." Journal of Geophysical Research **108**(D9): 4262, doi:10.1029/2002JD002633.

Grousset, F. E., P. Ginoux, et al. (2003). "Case study of a Chinese dust plume reaching the French Alps." Geophysical Research Letters **30**(6): 1277, doi:10.1029/2002GL016833.

Hansson, M. (1995). "Are changes in atmospheric cleansing responsible for observed variations of impurity concentrations in ice cores?" Annals of Glaciology **21**: 219-224.

Hewitt, C. D., R. J. Stouffer, et al. (2001). "Simulating the Last Glacial Maximum with the coupled ocean-atmosphere general circulation model HadCM3." Hadley Centre technical note **29**.

Hillamo, R. E., V.-M. Kerminen, et al. (1993). "Size distributions of atmospheric trace elements at Dye 3, Greenland - I. Distribution characteristics and dry deposition velocities." Atmospheric Environment **27A**(17/18): 2787-2802.

Husar, R. B., D. M. Tratt, et al. (2001). "Asian dust events of April 1998." Journal of Geophysical Research **106**(D16): 18317-18330.

Jaffrezo, J.-L., R. E. Hillamo, et al. (1993). "Size distributions of atmospheric trace elements at Dye 3, Greenland - II. Sources and transport." Atmospheric Environment **27A**: 2803-2814.

Joussaume, S. and K.E.Taylor (2001). "Status of the paleoclimate modeling intercomparison project (PMIP)." http://www-Isce.cea.fr/pmip/publications.

Kahl, J. D. W., D. A. Martinez, et al. (1997). "Air mass trajectories to Summit, Greenland: A 44-year climatology and some episodic events." Journal of Geophysical Research **102**(C12): 26861-26875.

Kohfeld, K. E. and S. P. Harrison (2001). "DIRTMAP: The geological record of dust." Earth-Science Reviews **54**(1-3): 81-114.

Kutzbach, J. E. and H. E. Wright (1985). "Simulation of the climate of 18,000 years BP: Results for the North American/North Atlantic/European sector and comparison with the geologic record of North America." Quaternary Science Reviews **4**: 147-187.

Legrand, M. R. and R. J. Delmas (1988). "Soluble impurities in four Antarctic ice cores over the last 30 000 years." Annals of Glaciology **10**: 116-120.

Mahowald, N., K. Kohfeld, et al. (1999). "Dust sources and deposition during the last glacial maximum and current climate: A comparison of model results with paleodata from ice cores and marine sediments." Journal of Geophysical Research **104**(D13): 15895-15916.

Mayewski, P. A., L. D. Meeker, et al. (1997). "Major features and forcing of high-latitude Northern Hemisphere atmospheric circulation using a 110,000-year-long glaciochemical series." Journal of Geophysical Research **102**(C12): 26345-26366.

Meeker, L. D., P. A. Mayewski, et al. (1997). "A 110,000-year history of change in continental biogenic emissions and related atmospheric circulation inferred from the Greenland Ice Sheet Project Ice Core." Journal of Geophysical Research **102**(C12): 26489-26504.

North Greenland Ice-Core Project (NorthGRIP) Members (in press, 2004). "High resolution Climate Record of the Northern Hemisphere reaching into the last Glacial Interglacial Period." Nature.

Peltier, W. R. (1994). "Ice age paleotopography." Science **265**: 195-201.

Petit, J. R., J. Jouzel, et al. (1999). "Climate and atmospheric history of the past 420,000 years from the Vostok ice core, Antarctica." Nature **399**: 429-436.

Petit, J. R., L. Mounier, et al. (1990). "Palaeoclimatological and chronological implications of the Vostok core dust record." Nature **343**: 56-58.

Porter, S. C. (2001). "Chinese loess record of monsoon climate during the last glacial-interglacial cycle." Earth-Science Reviews **54**: 115-128.
Porter, S. C. and Z. S. An (1995). "Correlation between climate events in the North Atlantic and China during the last glaciation." Nature **375**: 305-308.
Prospero, J. M., R. J. Charlson, et al. (1983). "The atmospheric aerosol system: An overview." Reviews of Geophysics and Space Physics **21**: 1607-1629.
Prospero, J. M., P. Ginoux, et al. (2002). "Environmental characterization of global sources of atmospheric soil dust identified with the NIMBUS 7 Total Ozone Mapping Spectrometer (TOMS) absorbing aerosol product." Reviews of Geophysics **40**(1): 1002, doi:10.1029/2000RG000095.
Prospero, J. M., M. Uematsu, et al. (1989). Mineral aerosol transport to the Pacific Ocean. Chemical Oceanography. J. P. Riley, R. Chester and R. A. Duce. New York, Academic Press. **10:** 187-218.
Pye, K. (1995). "The nature, origin and accumulation of loess." Quaternary Science Reviews **14**: 653-667.
Pye, K. and L.-P. Zhou (1989). "Late Pleistocene and Holocene aeolian dust deposition on north China and the northwest Pacific Ocean." Palaeogeography, Palaeoclimatology, Palaeoecology **73**: 11-23.
Rankin, A. M., E. W. Wolff, et al. (2002). "Frost flowers: Implications for tropospheric chemistry and ice core interpretation." Journal of Geophysical Research **107**(D23): 4683, doi:10.1029/2002JD002492.
Reader, M. C. and N. McFarlane (2003). "Sea-salt aerosol distribution during the Last Glacial Maximum and its implications for mineral dust." Journal of Geophysical Research **108**(D8): 4253, doi:10.1029/2002JD002063.
Ruth, U., D. Wagenbach, et al. (2002). "High resolution microparticle profiles at NGRIP: Case studies of calcium-dust relationship." Annals of Glaciology **35**: 237-242.
Ruth, U., D. Wagenbach, et al. (2003). "Continuous record of microparticle concentration and size distribution in the central Greenland NGRIP ice core during the last glacial period." Journal of Geophysical Research **108**(D3): 4098, doi:10.1029/2002JD002376.
Seinfeld, J. H. and S. N. Pandis (1997). Atmospheric Chemistry and Physics: From Air Pollution to Climate Change. New York, John Wiley & Sons.
Steffensen, J. P. (1988). "Analysis of the seasonal variation in dust, Cl^-, NO_3^-, and SO_4^{2-} in two Central Greenland firn cores." Annals of Glaciology **10**: 171-177.
Steffensen, J. P. (1997). "The size distribution of microparticles from selected segments of the Greenland Ice Core Project ice core representing different climatic periods." Journal of Geophysical Research **102**(C12): 26755-26763.
Stenni, B., V. Masson-Delmotte, et al. (2001). "An oceanic cold reversal during the last deglaciation." Science **293**: 2074-2077.
Sun, J. (2002). "Provenance of loess material and formation of loess deposits on the Chinese Loess Plateau." Earth and Planetary Science Letters **203**(3): 845-859.
Sun, J., M. Zang, et al. (2001). "Spatial and temporal characteristics of dust storms in China and its surrounding regions, 1960-1999: Relations to source area and climate." Journal of Geophysical Research **106**(D10): 10325-10333.
Svensson, A., P. E. Biscaye, et al. (2000). "Characterization of late glacial continental dust in the Greenland Ice Core Project ice core." Journal of Geophysical Research **105**(D4): 4637-4656.
Tegen, I. (2003). "Modeling the mineral dust aerosol cycle in the climate system." Quaternary Science Reviews **22**: 1821-1834.
Tegen, I., S. P. Harrison, et al. (2002). "The impact of vegetation and preferential source areas on global dust aerosol: Results from a model study." Journal of Geophysical Research **107**(D21): 4576, doi:10.1029/2001JD000963.
Voelker, A. H. L. and workshop participants (2002). "Global distribution of centennial-scale records for Marine Isotope Stage (MIS) 3: A database." Quaternary Science Reviews **21**: 1185-1212.
Wagenbach, D., F. Ducroz, et al. (1998). "Sea-salt aerosol in coastal Antarctic regions." Journal of Geophysical Research **103**(D9): 10961-10974.
Wemer, M., I. Tegen, et al. (2002). "Seasonal and interannual variability of the mineral dust cycle under present and glacial climate conditions." Journal of Geophysical Research **107**(D24): 4744, doi:10.1029/2002JD002365.
Wolff, E. W., A. M. Rankin, et al. (2003). "An ice core indicator of Antarctic sea ice production?" Geophysical Research Letters **30**(22,2158): doi:10.1029/2003GL018454.
Yang, X., K. T. Rost, et al. (2004). "The evolution of dry lands in northern China and in the Republic of Mongolia since the Last Glacial Maximum." Quaternary International **118-119**: 69-85.
Yu, G., S. P. Harrison, et al. (2001). Lake status records from China: Data Base Documentation. **4:** 1-243.

Yu, G., B. Xue, et al. (2003). "LGM lake records from China and an analysis of climate dynamics using a modelling approach." Global and Planetary Change **38**(3-4): 223-256.
Yu, G., B. Xue, et al. (2000). "Lake records and LGM climate in China." Chinese Science Bulletin **45**(13): 1158-1164.
Zhang, X. Y., R. Arimoto, et al. (1999). "Glacial and interglacial patterns for Asian dust transport." Quaternary Science Reviews **18**(6): 811-819.
Zhang, X. Y., H. Y. Lu, et al. (2002). "Atmospheric dust loadings and their relationship to rapid oscillations of the Asian winter monsoon climate: Two 250-kyr loess records." Earth and Planetary Science Letters **202**(3-4): 637-643.
Zhuo, Z., Y. Baoyin, et al. (1998). "Paleoenvironments in China during the Last Glacial Maximum and the Holocene Optimum." Episodes **21**(3): 152-158.
Zou, X. K. and P. M. Zhai (2004). "Relationship between vegetation coverage and spring dust storms over northern China." Journal of Geophysical Research **109**(D03): 104, doi:10.1029/2003JD003913.

3: Lithium in Greenland ice cores measured by ion chromatography

Marie-Louise Siggaard-Andersen[1], Jørgen Peder Steffensen[2] and Hubertus Fischer[1]

[1]Alfred-Wegener-Institute for Polar and Marine Research, Bremerhaven, Germany
[2]Department of Geophysics, Niels Bohr Institute for Astronomy, Physics and Geophysics, Copenhagen, Denmark

Printed in *Annals of glaciology,* Volume **35**, 2002, pages 243-249

Abstract: Ion chromatography is a widely used technique to analyse ice cores for ions like Na^+, NH_4^+, K^+, Mg^{2+}, Ca^{2+}, F^-, MSA^-, Cl^-, NO_3^- and SO_4^{2-} that are present in polar ice cores at ppb level. By using sample pre-concentration and an optimised separation technique we have been able to detect Li^+ in ice core samples in concentrations as low as 0.0001 $\mu eq \cdot kg^{-1}$ or 0.7 ppt by ion chromatography. During routine analysis of ions in ice cores, the lithium content has been evaluated and recorded. The IC technique used in these measurements and some exemplary IC data from the GRIP (Greenland Ice Core Project) and the NGRIP (North Greenland Ice Core Project) ice cores will be presented. By these data we introduce Li^+ concentration as a new parameter in the analysis of ice cores.

Like other ions Li^+ reflects climatic changes and shows seasonal cycles. On the basis of the geochemistry of lithium we suggest that Li^+ measured in the Greenland ice cores is derived from mineral dust. However data from the NGRIP ice core that represents the 8.2 ka BP Holocene cold event show a strong Li^+ signal that does not correlate with any other ionic component measured. This means that the lithium content in ice cores is a signal with its own pattern, which is not yet understood.

3.1 Introduction

Ion chromatography is a convenient and reliable method and is widely used to analyse soluble chemical components like Na^+, NH_4^+, K^+, Mg^{2+}, Ca^{2+}, F^-, MSA^-, Cl^-, NO_3^- and SO_4^{2-} in ice cores where these ions are present at the ppb level (e.g. Mayewski et al., 1997). Two of the main contributors to the Greenland ice core ion chemistry are sea salts and ions released from mineral dust particles. The Na^+ concentration is often taken as an indicator for the content of sea salt aerosols. Non-sea salt contributions to the contents of various ionic components in ice cores can be evaluated by subtraction of the sea salt contribution (e.g. De Angelis et al., 1997). The content in Greenland ice cores of soluble Ca^{2+} correlates well with the content of insoluble dust (Steffensen, 1997) and it is well established to use the Ca^{2+} concentration as an indicator for the content of dust aerosols (e.g. Fuhrer et al., 1999). The insoluble mineral dust aerosols are mostly aluminum silicates (e.g. Laj et al., 1997; Svensson et al., 2000). Iron and aluminum are therefore better tracers for insoluble dust aerosols than Ca^{2+}, but the amount of data from analysis of these elements in ice cores are limited due to the tedious analytical

technique. Contributions to ions in Greenland ice cores other than sea salt and mineral dust aerosols can be aerosols of biogenic or volcanic origin.

Very little has been reported about ion chromatographic measurements of lithium in geological samples. The reason for this is that up to now the ion chromatographic technique has been insufficient. Ion chromatographic methods for measuring Li^+ were optimised by Papoff et al. (1991), who measured Li^+ along with other cations using column switching, and by Singh and Abbas (1996), who measured only mono-valent alkali metals. After sample dilution they measured Li^+ in concentrations down to 0.5 $\mu eq \cdot kg^{-1}$. But since their work ion chromatographic techniques have improved markedly. Today the separation of all components of interest is easily performed in a single run and the procedures for measurements and data evaluations have become automated to a high degree. Lyons and Welch (1997) measured Li^+ concentrations in stream and lake samples during ion chromatographic analysis of chemistry in waters from the McMurdo Dry Valleys, Antarctica. They report a detection limit of 0.01 $\mu eq \cdot kg^{-1}$ and after sample dilution, they were measuring Li^+ concentrations down to about 0.1 $\mu eq \cdot kg^{-1}$. In this work we present an ion chromatographic method, where Li^+ concentrations down to 0.0001 $\mu eq \cdot kg^{-1}$ or 0.7 ppt can be measured and we introduce the Li^+ concentration as a new parameter in the analysis of ice cores.

	Upper crust	*Sea water*
Lithium (ppmw)	22	0.19
Li/Ca (eq./eq.)	0.0022	0.0014
Li/Na	0.0028	$0.061 \cdot 10^{-3}$
Li/Mg	0.0029	$0.27 \cdot 10^{-3}$
Na/Ca	0.76	23
Mg/Na	1.0	0.22
Mg/Ca	0.76	5.1

Table 3.1: *The average lithium and relative lithium abundance in the upper crust and seawater (from Holland (1984) and Wedepohl (1995). The ratios are given in equivalents/equivalents.*

Since sea salt and mineral dust aerosols are two of the main contributors to ion chemistry in Greenland ice cores, we consider the contribution of these two sources to the Li^+ content in our samples. In Table 3.1 the abundance of lithium relative to other elements in the Earth upper crust and in seawater is listed. In seawater the molar ratio between lithium and sodium is $0.061 \cdot 10^{-3}$ (Holland, 1984), which is much lower than the ratios we have measured. We therefore assume that the origin of lithium in Greenland ice cores is mainly mineral dust aerosols. This assumption is supported by recent analysis of single particle aerosol using aerosol time-of-flight mass spectrometry in air masses in Southern California. There Silva et al. (2000) detected lithium in soil dust particles, and Hughes et al. (2000) used lithium along with aluminium, iron and calcium as an indicator for mineral dust particles in the analysis of the evolution of various atmospheric particles. In Earth upper crust the lithium and calcium contents are 22 ppm and 29450 ppm (Wedepohl, 1995) corresponding to 3.1 $meq \cdot kg^{-1}$ and 1.47 $eq \cdot kg^{-1}$ respectively. Lithium has a very low solubility in water but a very high mobility during chemical weathering processes and replaces magnesium in rocks and minerals

(Heier and Billings, 1970). The lithium content in minerals varies (see Table 3.2) and the concentration of lithium in clays and sedimentary rocks are much higher than in igneous rocks and fresh basalts. In fresh basalts the contents of lithium is typically 5 ppm, whereas the contents in some clay minerals can be 150 ppm (Holland, 1984). Lithium is not likely replacing calcium in minerals and in marine carbonates the content of lithium is very low (Hoefs and Sywall, 1997). Because of this variation in lithium contents in minerals, the relative concentrations of Li^+, Mg^+ and Ca^{2+} measured in Greenland ice cores might be useful in the study of mineral composition of dust aerosols.

	Clay and Clay shales	*Sands and Silts*	*Carbonates*
Li_{qrt} (ppmw)	40	18	2
Li_{avg} (ppmw)	80	36	13
Li/Ca_{qrt} (eq./eq.)	0.0033	0.0010	0.00002
Li/Ca_{avg} (eq./eq.)	0.0045	0.0034	0.00013
Mg/Ca_{qrt} (eq./eq.)	0.87	0.41	0.02
Mg/Ca_{avg} (eq./eq.)	0.64	0.62	0.27

Table 3.2: *Lithium content in some quaternary (qrt) and average (avg) sediments in ppmw and ratios in equivalents between lithium and calcium in some quaternary sediments. Data are evaluated from Holland (1984) and from Hoefs and Sywall (1997).*

Here we present exemplary Li^+ profiles along with Ca^{2+} profiles from three different data series. One series is representing 70 years around 400 years BP from the North Greenland Ice core Project (NGRIP) Holocene ice core (personal communication from [H.B. Clausen], February [2001]) where a seasonal signal in the Li^+ profile can be seen and where Li^+ was measured in concentrations as low as 0.0001 $\mu eq \cdot kg^{-1}$ or 0.7 ppt. Another series is representing the Greenland Ice core Project (GRIP) ice core Greenland Stadial 21 to Greenland Inter Stadial 20 transition approximately 75 ka BP (Dansgaard et al., 1993; Walker et al., 1999). The third series we have chosen to present is from the NGRIP ice core representing approximately 170 years around the Holocene 8.2 ka BP cold event (personal communication from [H.B. Clausen], February [2001]). The 8.2 ka BP event has been described by e.g. Klitgaard-Kristensen et al. (1998) and has been analysed in the GISP2 ice core by Alley et al. (1997). In the NGRIP ice core series the lithium profile shows a strange and incomprehensible behaviour during this event.

3.2 Ice core samples

The GRIP ice core was drilled during the 1990, 1991 and 1992 summer field seasons and reached a depth of 3028 very close to bedrock (Dansgaard et al., 1993). The NGRIP1 ice core was drilled during the 1996 and 1997 summer field seasons and terminated at a depth of 1371 metres (Dahl-Jensen et al., in press).

Samples for ion chromatographic analysis were decontaminated and cut into 5.0 or 2.5 cm samples manually in a clean bench using a microtome knife and then stored

frozen in Coulter accuvettes. Except for a few samples from the GRIP ice core all the samples have been decontaminated and cut in the field.

From the NGRIP1 ice core the upper 350 metres were sampled for a continuous record in 5 cm resolution and below 350 metres depth selected sections were sampled.

3.3 Ion chromatographic method

The measurements of ions in the ice core samples were done using a DIONEX 500 micro bore ion chromatograph equipped with a two-channel set-up for simultaneous measurements of cations and anions. Each channel has a pre-concentration column, gradient pump, suppressor and a conductivity detector. The samples were decanted into 5-ml sample vials and injected into the ion chromatograph by an auto-sampler. From each sample a 3-ml portion was injected into the cation system and a 1.5-ml portion was injected into the anion system. The separation of the ionic components was done within 20 minutes for both cations and anions.

The cations were separated on Ionpac CS12 2mm columns using a gradient mixture of 20 meq·kg^{-1} methane-sulfonic acid and 18 MΩ water as eluent with a flow rate of 0.5 ml·min^{-1}. The initial eluent concentration was 9 meq·kg^{-1} methane-sulfonic acid with a gradient increase up to 16 meq·kg^{-1} between 2 and 12 minutes. Between 12 and 16 minutes the eluent concentration was constant at 16 meq·kg^{-1} and then changed back to 9 meq·kg^{-1} for the baseline to relax.

The application of a pre-concentration column decreases markedly the effect of the water dip in the beginning of the chromatograms and therefore a large sample volume can be injected. Since lithium is present in ice core samples in very low concentrations a large sample volume is essential for the detection of lithium. The decreased effect of the water dip is also an advantage because Li^+ is the first component in the cation chromatograms. With a low initial eluent concentration the lithium peak is distant to the water dip and a good separation of the first four components Li^+, Na^+, NH_4^+, K^+ is achieved. A high eluent flow rate ensures a low detection limit since the component peaks are easier to distinguish from baseline noise. Important for a low detection limit is a high chemical purity of the eluent and optimally working pump and suppressor. The gradient in the eluent concentration is applied for the components Mg^{2+} and Ca^{2+} to be measured along with the mono-valent cations within 20 minutes. The chromatograms were integrated using the Peaknet 4.30 software and the peak heights were used in the data evaluation except when the peak area seemed to be more reproducible. In Figure 3.1 the detector responses of the first four components in the cation chromatograms are shown for a standard solution and for a sample solution. The Li^+ concentration in the standard solution is 0.2 µeq·kg^{-1} and the Li^+ concentration in the sample was evaluated to 0.00025 µeq·kg^{-1}.

Reproducibility and linearity of the Li^+ response was tested on solutions with Li^+ concentrations of 0.2 µeq·kg^{-1}, 0.02 µeq·kg^{-1}, 0.002 µeq·kg^{-1} and 0.0002 µeq·kg^{-1}. The tests showed no significant deviation from linearity of the Li^+ response for concentrations down to 0.002 µeq·kg^{-1}. For 0.0002 µeq·kg^{-1} Li^+ the tests showed a positive deviation from linearity of less than +20%. This means that using a linear calibration curve Li^+ concentrations evaluated to around 0.0002 µeq·kg^{-1} are overestimated by less than 20%. The standard deviations for repeated measurements of solutions with Li^+ concentrations of 0.2, 0.02, 0.002 and 0.0002 µeq·kg^{-1} was <5%,

<5%, 10% and 10% –15% respectively. After standard solutions of 0.2 µeq·kg^{-1} Li^+ and 4.1 µeq·kg^{-1} Ca^{2+} two blank solutions were measured. In the first blanks an average of 0.0001 µeq·kg^{-1} Li^+ was measured with a reproducibility of 17% corresponding to a carry over of 0.07% of the previous standard solution. There was not detected any Li^+ in second blanks. For Ca^{2+} there was carry over of 4% in the first blanks.

During routine ion chromatographic measurements of ice core samples from various ice cores the Li^+ content was evaluated and recorded. The detection limits for components in the chromatograms depend on how well the system was running. For an optimally working system the detection limits, taken as three times the height of baseline noise, were 0.0001 µeq·kg^{-1} for Li^+ and 0.0002 µeq·kg^{-1} for Ca^{2+}. In practice calcium has a much higher detection limit of 0.05 µeq·kg^{-1} which is determined by blank concentrations. During automatic data evaluation the detection limit is controlled by parameters in the integration software and it was possible to detect Li^+ peaks smaller than corresponding to 0.0001 µeq·kg^{-1} in chromatograms of high quality. This means that Li^+ concentrations as low as 0.0001 µeq·kg^{-1} or 0.7 ppt. were evaluated. During routine IC measurements the limit for automatic detection of Li^+ could vary between 0.0001 and 0.0003 µeq·kg^{-1} depending of the quality of the chromatograms.

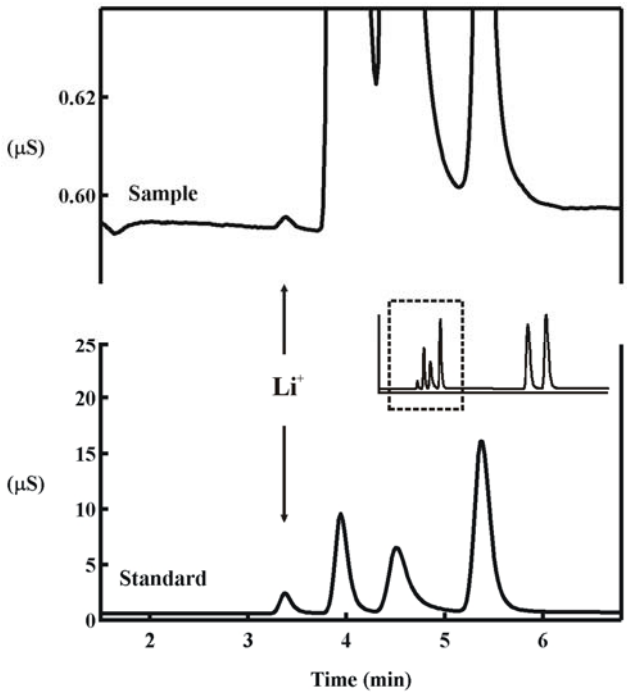

Figure 3.1: *The detector response vs. time for the first four components in the cation chromatograms is shown for a sample solution and for a standard solution. The cations measured are Li^+, Na^+, NH_4^+, K^+, Mg^{2+} and Ca^{2+}. The Li^+ concentration in the standard was 0.2 µeq·kg^{-1}. The sample concentration of Li^+ was evaluated to 0.0003±0.0001 µeq·kg^{-1}.*

For quantification of ion concentrations a single standard solution was used. Deviations from linearity in the detector response of very low Li^+ concentrations have not been taken into account in the data evaluations. Therefore Li^+ concentrations around

0.002 μeq·kg^{-1} have an error of 10% from reproducibility while Li^+ concentrations around 0.0002 μeq·kg^{-1} have a total error of 30-35% from reproducibility and deviations from linearity.

Contaminations of samples during manual sampling occasionally occur and show up as spikes in the data profiles. A typical source of contamination is fingerprints and so spikes in the sodium, potassium and chloride profiles are good indicators for sample contaminations. During the manual sampling of NGRIP samples 4.4% of the samples were marked as possibly contaminated. The marked samples have 91%, 76% and 33% higher average concentrations of sodium, potassium and chloride. For lithium the average concentration in the marked samples are 30% higher than in unmarked samples. This shows that a few samples have been contaminated with lithium during the manual sampling. We expect that contaminations that happened during manual sampling would have affected several of the measured components and that samples contaminated with lithium also is contaminated with other components. We therefore assume that sample data, which look like usual data with respect to components other than lithium, represent real ice core data with respect to lithium.

3.4 Presentation of data

Here we will show the Li^+ profiles along with the Ca^{2+} profiles for selected data series in order to characterise the pattern of Li^+ concentrations in ice cores. The complete data sets involving all the ionic components, that have been measured, will be presented and discussed elsewhere.

Holocene seasonals: From the upper 350 m IC-data profile of the NGRIP ice core Li^+ was measured in sample sections corresponding to approximately 250 metres. We selected a section from a depth of 96-109 metres for this presentation. The Ca^{2+} and Li^+ profiles from the series are shown in Figure 3.2. This section corresponds to a time span of approximately 70 years starting from approximately 400 years BP at 96 metres (personal communication from [H.B.Clausen], February [2001]). With the 5 cm sample resolution seasonal variations of ionic components can be recognized in the whole 350 metre data series and the Li^+ data show seasonal variations in line with Na^+ and Ca^{2+}. But the resolution of the data series is not good enough to show any details in the seasonal pattern. The average values of all the ionic components from the 96—109 metres section are typical for the whole 350-m series. The measured Li^+ concentrations in this series are ranging between 0.0001 and 0.004 μeq·kg^{-1} with an average of 0.0003±0.0001 μeq·kg^{-1}. The ratio between the average concentrations of Li^+ and Ca^{2+} is 0.0007±0.0002. This ratio is comparable to ratios of lithium and calcium contents in various minerals (see Table 3.2).

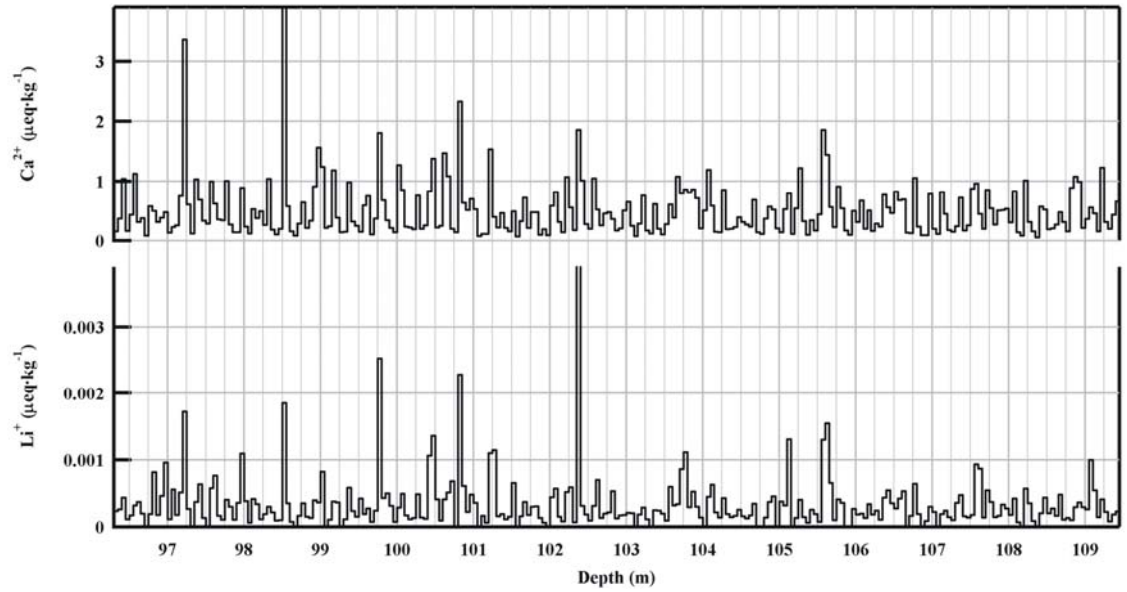

Figure 3.2: *NGRIP Holocene seasonals. Ca^{2+} and Li^{+} profiles in 5 cm resolution from a typical Holocene section of the NGRIP ice core. The section represents approximately 70 years around 400 years BP.*

A glacial Stadial/Interstadial transition: From the GRIP ice core a 5-m section at 2582.25-2587.2 metres depth was analysed. This section represents the transition from the Greenland Stadial 21 (GS-21) to Greenland Inter-stadial 20 (GIS-20) approximately 75 ka BP (Dansgaard et al., 1993; Walker et al., 1999). The Ca^{2+} and Li^{+} profiles are shown in Figure 3.3. The data show that the Li^{+} concentration is higher in the cold GS-21 climate period than in the warmer GIS-20. This response to a change in climate is a familiar pattern seen for most ionic components measured in ice cores (e.g. Mayewski et al., 1997). Although the Li^{+} profile looks noisy during the Inter Stadial the other data from this series does not show any sign of contamination.

The average Li^{+} concentrations and ratios between average concentrations of cations for the three climatic periods represented by the Holocene and the glacial transition data series have been evaluated and listed in Table 3.3. To compare the values of the different climatic periods the errors are estimated on the basis of data reproducibility. In Table 3.3 the ratio between Li^{+} and Ca^{2+} is varying with the highest value for the Holocene series and the lowest value for the GS-21 series whereas the ratio between $nssMg^{2+}$ (non sea salt Mg^{2+}) and Ca^{2+} seem to be constant for the three climate series. The ratio between Li^{+} and Na^{+} also seem to be constant.

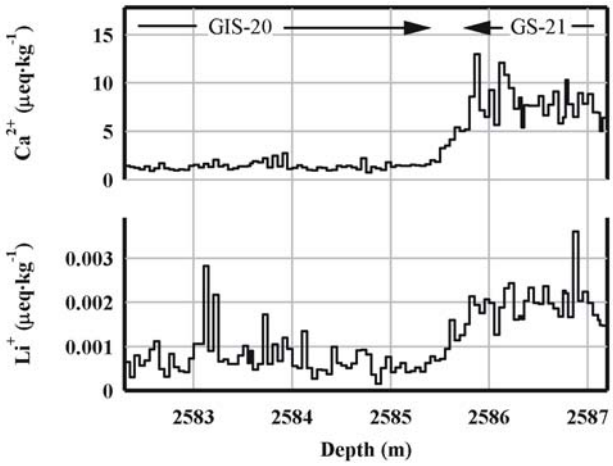

Figure 3.3: *Ca^{2+} and Li^{+} profiles from the GRIP ice core showing the transition between Greenland Stadial 21 and Greenland Inter Stadial 20 approximately 75 ka BP.*

Climate series	*Holocene* (NGRIP):	*GIS-20* (GRIP):	*GS-21* (GRIP):
Section	*96.3 – 109.45 m*	*2582.3 – 2585.3 m*	*2585.7 – 2587.2 m*
$\delta^{18}O$ (‰)	-35.47	-36.73	-41.58
Ca^{2+} (µeq·kg^{-1})	0.51±0.03	1.41±0.08	7.8±0.4
Li^{+} (µeq·kg^{-1})	0.0003±0.0001	0.0008±0.0001	0.0019±0.0002
Li/Na (eq/eq)	0.0010±0.0002	0.0013±0.0002	0.0011±0.0002
Li/Ca	0.00066±0.00014	0.00053±0.00008	0.00025±0.00004
Li/Mg	0.0019±0.0004	0.0016±0.0003	0.0010±0.0001
Li/nssMg	0.0034±0.0007	0.0022±0.0004	0.0012±0.0002
Na/Ca	0.65±0.07	0.41±0.04	0.22±0.02
Mg/Ca	0.36±0.04	0.33±0.03	0.26±0.03
nssMg/Ca	0.20±0.03	0.24±0.04	0.21±0.03

Table 3.3: *Average values of $\delta^{18}O$, average concentrations in µeq·kg^{-1} of Ca^{2+} and Li^{+} and ratios between average concentrations of various cations evaluated for three different climate series: A Holocene section of the NGRIP ice core, and two sections from the GRIP ice core representing the Greenland InterStadial-20 and the Greenland Stadial-21 climate series.*

Holocene 8,200 years BP cold event: Another NGRIP data profile to be presented here is from a 16.5-m series from a depth of 1221-1237.5 metres. The series represents approximately 170 years during the Holocene 8.2 ka BP cold event (personal communication from [H.B.Clausen], February [2001]). This series is particularly interesting with respect to the Li^{+} signal because the lithium content increases more than one order of magnitude and the lithium signal does not seem to correlate with any other of the ionic components measured.

In Figure 3.4 the $\delta^{18}O$ profile from NGRIP (personal communication from [S.J.Johnsen], [2001]) is shown together with the Ca^{2+} and Li^{+} profiles of this series. In the $\delta^{18}O$ profile the 8.2 ka BP event begins at approximately 1234.5 m depth and ends at

approximately 1219.5 m. Ca^{2+} concentrations are increasing slowly with time in the beginning of this depth interval and seem to decrease again later during the event. Li^{+} concentrations start to increase with time more suddenly at a depth of approximately 1232 m, which is later than the beginning of the event in the $\delta^{18}O$ profile. The Li^{+} profile continues to increase through the whole data series and reaches values at the end that are almost two orders of magnitude higher than the values from the deepest part of the core section. This pattern of the Li^{+} profile is not correlated to any other of the measured ionic components. Unfortunately, our Ca^{2+} and Li^{+} profiles are not covering the complete cold event so we do not know how the data profiles of Li^{+} and Ca^{2+} will respond to the end of the event at approximately 1219.5 metres. We have removed data from a few samples that were marked for possible contaminations. These samples had higher values in both Li^{+} and K^{+}, which is a good indicator for contamination. The rest of the data from this series does not show signs of contamination and the measured Li^{+} profile seems to be a real ice core signal. Samples were measured in random order, which excludes the possibility that the Li^{+} profile could be a systematic artefact from the measurements.

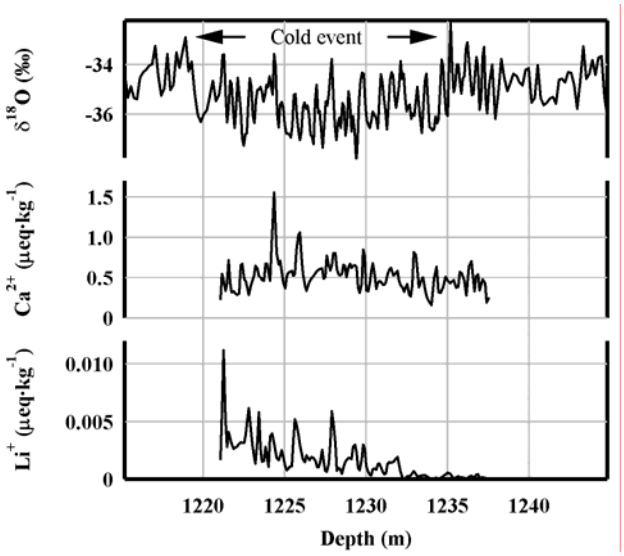

Figure 3.4: *$\delta^{18}O$, Ca^{2+} and Li^{+} profiles from the NGRIP ice core showing the Holocene 8.2 ka BP cold event. The Ca^{2+} and Li^{+} sections represent approximately 170 years. In the deeper part of these sections the Ca^{2+} and Li^{+} concentrations are similar to typical Holocene values.*

Four-metre averages of concentrations and ratios between average concentrations from this data series are listed in Table 3.4. The last column in this table shows values from the deepest part of the section. In the $\delta^{18}O$ profile this part represents the climate just prior to the cold event and the evaluated data from this part of the core have values that are typical for data from the NGRIP Holocene section at 9-350 metres depth. During the series the four-metre average value of $\delta^{18}O$ decreases about 1‰ and Ca^{2+} increases about 40%. Alley et al. (1997) report a decrease in $\delta^{18}O$ of 2 ‰ and an increase in Ca^{2+} of 60 % during the 8.2 ka BP event in the GISP2 ice core.

Depth section	*1221 – 1225 m*	*1225 – 1229 m*	*1229 – 1233 m*	*1233 – 1237.5 m*
$\delta^{18}O$ (‰)	-35.35	-36.07	-35.61	-34.97
Ca^{2+}(µeq.·kg^{-1})	0.54±0.03	0.61±0.03	0.50±0.03	0.43±0.02
Li^{+} (µeq.·kg^{-1})	0.0033±0.0005	0.0020±0.0002	0.0011±0.0001	0.0002±0.0001
Li/Na (eq./eq.)	0.012±0.002	0.0074±0.0001	0.0040±0.0006	0.0006±0.0001
Li/Ca	0.006±0.001	0.0033±0.0005	0.0023±0.0003	0.0005±0.0001
Na/Ca	0.50±0.05	0.45±0.05	0.57±0.06	0.78±0.08
Mg/Ca	0.36±0.04	0.34±0.03	0.36±0.04	0.41±0.04
nssMg/Ca	0.26±0.04	0.24±0.04	0.23±0.04	0.24±0.04

Table 3.4: *Average values of $\delta^{18}O$, average concentrations in µeq·kg^{-1} of Ca^{2+} and Li^{+} and ratios between average concentrations of various cations evaluated for 4-m sections from the NGRIP ice core Holocene 8.2 ka BP cold event series.*

3.5 Discussion

Holocene seasonals and glacial transition: In the data series from the NGRIP Holocene seasonal series and the GRIP GS-21/GIS-20 transition series we see that the Li^{+} profiles show the same pattern as Na^{+} and/or Ca^{2+}. We would expect this if the sources for Li^{+} are sea-salt and mineral dust. The ratios between the average values of Li^{+} and Na^{+} measured range between 0.0010±0.0003 and 0.0013±0.0004, which is 20 times higher than the Li/Na ratio of $0.06 \cdot 10^{-3}$ in seawater. This means that sea salt can only contribute 5% of the Li^{+} measured as long as no significant ion fractionation in sea salt aerosols occurs. Such a fractionation has not been observed in Greenland ice cores for other sea salt components. We therefore suggest that the Li^{+} measured in the Holocene seasonal series and the GS-21/GIS-20 transition series mainly is a dust derived component.

If Li^{+} originates from a mixture of different mineral types we expect to see varying ratios between Li^{+}, $nssMg^{2+}$ and Ca^{2+} concentrations as the composition of mineral types in the samples varies. In both series the Li/Ca ratio of individual samples varies and has a lower limit of 0.0002. This lower limit of the Li/Ca ratio fits well to the content of lithium in average marine carbonates (see Table 3.2). This supports the assumption that lithium in the Greenland ice cores is of terrestrial origin and has a potential application in the analysis of dust aerosols in Greenland ice cores.

Studies of insoluble dust particles in the GRIP ice core suggest that the origin of these particles is eastern and central China (e.g. Svensson et al., 2000). But the source of soluble calcium to the central Greenland ice cores and the relation to the insoluble dust are not completely understood. There is a difference in the calcium/dust ratio in different climatic periods (Steffensen, 1997). There is also a difference in the ratios between dust derived ionic components in different climatic periods (De Angelis et al., 1997). Laj et al. (1997) measured the insoluble part of the aerosols on filtered samples and the total content of elements in evaporated samples using micro probe techniques. They find that fractions of soluble K, Ca, S and Fe are different in different climatic periods and that the correlation between soluble and insoluble contents of these four elements is very poor. De Angelis et al. (1997) and Laj et al. (1997) suggest that a

change in source contribution to mineral dust aerosols in Greenland ice cores occurs during climate changes.

8.2 BP Holocene cold event: The data from the NGRIP 8.2 BP Holocene cold event show an increase in the Li^+ concentration of more than one order of magnitude. The Li^+ change that we see in the series is not correlated to any other of the measured ions. The Li^+ profile from 9-350 metres in the NGRIP ice core shows nothing that is similar to the 8.2 ka BP series. Therefore the data from the 8.2 ka BP event represents a special event with respect to Lithium. We cannot say if the Li^+ change that we see in the 8.2 ka BP data series is directly related to the cold event. The time delay of the increase of Li^+ concentrations relative to the decrease in the $\delta^{18}O$ and the missing decrease later during the cold period suggest that the pattern of the Li^+ concentrations seen in the series are not directly linked to the temperature drop. But since the 8.2 ka BP event is a special climate event, the increase in Li^+ could be indirectly related to some climate changes taking place during the event.

Some clay minerals have relative lithium and calcium contents that correspond to the high ratio of the measured concentrations of Li^+ and Ca^{2+} in the 8.2 ka BP series. But it is unlikely that such a high increase in the measured Li^+ concentration and no significant change in other dust-derived components is only an effect of a change in mineral composition due to changes in source contribution. We therefore have to look for an additional source to Li^+ in this series. However we have no candidate for such a source. To understand the lithium chemistry of the 8.2 ka BP series, additional ion chromatographic measurements to extend the data series would be helpful to clarify if the concentration of soluble lithium increases further and for how long time the lithium event takes place. Analysis of the insoluble fraction of components and an analysis of the mineralogy in this ice core series would also be of great value to study whether a change in mineral composition or a change in the soluble fraction of lithium has caused the increased Li^+ concentrations and what kind of changes in climate could be the reason for such a change in lithium. Since the isotopic composition of lithium varies in material of different geological origin (e.g. Hoefs and Sywall, 1997) an analysis of the isotopic composition of lithium in this ice core series might give some evidence whether the lithium is of volcanic origin or if it comes from secondary minerals.

3.6 Conclusion

The main result of this work is the introduction of the Li^+ ion in the ice core analysis. We have shown that it is possible to measure a reliable lithium signal from ice cores in concentrations down to 0.0001 $\mu eq \cdot kg^{-1}$ using ion chromatography with a reproducibility of 15% for concentrations close to the detection limit.

The data profiles of Li^+ from a NGRIP Holocene seasonal series and from the GRIP GS21/GIS20 transition series demonstrates that Li^+ data from ice cores have a potential application in the analysis and interpretations of ice core dust chemistry. Future analysis of the ice core chemistry of lithium may give a better insight into the chemistry of the dust derived ionic components and the relation between soluble calcium and dust in ice cores. The Li^+/Ca^{2+} relation can contribute to a characterization of calcium sources and to an analysis of potential solubility effects on mineral dust particles. The Li^+ component might also give some new information about ice core chemistry as

suggested by the independent behavior of the Li^+ component to other species during the 8.2 BP Holocene cold event.

The NGRIP 8.2 ka cold event series represent a special lithium event where the source of lithium to the ice core samples is unknown. Further ion chromatographic measurements along with analysis of the insoluble fraction and isotopic composition of lithium in this series would give information about the origin of the Li^+ measured in this series.

Acknowledgements: The GRIP project is organized by the European Science Foundation with eight nations (Belgium, Denmark, France, Germany, Iceland, Italy, Switzerland, and United Kingdom), and the EEC. The NorthGRIP project is directed and organized by the Department of Geophysics at the Niels Bohr Institute for Astronomy, Physics and Geophysics, University of Copenhagen. It is being supported by Funding Agencies in Denmark (SNF), Belgium (NFSR), France (IFRTP and INSU/CNRS), Germany (AWI), Iceland (RannIs), Japan (MECS), Sweden (SPRS), Switzerland (SNF) and the United States of America (NSF). We thank GRIP and NGRIP participants and supporters for their cooperative effort. We also thank reviewers for useful comments.

3.7 References

Alley, R. B., P. A. Mayewski, et al. (1997). "Holocene climatic instability: A prominent widespread event 8200 yr ago." Geology **25**(6): 483-486.

Dahl-Jensen, D., N. Gundestrup, et al. (2002). "The NorthGRIP deep drilling program." Annals of Glaciology **35**: 1-4.

Dansgaard, W., S. J. Johnsen, et al. (1993). "Evidence for general instability of past climate from a 250-kyr ice-core record." Nature **364**(6434): 218-220.

De Angelis, M., J. P. Steffensen, et al. (1997). "Primary aerosol (sea salt and soil dust) deposited in Greenland ice during the last climatic cycle: Comparison with east Antarctic records." Journal of Geophysical Research **102**(C12): 26681-26698.

Heier, K. S. and G. K. Billings (1970). Lithium. Handbook of Geochemistry. K. H. Wedepool. Berlin-Heidelberg, Springer Verlag**:** 3E1-3O1.

Hoefs, J. and M. Sywall (1997). "Lithium isotope composition of Quaternary and Tertiary biogene carbonates and a global lithium isotope balance." Geochimica et Cosmochimica Acta **61**(13): 2679-2690.

Holland, H. D. (1984). The Chemical Evolution of the Atmosphere and Oceans. Princeton, New Jersey, Princeton University Press.

Hughes, L. S., J. O. Allen, et al. (2000). "Evolution of atmospheric particles along trajectories crossing the Los Angeles basin." Environmental Science and Technology **34**(15): 3058-3068.

Klitgaard-Kristensen, D., H. P. Sejrup, et al. (1998). "A regional 8200 cal. yr BP cooling event in northwest Europe, induced by final stages of the Laurentide ice-sheet deglaciation?" Journal of Quaternary Science **13**(2): 165-169.

Laj, P., G. Ghermandi, et al. (1997). "Distribution of CA, Fe, K, and S between soluble and insoluble material in the Greenland Ice Core Project ice core." Journal of Geophysical Research **102**(C12): 26615-26623.

Lyons, W. B. and K. A. Welch (1997). "Lithium in waters of a polar desert." Geochimica et Cosmochimica Acta **61**(20): 4309-4319.

Mayewski, P. A., L. D. Meeker, et al. (1997). "Major features and forcing of high-latitude Northern Hemisphere atmospheric circulation using a 110,000-year-long glaciochemical series." Journal of Geophysical Research **102**(C12): 26345-26366.

Papoff, P., M. Betti, et al. (1991). "Optimization of the procedure for the determination of alkali and alkaline-earth elements in sea-water by suppressed ion chromatography." Journal of Chromatography A **259**: 259- 271.

Silva, P. J., R. A. Carlin, et al. (2000). "Single particle analysis of suspended soil dust from Southern California." Atmospheric Environment **34**: 1811-1820.

Singh, R. P. and N. M. Abbas (1996). "Suppressed ion chromatographic determination of lithium, sodium, ammonium and potassium concentrations in sub-surface brines." Journal of Chromatography A **733**: 93-99.

Steffensen, J. P. (1997). "The size distribution of microparticles from selected segments of the Greenland Ice Core Project ice core representing different climatic periods." Journal of Geophysical Research **102**(C12): 26755-26763.

Svensson, A., P. E. Biscaye, et al. (2000). "Characterization of late glacial continental dust in the Greenland Ice Core Project ice core." Journal of Geophysical Research **105**(D4): 4637-4656.

Walker, M. J. C., S. Björck, et al. (1999). "Isotopic "events" in the GRIP ice core: a stratotype for the Late Pleistocene." Quaternary Science Reviews **18**: 1143-1150.

Wedepohl, K. (1995). "The composition of the continental crust." Geochim. Cosmochim. Acta . **59**(7): 1217-1232.

4: Evidence from the NorthGRIP ice core for rapid development of playa areas from Western Chinese lakes reinforced by the 8.2 ka BP Holocene cold event

This section is based on a poster titled "A lithium anomaly observed in the NorthGRIP ice core." presented at the Goldschmidt conference on Geosciences, Copenhagen 2004 by Marie-Louise Siggaard-Andersen, Jørgen Peder Steffensen and Henrik Brink Clausen, Department of Geophysics, University of Copenhagen, Juliane Mariesvej 30, 2100 Kbh,Ø.

Abstract: Greenland ice cores contain trace amounts of wind blown mineral dust deposited onto the ice sheet. A fraction of the dust material is partly soluble. Analysis of soluble ions in the NorthGRIP ice core has revealed a lithium anomaly in the dust material around the 8.2 ka BP Holocene cold event. This anomaly is characterized by a sudden increase in soluble lithium concentrations, still increasing over at least one century, and reaching up to two orders of magnitude higher concentrations than prior to the event. This lithium-anomaly occurs while none of the other soluble ions measured show similar anomalies. Such an increase of a single soluble species is a unique event in the ice core.
Geochemical properties of lithium suggest that the increase in soluble lithium concentrations is due to lithium enrichments in the dust material characteristic for rock-water interactions in the dust source area. Mineral dust in Greenland ice cores has provenance mainly in Western and North-Western Chinese desert areas. We have searched for special geological and climate conditions in these areas around the 8.2 ka BP event that can explain increased lithium concentrations observed in the NorthGRIP ice core.
Here we suggest that the lithium anomaly observed in the NorthGRIP ice core is a signature from changes that followed the transition in the water balance in the dust source area.

4.1 Background

The 8.2 ka BP event: The most prominent climate event during the last 10 ka seen in Greenland $\delta^{18}O$ records is a cold episode around 8.2 ka BP (BP = Before Present 1950 AD) that lasted approximately 200 years (Johnsen et al., 1992) (see Figure 4.1). As indicated from marine sediment cores, the 8.2 ka BP event is caused by sudden drainage into the Labrador Sea of enormous Laurentide melt-water lakes succeeding a long term enhanced freshwater flux from the break-up of a partly marine based Northern Labrador ice sheet (Klitgaard-Kristensen et al., 1998; Barber et al., 1999). Changes in ocean thermo-haline circulation resulted in a temperature drop in the Northern and Tropical Atlantic regions and severe drought in low latitudes (Hughen et al., 1996; Alley et al., 1997; Grafenstein et al., 1998). The cooling scenario of the 8.2 ka BP event has raised concern about consequences of global warming associated with greenhouse effects inducing an increased fresh-water flux into high latitude oceans from melt water or from increased precipitation (Broecker, 1997). Also the drought scenario of the 8.2 ka BP event is investigated with respect to perspectives on drought and implications for the future (CLIVAR/PAGES/IPCC, 2003).

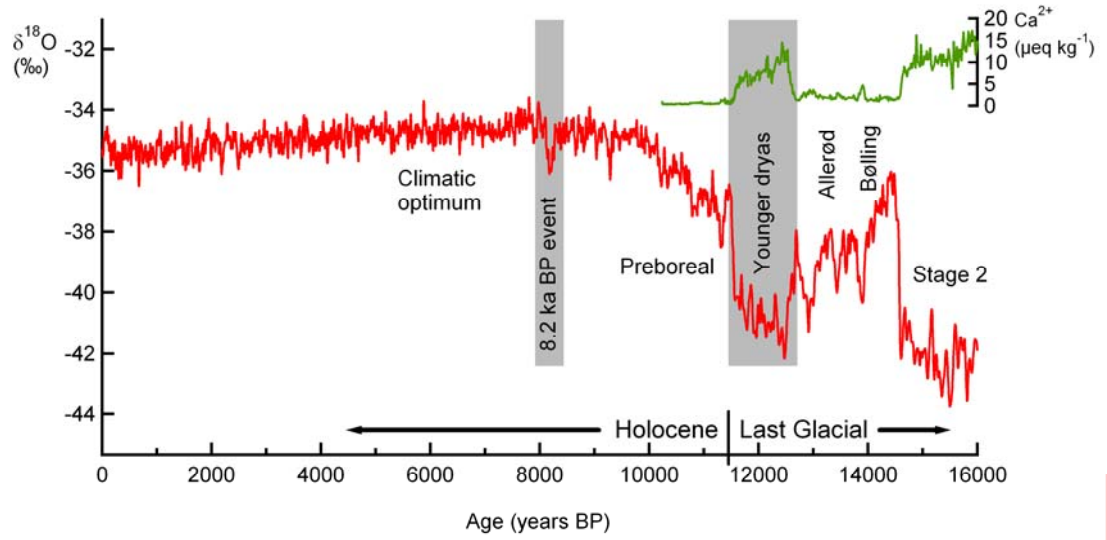

Figure 4.1: *The climate record for the last 16 ka from the NorthGRIP ice core ($\delta^{18}O$ data from Sigfus Johnsen, Geophys. Dept. Univ. Copenhagen, unpublished data). The top curve shows Ca^{2+} concentrations that represent contents of mineral dust.*

The 8.2 ka BP event in the NorthGRIP ice core: A detailed look at the NorthGRIP $\delta^{18}O$ record shows that the 8.2 ka BP event represents a well-defined cold time interval (see Figure 4.2). Within this interval soluble calcium concentrations are increased, but not beyond the general variation in the Greenland Holocene calcium ice core records from GRIP (Fuhrer et al., 1993) and GISP2 (O`Brien et al., 1995; Alley et al., 1997). As indicated in Figure 4.2 lithium concentrations, however, increase suddenly one order of magnitude some time after the 8.2 ka BP cooling. This increase continues during the cold period and reaches concentrations that are two orders of magnitude higher than concentrations prior to the event. Unfortunately we do not have data representing the end of the cold period and immediately after but a series of lithium concentrations in the NorthGRIP ice core representing the last 2000 years (unpublished data) shows concentrations all through this series corresponding to the level prior to the 8.2 ka BP event. The lithium anomaly observed in the NorthGRIP ice core of the 8.2 ka BP event is not associated with a corresponding anomaly in any other ion species measured.

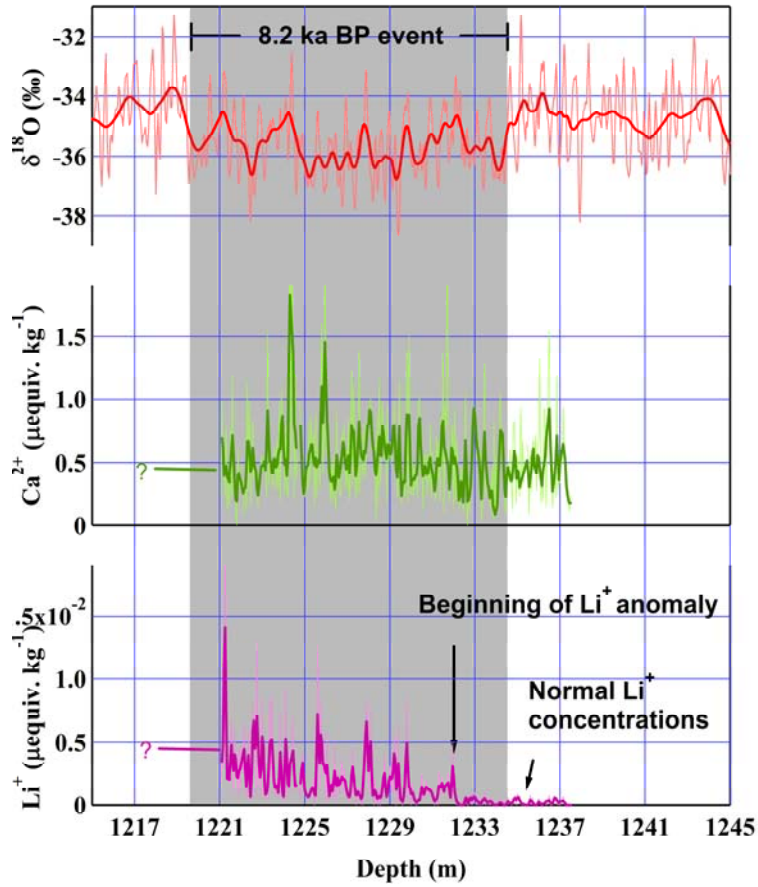

Figure 4.2: *Detailed analysis of soluble ions in the NorthGRIP ice core was performed for a section representing most of the cold period of the 8.2 ka BP event. Only the lithium record responds significantly to the dry and cold conditions during this period.*

Geochemical properties of lithium: The abundance of lithium in Earth's crust is small in view of its small atomic weight. Lithium fits poorly into mineral crystal structures and is therefore more abundant in magma than in igneous rocks. Pure lithium minerals are rare but occur as pegmatite, which is the last mineral crystallizing from a magma chamber. Li^+ is very little soluble in water, but the solubility increases with temperature. Therefore hot springs often contain relatively high concentrations of lithium and ocean waters are provided with lithium from midocean spreading zones where hot magma is injected directly up onto the ocean floor (Holland, 1984).
Rock-water interactions play an important role in lithium's geochemical properties. Although lithium is almost insoluble in water, it is rather mobile during contact between rocks and streaming water, where lithium is leached from the parent rock and permeates into clay minerals by ion exchange typically with magnesium (Heier and Billings, 1970). Clay-minerals can therefore be highly enriched in lithium depending upon the weathering history. Also salt-lake brines in basins with no out-flow and long-term alternating water balances can accumulate large amounts of lithium.
The technique used for measuring soluble lithium in extremely low concentrations in ice cores has been developed recently and until now only little is known about lithium in ice cores (Siggaard-Andersen et al., 2002).

The geochemical properties of lithium suggest that the lithium anomaly at 8.2 ka BP observed in the NorthGRIP ice core is a source related lithium enrichment of the dust material.
A lithium anomaly in atmospheric dust could be a result of regional changes in source emission properties due to regional changes in vegetation or aridity. Alternatively, decreased lake-levels could result in exposure of lithium-rich lake sediments, enhanced rock-water interaction in the source area prior to the 8.2 ka BP event could result in high production of Li salts or Li-rich clay minerals, and larger supply to lakes of water from hot springs could enhance the lithium content in lake sediments. These possible scenarios for increases in the Li content in the dust-material suggest a major change in the water balance in the dust source region around 8.2 ka BP.

Provenance of dust in the NorthGRIP ice core: Dust in Greenland ice cores has been wind-transported by westerly winds from the Asian continent. Satellite observations of atmospheric dust show that Chinese deserts are major global dust sources (Prospero et al., 2002).
Neodymium (Nd) and Strontium (Sr) isotope analyses of the mineral dust deposited recently at NorthGRIP have shown that this dust material origins mainly from the Taklimakan desert in the Tarim basin north of the Tibetan Plateau (Bory et al., 2002; Bory et al., 2003a) (see Figure 4.3). The Tarim basin is a major dust source area for Greenland because of a high frequency in this area of spring dust-storms and because dust in the Tarim basin is uplifted particularly high into the upper troposphere where it is driven east-ward by the westerlies (Bory et al., 2003a). In contrast, dust from other Chinese deserts is mainly deposited down-wind onto Chinese loess deposits (Zhang et al., 1999; Sun, et al., 2001) or transported by mid-tropospheric winds to the North Pacific (Bory et al., 2003a).
However, salt brines in the Qaidam basin, which is located east of the Tarim basin (see Figure 4.3), accounts for 80% of Chinese lithium reserves or 1/3 of the lithium reserves of all salt lakes in the world (Peihua and Pingxi, 1999). Satellite observations show significant dust activity in the Qaidam basin (Prospero et al., 2002), and observations of dust-storms show some occurrence of dust-storms in the Qaidam basin at present (Sun, 2002). This means that a small fraction of the dust material in Greenland ice cores could come from the Qaidam basin. Since air dynamics for uplift of dust to the upper troposphere is dependent on topographic conditions we can assume that the major dust source areas at 8.2 ka BP were the same as at present. We will therefore seek for environmental changes around 8.2 ka BP in the region of desert areas north of the Tibetan Plateau that could effect sudden lithium enrichments in the dust material in the NorthGRIP ice core.

Figure 4.3: *Source provenance (Tarim basin) and transport path for dust deposited onto the Greenland ice sheet. The lithium anomaly observed in the NorthGRIP ice core might origin from the Qaidam basin.*
(The figure is modified from Satellite Imagemap © 1999 Planetary Visions Limited).

4.2 History of lake status in the dust source area

Due to variations in monsoonal and continental precipitations and glacier melt over the last 30 ka, large changes in the water budget occurred all over China in this period. During the last glacial period inland basins in Western China were occupied by large lakes, which, because of less precipitation and higher evaporation during Holocene, now have dried out and turned into salt lakes or playas (Yu et al., 2001). About 276 Chinese saline lakes are located mainly in the Western and Northern China. Lacrustine sediments have been deposited in these lakes all through the Pleistocene and can be up to 3000 m thick. The development of Chinese lakes can be recovered in lake-core records of pollen, shells and algae as well as contents of gypsum and halite. Changes of lake-levels recorded in lake sediments are good indicators of regional precipitation and temperature variations.
The latest 30 ka sequence of lake status in Western Chinese lakes identifies three periods of relatively high lake level of which the highest was before 28 ka BP, the second highest was 21-17 ka BP and the lowest high-level stand was 7-6 ka BP (Yu et al., 2000). Between these wet periods conditions were dry as indicated by salt-layers in the sediment records.

Lake status in the Tarim and Qaidam basins: The Tarim pendi is located in the Xinjiang province north of the Tibetan plateau and the Qaidam pendi is located in the Qinghai province east of the Tarim basin. Both locations are in the arid Western China.
The Tarim and Qaidam pendi's are large intermountain sedimentary high altitude basins. Both basins have no outflow and hence evaporation has a major influence on the water balance. Salt lakes in the basins are fed with water from mountain run-off and precipitation over large catchments. Some of the lakes get a small amount of water from ground water or hot springs associated with underground tectonic faulting (Yu et al., 2001). At present the annual evaporation in these areas is around 3000 mm, which is more than one order of magnitude larger than the annual precipitation around 50 mm.

The Tarim basin was until recently (1950) drained into three lakes in the Lop basin in the eastern part of the Tarim basin, but because of human activities in the region the Tarim river stopped discharging water into the Lop Nur lake and in 1972 the lake completely dried out (Xinhua News Agency, September 9, 2004). The Lop basin is rich in evaporites (Beijing Time, Monday, November 24, 2003) that might contribute to dust deposited onto the Greenland ice sheet. In Figure 4.4 is shown a satellite image of the Lop Nur Lake. Former lake shore-lines made up of evaporitic deposits are clearly visible. However we will exclude playas in the Lop basin as a possible source for lithium because the resent drying of the lake is not followed by higher ice core concentrations of soluble minerals and because cores from the Lop basin playa show high lake stand around 8.2 ka BP and no evidence of major changes in the water balance around that time (see Figure 4.5).

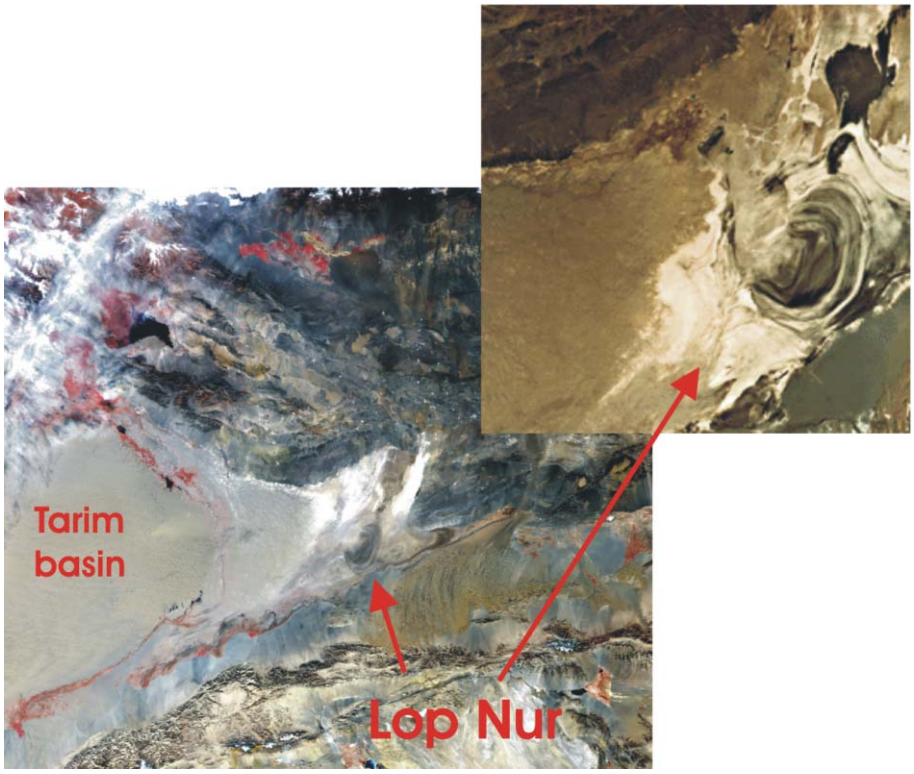

Figure 4.4: *Satellite images of the Lop Nur lake playa located in the eastern part of the Tarim basin. Mineral deposits around the playa indicate former lake shore-lines. Large picture: EO Newsroom: New Images - The Wandering Lake (http://earthobservatory.nasa.gov). Small picture: Geomorphology from Space, Goddard Space Flight Center, Distributed Active Archive Center, (http://daac.gsfc.nasa.gov)*

We will instead consider the Qaidam basin located north of the Tibetan plateau south-east of the Tarim basin. Lake cores from the Qaidam basin show that the water balance here changed significantly around 8.2 ka BP. Nine of 33 salt-lakes in the Qaidam basin are located within the Chaerhan (also Qarhan) playa area, at 36.63-37.22 ºN and 93.72-96.25 ºE, at an altitude of 2675 m.a.s.l. The Chaerhan playa contains 1/3 of the global playa resources of lithium (Peihua and Pengxi, 1999). The stratigraphy of deep cores taken from the playa and a lacustrine shell-ridge 29 m higher than the lowest lying salt-

lake indicate that there was a large freshwater lake in the basin until 25 ka BP when the lake became salt. Around 8 ka BP the Chaerhan salt lake turned into a playa (Yu et al. 2001) that today, with an area of 5856 km^2, is one of largest playa surfaces in the world. During the last 25 ka at least three salt layers (S1-S3) were deposited across most parts of the Chaerhan Basin. Intercalated with these salt layers are units, indicating intervals of relatively fresh water-conditions. The area of the youngest salt layer deposited during the last 8 ka playa phase is more than two times larger than the previous layer, deposited during a shallow salt-lake phase, indicating that water supply was significantly different during the two phases of the lake.

A more detailed record of lake status changes in the Chaerhan salt lake is provided by a 101 m long sedimentary core (Core CK2022) taken from the playa surface at higher elevation. The lake-status record obtained from this core is summarized in Figure 4.5 The characteristics of distinct sequences, dated according to the ^{14}C chronology that is somewhat younger than the calendar time scale, is described in Yu et al., (2001). Here is given a short summary: Salt layers (S2-1 and S2-2) indicate that during time-periods of 20.6-16.0 ^{14}C ka BP and 15.0-9.3 ^{14}C ka BP the lake was shallow. The area of the salt layer formed during this period was 2300 km^2, which is less than half the area of the present playa. A layer formed between 9.3-8.1 ^{14}C ka BP contains only 20% evaporite minerals suggesting that the lake became deeper. This layer is succeeded by a salt-layer (S3-1) formed during 8.12-4.94 ^{14}C ka BP suggesting the lake became shallower and more saline. Between 4.94-3.80 ^{14}C ka BP the lake became somewhat less saline and deeper than formerly. Finally the uppermost layer with an area of the salt deposit larger than any of the other salt units found in Chaerhan represents the most arid phase in the history of this basin.
Evaporite contents in the CK2022 core and Lake Status Coding, indicating lake stands, (after Yu et al., 2001) are given in Figure 4.5. Here is also shown temporal changes in lake level and precipitation evaluated from the CK2022 core (after Lehmkuhl and Haselein, 2000).

Another salt-lake in the Qaidam basin, Da Chaidan (also Da Qaidam) salt lake, is located 37.83 ºN, 95.23 ºE, 3110 m above sea level and is one of two salt lakes remaining from a mega fresh water lake, which began to shallow around 30 ka BP. The characteristics of distinct sequences as described by Yu et al., (2001) show that sediments deposited from 9.0-7.08 ^{14}C ka BP are clay-rich indicating relatively fresh water and high lake stand during this period. The overlying layer is rich in halite indicating a shallowing of the lakes.

The Da Chaidan salt lake is located at lower altitude than the position of the CK 2022 core and may therefore respond to a shallowing of lakes in the Qaidam basin later (7.08 ^{14}C ka BP) than indicated by the CK 2022 core (8.1 ^{14}C ka BP).

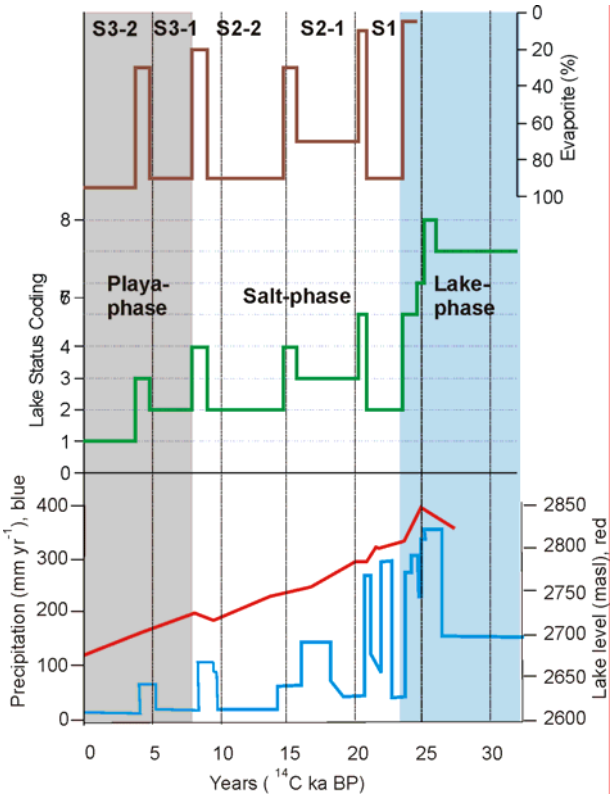

Figure 4.5: *The top curve shows evaporate contents in lake core CK2022 from the Chaerhan playa (after Yu, 2001). Salt layers S1-S3 are indicated on the curve. The middle curve shows Lake Status Coding by G.Yu and S.P.Harrison (from Yu, 2001). The bottom curves show precipitation (blue) and lake-stand of the Chaerhan lake (red) evaluated from the CK2022 core (after Lehmkuhl and Haselein, 2000).*

4.3 Water balance in Western China

Glacier melting: Glaciers in Western China were widely expanded during the last glacial maximum (Zhuo et al. 1998). During the Holocene optimum Western Chinese glaciers rapidly retreated. Glaciers in the West Kunlun mountain area, south-west of the Tarim basin, were 2.2 times larger in area during LGM than at present while glaciers in the east Kunlun mountain area, south of the Qaidam basin, were 144 times larger in area than at present (Shi et al., 2002). The large change in glacier area in east Kunlun is due to the monsoonal precipitation conditions (Shi et al., 2002).
Wet and warm climatic conditions during the Holocene optimum resulted in more rainfall and more glacier melt water draining to lakes and seas (He et al., 2004). Many lakes in North Eastern China and on the Tibetan Plateau received melt-water to form large lakes (Zhuo et al., 1998). The relatively high lake stand in the Qaidam basin prior to 8 ka BP could be a result of glacier melt. Water streams from catchments and glacier melt could have leached large amount of lithium and caused enhanced accumulation of lithium in lake sediments. The succeeding cold conditions during the 8.2 ka event could have reduced mountain glacier run-off and caused shallowing of lakes whereby dust from lithium rich playas could be exposed to the atmosphere. However glacier retreat

was relatively slow before 8 ka BP (Zhou et al., 1998). Furthermore synchronous increases in water balance and ice balance in Tibet and Xinjiang around LGM has been reported in Chinese literature (e.g. Yu et al., 2000). Coarse particles in the Chaerhan lake sediments representing small glacier advances at about 9 and 4.5 ka BP are coinciding with the periods of enhanced lake-stands (Lehmkuhl and Haselein, 2000). The high lake stand in the Qaidam basin prior to the 8.2 ka BP event is therefore more likely an effect of enhanced precipitation.

Monsoonal circulation: Precipitation and temperatures in China are influenced by the Asian monsoonal circulation, which is a complicated and unique climate system. The Asian monsoon system has three relatively independent subsystems; the East Asian monsoon, the Indian monsoon, and the Tibetan plateau monsoon (see Figure 4.6). The East Asian monsoon is controlled by the land-ocean contrast induced by sun-heating of the South East Asian continent and brings moist air to Eastern China from the Pacific during summer. The Indian monsoon circulation is associated with convection of moist air in the inter-tropical convergence zone and brings moist marine air from the Indian Ocean to Western China during summer (An et al., 2000). The winter monsoon is associated with the Siberian high pressure system and brings dry and cold continental air from the north and north-west to Western and Central China. The Tibetan Plateau monsoon is controlled by sun heating of the plateau it selves and interacts with the winter monsoon and the Indian summer monsoon systems.

Western and North-Western China is located too far inland for the Asian summer monsoons to bring significant amounts of precipitation from the Pacific and Indian Oceans why this area is arid and occupied by large deserts. North-Western China is during summer provided with moisture by continental westerly winds associated with the jet-stream. During winter the jet-stream moves south but the Tibetan Plateau splits the jet-stream and the northern branch passes over North-Western China. Western China is therefore dominated by westerly winds throughout the year (Lehmkuhl and Haselein, 2000; Yu et al., 2003; He et al., 2004). The summer and winter wind systems in East Asia are shown in Figure 4.6 where also present day ranges of the different Asian monsoons are roughly indicated (After Yu et al, 2003). During the glacial period a weak East Asian summer monsoon resulted in dry conditions in Eastern China while stronger westerlies brought more moisture to Western China, where conditions due to more precipitation and less evaporation were much wetter than today (Yu et al., 2000;Yu et al., 2003).

Ice core records from Gulian ice cap located south west of the Tarim basin (Thompson et al., 1997), and from the Dunde ice cap located north of the Qaidam basin (Thompson et al., 1989), reflect continental and monsoonal precipitation regimes respectively (He et al., 2004) (see Figure 4.7). Penetration of the Indian monsoon results in high summer rain fall on the central and eastern Tibetan Plateau (Yu et al., 2001). Also some East Asian monsoon rain falls in the eastern part of the Tibetan plateau. Shi et al., (2001) connected precipitation in the Qaidam basin with the Indian summer monsoon.

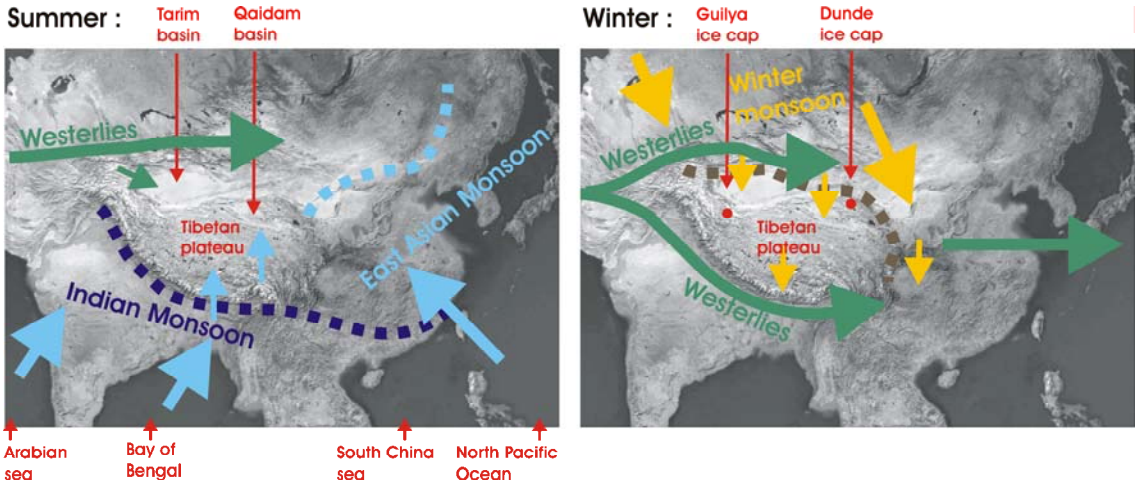

Figure 4.6: *Main wind directions in central Asia for summer and winter (modified after Lehmkuhl and Haselein, 2000). Range limits for the different monsoons at present are indicated (after Yu et al, 2003). The East Asian summer monsoon is governing Eastern, and North-Eastern China while the Indian summer monsoon is governing Southern China and Southern Tibet and, modified by the plateau summer monsoon, also parts of the Tibetan plateau. The Asian winter monsoon governs almost the whole of Western and Central China. On the Tibetan Plateau the winter monsoon becomes associated with the plateau winter monsoon. The Tarim and Qaidam basins are indicated on the left Figure. Locations of the Guliya and Dunde ice caps are indicated on the right plot.*

The monsoonal circulation exerts large changes in intensity and range on a Milankowitch timescale (An, 2000), and on a millennial time scale as well (e.g. An, 2000; Gupta et al., 2003). Due to different controls the Asian monsoons vary asynchronously (He et al, 2004), (An et al., 2000), (Shi et al., 2001).

Regional changes in precipitation: Conditions for precipitations in the regions around the Tarim and the Qaidam basins can be derived from the Guliya and the Dunde ice cores respectively (see Figure 4.7). The continental Guliya ice core shows high $\delta^{18}O$ during 11.5-7.0 ka BP, refecting the Holocene optimum with high temperatures. In contrast decreases in $\delta^{18}O$ in the Dunde ice core might reflect monsoon penetration further inland, with increases of monsoonal precipitation as well as higher temperatures in the periods 8.5-9 ka BP and around 5-6 ka BP (He et al., 2004). These periods of higher monsoonal precipitation at the Dunde ice cap are consistent with periods of enhanced precipitation in the Qaidam basin derived from the CK 2022 core from the Chaerhan salt lake.

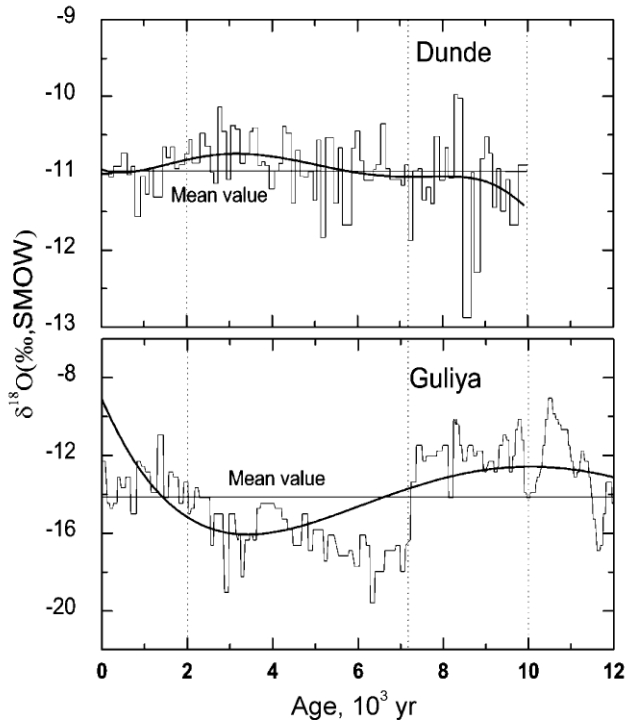

Figure 4.7: $\delta^{18}O$ *records from the Dunde and the Guliya ice cores reflecting monsoonal and continental precipitation respectively (from He et al., 2004).*

An et al., (2000), found that the zone of peak rainfall conditions associated with the East Asian summer monsoon shifted latitudinally across China during the Holocene in response to natural variations in solar radiation. However, while northern hemisphere insolation increased before 15 ka BP, the East Asian Monsoon did not increase until 9 ka BP due to remnant ice sheets, low atmospheric concentrations of CO_2 and low air temperatures (An et al., 2000). Due to the high altitude of the Tibetan Plateau this region responses earlier and is more sensitive to global climate changes. Thus the Holocene optimum occurred earlier and lasted longer on the western part of the Tibetan plateau that on the eastern part that is influenced by lower altitude monsoonal climate (He et al., 2004). In South-Western China precipitation peaked at 12 ka BP in association with the development of the tropical Indian summer monsoon that was favoured due to a warming of the Tibetan Plateau between 15 and 12 ka BP and a significant rise of sea level (An et al., 2000). An Indian monsoon proxy from the continental margin of Oman, Arabian Sea, indicates that the Indian monsoon was enhanced around 10 ka BP and again at 8.8 ka BP (Gupta et al., 2003). Decreases in snow and ice cover on the Tibetan plateau after the transition might have assisted in a strengthened monsoon in the Qaidam basin at 10-8 ka BP (An et al., 2000). This means that both the Indian and the East Asian monsoons were intensified prior to 8 ka BP and ranging further inland.

Gupta et al., 2003, found discrete intervals of weakened strength of the Indian summer monsoon throughout the Holocene correlating with millennia scale cold events in the

North Atlantic where the North Atlantic 8.2 ka BP cold event appears prominent in the Indian monsoon proxy record (see Figure 4.8).

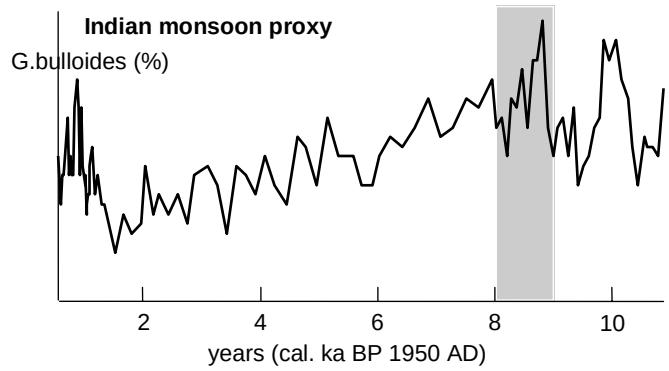

Figure 4.8: *Indian monsoon proxy from the Continental margin of Oman, Arabian Sea, given as the percentage of G.bulloides that is planktonic foraminifera, which is sensitive to the monsoonal atmospheric pressure gradient. The long term trend during Holocene matches changes in July insolation. The record shows intensified Indian monsoon at 10 ka BP and at 8.8 ka BP, and a weakening around 8.2 ka BP. (Data are from Gupta et al., 2003b)*

4.4 Discussion and Conclusions

The observed lithium anomaly around 8.2 ka BP in the NorthGRIP ice core suggest that the aerosol dust material was enriched in lithium as an effect of rock water interaction in the Western Chinese desert dust source areas.

A lake status record from the Chaerhan lake located in the Qaidam basin shows evidence that the lithium anomaly in the NorthGRIP ice core around 8.2 ka BP is simultaneous with the occurrence of the Chaerhan salt lake becoming a playa around 8 ka BP, thereby exposing large areas of lake sediments. A connection between this event and the NorthGRIP lithium anomaly is further supported by the high abundance of lithium in the Chaerhan lake playa.

The sedimentation of evaporitic minerals all through the period from 8 ka BP and to present is not reflected in Greenland ice cores. The lithium anomaly seen in the NorthGRIP ice core is therefore likely not to arise from evaporites but rather from clay-minerals deposited during high lake stands and exposed immediately after the shallowing.

The lake sediments might have become rich in lithium after a period of larger supply of water to the catchments from monsoonal precipitation.

The rapid increase in lithium seen in the NorthGRIP ice core shortly after the onset of the 8.2 ka BP cooling suggest a link between the development of the Chaerhan playa and the 8.2 ka BP cooling.

A weakening of the Asian monsoons during the 8.2 ka BP indicated by monsoonal proxies suggest that the 8.2 ka BP event effected a retreat of the range of monsoonal precipitation from inland Western China. Reduced precipitation combined with high evaporation during the Holocene optimum could have resulted in rapid changes from relatively wet into very dry conditions.

Disregarding the possibility of a contribution of lithium to the lakes in association with tectonic activity our work suggests that analyses of lithium in Greenland ice cores reveals details in rapid changes in regional monsoonal patterns in the Western Chinese dust source areas.

4.5 References

Alley, R. B., P. A. Mayewski, et al. (1997). "Holocene climatic instability: A prominent widespread event 8200 yr ago." Geology **25**(6): 483-486.

An, Z. (2000). "The history and variability of the East Asian paleomonsoon climate." Quaternary Science Reviews **19**: 171-187.

An, Z., S. C. Porter, et al. (2000). "Asynchronous Holocene optimum of the East Asian monsoon." Quaternary Science Reviews **19**(8): 743-762.

Barber, D. C., A. Dyke, et al. (1999). "Forcing of the cold event of 8,200 years ago by catastrophic drainage of Laurentide lakes." Nature **400**: 344-348.

Bory, A. J.-M., P. E. Biscaye, et al. (2003). "Two distinct seasonal Asian source regions for mineral dust deposited in Greenland (NorthGRIP)." Geophysical Research Letters **30**(4): doi:10.1029/2002GL016446.

Bory, A. J.-M., P. E. Biscaye, et al. (2002). "Seasonal variability in the origin of recent atmospheric mineral dust at NorthGRIP, Greenland." Earth and Planetary Science Letters **196**(No. 3-4): 123-134.

Broecker, W. S. (1997). "Thermohaline circulation, the Achilles Heel of our climate system: Will Man-Made Co_2 upset the current balance?" Science **278**: 1582-1588.

CLIVAR/PAGES/IPCC Workshop (2003). A multi-millennia perspective on drought and implications for the future. Tucson, AZ**:** 1-34.

Fuhrer, K., A. Neftel, et al. (1993). "Continuous measurements of hydrogen peroxide, formaldehyde, calcium and ammonium concentrations along the new GRIP ice core from Summit, central Greenland." Atmospheric Environment , Part A **27**(12): 1873-1880.

Gupta, A. K., D. M. Anderson, et al. (2003). "Abrupt changes in the Asian southwest monsoon during the Holocene and their links to the North Atlantic Ocean." Nature **421**: 354-357.

He, Y., T. W. H., et al. (2004). "Asynchronous Holocene climatic change across China." Quaternary Research **61**(1): 52-63.

Heier, K. S. and G. K. Billings (1970). Lithium. Handbook of Geochemistry. K. H. Wedepool. Berlin-Heidelberg, Springer Verlag**:** 3E1-3O1.

Holland, H. D. (1984). The Chemical Evolution of the Atmosphere and Oceans. Princeton, New Jersey, Princeton University Press.

Hughen, K. A., J. T. Overpeck, et al. (1996). "Rapid climate changes in the tropical Atlantic region during the last deglaciation." Nature **380**: 51-54.

Johnsen, S. J., H. B. Clausen, et al. (1992). "Irregular glacial interstadials recorded in a new Greenland ice core." Nature **359**(6393): 311-313.

Klitgaard-Kristensen, D., H. P. Sejrup, et al. (1998). "A regional 8200 cal. yr BP cooling event in northwest Europe, induced by final stages of the Laurentide ice-sheet deglaciation?" Journal of Quaternary Science **13**(2): 165-169.

Lehmkuhl, F. and F. Haselein (2000). "Quaternary paleoenvironmental change on the Tibetan Plateau and adjacent areas (Western China and Western Mongolia)." Quaternary International **65-66**: 121-145.

O'Brien, S. R., P. A. Mayewski, et al. (1995). "Complexity of Holocene climate as reconstructed form a Greenland ice core." Science **270**: 1962-1964.

Peihua, M. and Z. Pengxi (1999). "Lithium resources in China's salt lakes & its sustainable development." Bulletin of the Chinese Academy of Sciences **13**(3): ??

Prospero, J. M., P. Ginoux, et al. (2002). "Environmental characterization of global sources of atmospheric soil dust identified with the NIMBUS 7 Total Ozone Mapping Spectrometer (TOMS) absorbing aerosol product." Reviews of Geophysics **40**(1): 1002, doi:10.1029/2000RG000095.

Shi, Y. (2002). "Characteristics of late Quaternary monsoonal glaciation on the Tibetan Plateau and in East Asia." Quaternary International **97-98**: 79-91.

Siggaard-Andersen, M.-L., J. P. Steffensen, et al. (2002). "Lithium in Greenland ice cores measured by ion chromatography." Annals of Glaciology **35**: 243-249.

Sun, J. (2002). "Provenance of loess material and formation of loess deposits on the Chinese Loess Plateau." Earth and Planetary Science Letters **203**(3): 845-859.

Sun, J., M. Zang, et al. (2001). "Spatial and temporal characteristics of dust storms in China and its surrounding regions, 1960-1999: Relations to source area and climate." Journal of Geophysical Research **106**(D10): 10325-10333.

Thompson, L. G., E. Mosley-Thompson, et al. (1995). "Late Glacial Stage and Holocene tropical ice core records from Huascarán, Peru." Science **269**: 46-50.

Thompson, L. G., T. Yao, et al. (1997). "Tropical climate instability: The Last Glacial Cycle from a Qinghai-Tibetan Ice Core." Science **276**: 1821-1825.

von Grafenstein, U., H. Erlenkeuser, et al. (1998). "The cold event 8200 years ago documented in oxygen isotope records of precipitation in Europe and Greenland." Climate Dynamics **14**: 73-81.

Xuncheng, X. and F. Shangyue (2000). "Research progress of desert science in China." Chinese Science Bulletin **45**(24): 2209-2213.

Yang, X., K. T. Rost, et al. (2004). "The evolution of dry lands in northern China and in the Republic of Mongolia since the Last Glacial Maximum." Quaternary International **118-119**: 69-85.

Yu, G., S. P. Harrison, et al. (2001). Lake status records from China: Data Base Documentation. **4:** 1-243.

Yu, G., B. Xue, et al. (2003). "LGM lake records from China and an analysis of climate dynamics using a modelling approach." Global and Planetary Change **38**(3-4): 223-256.

Yu, G., B. Xue, et al. (2000). "Lake records and LGM climate in China." Chinese Science Bulletin **45**(13): 1158-1164.

Zhang, X. Y., R. Arimoto, et al. (1999). "Glacial and interglacial patterns for Asian dust transport." Quaternary Science Reviews **18**(6): 811-819.

Zhuo, Z., Y. Baoyin, et al. (1998). "Paleoenvironments in China during the Last Glacial Maximum and the Holocene Optimum." Episodes **21**(3): 152-158.

5: Soluble and insoluble chemistry of lithium in the EPICA DomeC ice core

This chapter is based a poster presented at the EPICA session, EGU, Nice, April 26'th, 2004, by: M.-L. Siggaard-Andersen (1,2), P. Gabrielli (3,4), J. P. Steffensen (2), Trine Strømfeldt (2), C. Barbante (3), C. Boutron (4), H. Fischer (1), H. Miller (1) .

1) Alfred Wegener Institute for Marine and Polar Research, Columbusstrasse, 27568 Bremerhaven, Germany. 2) Department of Geophysics, University of Copenhagen, Juliane Mariesvej 30, 2100 Kbh Ø, Denmark. 3) Department of Environmental Sciences, University of Venice, Ca' Foscari, I-30123 Venice, Italy. 4) Laboratoire de Glaciologie et Géophysique de l'Environnement, B.P. 96, 38402 Saint Martin d'Hères, Cedex, France.

Abstract: The EPICA DomeC (EDC) ice core has provided numerous records of mineral dust species obtained by different analytical methods. Using improved techniques of ion chromatography (IC) and Inductively Coupled Plasma - Sector Field Mass Spectroscopy (ICP-SFMS) it was possible to measure lithium, which was recently introduced among the dust species in the ice core records. The lithium ions are present in ice cores in various salts and clay minerals, but in very low concentrations. The two complementary EDC records of soluble and total contents of lithium, obtained using the IC and ICP-SFMS techniques, have given the opportunity to analyse soluble and insoluble properties of the dust material.

We investigated records of soluble Li^+ and Ca^{2+}, obtained by IC; records of insoluble mineral particles, obtained by Coulter Counting (CC); and records of total contents of Li^+ and Ba^{2+} obtained by ICP-SFMS. First we noticed that the solubility of Li changes significantly along the record. For the glacial period and for the Antarctic Cold Reversal (ACR) a large fraction, up to 75 %, of the total Li content is present as insoluble minerals whereas for the Holocene part all Li^+ is present as soluble salts. Our analysis suggests that the changes in solubility of Li along the EDC ice core are related to changes in mineral composition of the dust rather than to changes in pH of the ice.

A large difference in characteristics of the dust for the Holocene and for the glacial parts of the records is a general feature in our comparisons. In the glacial part the various records correlate linearly on logarithmic scales, indicating that the dust has been subject to mineral fractionation processes. For the Holocene part the correlations between different dust species is significantly different and much less pronounced.

Correlations of the soluble Li series with series for the various particle size fractions show that for the glacial part soluble Li is mainly related to particles with a diameter around 0.8-1μm, which is much smaller than the particle volume mode around 2 μm in diameter. In contrast the content of lithium in the Holocene part shows an increasing trend with increasing particle volume mode suggesting a relationship with large particles.

The trend for soluble Li over the transition shows some features similar to the unexpected increasing trend for the particle mode that recently was observed by Delmonte et al., (2002), in the EDC ice core.

From our analysis it seems that the dust characteristics in the EDC ice core for the glacial period represent a dust material that more or less disappeared after the ACR due to weakened conditions for transport, whereas the dust characteristics for the Holocene

part represent a partly different dust material that was introduced to DomeC after the transition.

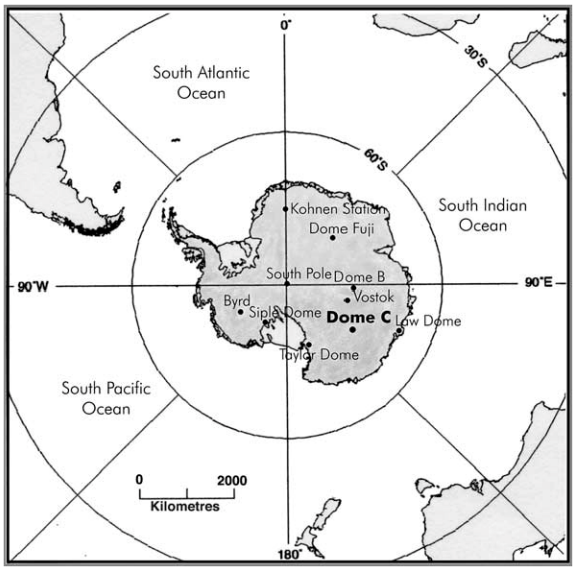

Figure 5.1: *Map of Antarctica with selected ice core sites marked on it (from Stenni et al., 2003). Located in West Antarctica are only the Byrd and Siple stations. The other sites are located in East Antarctica.*

5.1 Introduction

The EPICA DomeC ice core: Dome Concordia (DomeC) in East Antarctica (75° 06'S, 123° 23'E) is located 3233 m above sea level and 800 km from the nearest coast, which lies in the direction towards the Indian Ocean. In 1977-1978 an ice core (old DomeC) had already been drilled at this site (Lorius et al., 1979; Jouzel et al., 1982). In 1996/1997 the European Project for Ice Coring in Antarctica (EPICA) started a new DomeC deep drilling 50 km from the site of the old DomeC ice core. In the 1998/1999 field season the drill got stuck at a depth of 788 m and started again from the surface in the season 2000/2001 (EPICA community members, 2004). The 788 m of ice core obtained during the 1996-1999 seasons (EDC-96) covers the East Antarctic climate history over the last 45,000 years.

45,000 years East Antarctic climate history from the EDC-96 ice core: The 788 m long EDC-96 ice core covers the time period of Holocene and the later part of the last glacial, including the Antarctic warming events A2 and A1 with maximum temperatures around 45 ka BP and 38 ka BP respectively. The EDC-96 climate record of deuterium (δD), (Jouzel et al., 2001; Stenni et al., 2003) is shown in figure 5.2.
The last transition started around 19 ka BP, where Antarctic temperatures began slowly to increase until around 11 ka BP. Within this period an Antarctic Cold Reversal (ACR), 14-12.5 ka BP, interrupted the warming trend. After 12.5 ka BP Antarctic temperatures

started to increase again and reached shortly after a climatic optimum that lasted until 9.5 ka BP.
Schwander et al. (2001), established a tentative chronology for the 788 m long EDC-96 ice core using a simple flow model and well known time markers.
Synchronizations of Antarctic and Greenland ice core records using the global variations in the methane concentrations have shown that the ACR is roughly in anti phase with the Bølling/Allerød warming in the north (Blunier et al., 1997) and that the Antarctic warming events, A1 and A2, are asynchronous counterparts to the large Dansgaard/Oeschger events 8 and 12 (Blunier et al., 1998; Blunier and Brook, 2001), which are observed in the Greenland ice cores (e.g. Dansgaard et al., 1993). Stocker and Johnsen, (2003), explained the Antarctic/Greenland climate anti phase relationship in a simple thermodynamic model for the Atlantic see saw involving the southern ocean as a heat reservoir.

Records of chemical impurities: Antarctic ice core records of mineral dust and sea salt respond strongly to climate changes and reflect source strengths and conditions for transport with high concentrations for cold climate conditions (Petit et al., 1981; Legrand et al., 1988; Petit et al., 1999).

Soluble Na^+ is an indicator for the contents of sea salt and is used to determine sea salt contributions to other measured ionic species such as Ca^{2+}, which mainly is derived from mineral dust (Röthlisberger et al., 2002). The dust might contribute little to the soluble Na^+ contents (Röthlisberger et al., 2002; Bigler et al., in preparation).
Ca represents an alkaline constituent ($CaCO_3$) that balances the relatively high ice core concentrations of sulphuric acid and nitric acid, which are produced by marine biological activity in the Southern Ocean and locally in the atmosphere during lightning (Legrand et al., 1988). For dust concentrations above a certain threshold, acidity effects on freshly deposited sea salt chloride are limited (Röthlisberger et al., 2003). The opposite effect on solubility of mineral dust species from atmospheric acidity was considered by Laj et al., (1997).
Isotope analyses (Nd and Sr) of glacial dust material from the old DomeC and the Vostok ice cores have suggested a source provenance in Patagonia (Argentina) possibly mixed with a smaller fraction of dust from South Africa or Australia (Grousset et al., 1992; Basile et al., 1997). A more recent analysis of glacial dust from the EDC-96 (EDC from now on) ice core and from other ice cores located in East Antarctica confirms a Patagonian provenance (Delmonte et al., 2004). A very recent and more detailed analysis has shown that dust deposited during the glacial period in East Antarctica was distinctly of Patagonian origin but that the provenance might have changed within South America during the Holocene (Bory et al., oral presentation at the European Geosciences Union conference , Nice, April 2004).
Because of the very low snow accumulation rate at DomeC (1-3 $cm \cdot a^{-1}$) it is assumed that dust and sea salt aerosol in the EDC ice core mainly is deposited under dry conditions. Contents of chemical impurities are therefore often reported in terms of fluxes rather than in terms of concentrations (e.g. Röthlisberger et al., 2002).
In Greenland ice cores warmer climate conditions are associated with smaller particle size modes as atmospheric transport becomes less vigorous (Ruth et al., 2003). However in the EDC ice core an unexpected increase in particle size mode during the transition from the LGM to the Holocene was recently observed and explained as an effect of

better conditions for transport of dust to East Antarctica after the transition (Delmonte et al., 2002). Based on this finding it has been suggested that decreases in dust fluxes over the last transition in the EDC ice core reflect decreased source emission due to changes of weathering and vegetation cover in the source environment (Röthlisberger et al., 2002; Delmonte et al., 2002). However a more recent work by Delmonte et al., (2004), has shown that the increase in particle size mode observed in the EDC ice core is a regional effect in the DomeC area indicating an increased complexity of dust transport to East Antarctica.
Although the records of sea salt and dust show similar patterns, changes in sea salt fluxes are considered differently from changes in dust fluxes. The decrease in the sea salt flux over the transition has been attributed to a decreasing intensity of meridional atmospheric circulation (Stenni et al., 2001), a decreased contribution to sodium from dust and a reorganization of the atmospheric circulation after the ACR (Röthlisberger et al., 2002), and a decreased extent of sea ice (Wolff et al., 2003).
Changes in source strength and environments and changes in conditions for transport will affect the characteristics of the dust material differently. Here we performed a detailed investigation of chemical and physical properties of the EDC dust material as reflected in the records of soluble Li^+ and Ca^{2+}, total Li and Ba, dust mass and size characteristics in order to see how these properties are affected by climate changes.

5.2 Data and experimental methods

Soluble ions: From the top 588 m of the EDC-96 ice core 55 cm long strips for IC analysis were cut in the field and distributed between 5 European laboratories, where the strips where manually decontaminated and cut into 2.5 or 5 cm sub-samples before they were melted and measured.
From 588 m to 788 m samples for IC analyses were collected from excess melt water during continuous flow analysis. The sample depth interval varies roughly between 10 cm and 50 cm depending on the amount of excess melt water from the flow analysis. The IC Na and Ca records are measured in parallel with the high resolution Na and Ca records obtained by Continuous Flow Analysis (Littot et al., 2002).
The IC record shows strong inter-laboratory dissimilarities in average contents for several components (Littot et al., 2002). However the IC Na record from all 5 laboratories over the whole length of the ice core is relatively consistent (see figure 5.2).
For this work we have used data measured at the Dept. of Geophysics, University of Copenhagen, where an optimized IC technique was developed for the detection of soluble Li and where manually cut IC samples also were analysed by Coulter Counter for concentrations and size characteristics of insoluble particles. The IC technique used is described in Chapter 9.

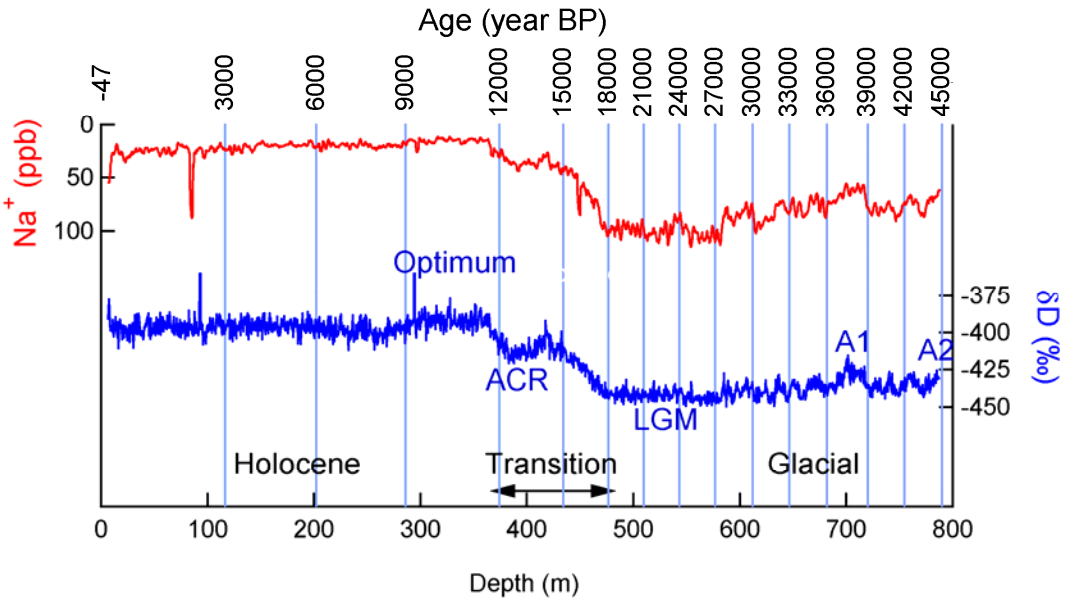

Figure 5.2: *The EDC-96 IC-record of soluble Na^+ obtained from 5 European laboratories and the deuterium record (δD) (Jouzel et al., 2001, and Stenni et al., 2003). The sodium record is shown on a reversed axis for comparisons with the δD record. The records reflect the Antarctic warm events A1 and A2, the Last Glacial Maximum (LGM), the transition, the Antarctic Cold Reversal (ACR), and the Holocene. The dating shown is based on the EDC-1 chronology from Schwander et al., (2001).*

Particle characteristics: Particle concentrations and size characteristics used in this work was measured at the Geophysics department, University of Copenhagen from excess IC sample volumes. From each manually cut sample bag, 4-6 samples had a sufficient volume to be analysed using Coulter Counting.
To 4.8 ml of sample from the IC measurements 1.2 ml 10% NaCl were added and measured in a Coulter Counter with a 30 µm aperture (see figure 5.3). Particles in a 500 µl sample volume were counted into 256 size resolving channels corresponding to logarithmic diameter intervals and covering the size range of 0.4-14 µm. The calibration constant K_d of 321.46 was obtained using 2.20 µm diameter latex particles. With the current set to 1600 µA and the gain set to 8, particle diameters corresponding to each channel was calculated as:

$$Diameter = K_d \frac{1}{\sqrt[3]{gain \cdot current}} \cdot (2)^{\left(\frac{X-256}{50}\right)}.$$

The log linearity of particle size detection was tested using latex particles with a radius of 5.06 µm.

Particles in a liquid suspension are not homogeneously distributed, and they have a tendency to settle by gravity. Repeated sample particle counting showed in most cases

reproducibility better than ±15%. In the size distribution, around 0.7 µm, a sharp artificial peak appeared, possibly due to micro bubbles generated in the purifying water system. This peak does not disturb the particle log normal distribution with a volume mode around 2 µm in diameters.

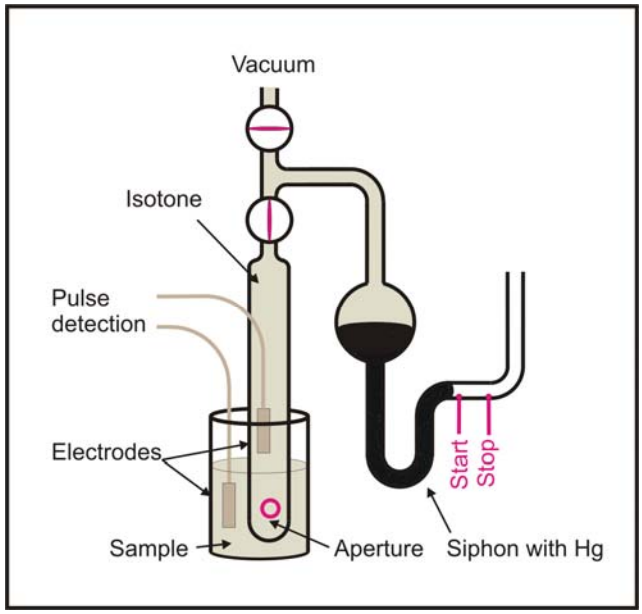

Figure 5.3: *Basic principle of a Coulter Counter. Sample flow through the aperture is driven by the siphon effect. The distance between the two contacts in the siphon corresponds to a well defined volume. The sample is added NaCl solution to obtain electrolytic properties, so an electrical current can run between the two electrodes. When particles are passing through the aperture, they affect the electrical resistance, and are detected as a pulse in the current. The size of the pulse depends on particle volume. The setup is placed inside a Faraday cage to reduce electrical noise.*

Total elemental contents: Discrete 55 cm sample strips for ICP-SFMS measurements were decontaminated in ultra-clean environments at the Laboratoire de Glaciologie et Géophysique de l'Environnement, Grenoble. From each strip two adjacent samples with a length of 20 cm were obtained. From each sample a 5ml aliquot was analysed for total Li and Ba, both essentially of crustal origin, using using ICP-SFMS at the Department of Environmental Science, University of Venice (Planchon et al., 2001; Gabrielli et al., 2004).

5.3 Analyses and results

The records of soluble and insoluble lithium: The EDC record of lithium is the first Antarctic lithium ice core record. The soluble Li/Na ratio in the ice core is 8-10 times higher than the corresponding molar ratio of 0.00006 in sea water (Holland, 1984). Therefore we consider soluble Li as well as total Li in the EDC ice core to be essentially a mineral dust species. The detection limit for Li is around 1 ppt for both IC (Siggaard-Andersen et al., 2002) and ICP-SFMS (Planchon et al., 2001; Gabrielli et al., 2004) which is sufficient for quantitation of Li in the EDC ice core.

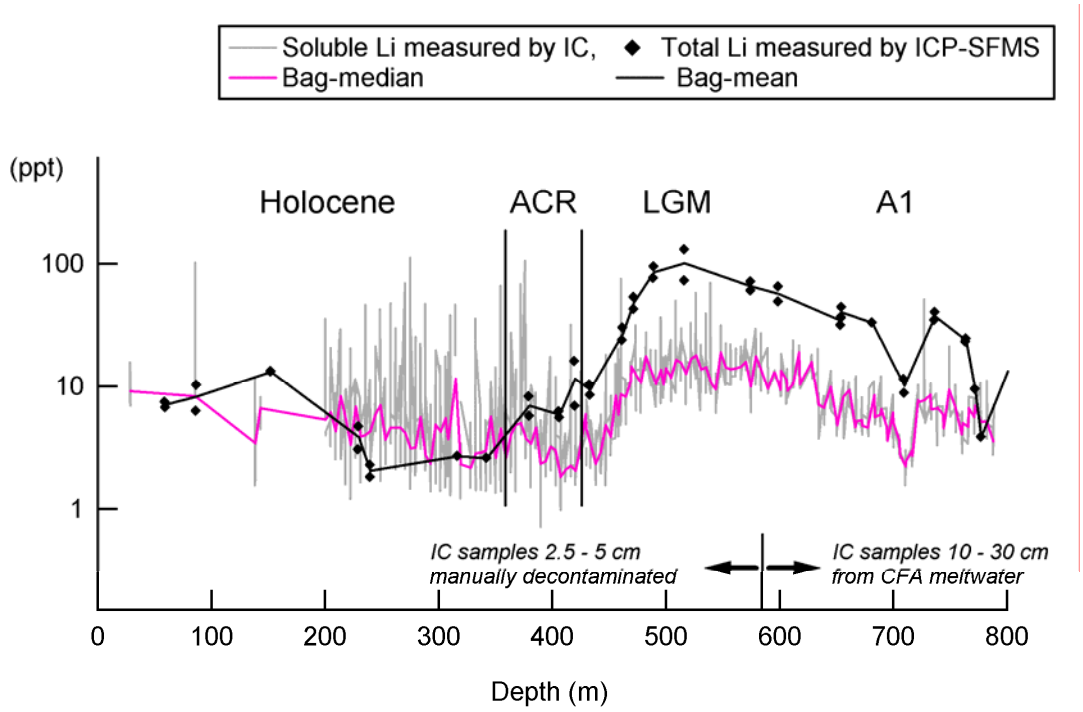

Figure 5.4: *Soluble lithium concentrations measured by IC versus total lithium concentrations measured by ICP-SFMS. The detection limit is 1 ppt for both methods.*

The record of soluble Li shows high spikes in the upper part of the ice core (see Figure 5.4). This could be an effect of the sampling procedure which was changed at around 590 m from manual sample cutting of frozen samples to sampling from excess melt water from continuous flow analysis. However the frequency and magnitude of spikes varies within the section of manually cut samples and seems to be affected by sample time interval.

For the IC measurements the average blank value was below 1 ppt; therefore it is unlikely that blank contributions have affected the measured sample values. Inaccuracy of the Li concentrations was less than 10 % in the interval of 1.4 – 5600 ppt. We therefore have great confidence with the record of soluble Li^+. Although we can not explain the occurrence of high spikes in the Holocene part of the record we believe they represent impurities in the ice; not an artefact from sampling or measurements. Bag-means and bag-medians represent means and medians of 55 cm ice core strips. Since

bag-medians are not influenced by the spikes we have preferred to use those instead of bag-means.

A comparison of the two Li records shows that the solubility of Li changes significantly along the record. For the glacial period and until the end of the ACR up to 75 % of the Li is insoluble whereas for the Holocene part apparently all of the Li is soluble.
As expected for warm climate periods, concentrations of total Li decrease significantly by the end of the ACR whereas concentrations of soluble Li seem to be unaffected by the warming after the ACR.

Mineral fractionation process: The analyses presented here are based on simple hypotheses of source strength and transport. A further simplification is the use of concentrations rather than fluxes as we do not correct for sea salt contributions to the various species analysed. The sea salt contribution to soluble Ca^{2+} is 24 % ± 10 % for the Holocene, and 8 % ± 2 % for the glacial period, which is not a negligible amount, yet it does not affect our analysis.

Fractionation of mineral dust during long-range atmospheric transport is a well known phenomenon (e.g. Johnson, 1976, and Arnold et al., 1998). Dust size and mineral characteristics in a moving air parcel is modified over time due to different aerosol life-times, τ, for different size fractions of the particles. The time development of concentrations in a moving air parcel for an aerosol species with life-time τ, can be expressed as:

$$C(t) = C_0 \exp\left(-\frac{t - t_0}{\tau}\right).$$

or $\ln C(t) = -(t - t_0)/\tau + \ln C_0$.
From the expression above it follows that, if the dust records mainly reflect climate induced variations in transport times, different fractions of the dust material will be related through a power law, i.e. linearly related on logarithmic scales. This effect of fractionation on ice core concentrations will be described more detailed in chapter 6.

Soluble Li enrichment in Holocene: For the glacial part, soluble Li^+ and Ca^{2+} are almost linearly correlated with a Li^+/Ca^{2+} ratio around 0.001. For LGM, however, the relative concentrations of Li^+ are slightly lower (see Figure 5.5 top right). During the Holocene the correlation between soluble Li^+ and Ca^{2+} deteriorates and the relative contents of soluble Li^+ are markedly higher.

Total Li and Ba: In a log-log plot, the ratio between total contents of Li and Ba shows a linear decrease with increasing Ba contents for the glacial period (see figure 5.5 top left). This trend indicates an effect of mineral fractionation during transport, where Li has a longer atmospheric lifetime than Ba (see chapter 2.6). In the glacial part the variation of the total Li content is mainly due to variations in contents of insoluble Li (see Figure 5.4). The trend for the Li/Ba ratio seen in figure 5.5 therefore indicates that both soluble and insoluble Li has a larger atmospheric life-time than Ba.
For the Holocene the correlation between Li and Ba is missing and the content of Li is relatively larger than corresponding to the trend for the glacial part of the record. This indicates that the higher relative content of soluble Li^+ in Holocene, as seen in Figure

5.5 top right, is not an effect of pH in the ice but is due to a relatively higher content of soluble Li rich minerals.

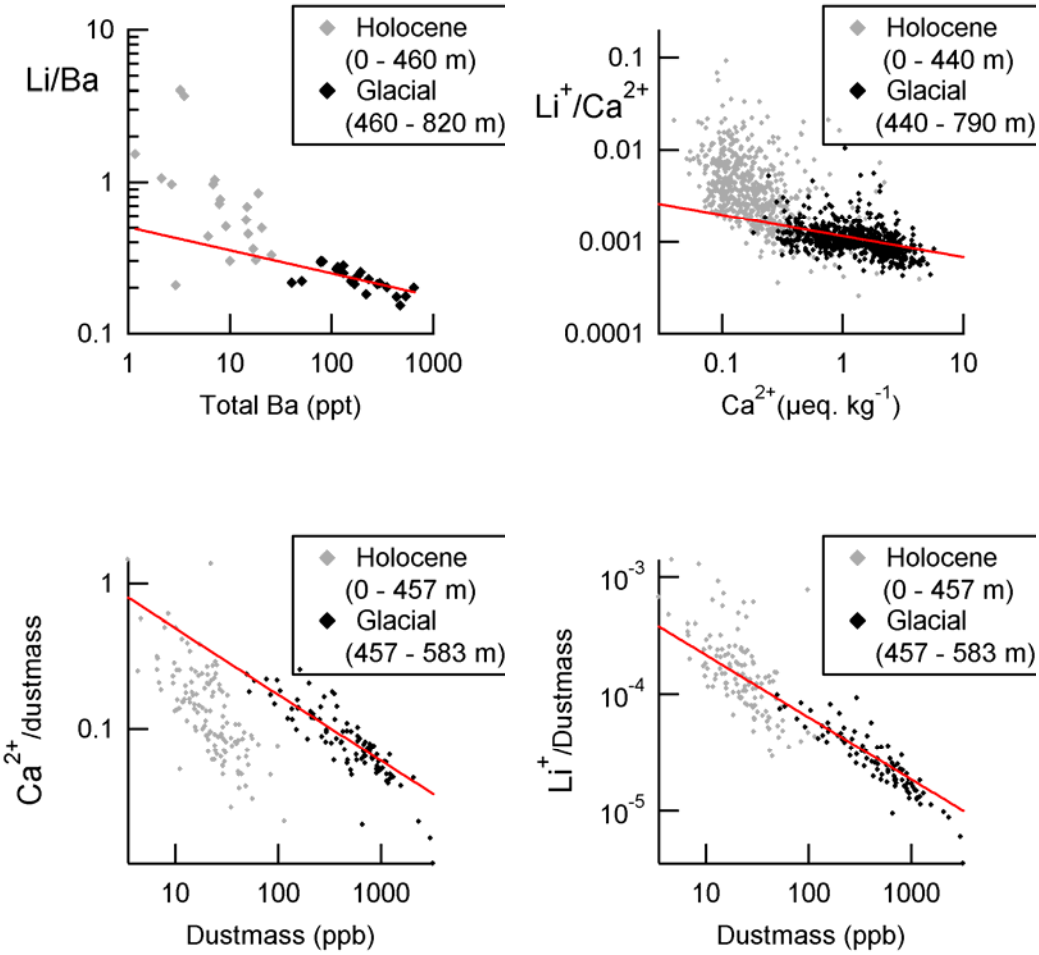

Figure 5.5: *Trends in relative contents of dust species. A linear trend on log-scales indicates a transport effect. The red lines show linear trends (on log-scales) for the glacial parts. Top left; total Li/Ba ratio versus total Ba. Top right; soluble Li^+/Ca^{2+} ratio versus soluble Ca^{2+}. Bottom left; soluble Ca^{2+}/dust mass ratio versus dustmass. Bottom right; soluble Li^+/dust mass ratio versus dustmass. All ratios are mass ratios except for the Li^+/Ca^{2+} ratio (top right) that is given in equivalents ratio. The conversion factors for $\mu eq \cdot kg^{-1}$ to ppb is 6.94 for Li and 20.04 for Ca (molar mass divided by charge number).*

Soluble Li^+ and Ca^{2+} versus insoluble dustmass: The Ca^{2+}-dust mass ratio and the Li^+-dust mass ratio for the glacial period show a decreasing trend with increasing dust mass consistent with a transport effect (see figure 5.5 bottom left and right). Such trends are also seen for the Holocene period. The shift in position of the trend line seen for the Li^+-dust mass ratio could be an effect of a change in snow accumulation, but for the

Ca^{2+}-dust mass ratio, the trend for the Holocene part is markedly different from the trend for the glacial period.

Particle characteristics: The volumes (masses), *V*, of dust particles versus diameter, *d*, are nearly log-normal distributed. Size distributions of insoluble dust particles are characterized by the modes (μ; diameter or radius) and the relative standard deviation (σ = std − log(μ)) of a log-normal distribution of $\partial V / \partial \log(d)$.
An increase in particle size mode over the transition was recently observed in the EDC ice core (Delmonte et al., 2002). The particle characteristics from EDC shown here is consistent with the one from Delmonte et al. (2002). The observed increase in size mode is opposite to what would be expected on the basis of observations in Greenland ice cores, where warmer climate conditions are associated with smaller particle size mode as atmospheric transport becomes less vigorous (Ruth et al., 2003). At the beginning of the transition the particle size mode decreases, as expected, synchronously with the mass concentrations. This tendency shifts abruptly at a depth of around 450 m where the particle size mode increases and remains high all through ACR and the Holocene while the dust mass decreases as the climate is getting warmer (see Figure 5.6).

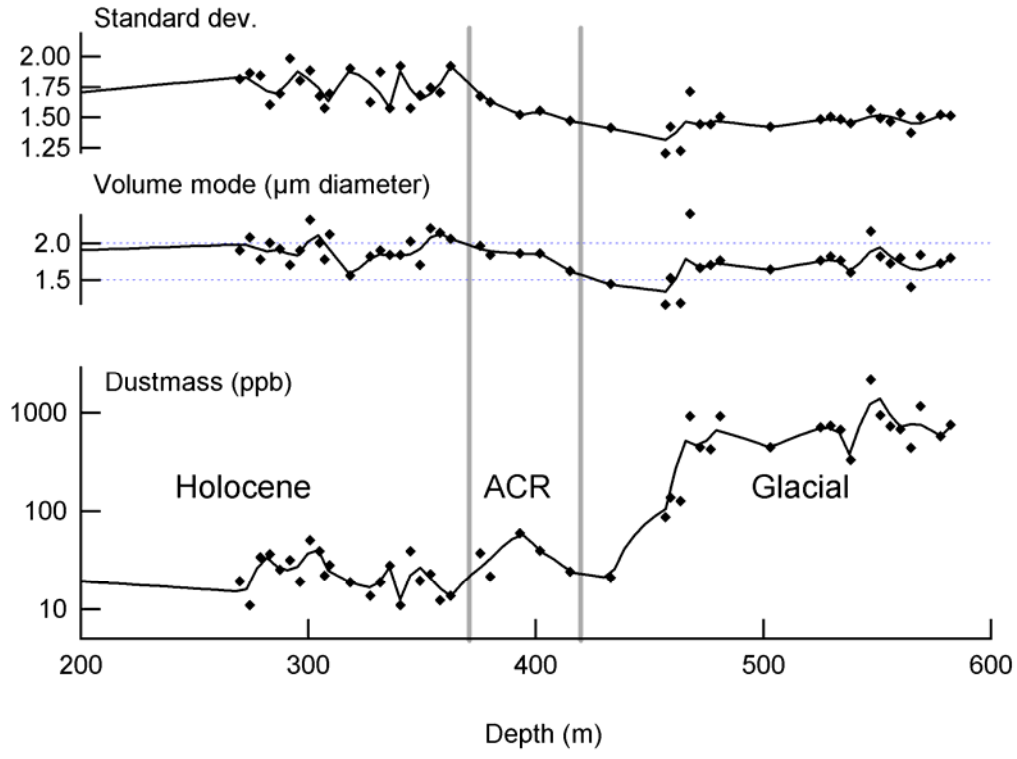

Figure 5.6: *Particle characteristics measured using Coulter Counter and evaluated on bag averages. The bottom curve shows dust mass concentrations. The middle curve shows particle volume mode and the top curve shows the relative standard deviation of the log-normal volume distribution. The size mode shows an unexpected increase after the transition.*

Soluble Li^+ and Ca^{2+} and size characteristics: We have correlated series of soluble Li and Ca concentrations with series of particle size fractions. The Holocene and glacial

sub-series were correlated separately. The size resolving channels from the Coulter Counting were added together three by three.

Influence on correlations from Poison statistics of particle counts for a given size interval was evaluated as the factor

$$\frac{\sqrt{N^2 - \left(\sum \sqrt{n}\right)^2}}{N}$$

where N is the total number of counts along the series and n is the number of counts in each sample. The factor is insignificant for a wide range of sizes. The factor was below 0.9 for particles larger than 6.6 μm for the glacial series, and for particles larger than 3.5 μm for the Holocene series.

For the glacial period the observed correlation curves for Li^+ and Ca^{2+} are nearly proportional. Soluble Ca^{2+} correlates best with particles around 1 μm in diameter and soluble Li^+ correlates best with particles around 0.8-1.0 μm in diameter (see Figure 5.7, left) indicating that soluble Li^+ and Ca^{2+} both mainly are related to the very small particles that usually is dominated by clay minerals.
For the Holocene series correlations are limited because of less accuracy in the low concentration range both for particle counts and for IC measurements (see Figure 5.7 right). However using bag-medians for Li^+ and bag-averages for particle characteristics there seems to be for the Holocene part an increasing trend for Li^+ concentrations with increasing size mode (see Figure 5.8, right), suggesting that Li^+ in this part is associated with large particles. To verify the $R^2 = 0.33$ for the correlation between Li^+ concentrations and size mode, we performed "students test" and found for the 95 % significance limit with $t = 1.708$ and a degree of freedom $f = 25$: $R^2 = (f / t^2 + 1)^{-1} = 0.10$ which means that the trend between Li^+ concentrations and size mode during the Holocene is significant.
A relationship with very small particles for soluble Li^+ in the glacial part is further confirmed from the increasing trend of the soluble Li^+-dust mass ratio against the mass fraction of particles in the interval 0.9-1.1 μm diameter (see Figure 5.8, left). Soluble Ca^{2+} has a similar relationship with the 0.9-1.1 μm size fraction (not shown) in the glacial part.

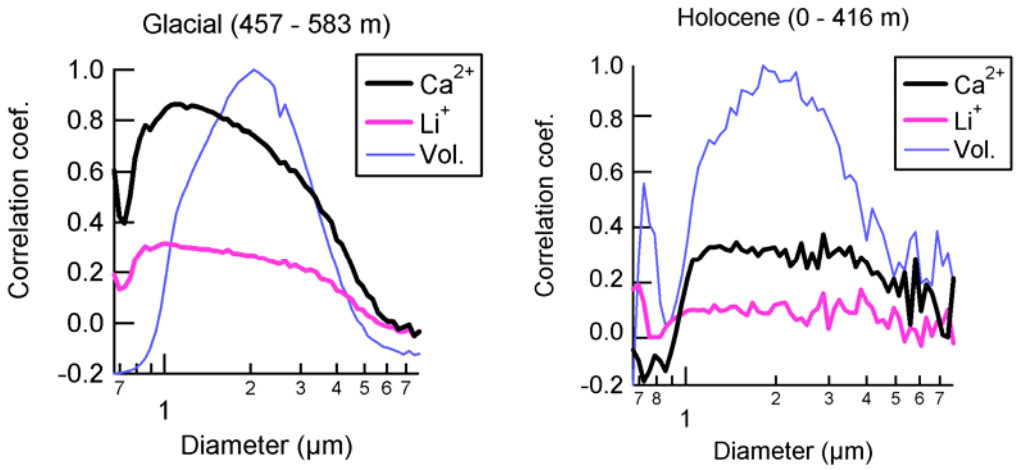

Figure 5.7: *Correlations between series of soluble Li^+ (pink) and Ca^{2+} (black) concentrations and particles for varying size intervals: for the glacial (left) and for the Holocene (right). The thin blue curves indicate the volume distribution (Vol.). For the glacial the correlations show that both Li^+ and Ca^{2+} are associated with small particles.*

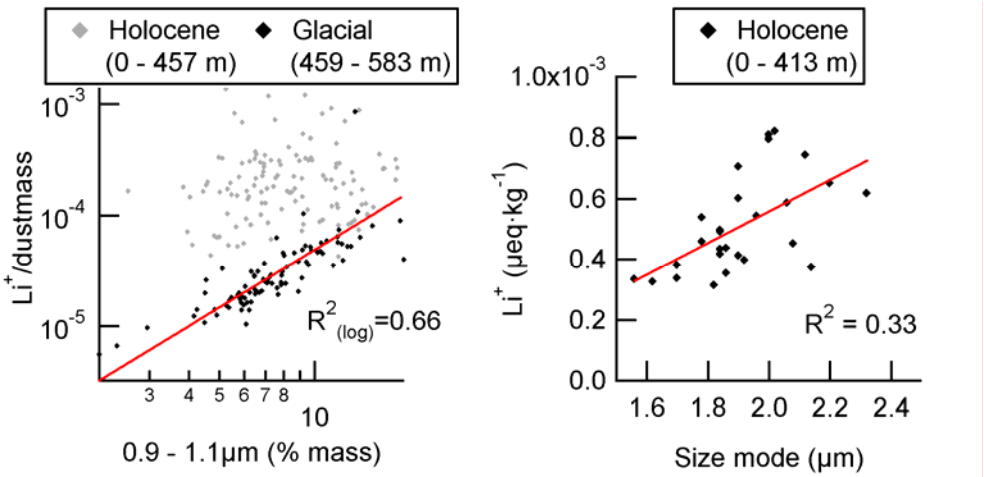

Figure 5.8: *The left figure shows the soluble Li^+-dustmass mass ratio versus the mass fraction of particles in the size interval 0.9-1.1 µm diameter. To the right is shown Li^+ bag-median concentrations versus particle volume mode (diameter) for Holocene bag averages.*

5.4 Discussion

Based on the linear relationships on log-scales for the glacial dust material, we have matched different records on different logarithmic scales (see Figure 5.9).
At the depth of around 450 m (after the onset of the transition), which corresponds to approximately 16 ka BP, the curves starts to diverge and from a depth of around 360 m (end of the ACR) they propagate in the plot at different levels, illustrating the change in dust characteristics.

Changes in dust concentrations along the series of the last glacial in the EDC ice core (e.g. during A1 and A2) has in recent papers been explained by changes in source load (Delmonte et al., 2002), (Röthlisberger et al., 2002). However for the period from 45 ka BP and until around 16 ka BP (around 458 m depth), the chemical and size characteristics seem to be mainly affected by fractionation during transport. This means that during the glacial period source load could be nearly constant and that warming is likely to be associated with less favorable conditions for dust transport.

Around 16 ka BP the dust material changes character abruptly. Our analyses have shown that the different chemical and size characteristics of the glacial and the Holocene dust material cannot be explained as effects of changed transport time, snow accumulation rates or pH.
The change in particle mode after the transition observed in the EDC ice core was recently explained as a regional transport effect involving vertical fractionation effects in the transport system (Delmonte et al., 2004). Some observations done in the present analysis are consistent with this. The Ca^{2+}-dust mass ratios in Holocene are similar to the corresponding glacial ratios although concentrations in the ice core are much lower during Holocene. However the trend for the particle size mode over the transition shows similarities with the trend for soluble Li^{+} concentrations supporting a connection between the high Li^{+} concentrations and the large particle sizes for Holocene, which is in contrast to the glacial part where soluble Li^{+} is related to the very small particles. The increased relative Li content for Holocene and the change in the matching size fraction for Li^{+} combined, suggest that chemical and size characteristics of the dust in the EDC ice core for the Holocene and the glacial respectively represent two different dust materials. In the glacial period, Li containing dust material seems to be related to the clay fraction, while in the Holocene dust material the 100% solubility of Li indicates that it is related to evaporite minerals.

The relatively weak correlations between dust species together with a large standard deviation of particle sizes for the Holocene could be an effect of a mixed composition of different dust materials during the Holocene.

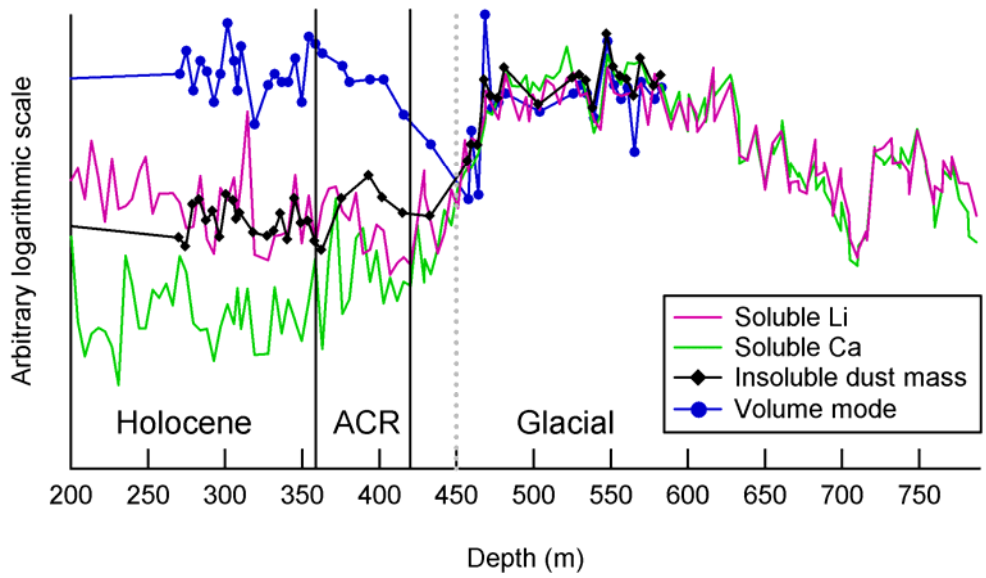

Figure 5.9: *Reconstruction of the change in particle characteristics over the transition. Soluble Li^+ and Ca^{2+} are bag-medians and bag-means respectively. Dust mass and volume mode are evaluated on the basis of bag-means. Around the depth of 450 m (after the onset of the transition) the curves begin to diverge and from around 360 m (end of ACR) they propagate at different levels.*

5.5 Conclusions

Based on the two complementary records of soluble and total Li from the EDC ice core we have made detailed studies of the chemical properties of the EDC dust material.
A high content of soluble Li^+ relative to Ca^{2+} during the Holocene could be an acidity effect. A comparison of total Li and Ba, with Ba as a crustal indicator, showed that the dust was enriched in Li during the Holocene while a comparison with dust mass showed instead depletion in the Ca content during the Holocene. These properties indicate different chemical characteristics of the dust material for the glacial and for the Holocene.
During the glacial, the mineral dust had well defined properties, and seems to have been affected mainly by transport times as indicated by a linear relationship between different dust species on log-scales. At around 16 ka BP, 3 ka after the onset of the transition, the characteristics of the dust material changed abruptly. In the glacial dust material Li seems to be related to the clay fraction whereas in the Holocene dust material Li appears to be related to evaporate minerals.

Insoluble Li is representing a glacial dust material, which more or less disappeared from the air mass at DomeC after the Antarctic Cold Reversal; possibly due to a weakened transport as climate became warmer. The large particle mode after the transition seems to be associated with a different dust material that was introduced to the air mass over

DomeC around 16 ka BP and which co-existed there with the glacial dust material during the Antarctic Cold Reversal.

Acknowledgement: This work is a contribution to the EPICA project. The EPICA project is a joint ESF/EC scientific programme, funded by the European commission and national contributions from Belgium, Denmark, France, Germany, Italy, the Netherlands, Norway, Sweden, Switzerland, and the United Kingdom.

5.6 References

Arnold, E., J. Merrill, et al. (1998). "The effect of source area and atmospheric transport on mineral aerosol collected over the North Pacific Ocean." Global and Planetary Change **18**(3-4): 137-159.

Basile, I., F. E. Grousset, et al. (1997). "Patagonian origin of glacial dust deposited in East Antarctica (Vostok and Dome C) during glacial stages 2, 4 and 6." Earth and Planetary Science Letters **146**: 573-589.

Bigler, M. (2004). "The continental contribution to the water-soluble mean aerosol deposited on the East Antarctic plateau derived from the EPICA Dome C ice core." in preparation.

Blunier, T. and E. J. Brook (2001). "Timing of millennial-scale climate change in Antarctica and Greenland during the last glacial period." Science **291**: 109-112.

Blunier, T., J. Chappellaz, et al. (1998). "Asynchrony of Antarctic and Greenland climate change during the last glacial period." Nature **394**: 739-743.

Blunier, T., J. Schwander, et al. (1997). "Timing of the Antarctic cold reversal and the atmospheric CO_2 increase with respect to the Younger Dryas event." Geophysical Research Letters **24**(21): 2683-2686.

Dansgaard, W., S. J. Johnsen, et al. (1993). "Evidence for general instability of past climate from a 250-kyr ice-core record." Nature **364**(6434): 218-220.

Delmonte, B., J. R. Petit, et al. (2004b). "Dust size evidence for opposite regional atmospheric circulation changes over East Antarctica during the last climatic transition." Climate Dynamics(in press).

Delmonte, B., J. R. Petit, et al. (2002). "Glacial to Holocene implications of the new 27000-year dust record from the EPICA Dome C (East Antarctica) ice core." Climate Dynamics **18**(8): doi: 10.1007/s00382-001-0193-9.

EPICA community members (2004). "Eight glacial cycles from an Antarctic ice core." Nature **429**(6692): 623-628.

Gabrielli, P., F. Planchon, et al. (2004). "Trace elements in Vostok Antarctic ice during the last four climatic cycles." Submitted to Earth Planet. Sci. Lett.

Grousset, F. E., P. E. Biscaye, et al. (1992). "Antarctic (Dome C) ice-core dust at 18 k.y. B.P.: Isotopic constraints on origins." Earth and Planetary Science Letters **111**: 175-182.

Holland, H. D. (1984). The Chemical Evolution of the Atmosphere and Oceans. Princeton, New Jersey, Princeton University Press.

Johnson, L. R. (1976). "Particle-size fractionation of eolian dusts during transport and sampling." Marine Geology **21**: M17-M21.

Jouzel, J., V. Masson, et al. (2001). "A new 27 ky high resolution East Antarctic climate record." Geophysical Research Letters **28**(16): 3199-3202.

Jouzel, J., L. Merlivat, et al. (1982). "Deuterium excess in an East Antarctic ice core suggests higher relative humidity at the oceanic surface during the last glacial maximum." Nature **299**(5885): 688-691.

Laj, P., G. Ghermandi, et al. (1997). "Distribution of CA, Fe, K, and S between soluble and insoluble material in the Greenland Ice Core Project ice core." Journal of Geophysical Research **102**(C12): 26615-26623.

Legrand, M. R., C. Lorius, et al. (1988). "Vostok (Antarctica) ice core: Atmospheric chemistry changes over the last climatic cycle (16,000 years)." Atmospheric Environment **22**(2): 317-331.

Littot, G. C., R. Mulvaney, et al. (2002). "Comparison of analytical methods used for measuring major ions in the EPICA Dome C (Antarctica) ice core." Annals of Glaciology **35**: 299-305.

Lorius, C., L. Merlivat, et al. (1979). "A 30,000-yr isotope climatic record from Antarctic ice." Nature **280**: 644-648.

Petit, J.-R., M. Briat, et al. (1981). "Ice age aerosol content from East Antarctic ice core samples and past wind strength." Nature **293**(5831): 391-394.

Petit, J. R., J. Jouzel, et al. (1999). "Climate and atmospheric history of the past 420,000 years from the Vostok ice core, Antarctica." Nature **399**: 429-436.

Planchon, F. A. M., C. F. Boutron, et al. (2001). "Ultrasensitive determination of heavy metals at the sub-picogram per gram level in ultraclean Antarctic snow samples by inductively coupled plasma sector field mass spectrometry." Analytica Chimica Acta **450**(1-2): 193-205.

Röthlisberger, R., R. Mulvaney, et al. (2003). "Limited dechlorination of sea-salt aerosols during the last glacial period: Evidence from the European Project for Ice Coring in Antarctica (EPICA) Dome C ice core." Journal of Geophysical Research **108**(D16): 4526, doi:10.1029/2003JD003604.

Röthlisberger, R., R. Mulvaney, et al. (2002). "Dust and sea salt variability in central East Antarctica (Dome C) over the last 45 kyrs and its implications for southern high-Iatitude climate." Geophysical Research Letters **29**(20,1963): doi:I0.1029/2002GL015186.

Ruth, U., D. Wagenbach, et al. (2003). "Continuous record of microparticle concentration and size distribution in the central Greenland NGRIP ice core during the last glacial period." Journal of Geophysical Research **108**(D3): 4098, doi:10.1029/2002JD002376.

Schwander, J., J. Jouzel, et al. (2001). "A tentative chronology for the EPICA Dome Concordia ice core." Geophysical Research Letters **28**(22): 4243-4246.

Siggaard-Andersen, M.-L., J. P. Steffensen, et al. (2002). "Lithium in Greenland ice cores measured by ion chromatography." Annals of Glaciology **35**: 243-249.

Stenni, B., J. Jouzel, et al. (2003). "A late-glacial high-resolution site and source temperature record derived from the EPICA Dome C isotope records (East Antarctica)." Earth and Planetary Science Letters **217**: doi:10.1016/S0012-821X(03)00574-0.

Stenni, B., V. Masson-Delmotte, et al. (2001). "An oceanic cold reversal during the last deglaciation." Science **293**: 2074-2077.

Stocker, T. F. and S. J. Johnsen (2003). "A minimum thermodynamic model for the bipolar seesaw." Paleoceanography **18**(4): 1087, 10.1029/2003PA000920.

Wolff, E. W., A. M. Rankin, et al. (2003). "An ice core indicator of Antarctic sea ice production?" Geophysical Research Letters **30**(22,2158): doi:10.1029/2003GL018454.

6: Ion chemistry in the NorthGRIP ice core as a signal of aerosol transport

This chapter is based on work presented at: Swiss Polar Research Summer School, Riederalp 2002 (poster); AGU fall meeting, San Fransisco December 2002, A72A-0150 (poster); EGS-AGU-EUG joint assembly, Nice, France April 2003, CR7 EAE03-A-11932 (oral).

Authors:

[1]Marie-Louise Siggaard-Andersen, [1]Hubertus Fischer, [2]Jørgen Peder Steffensen, [4]Margareta Hansson, [3]Regine Röthlisberger, [5]Kumiko Goto-Azuma, [6]Matthias Bigler, [1]Heinz Miller

Addresses:

(1) Alfred Wegener Institute for Polar and Marine Research, Columbusstrasse, Bremerhaven 27568, Germany, (2) Department of Geophysics, University of Copenhagen, Juliane Maries Vej 30, Copenhagen 2100, Denmark, (3) NCCR-Climate University of Bern Erlachstrasse 9a, CH-3012 Bern (Switzerland), (4) Department of Physical Geography and Quaternary Geology, University of Stockholm , Stockholm 106 91, Sweden, (5) National Institute of Polar Research, 1-9-10 Kaga, Itabashi-ku, Tokyo 173-8515, JAPAN, (6) Physikalisches Institut der Universitaet Bern, Abteilung für Klima- und Umweltphysik, Sidlerstrasse 5, CH-3012 Bern.

Abstract: The NorthGRIP ice core provides continuous records of sea salt and mineral dust aerosols from the last glacial period. A large number of soluble ions were analysed by ion chromatography and have opened up for new possibilities looking into details in the relationship between ion composition and climate conditions. Concentrations of sea salt and dust measured in Greenland ice cores reflect source strength and conditions for long-range transport of aerosols.

We have analysed the NorthGRIP record of Li^+, Na^+, K^+, Mg^{2+}, Ca^{2+}, F^-, Cl^-, and SO_4^{2-} that are mainly derived from sea salt and mineral dust aerosol. We introduce a statistical method to extract characteristics of ion composition. From this characteristics, source strengths and transport properties can be quantified.

Changes in ion composition seem to be related to changes in particle size distribution as an effect of fractionation during atmospheric transport. Applying a simple transport model, variations in ion concentrations can be explained in terms of large-scale transport patterns and varying transport efficiency. Our analysis of ion compositions during Marine Isotope Stage 3 suggests that ion concentrations during this period are mainly affected by changes in transport efficiency. Furthermore our analysis shows that large-scale transport patterns changed only little during the D/O events.

6.1 Introduction

Ice cores from Greenland provide information on the climate during the last glacial cycle. This information is based on records of stable isotopes in the ice and of various chemical aerosol species. The isotope records from the GRIP (Greenland ice core project) and GISP2 (Greenland ice sheet project 2) ice cores revealed details of 24 interstadials, the so-called Dansgaard/Oeschger (D/O) events, which are characteristic large abrupt warm climate events disrupting the glacial conditions (Dansgaard et al., 1993). During recent years a new deep ice core from the North Greenland Ice core Project (NorthGRIP) has been drilled at 72.20 °N, 42.32 °W, 324 km from the Greenland Summit, with the goal of providing high resolution details of the climate history during the last interglacial period (Dahl-Jensen et al., 2002). The NorthGRIP drilling reached bedrock in the summer of 2003 and recovered a new high-resolution and undisturbed climate record reaching back into the last interglacial period (NorthGRIP members, 2004), adding new continuous records of the climate history of the last glacial cycle to the records from GRIP and GISP2.

Many detailed analyses of chemical impurities were performed on the GRIP and GISP2 ice cores. Results from these analyses are presented in numerous papers in the Journal of Geophysical Research special issue on Greenland Summit Ice Cores (JGR special issue, 1997). A continuous record of soluble ions was measured along the GISP2 ice core using ion chromatography (IC), providing a complete series of ion chemistry over the last glacial cycle (Mayewski et al., 1994; O'Brien et al., 1995; Mayewski et al., 1997). In the GRIP ice core, continuous high-resolution records of soluble calcium (Ca^{2+}), ammonium (NH_4^+), hydrogen peroxide (H_2O_2), and formaldehyde (HCHO) were measured using continuous flow analysis (Fuhrer et al., 1993; Fuhrer et al., 1996; Fuhrer et al., 1999). In the GRIP ice core, IC analyses of soluble ions were performed discontinuously along the ice core (Legrand et al., 1993; De Angelis et al., 1997; Legrand et al., 1997; Fuhrer and Legrand, 1997) and additionally in high resolution in selected depth intervals where also insoluble dust characteristics were measured using Coulter counting (De Angelis et al., 1997; Steffensen, 1997). In the GRIP ice core detailed micro-analyses on dust samples from selected depth intervals were also performed in order to obtain records of mineral characteristics (Maggi, 1997) and soluble/insoluble contents of Ca, Fe, K, and S (Laj et al., 1996; Laj et al., 1997).

The chemical impurities in Greenland ice cores are mainly derived from sea salt and mineral dust aerosols, which have been long-range wind transported from marine and continental source areas respectively. High ice core concentrations of dust and sea salt reflect cold climate conditions with enhanced source load and better conditions for transport.

The analyses of dust and sea salt in the GRIP and GISP2 ice cores have led to many discussions on possible climate effects acting on the cycles of dust and sea salt aerosol. A major issue in these discussions has been which factor is the most important for variations in fluxes in Greenland; source emission or transport efficiency. These discussions were encouraged by observations of systematical patterns in the records and abrupt changes in characteristics during transitions between climate regimes. However the discussions have led to very different conclusions. An understanding of climate impacts on source emission and transport is required to

assist interpreting ice core records of chemical impurities.

In order to identify the source location for mineral dust deposited in Greenland, comparative analyses of Nd, Sr, and Pb (neodymium, strontium, and lead) isotope compositions and clay mineralogy in dust samples from the GRIP and GISP2 ice cores, and dust material from potential source areas were performed (Biscaye et al., 1997; Svensson et al., 2000). These analyses suggested that East Asian deserts are the most probable dust source areas for Greenland and further that the source areas did not change significantly during times of large variations in dust fluxes and dust grain sizes. Biscaye et al. (1997) concluded on the basis of these findings that high ice core concentrations of dust during the Last Glacial Maximum (LGM) are mainly due to enhanced transport intensity.

Maggi (1997) found that systematic changes in the mineralogy during the D/O events occurred too rapid to be explained by changes in processes of soil genesis and chemical weathering and suggested that these changes were caused by atmospheric dynamical factors, such as the shifting polar front. Biscaye et al. (1997) suggested that changes in clay mineralogy could be due to a particle size fractionation of dust aerosol within the source area.

Mayewski et al. (1994) inferred covariance in concentrations of ionic species from sea salt and mineral dust in the GISP2 ice core as a polar circulation index. Further they explained systematic enrichment in dust and an opposite decline in sea salt species for cold periods as enhanced efficiency of transport from more distant source areas and effects of reduced open ocean surface due to enhanced sea ice extent and iceberg discharges.

De Angelis et al. (1997) and Laj et al. (1997) both observed a systematic enrichment of soluble calcium for cold periods and suggested an additional contribution to calcium minerals from continental shelves, which have been exposed due to changing sea level. However, their observations are in contrast to the observation of Steffensen (1997) of a systematic decline in contents of soluble calcium relative to dust mass during cold periods. This discrepancy seems to be a systematic feature of the dust material, which also show a systematic change of particle size characteristics with changes in dust mass as observed in the GRIP ice core (Steffensen, 1997).

A high resolution dust record from Fuhrer et al. (1999) showed that changes in dust concentrations during rapid climate changes occur more abruptly than changes in isotope compositions. Fuhrer et al. (1999) suggested that higher dust concentrations for cold climate periods mainly reflected a combined effect of increased turbulence in the source area and enhanced wind transport.

Modellers have also contributed to this discussion. Atmospheric General Circulation Models (AGCM) have been used to simulate long-range aerosol transport to the Greenland ice sheet. The simulated climate effect on transport efficiency is not large enough to account for the enhanced LGM concentrations of mineral dust aerosols in Greenland ice cores (Tegen, 2003). Therefore simulations of past and present dust depositions in Greenland have been mainly focused on parameterizations of the soil surface properties in the source areas that affect dust emissions.

In general the simulations obtain realistic ice core concentrations but under unrealistic conditions. Andersen et al. (1998) simulated an unrealistic high source contribution from North African desert areas. Mahowald et al. (1999), used a model for vegetation cover, and obtained more realistic source areas but an unreal-

istic expansion of source areas for the LGM. Tegen et al. (2002) used a better model for source areas and also a model for seasonal changes in vegetation but their simulation did not obtain realistic dust fluxes in remote areas such as Greenland. Werner et al. (2003) extended the model of Tegen at al. (2002) and obtained realistic dust fluxes in Greenland for LGM but due to an unrealistic effect on deposition from the regional hydrological cycle. Recent AGCM simulations of sea salt concentration in Greenland ice cores considered contributions to sea salt aerosol from sea ice brines and concluded that sea ice brines was far the most important source to sea salt in Greenland (Reader and McFarlane, 2003). However their parameterization was unrealistic because it was based on permanent sea ice coverage where only freshly formed sea ice produces sea salt aerosol (Wagenbach et al., 1998). Reader and McFarlane, (2003), suggested that dissimilarities for both dust and sea salt between simulated and measured ice core concentrations were due to model underestimation of wind extremes and errors in model transport pattern.

New continuous high-resolution records of soluble chemical species and mineral dust particles from the NorthGRIP ice core (Rothlisberger et al., 2002; Ruth et al., 2002) open up for new detailed studies of rapid climate changes. Ruth et al. (2003) presented a continuous record of particle concentrations and size distributions from the NorthGRIP ice core and explained a systematic climate effect on particle size modes as an enhanced long-range atmospheric transport efficiency during cold climate conditions. Despite this finding, however, they could not quantitatively explain the strong influence of climate conditions on ice core concentrations of mineral dust particles and they suggested that a source effect dominantly influenced ice core concentrations of mineral dust.

Here we present a NorthGRIP record of soluble ions measured by ion chromatography and introduce two new ionic species, Li^+ and F^-, to the series of continuous records from central Greenland ice cores covering the last glacial period.

The finding of a transport effect on particle size distributions by Ruth and others (2003) has lead us to consider systematic changes in ion composition as an effect of transport rather than a source effect. The discrepancy between the observations in the GRIP ice core of systematic properties, where the soluble calcium contents either increases or decreases relative to other dust species during cold periods, can be explained as a transport effect on the dust material. We extend this approach and explain ion compositions as mainly an effect of different depletions for different aerosol types during long-range transport.

We have analysed composition of soluble Li^+, Na^+, K^+, Mg^{2+}, Ca^{2+}, F^-, Cl^-, and SO_4^{2-} that are all mainly derived from sea salt and mineral dust aerosols. For this analysis we have developed a statistical method to extract ion composition characteristics so that we can quantify effects of source contribution and long-range transport properties. The method is based on empirical orthogonal function analysis (EOF), which is a well-established method used in many contexts to assess the dominant variability in a multi-variate record. We infer a physical interpretation, related to large-scale transport patterns, on the basis of the statistical parameters we obtain from the analysis.

6.2 The NorthGRIP ion record

Sampling and Measurements

Ice core samples for IC analyses were collected from decontaminated melt water used in high resolution flow analysis (CFA) performed in the field during the NorthGRIP 2000 field season (Dahl-Jensen et al., 2002). The CFA was performed using the Bern CFA system (Röthlisberger, 2000). The melt water samples were collected continuously in 55 cm resolution in Coulter Counter polystyrene accuvettes in a clean air laminar flow bench and hereafter immediately frozen. The sampling covers the ice core depth interval from 1404.70 m to 2930.40 m. The samples were stored frozen until measurements that took place in clean room facilities. Samples from the depth section of 1404.70 - 2025.65 m were analysed at the Dept. of Meteorology, University of Stockholm. The remaining samples were analysed at the Dept. of Geophysics, University of Copenhagen. Because our statistical analysis only includes data measured in Copenhagen, the following description of laboratory procedures, ion chromatographic system and method refer to the analyses performed in Copenhagen.

In a clean air laminar flow bench the samples were decanted into 5 ml Dionex vials, which were closed with a filter cap. Prior to use the vials were rinsed thoroughly in super quality (SQ) water (>18 MΩ) from an Elga water purifying system. Filter caps were rinsed successively in methanol and SQ water in an ultrasonic bath. Vials and filter caps were re-used after rinsing four times in SQ water. Measurements were performed using a Dionex 500 micro bore ion chromatograph (IC) equipped with a two channel setup for simultaneous measurements of cations and anions. Each channel was equipped with a pre concentrator column, a gradient pump, a suppressor and a conductivity detector. The samples were injected from the 5 ml vials into the IC system by an auto sampler. From each sample 3 ml and 1.5 ml were injected into the cation and anion pre concentrator columns, respectively. The cations were separated on a 2 mm Ionpac CS12 column eluted with a gradient mixture of methanesulfonic acid (MSA) and SQ water. The anions were separated on a 2 mm Ionpac AS14 column eluted with a gradient mixture of $Na_2B_4O_7$ and SQ water.

The measured concentrations were all far above the detection limit. Within the range of measured concentrations inaccuracies were less than 10% for all the species.

Characteristics of the ion record

The continuous NorthGRIP ion record covers the time interval from the Preboreal and back to around 110 ka BP. The time scale used in this work is the ss09sea chronology from Johnsen et al. (2001). Each 55 cm sample covers a time interval spanning 10–100 years depending on the annual layer thickness (personal communication from Sigfus Johnsen, 2003). We present here the IC records of eight soluble ion species Li^+ (lithium), Na^+ (sodium), K^+ (potassium), Mg^{2+} (magnesium), Ca^{2+} (calcium), F^- (fluoride), Cl^- (chloride), and SO_4^{2-} (sulphate) that are dissolved mainly from sea salt and mineral dust. The records of ion concentrations are shown in Figure 6.1. Ion concentrations are here given in μeq·kg^{-1}(micro equivalents (mole

times charge number) per kg). Conversion factors between ppb (mass fraction in parts per billion) are given in Table 6.1.

Greenland ice core records of ions derived from sea salt and mineral dust from the last glacial period reflect the climate with high concentrations indicating cold climate conditions. The Dansgaard/Oeschger events are highly pronounced in the ion records where Ca^{2+} is the most prominent climate indicator with changes in concentrations of one order of magnitude during the Dansgaard/Oeschger events.

The ion records show long term trends in the climate history generally with low concentrations during the warm MIS 5 (Marine Isotope Stage) and high concentrations during the cold stages MIS2 and MIS4. Despite the low resolution, a few volcanoes can be seen in the records of SO_4^{2-}, Cl^-, and F^-. Most prominent is the Z2 eruption at a depth of 2359 m (around 56 ka BP), where the F^- record shows a particularly strong excursion. Unusual for volcanic signals, the Z2 eruption also exhibits strong signals in the Na^+ and Ca^{2+} records.

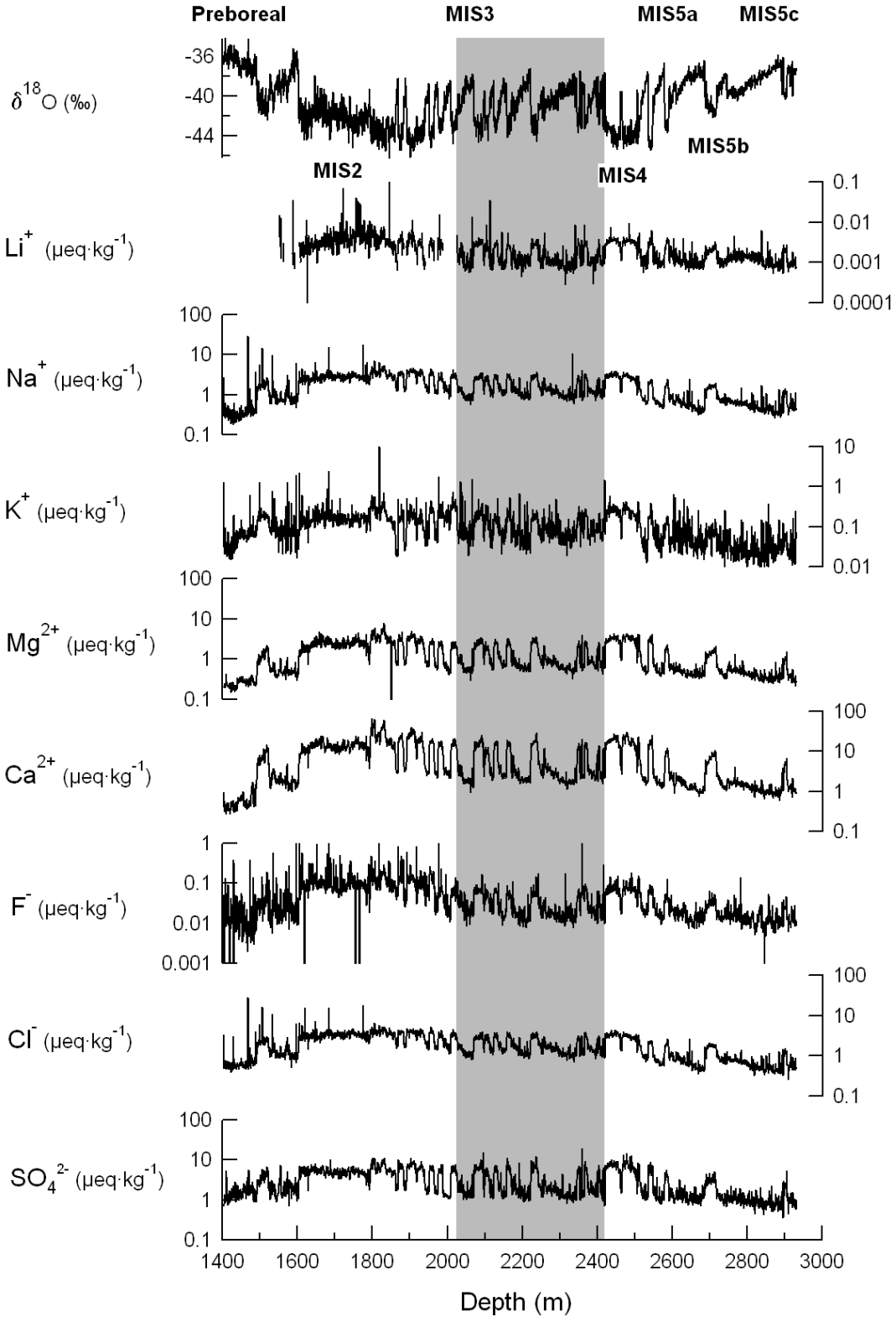
Preboreal
MIS3
MIS5a
MIS5c
MIS5b
MIS2
MIS4
δ18O (‰)
-36
-40
-44
Li+ (μeq·kg-1)
0.1
0.01
0.001
0.0001
Na+ (μeq·kg-1)
100
10
1
0.1
K+ (μeq·kg-1)
10
1
0.1
0.01
Mg2+ (μeq·kg-1)
100
10
1
0.1
Ca2+ (μeq·kg-1)
100
10
1
0.1
F- (μeq·kg-1)
1
0.1
0.01
0.001
Cl- (μeq·kg-1)
100
10
1
0.1
SO42- (μeq·kg-1)
100
10
1
0.1
1400
1600
1800
2000
2200
2400
2600
2800
3000
Depth (m)

Figure 6.1: (Previous page) *Concentrations of eight different ionic species measured in the NorthGRIP ice core shown together with the $\delta^{18}O$ record (top curve). The ion concentrations are shown on logarithmic scales all ranging over three decades. Marine Isotope Stages (MIS) are indicated at the top. The ion records show different long-term trends, and therefore it is not suitable to perform a statistical analysis of the whole record. The grey bar indicate the section we have chosen for our statistical analysis of ion concentrations.*

	$ppb/\left(\mu eq \cdot kg^{-1}\right)$
Li^+	6.941
Na^+	22.99
K^+	39.10
Mg^{2+}	12.15
Ca^{2+}	20.04
F^-	19.00
Cl^-	35.45
SO_4^{2-}	48.03

Table 6.1: *Conversion factors for concentrations of different ions between the units of $\mu eq{\cdot}kg^{-1}$ (micro equivalents (charge units) per kg) and ppb (mass fraction in parts per billion). The factors are molar mass divided by charge number.*

The records from MIS3 show no major long term trends but are dominated by frequent Dansgaard/Oeschger events (IS5 - IS17). Typical ion concentrations for interstadial and stadial climate conditions during MIS 3 are shown in Table 6.2. The high variability in climate conditions during MIS3 makes this period very suitable for statistical analyses of ion composition. For such analysis we have selected the depth section from 2025.65 to 2421.10 m corresponding to a time interval from 36.5 to 60.2 ka BP (marked in grey in Figure 6.1). The selected section contains climate variability corresponding to the Dansgaard/Oeschger events 8 -17 and the chemical signature of the Z2 eruption. In this section each sample represents a time interval ranging 20 to 40 years (personal communication from Sigfus Johnsen, 2003).

Origin of ions Soluble Ca^{2+} is mainly derived from mineral dust while soluble Na^+ is mainly derived from sea salt aerosol. Therefore records of soluble Ca^{2+} and Na^+ are often used as indicators for continental and marine inputs, respectively.

The dominant ions in sea salt are Cl^- and Na^+. In Greenland ice cores Cl^- and Na^+ are present in nearly the same molar ratio as in sea salt and they may as a first approximation be taken as representing only sea salt aerosol, although small contributions to these ions could come from dust minerals (De Angelis et al., 1997; Mayewski et al., 1997). Sea salt aerosol contributes also to concentrations of the other ions in the analysis; i.e. to Ca^{2+}, Mg^{2+}, K^+, F^-, and SO_4^{2-}. This sea salt (ss) contribution is calculated from the Na^+ contents using the relative contents in sea salt (see Table 6.2). De Angelis et al. (1997) did a detailed analysis of soluble chemistry of dust and sea salt in the GRIP ice core in order to identify the non-sea salt (nss) contribution to Na^+.

Mineral dust aerosols consist of a mixture of dust minerals from which ions dissolves in proportions dependent of the mineral type and history of chemical weathering. In glacial ice, Ca^{2+}, Mg^{2+}, SO_4^{2-}, K^+, Li^+, and F^- can be considered as representing mineral dust aerosols, although small amounts of these ionic species origin from sea salt and volcanic events. Sea salt contributes to K^+ with a relatively large fraction.

Ca^{2+}, Mg^{2+}, and SO_4^{2-} are the dominating dust components in soluble ion chemistry in glacial ice. They are dissolved from readily soluble minerals like calcite, dolomite and gypsum (Laj et al., 1997). K^+, $Li^+$and F^- are present in ice core samples only in trace amounts and are probably dissolved mainly from less soluble minerals, such as clays.

In warm periods biological activity is a dominant contribution to SO_4^{2-} but this contribution can be ignored in glacial ice because of less biological activity and increased contribution to SO_4^{2-} from mineral dust.

	S *avg (std)*	*IS* *avg (std)*	*S* *sea salt*	*IS* *sea salt*	*sea salt* / Na^+
Li^+	0.0029 (0.0005)	0.001(0.001)	6 %	5 %	$6.04{\cdot}10^{-5}$
Na^+	2.8 (0.4)	1.2 (0.3)	≡100 %	≡100 %	≡1
K^+	0.19 (0.06)	0.1(0.1)	31 %	28 %	0.0219
Mg^{2+}	2.5 (0.4)	0.8 (0.2)	12 %	17 %	0.113
Ca^{2+}	15.1(3.4)	2.9 (0.7)	<1 %	1 %	0.0219
F^-	0.06 (0.02)	0.02 (0.01)	<1 %	1 %	$0.13{\cdot}10^{-3}$
Cl^-	3.1(0.4)	1.5 (0.4)	104 %	95 %	1.16
SO_4^{2-}	6.5 (1.5)	1.9 (0.7)	3 %	4 %	0.0603

Table 6.2: *Average ion concentrations* $\left(in\ \mu eq \cdot kg^{-1}\right)$ *in the NorthGRIP ice core for stadials (S) and interstadials (IS) during MIS3. Standard deviations are indicated in parenthesis. Contributions from sea salt (in % of total content) are also shown. Sea salt contributions are estimated on the basis of the* Na^+ *concentration and relative contents in sea water, which is shown in the last column for the measured ion species (from Holland, 1984).*

Systematic patterns of ion concentrations

Concentrations versus δ^{18}O: Ion concentrations show a strong relationship with δ^{18}O. In Figure 6.2 is shown logarithmic Mg^{2+} concentrations versus δ^{18}O for the NorthGRIP MIS3 section, which is analysed here (indicated with grey in Figure 6.1). The δ^{18}O curve has been reversed for comparisons. The two curves show slightly different patterns indicating that they represent different physical influences. However, the synchronous variations is undoubtedly indicating a strong climate influence acting on both parameters.

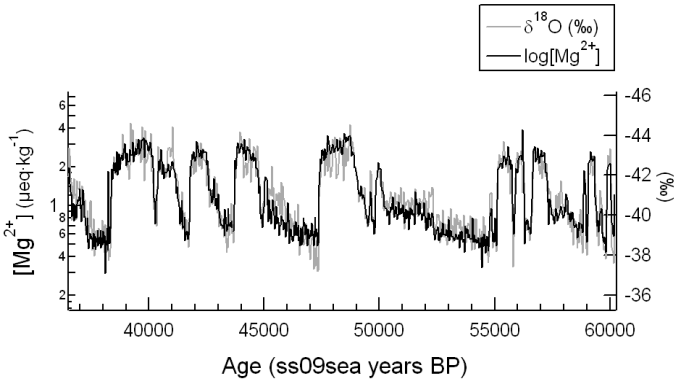

Figure 6.2: *Logarithmic Mg^{2+} concentrations and reversed $\delta^{18}O$ in the NorthGRIP record for the ice core section indicated in grey in Figure 6.1.*

Log-normal distributions: The main variation in the ice core records of $\delta^{18}O$ and of soluble ions is due to changes in climate between the distinctly different climate regimes of the Holocene and of stadials and interstadials. For each of the climate regimes, ion concentrations show a nearly log-normal distribution. In Figure 6.3 is shown the distribution of logarithmic Mg^{2+} concentrations during MIS3. The logarithmic concentrations are grouped into two separate nearly normal distributions corresponding to stadials and interstadials.

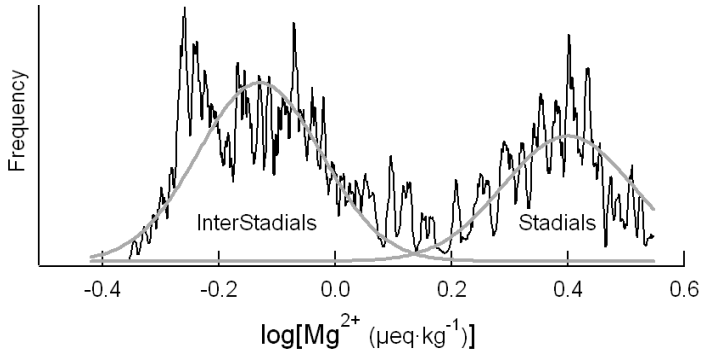

Figure 6.3: *Logarithmic ion concentrations within the same climate regime is nearly normal distributed. Here is shown distributions of logarithmic Mg^{2+} concentrations for stadials and interstadials climates during MIS3.*

Particle size mode: A systematic relationship between the modes of the particle size distribution and dust mass concentration was observed both in the GRIP ice core (Steffensen, 1997) and in the NorthGRIP ice core (Ruth et al., 2003). This systematic relationship was explained by Ruth et al. (2003) as an effect of changing

transport times. The explanation was based on a model for size fractionation during transport. In Figure 6.4 is shown the continuous record of particle size mode versus dust mass in the NorthGRIP ice core.

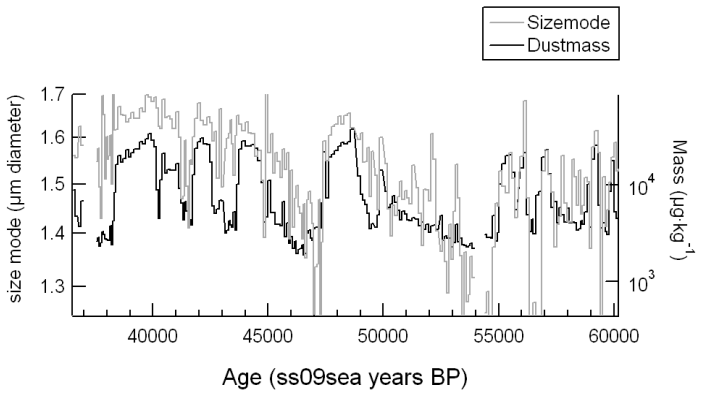

Figure 6.4: *Particle size mode versus dust mass concentration in the NorthGRIP ice core section marked with grey in Figure 6.1. (The data are from Ruth et al. (2003)).*

Systematic relationship of ion concentrations: For analysis of ice core records of soluble ions it is often assumed that ratios between ion concentrations reflect source characteristics and therefore linear approximations of ion concentration relationships are often made in order to identify climatic effects in source regions. The systematic non-linear patterns of ion compositions in Greenland ice cores, observed in the GRIP and GISP2 ion records, have been described in different ways. De Angelis et al. (1997), and Steffensen (1997) considered linear approximations for stadial and interstadial periods separately, whereas Mayewski et al. (1994) made a cubic approximation to the non-linear patterns. However, our observations on the NorthGRIP ion record shows that for glacial conditions the systematic patterns of ion compositions can be well approximated using a power law, describing the relationship between ion concentrations, C_A and C_B, of two different ionic species A and B:

$$C_A = K \cdot {C_B}^{\alpha} \tag{1}$$

and hence logarithmic ion concentrations can be approximated by a linear relationship:

$$\ln(C_A) = \ln K + \alpha \cdot \ln(C_B)\,. \tag{2}$$

In Figure 6.5 is illustrated the linear relationship between logarithmic ion concentrations. Concentrations of Cl^- and Na^+ appears in Greenland ice cores in nearly the same ratio as in sea salt ($[Cl^-]/[Na^+] = 1.16$). The relationship between concentrations of Cl^- and Na^+ is approximated well by a linear approximation, but show however, slightly systematic non-linear features due to fractionation processes and to other contributions than sea salt. For the relationship between concentrations

of $Mg^{2+}$and Ca^{2+} a power law is obviously a better approximation that the linear approximation. The same is true for the concentrations of Na^{+} and Ca^{2+}.

Using a linear relationship between logarithmic ion concentrations, ion composition in Greenland ice cores for the glacial period can be characterized by the parameters K and α. These parameters can be obtained by linear regression. However, linear regression is sensitive to noise and to source contributions not consistent with the power-law. Instead we use empirical orthogonal function (EOF) analysis on the complete array of logarithmic ion concentrations. On the basis of the EOF principal component we get a unique determination of the characteristic parameters.

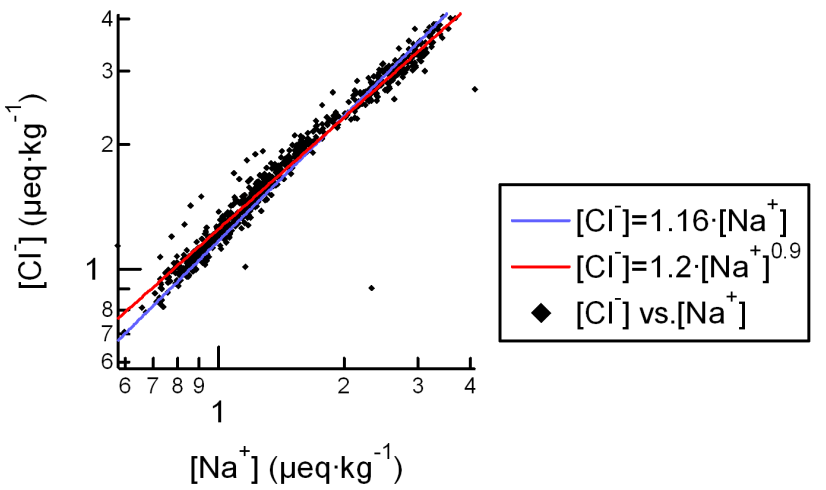
[Cl-] (µeq·kg-1)
[Na+] (µeq·kg-1)
[Cl-]=1.16·[Na+]
[Cl-]=1.2·[Na+]0.9
[Cl-] vs.[Na+]

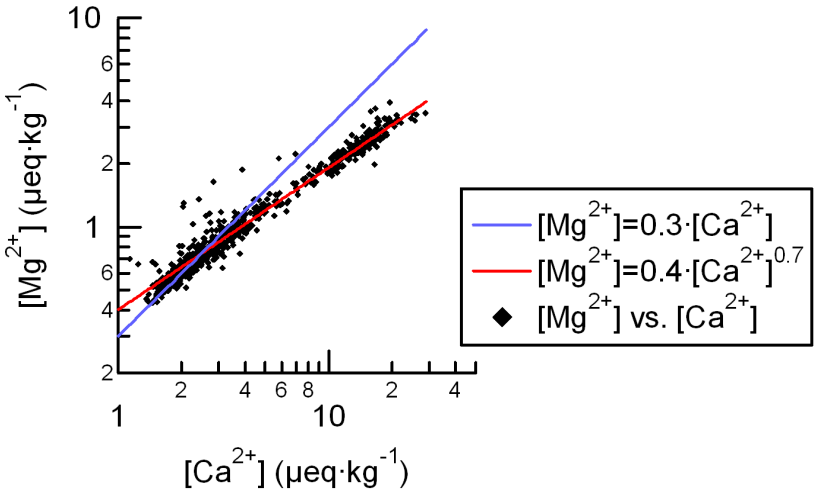
[Mg2+] (µeq·kg-1)
[Ca2+] (µeq·kg-1)
[Mg2+]=0.3·[Ca2+]
[Mg2+]=0.4·[Ca2+]0.7
[Mg2+] vs. [Ca2+]

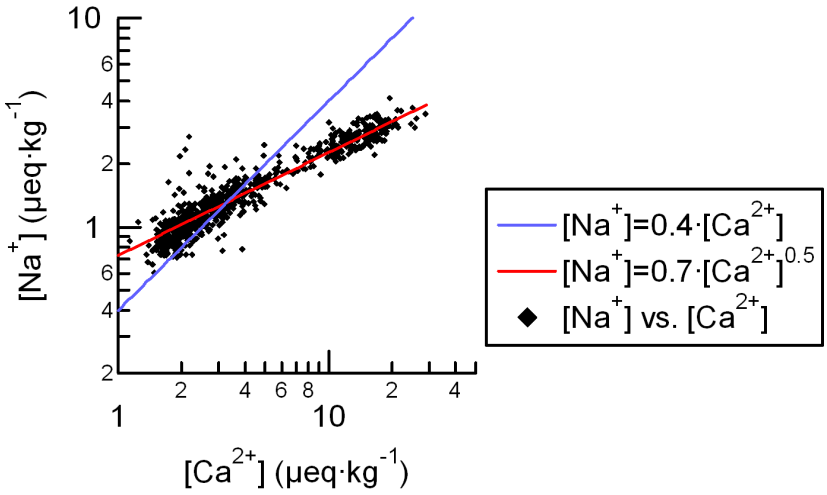
[Na+] (µeq·kg-1)
[Ca2+] (µeq·kg-1)
[Na+]=0.4·[Ca2+]
[Na+]=0.7·[Ca2+]0.5
[Na+] vs. [Ca2+]

Figure 6.5: (Previous page) *Ion concentrations for MIS3 on logarithmic scales (black dots), linear approximations (blue lines) and power law approximations (red lines).*

The two species Cl^- and Na^+ are both mainly from sea salt as indicated by their nearly linear relationship (top). Mg^{2+} and Ca^{2+} that both mainly are derived from mineral dust, clearly have a linear relationship on logarithmic scales, but not on linear scales (middle). The relationship between Na^+ and Ca^{2+} is also well described by a power law (bottom).

Systematic non-linear properties were observed in the GRIP ice core records of soluble Ca^{2+} and dust mass (Steffensen, 1997). These properties were described by linear approximations for stadials and interstadials, respectively. Figure 6.6 shows Ca^{2+} concentrations versus dust mass in the GRIP ice core. As seen in the figure this relationship is well-described by a power law.

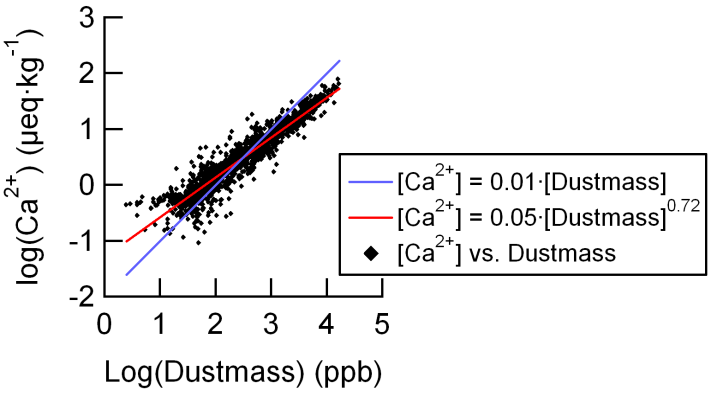

Figure 6.6: *Logarithmic Ca^{2+} concentrations ($\mu eq \cdot kg^{-1}$) versus logarithmic dust mass concentrations (ppb) in the GRIP ice core. The blue line is a linear approximation and the red line is a power law approximation. Data are from Steffensen (1997).*

Ice core concentration vs. flux estimates: Snow accumulation rates on the Greenland ice sheet changes with changing climate conditions. In the North GRIP ice core, accumulation rates varies a factor of 4 between present and LGM and a factor of ≈ 2 during the D/O events (Personal communication from Sigfus Johnsen, 2003). Therefore, for analysis of ionic species in ice cores, it is often discussed whether to use the measured concentrations or flux estimates. We prefer to perform our analysis on ion concentrations not on flux estimates. Firstly because we prefer to maintain the analysis as simple as possible. Flux estimates are a manipulation of the data that could introduce unwanted artefacts to the data. Secondly, several authors have pointed out that concentrations of sea salt and mineral dust aerosols in Greenland ice cores better represent the atmospheric concentrations than flux estimates (Alley et al., 1995; Meeker et al., 1997; De Angelis et al., 1997). In

this work we also made a small study of possible influences from accumulation rates which gave the conclusion that changing accumulation rates have minor effect on ion concentrations. Based on an analysis of the GISP2 ice core record of accumulation rates and ion concentrations, Mayewski et al. (1997) suggested that synchronous variations in ion concentrations and accumulation rates is an effect of climate acting on both parameters rather than an effect of accumulation rates controlling ion concentrations.

6.3 Statistical method

EOF analysis was used in several analyses of the GISP2 ice core ion records (O'Brien et al., 1995; Mayewsky et al,. 1994; Mayewski et al., 1997; Meeker et al., 1997; Yiou et al., 1997). O'Brien used the EOF analysis to identify periodic properties in the ion record throughout the Holocene period. Based on the assumption of a well mixed atmosphere, Mayewski et al. (1997) used the EOF principal component to define a polar circulation index (PCI), which they used for periodic component analysis in order to identify orbital forcing in the atmospheric circulation.

EOF analysis is a linear transformation of data variables and therefore has limitations when applied to non-linearly related variables. The EOF analyses performed on the GISP2 ion record were made on the measured concentrations which are clearly non-linearly related. It was assumed that non-linear properties, identified in the second EOF component, reflected climate effects acting on sources, e.g. on sea ice cover, iceberg discharges, and extent of the atmospheric polar cell (Mayewski et al., 1994). The second and lower components derived from an EOF analysis might contain negative contributions from variables for what reason it has been argued that they cannot be physically meaningful (Marsh and Ditlevsen, 1997; Ditlevsen and Marsh, 1998). Non-linear properties in Greenland ion records might reflect a systematic property of the physical processes in the climate system acting on the dust and sea salt cycles. In that case the second and lower ranging EOF components are just representing the same variability as

the principal component. Furthermore, in Greenland ice core records, ion concentrations are log-normal distributed and therefore, as pointed out by Yiou et al. (1997), covariance are not correctly estimated when performed directly on ion concentrations, and should for that reason be performed on logarithmic ion concentrations instead.

Our method differs from previous EOF analyses of ion records in the sense that we perform the analysis on logarithmic concentrations, where we have found linear relationships, and where the variables are normal distributed. Therefore our method offers some applications that conventional EOF analysis of ion records does not. We use the analysis to separate each ion series into a series representing the common variance (principal component) and a residual series. From the statistical parameters of the principal component we obtain characteristics of the ion composition. Assuming that this characteristics represent the physical influence from climate on the ion concentrations we interpret the statistical parameters as physical parameters. Based on a simple transport model we use the statistical parameters to indicate large-scale transport patterns and physical influences during transport. In

the following we give a detailed description of our method.

Principles of EOF analysis: The principle of EOF analysis is shortly summarized by Yiou et al. (1997) and Meeker et al. (1997). We also give a short summary of EOF analysis here.

EOF analysis is a covariance analysis of multivariate data series $(y_i(t))$. The M variables y_i ; $i = 1, .., M$ form a set of basis vectors. The data set is represented by a $M \times N$ matrix, D, where the rows represent the M variables (the ion species) and the columns represent the N discrete samples. The data covariance matrix is an $M \times M$ matrix, constructed by $\frac{1}{(N-1)} D\, D^T$ where each element (i, j) represents the covariance between variables y_i and y_j. In practice EOF analysis consists of a linear transformation of the basis vectors (variables) that diagonalize the data covariance matrix. During this diagonalization, which is a unique transformation, the basis vectors are transformed into a set of orthogonal eigenvectors EOF_1, EOF_2,.. with corresponding time expansions $E_1(t)$, $E_2(t)$,.. which are mutually uncorrelated. The time expansions are weighted sums of all the measured data series $(y_i^m(t))$, weighted according to their covariance with the $E_i(t)$'s. The diagonal elements of the transformed covariance matrix are the variances $V_1, V_2, ..$ of the new orthogonal time series. The eigenvector of the highest variance (EOF_1) is referred to as the principal component.

By normalizing the variables before the analysis, the data covariance matrix becomes identical to the correlation matrix, and the same variance is attributed to each variable in the analysis. The use of normalized variables has an advantage for analysis of ion records where different ions have markedly different variances.

Although EOF analysis in principle just reflects systematic patterns (covariance) in the data, EOF analysis is often used in time series analysis to extract time series that represents common variations in the data. We will use the principal component vector EOF_1 to obtain statistical parameters characterizing ion composition in ice cores, and the principal component time series $E_1(t)$ to obtain, for each variable i, a proportional model time series $y_i^M(t)$. Based on the residuals $\left(y_i^R = y_i^m - y_i^M\right)$ we also characterize non-linear properties in the data as explained in the following.

The climate signal from ion concentrations

Our analysis focuses on three different features in Greenland ice core records of the last glacial period: 1) the systematic relationship between concentrations of different ions, 2) the strong coupling between ion concentrations and climate and 3) the pronounced climate variability represented by the D/O events.

Measured ion concentrations (C^m) in ice cores vary due to changes in climate (C^{climate}), contributions from special events, such as volcanic eruptions, (C^{events}), and noise, such as analytical imprecision, (C^{noise}), thus the measured ion concentrations can be broken down into the three additive terms:

$$C^m = C^{\text{climate}} + C^{\text{events}} + C^{\text{noise}}$$

In the following we attempt to isolate and characterize the climate signal (C^{climate}) in the series (C^m) of measured ion concentrations.

Using the power function to describe the systematic relationship between ions, we separate the climate signal further into a contribution (F^{power}), for which the power law is valid, and a second order term (F') representing deviations from the power law: i.e. $C^{\text{climate}} = (F^{\text{power}} + F')$. At this stage we assume that the second order term is negligible compared to F^{power}, i.e. $F' \ll F^{\text{power}}$.

Given that variability in ion records mainly reflects changing climate conditions we introduce a parameter p that indicates climate conditions and defining $f^P \equiv \ln(F^{\text{power}})$ we assume:

$$f^P(p) = c^0 - \lambda\, p \tag{3}$$

$$F^{\text{power}}(p) = C^0 \exp(-\lambda\, p) \tag{4}$$

where $c^0 = \ln(C^0)$. The strength C^0 and the sensitivity λ are ion specific parameters (C_i^0 and λ_i), which are related to the parameters α and K in the power law ($C_A = K \cdot {C_B}^{\alpha}$) through the expressions $\left(\alpha = \lambda_A \cdot \lambda_B^{-1}\right)$ and $\left(K = C_A^0 \cdot (C_B^0)^{-\alpha}\right)$.

Since p is an undetermined parameter (only the variation is known) so are the parameters c^0, C^0 and λ at this stage. However, c^0 is proportional to the mean, $avg(f^P)$, and λ is proportional to the standard deviation, $std(f^P)$ of the series $f^P(t)$. Later in this paper we will discuss the understanding of the physical and climatic aspects of the parameters C^0 and λ.

Climate series: We apply expression (3) to the series of measured logarithmic concentrations $c^m(t) = \ln[C^m(t)]$:

$$c^m(t) = f^P(t) + f^{\text{residual}}(t)$$

where $f^P(t)$ represent the time evolution of f^P in expression (3) and the residual $f^{\text{residual}}(t)$ represents the combination of noise, contributions from special events e.g. volcanic eruptions, and a second order climate signal.

The series $f_i^P(t)$ in expression (3) are mutually proportional. Provided that the series $f_i^P(t)$ represent the major variability in the data, and further that they are statistically independent of the series $f^{\text{residual}}(t)$, their variability is well represented by the principal component series $E_1(t)$ of an EOF analysis of the multi-variate record of measured logarithmic ion concentrations $c^m(t)$.

Normalization: We normalize the logarithmic ion concentrations prior to the EOF analysis to attribute the same variance to each ion species. The normalized concentrations c_i^n are obtained by

$$c_i^n = \frac{[c_i^m - avg(c_i^m)]}{std(c_i^m)}. \tag{5}$$

We then perform the EOF analysis without any other prior manipulation of the data like averaging or filtering so that all information in the data of the relationship between concentrations of different ions stays intact.

At first in this analysis we do not take into account that the 55 cm samples are weighted differently by time. Later we show how we may treat sample time weighting.

Climate series reconstruction ("back-wards normalization"): The principal component series is a weighted sum of the normalized series, $c_i^n(t)$, with weight factors given by the basis vector components, $EOF_{1,i}$; i.e. $\left(E_1(t) = \sum_i \left[EOF_{1,i} \cdot c_i^n(t)\right]\right)$. Similarly the normalized time series $c_i^n(t)$ can be expressed as a weighted sum of EOF components $\left(c_i^n(t) = \sum_j \left[EOF_{j,i} \cdot E_j(t)\right]\right)$ and so, using expression (5), logarithmic ion concentrations are expressed as:

$$c_i^m = avg(c_i^m) + std(c_i^m) \cdot \left(\sum_j \left[EOF_{j,i} \cdot E_j(t)\right]\right) \tag{6}$$

The term $[EOF_{1,i} \cdot E_1(t)]$ represent the contribution from $c_i^n(t)$ to the principal component and vice versa. Replacing the sum over EOF components, j, in the expression above with the single term $[EOF_{1,i} \cdot E_1(t)]$, we obtain instead of $c_i^m(t)$ a set of model series $c_i^M(t)$:

$$c_i^M(t) = avg(c_i^m) + std(c_i^m) \cdot [EOF_{j,i} \cdot E_j(t)] \tag{7}$$

that well represents $f_i^P(t)$ in expression (3); i.e. $f_i^P(t) \approx c_i^M(t)$. The uncertainty between the two terms lies in the fact that $f^P(t)$ is a function of climate only, whereas $c_i^M(t)$ is a weighted sum of all the variables in the analysis and therefore contain also non-climate contributions such as volcanic signals.

Performing the "back-wards normalization" described in expression (7), the model series $c_i^M(t)$ will have the same averages as the series $c_i^m(t)$. However non-climate contributions to ion concentrations are likely to be larger than 0 in averages. Assuming that special events, such as volcanic eruptions, take place over a much shorter time than variations in climate, we will correct for non-climate contributions to $avg(c_i^m)$ by sorting out spikes; i.e. by replacing $avg(c_i^m)$ in expression (6) by the average $avg^*(c_i^m)$ of a median filtered series of c_i^m:

$$c_i^M(t) = avg^*(c_i^m) + std(c_i^m)\, EOF_{1,i}\; E_1(t) \tag{8}$$

and so $avg(c_i^M) = avg^*(c_i^m)$. Figure 6.7 shows an example of a model series $c^M(t)$ and residuals $c^R(t)$ obtained by expression (8) for logarithmic concentrations of SO_4^{2-}. Corresponding series of ion concentrations are calculated as:

$$C_i^M(t) = \exp\left[c_i^M(t)\right].$$

The residuals $C^R = C^m - C^M$ appears differently from the c^R. For concentrations of the major ions, which shows only few spikes, the correction for spikes (non-climate contribution) in expression (8) has no significant effect. For ion series containing many spikes, the correction is only of minor influence. An example of model concentrations and residuals for F^- is shown in Figure 6.8. In the case of F^- the non-climate contribution corresponds to 3.3 % in concentrations.

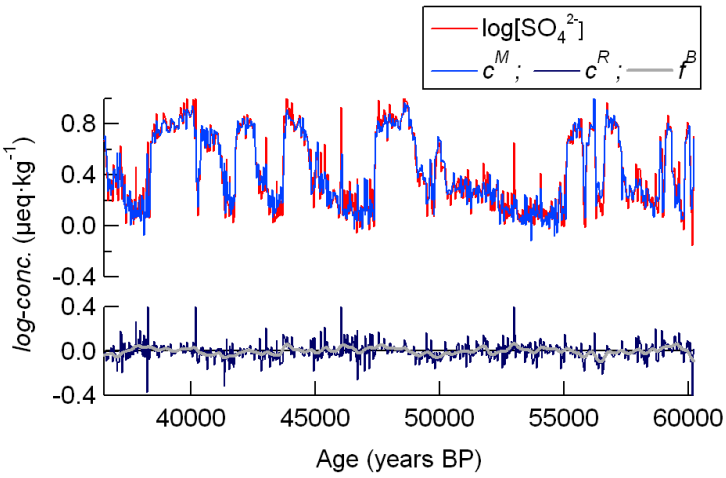

Figure 6.7: *Example of a model series obtained by back normalization of the EOF principal component using expression 8. The series f^B is a box filter of the residual c^R showing non-linear properties on time scales of the D/O events and longer.*

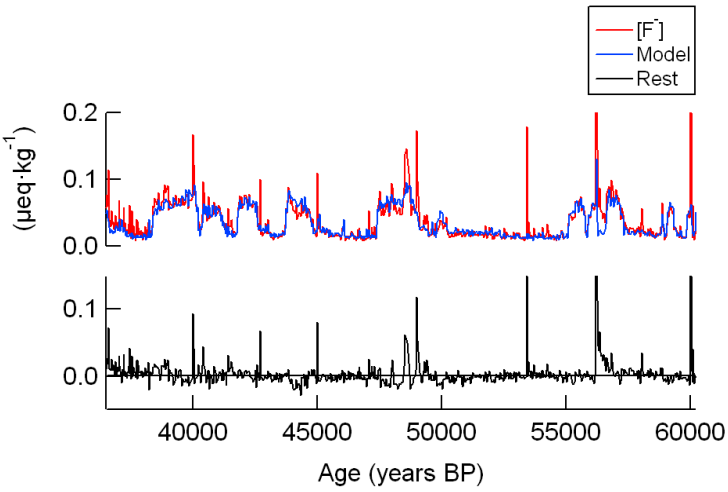

Figure 6.8: *Example of model concentrations and residuals for F^-.*

The residual series - investigation of the robustness The residual series $\left(c^R(t) = c^m(t) - c^M(t)\right)$ are just as important records as the series $c^M(t)$ because they also may contain information about climate processes. However, the model series $c_i^M(t)$ are proportional to the principal component series that in principle is a weighted sum of the series of all the variables included in the analysis. Therefore the individual $c_i^M(t)$ series are sensitive to ion specific signals in series for other components. One example is the Z2 volcanic eruption that appears in the constructed climate series and which is compensated for in the residuals by a negative spike.

In order to investigate the robustness of the principal component time series $E_1(t)$ and the proportional series $c_i^M(t)$ against influence from the individual ion series,

we have quantified the influences of each individual ion series $c_i^m(t)$ by repeating the analysis excluding the variable i and then again including it twice. Hereby we obtained the series $(E_{1-})_i$ and $(E_{1+})_i$ with variances $(V_{1-})_i$ and $(V_{1+})_i$ respectively, differing from E_1 due to the influence from the variable i. Performing this procedure for all the variables we determined the significance band $\sigma(t)$ of $E1(t)$ as the sum of influences by all ionic components:

$$\sigma(t)^2 = V_1 \sum_i \frac{1}{2} \left(\left(\frac{E_1(t)}{\sqrt{V_1}} - \frac{E_{1-}(t)}{\sqrt{V_{1-}}} \right)_i^2 + \left(\frac{E_1(t)}{\sqrt{V_1}} - \frac{E_{1+}(t)}{\sqrt{V_{1+}}} \right)_i^2 \right). \tag{9}$$

Around the residuals c_i^R the corresponding band $(\pm EOF_i^1 \cdot std(c_i^m) \cdot \sigma(t))$ represent the limit of influences from individual ion series on c_i^R. We therefore consider this band as significance limits for ion-specific residual signals. In Figure 6.9 is shown an example of significance bands for Mg^{2+}. The significance band show that for Mg^{2+} the residuals is mainly influenced by noise in the other ion series and therefore do not represent significant non-linear contributions to Mg^{2+}.

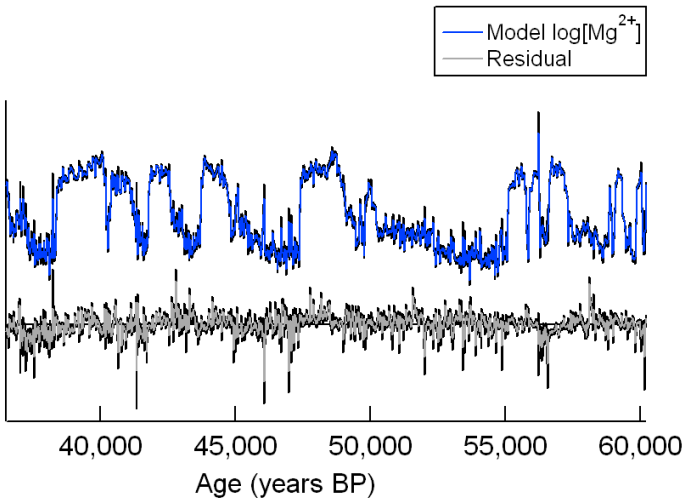

Figure 6.9: *Result from the robustness test shown for Mg^{2+}. The significance band show that for Mg^{2+} the residuals are mainly influenced by noise in the other ion series.*

Parameter estimations

Determination of λ: We now want to determine the parameter λ in expressions (3) and (4). Since p is an undetermined parameter so is λ, but as already pointed out, λ is proportional to the standard deviation of $f^P(t)$. In the following we therefore refer to λ as the standard deviation $std(c^M)$ of the model series c^M:

$$\lambda_i \equiv std(c_i^M) = EOF_i^1 \sqrt{V_1}\, std(c_i^m). \tag{10}$$

Uncertainty to λ: Although the parameters λ_i's are unequivocally determined from expression (10), they might change if we excluded variables or added new variables to the analysis. In order to determine an uncertainty to the λ_i's we use the procedure as in the robustness test described above in order to evaluate influences on λ_i from all the variables. For each repeated analysis excluding one variable j or including it twice we obtain a set of λ_{i-} and λ_{i-} respectively. The uncertainty $\sigma(\lambda_i)$ to λ_i we determine as:

$$\sigma(\lambda_i)^2 = \sum_{j \neq i} \frac{1}{2} \left((\lambda_i - \lambda_{i-})_j^2 + (\lambda_i - \lambda_{i+})_j^2 \right) + (\lambda_i - \lambda_{i+})_i^2 \tag{11}$$

Non-linear properties of logarithmic data: Parameters achieved from the EOF principal component characterize only the linear properties of the logarithmic ion concentrations. Non-linear features of logarithmic ion concentrations may also be used for characterization. Based on the residual series $c^R = c^m - c^M$ we want to define a deviation $\Delta\lambda$ from the linear relationship characterized by λ. We may consider $\Delta\lambda$ as a second order term to λ. Therefore in order to define a parameter $\Delta\lambda$, matching λ, that characterizes non-linear properties of logarithmic ion concentrations, we make use of the fact that the EOF components are statistically independent, i.e. the variances are related according to: $Var(c^m) = Var(c^M) + Var(c^R)$. Further we use that $\lambda \equiv std(c^M) = \sqrt{Var(c^M)}$ and define $\lambda + \Delta\lambda \equiv \sqrt{Var(c^m)} = \sqrt{\lambda^2 + Var(c^R)}$ i.e.:

$$\Delta\lambda \equiv \sqrt{\lambda^2 + Var(c^R)} - \lambda \tag{12}$$

The residuals (c^R) from the EOF analysis represent, in addition to the non-linear response to climate conditions, signals from special events, noise and contributions from other variables in the analysis.

We can confine the estimation of the non-linearity, $\Delta\lambda$, to account only for climate responses by substituting c^R with a box-filtered series f^B that is preserving only variability on a time scale of the D/O events and longer (an example of a box-filtering of the residuals is shown in Figure 6.7). We then assume that the filtered residual is uncorrelated to the model series (i.e. $Var(c^P) = Var(c^M) + Var(f^B)$) and substitute $Var(c^R) \longrightarrow Var(f^B)$ in equation (12):

$$\Delta\lambda = \sqrt{\lambda^2 + Var(f^B)} - \lambda. \tag{13}$$

The statistical properties of $\Delta\lambda$ is illustrated in a geometric representation in Figure 6.10.

$\Delta\lambda$ represent both systematic non-linear patterns and effects from underlying trends in the series. Both of these effects are limiting factors on the power law approximation. Therefore $\Delta\lambda$ may serve as a significance limit for the power law represented by λ.

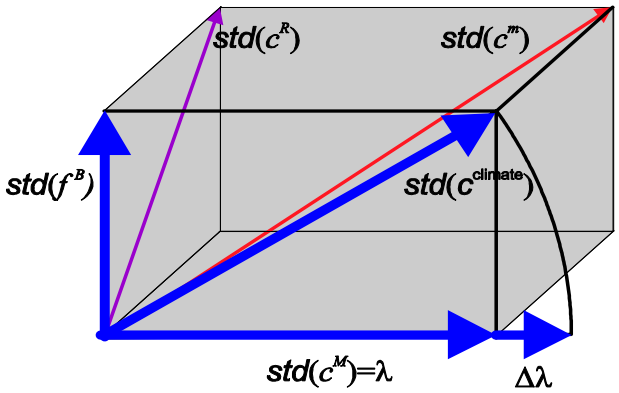

Figure 6.10: *Geometric representation of standard deviations of the series obtained by a separation of the logarithm of the measured concentrations are represented by* $c^m = \ln(C^m)$ *into a model series* c^M *obtained from the EOF analysis and a residual series* $c^R = c^m - c^M$.

$c^{\text{climate}} = c^M + f^B$ *represent the dominant climate contribution to the series of* c^m, *where* f^B *is the filtered residual series.* $\lambda \equiv std(c^M)$ *is the sensitivity to climate conditions given as the standard deviation to* c^M.

We can consider the box filtered residual f^B as a second order climate contribution f' and describe the climate signal in logarithmic ion concentrations as: $c^{\text{climate}} \approx c^M + f^B$, and in concentrations as: $C^{\text{climate}} = C^M + F'$, where $F' = C^M \cdot [\exp(f') - 1]$. However, in case of many spikes in the residual series, a median filter should be used instead of a box filter. Because of noise from other variables in the residual series it is not suitable to evaluate the series f' and F'. In our analysis we are therefore not going in detail in climate series reconstructions. We will instead focus on the residual series with significance limits attached.

Reconstructing the power law: The parameters α and K in equation (1), for the relationship between two species A and B is given by $\alpha_{AB} \equiv \lambda_A/\lambda_B$ and $\ln(K_{AB}) = avg^*(c_A^m) - \alpha_{AB}\ avg^*(c_B^m)$.

In Table 6.3 we show parameters α_i, K_i relating the model concentrations C_i^M of the different ions to the model concentration C_{Ca}^M for Ca^{2+}. These parameters are given by $\alpha_i \equiv \lambda_i/\lambda_{\text{Ca}}$ and $\ln(K_i) = avg^*(c_i^m) - \alpha_i\ avg\left(\ln C_{\text{Ca}}^M\right)$.

Uncertainty estimates: Errors $\Delta\alpha$ and $\Delta\ln(K)$ are evaluated on the basis of $\Delta\lambda$ using Taylor's error propagation formula. ΔK is determined by $\Delta K = K(\exp[\Delta\ln(K)] - 1)$.

$\Delta\lambda$ reflect variability in the amplitude of the logarithmic series. We therefore assume that the error to avg^* is of the same magnitude as $\Delta\lambda$.

Instead of the natural logarithm (ln), we may use $\log_{10}$ in the analysis. In that case model series are estimated as: $C_i^M(t) = 10^{\left[c_i^M(t)\right]}$, and K_i and ΔK will be evaluated according to $\log_{10}(K_i) = avg^*(c_i^m) - \alpha_i\ avg\left(\log_{10} C_{\text{Ca}}^M\right)$ and $\Delta K_i = K_i(10^{\Delta\log_{10} K_i} - 1)$

Weighting by time: In order to obtain a comparable ion composition characteristics from the analysis, we want to take sample time intervals into account. This we may do by performing the substitution

$$\frac{1}{1-N}\sum_{n=1}^{N} X_n; \frac{1}{N}\sum_{n=1}^{N} X_n \longrightarrow \frac{1}{t}\sum_{n=1}^{N} X_n \cdot \Delta t_n \tag{14}$$

where index n refers to the individual samples and Δt_n refers to the time interval of that sample. This substitution is relevant for the evaluations of elements in the data covariance matrix $(X_n = (x_n - \overline{x})(y_n - \overline{y}))$, variances $\left(X_n = (x_n - \overline{x})^2\right)$ and averages $(X_n = x_n)$. The standard deviations and the normalized data values are determined using the time weighted parameters of variance and average. For the analysis presented here, the results are not significantly different whether we take sample time intervals into account or not. However, the substitutions in expression (14) offer the opportunity to compare ion composition characteristics from different ice cores for which suitable time scales are available.

6.4 Transport model

A power law relationship between concentrations of different ions can be a result of a single physical process acting on the ions. Here we discuss the possible influences on aerosols during long-range transport. Enormous amounts of dust and sea salt are emitted into the atmosphere, but only trace amounts of these aerosols are reaching Greenland. This suggests that conditions for transport has a major influence on concentrations in Greenland ice cores and that concentrations of dust and sea salt vary with varying conditions for transport. A fractionation process during transport could be responsible for the different sensitivities of the different soluble ions to changed climate conditions and result in a power law relationship between ion concentrations.

Here we apply a transport model to the ions in Greenland ice cores. First we consider very simple physical processes in order to get an understanding of how transport conditions can influence the relationship between ion concentrations in Greenland ice cores. In the simple model we assume that changing climate conditions are associated with changes in wind speeds. Later we will discuss the results from the statistical analysis of ion composition and also extend the transport model and apply a more realistic view, of physical processes influencing ion concentrations.

One-dimensional transport model

Assuming a constant initial size distribution Ruth et al. (2003) explained a systematic change in particle sizes in the NorthGRIP ice core as an effect of size fractionation during transport. For cold periods particles are less fractionated due to shorter transport times as a consequence of better conditions for transport. We have extended this view to explain also systematic variations in ion composition.

Analysis of Nd (neodymium) and Sr (strontium) isotope composition and clay mineralogy of the mineral dust material in central Greenland ice cores has shown that this material is most likely from East Asian desert areas (Biscaye et al., 1997),

(Svensson et al., 2000). We can therefore consider the dust source area as a relatively small area with a single location (point source) and apply a simple one-dimensional model where aerosol is emitted from a point source and then follow a well defined transport path to the ice sheet (see Figure 6.11). This model is similar to the model used by Ruth et al. (2003) to describe particle size fractionation.

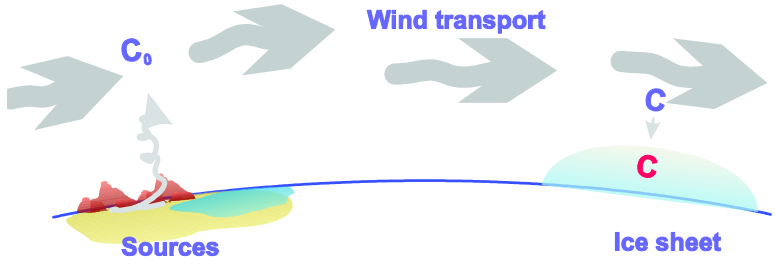

Figure 6.11: *Simple one dimensional transport model for dust deposition in Greenland.*

Aerosol in a moving air parcel: To begin with, we consider a model of a moving air parcel with an initial aerosol concentration of $C^{\mathrm{air},0}$ at $t = 0$. Concentrations C^{air} of aerosol in a moving air parcel are generally described to first order by

$$C^{\mathrm{air}}(t) = C^{\mathrm{air},0} \exp\left[-\frac{t}{\tau}\right] \tag{15}$$

where t is the atmospheric residence time and τ is atmospheric aerosol lifetime.

Assuming that the air parcel is driven by a constant wind speed we replace time, t, in expression (15) with transport distance $(r - r^0)$ divided by wind speed v, i.e. $t \longrightarrow (r - r^0)/v$:

$$C^{\mathrm{air}}(r - r^0) = C^{\mathrm{air},0} \exp\left[-\frac{(r - r^0)}{v} \cdot \frac{1}{\tau}\right]$$

An air parcel moving along a fixed trajectory: Now we follow an air parcel along a fixed trajectory, $L = \left(r^{\mathrm{ice}} - r^{\mathrm{source}}\right)$, from aerosol uplift in the source area until it passes over the ice sheet. Assuming that concentrations in the ice are proportional to air concentrations, $C^{\mathrm{ice}} = \gamma C^{\mathrm{air}}$, we can express aerosol concentrations in the ice as a function of wind speeds:

$$C^{\mathrm{ice}}(v) = \gamma C^{\mathrm{air},0} \exp\left[-\frac{L}{\tau} \cdot \frac{1}{v}\right] \tag{16}$$

If we substitute $L/\tau \rightarrow \lambda$ and $1/v \rightarrow p$ we obtain from expression (16) a one dimensional transport model of the form

$$C^{\mathrm{ice}}(p) = C^{\mathrm{ice},0} \exp(-\lambda p) \tag{17}$$

that is identical to expression (4) in the previous section.

In the simple model of expression (17) the strength, $C^{\mathrm{ice},0}$, indicates the atmospheric concentrations at the source (point source) and $C^{\mathrm{ice}}(p)$ indicates the atmospheric aerosol concentration over Greenland after depletion in air concentration during transport along the path length L and under the climate conditions given by $p = 1/v$.

Assuming a constant emission of aerosol at the source and a constant transport path to Greenland, aerosol concentrations in Greenland will vary with varying climate conditions associated with varying wind speeds. The sensitivity λ to changes in wind speeds is proportional to the length L of the trajectory and inversely proportional to the aerosol lifetime τ.

Simple fractionation model: We now consider fractionation of aerosol species in a moving air parcel. Different aerosol species A and B in a moving air parcel with air concentrations C_A^0 and C_B^0 for $t = 0$ and else $C_A(t)$ and $C_B(t)$, and with different atmospheric life times τ_A and τ_B, are fractionated along the transport route according to

$$\left(\frac{C_A}{C_B}\right)_{(t)} = \left(\frac{C_A^0}{C_B^0}\right)\left(\frac{C_B(t)}{C_B^0}\right)^{(\alpha-1)} \tag{18}$$

where the fractionation factor α is given by the ratio τ_A/τ_B of the atmospheric aerosol lifetimes for the two aerosol species. Expression (18) can be written in the form of a power law:

$$C_A(t) = K \cdot C_B(t)^{\alpha}$$

For a fixed trajectory we can substitute the time $t \longrightarrow L/v$ and the fractionation factor $\alpha = \tau_A/\tau_B \longrightarrow \lambda_A/\lambda_B$. Therefore, using the one-dimensional transport model, we can explain the power law relationship between ion concentrations in Greenland ice cores as an effect of aerosol fractionation during transport where the fractionation factor, α, is given by the power in the power law.

Fractionation model in a complex transport system

The one-dimensional transport model described above is valid for single air parcels, but is far to simple to apply to ice core records that do not resolve into single precipitation events.

In the dust storm season large plumes of mineral dust are long-range transported from Asian deserts and across the North Pacific. During this transport, fractionation of the dust minerals likely occurs and can result in a power law relationship for dust derived soluble ions in Greenland ice cores. However, sea salt and mineral dust in Greenland ice cores are the result of different trajectories and we therefore cannot consider aerosol fractionation in a moving air parcel to explain the relationship for dust and sea salt species. Instead we consider the depletions of the aerosols during transport independently. In equation (18) we may substitute t and $\alpha = \tau_B/\tau_A$ with p and $\alpha = \lambda_B/\lambda_A$, but in a complex transport system p no longer is represented directly by inverse wind speeds, as in the simple one-dimensional transport model. Instead p is a parameter indicating transport efficiency for a given climate regime. This has implication for the strength, $C_i^{\mathrm{ice},0}$, which can no longer be considered as representing air concentrations in the source area, but rather as a

regional source strength, dependent both on source emission and on the large-scale transport patterns.

Seen in a complex transport system the climate parameter, p, indicate a generalized transport efficiency (inversed), the strength, C^0, indicate regional source strength, dependent on both source load and large scale transport patterns, and the sensitivity, λ, reflect physical properties related both to processes influencing the aerosols during transport and to the large-scale transport patterns.

When applied to explain the relationship between ions in the NorthGRIP ion record, the transport model assumes that aerosol emissions and the large-scale transport patterns are constant during transitions between D/O events whereas transport efficiencies are varying synchronously with changing climate conditions. These assumptions are extreme simplifications when compared to the detailed reconstructions of aerosol emissions and transport that are performed on the basis of models and proxy-records. However, on the basis of our analysis we will be able to discuss the importance of transport efficiency relative to other effects on ion concentrations. Furthermore based on the residual time series, which we obtain from our analysis, we will be able to discuss possible systematic changes and long-term changes in large scale transport patterns.

6.5 Results

We analysed ion composition in a section of the NorthGRIP ice core corresponding to a time period within MIS3. We have weighted the sample data by sample time interval according to expression (14) using the ss09sea chronology from Johnsen et al. (2001).

EOF analysis of eight ionic components: The principal component of the EOF analysis of eight ion series explains 86 % of the total variance of the logarithmic ion concentrations and between 93 % and 96 % of the variance for the five dominant ions Ca^{2+}, Mg^{2+}, SO_4^{2-}, Na^+ and Cl^-. For F^-, K^+, and Li^+ only 74 %, 64 %, and 76 % of the variances are explained. The relatively low percentages for those three ions are mainly caused by a high contribution to the variance from spikes. We can demonstrate the effect from spikes by evaluating the variances obtained by a running 5-point median filter on normalized data series. These variances only differ a few % from the variances explained by the EOF principal component (see Table 6.3).

We evaluated significance bands, σ, for the principal component time series according to equation (9). Significance bands for the principal component series is represented in the top curves in Figures 6.12.a and 6.12.b. Attaching corresponding significance bands to the residual series for each variable, we can show that these series represent significant ion specific features.

Estimation of parameters: Statistical parameters for the logarithmic ion concentrations and model series (c_i^m and c_i^M) is shown in Table (6.3), where λ is given as $std(c^M)$. The sensitivity, λ, is highest for Ca^{2+} with $\lambda = 0.839 \pm 0.005$ and lowest for Cl^- with $\lambda = 0.412 \pm 0.009$. The term avg^* is obtained by a 5 points (2.75 m)

running median filtering. The uncertainty, σ_λ, to λ is estimated according to expression (11). The non-linearity, $\Delta\lambda$, represent systematic and long term deviations from λ and was estimated according to equation (13). The estimation of $\Delta\lambda$ was based on a 9 point (or 4.95 m) box filtering of the residual c^R. $\Delta\lambda$ is significantly higher for the ions, Li^+, K^+, and F^-, which is likely to be an effect of the large noise in these series that might be weighted incorrectly when working on logarithmic data. However, these ions are associated with clay minerals and therefore noise in their series could also be an effect of chemical weathering in the source areas. For the major ions $\Delta\lambda$ is highest for Ca^{2+}, with $\Delta\lambda = 0.008$, reflecting the systematic non-linear features for logarithmic Ca^{2+}concentrations.

Power law characteristics α and K, describing ion concentrations in terms of model concentrations for Ca^{2+} (C^M_{Ca}) are shown in Table (6.4), where the first column show the correlation between model concentrations and measured concentrations. The correction for spikes ($avg \longrightarrow avg^*$) has only little influence on the results. We estimated the effect (the non-climate contribution; N.C.C.) of the substitution $avg^* \longrightarrow avg$ in expression (8) where avg^* is the average of the 5 point running median filtered logarithmic ion concentrations (shown in the last column in Table 6.4). For Mg^{2+}, the concentrations are corrected by only 0.4 % whereas K^+ and F^- concentrations are corrected by 3.1 % and 3.3 % respectively. The model series and residuals for all components are shown in Figures 6.13.a-6.13.c.

	% var EOF1	*% var r.m.*	*avg*	*avg**	*std*	λ	σ_λ (%)	$\Delta\lambda$
Li^+	77	75	-6.48	-6.50	0.555	0.486	0.001	0.0182
Na^+	95	92	0.44	0.44	0.459	0.447	0.004	0.0043
K^+	64	67	-2.30	-2.33	0.647	0.519	0.001	0.0439
Mg^{2+}	96	94	0.14	0.14	0.606	0.594	0.008	0.0048
Ca^{2+}	95	96	1.57	1.57	0.859	0.839	0.005	0.0081
F^-	74	79	-3.53	-3.56	0.733	0.631	0.008	0.0528
Cl^-	93	92	0.61	0.61	0.427	0.412	0.009	0.0071
SO_4^{2-}	93	90	0.99	0.98	0.678	0.654	0.003	0.0068

Table 6.3: *Statistical parameters for the measured series $c^m = \ln(C^m)$ and the model series $c^M = \ln(C^M)$. The first two columns shows % variance of the normalized series, c_i^n, represented by respectively the principal component of the EOF analysis and by a 5 point running median. The next two columns show averages of c^m and c^M respectively, where $avg(c^M) = avg^*$ is the average of 5 point median filtered series c^m. The last four columns show $std(c^m)$, $\lambda \equiv std(c^M)$, σ_λ and $\Delta\lambda$ respectively. σ_λ represent the uncertainty to estimations of λ from the set of variables. $\Delta\lambda$ represents variations of λ along the series analysed.*

	corr.	$\alpha_{i,\mathrm{Ca}}$	$\Delta\alpha_{i,\mathrm{Ca}}$	*K*	$\Delta K(\%)$	*N.C.C. (%)*
Li^+	0.49	0.58	0.02	0.00061	4.1	2.0
Na^+	0.98	0.53	0.01	0.68	0.6	0.6
K^+	0.48	0.62	0.05	0.037	3.1	3.1
Mg^{2+}	0.98	0.71	0.01	0.38	0.4	0.4
Ca^{2+}	0.97	1	0.01	1	0.4	0.4
F^-	0.39	0.75	0.06	0.0088	3.3	3.3
Cl^-	0.96	0.49	0.01	0.86	0.6	0.6
SO_4^{2-}	0.95	0.78	0.01	0.78	1.7	1.7

Table 6.4: *Parameters relating ion concentrations by the power law. The first column is the correlation between model concentrations and measured concentrations. K represent ion concentrations in the case of* $\left[Ca^{2+}\right]$ *=1 eq·kg*$^{-1}$*. The last column show the non-climate contribution (N.C.C. in % of measured ion concentrations).*

Investigation of residual signals The residual series $c^R = c^m - c^M$ are shown in figures (6.12.a and 6.12.b). The model time series, $c^M(t)$, are all proportional to the principal component series, $E_1(t)$, shown as the top curve in both figures. The residuals are therefore scaled relative to the top curve according to their magnitude relative to $c^M(t)$. Together with the principal component series the residuals constitute an alternative representation of the data record. In principle these residuals are just a result of the linear transformation performed by the diagonalization of the covariance (correlation) matrix, but with significance limits attached, they represent ion specific signals.

Figure 6.12.a shows the residual for the 5 major ions, Ca^{2+}, Mg^{2+}, SO_4^{2-}, Na^+, and Cl^-. Ca^{2+} shows significant residuals during stadials except for S-10, S-15 and S-16. Mg^{2+} and SO_4^{2-} show no major systematic patterns in their residuals. The sea salt species Na^+ and Cl^- show in their residuals significant systematic patterns, slightly more pronounced for Cl^-, with generally large residuals during the interstadials except for the very warm periods.

Figure 6.12.b shows the residuals for the three species K^+, F^-, and Li^+. They all show large residuals and obviously have added a lot of noise to the principal component. Some systematic patterns could be a consequence of the analysis being performed on logarithmic data, where noise with constant amplitude appears larger during intervals with low concentrations. During interstadial IS-15, F^- shows a large residual in association with the Z2 eruption. The signal is decaying backwards in time and reach back into stadial 15. One may speculate whether this decay is an exceptional firn effect, where F^- has diffused all the way through the firn during deposition, or if it is an effect of the sampling procedure.

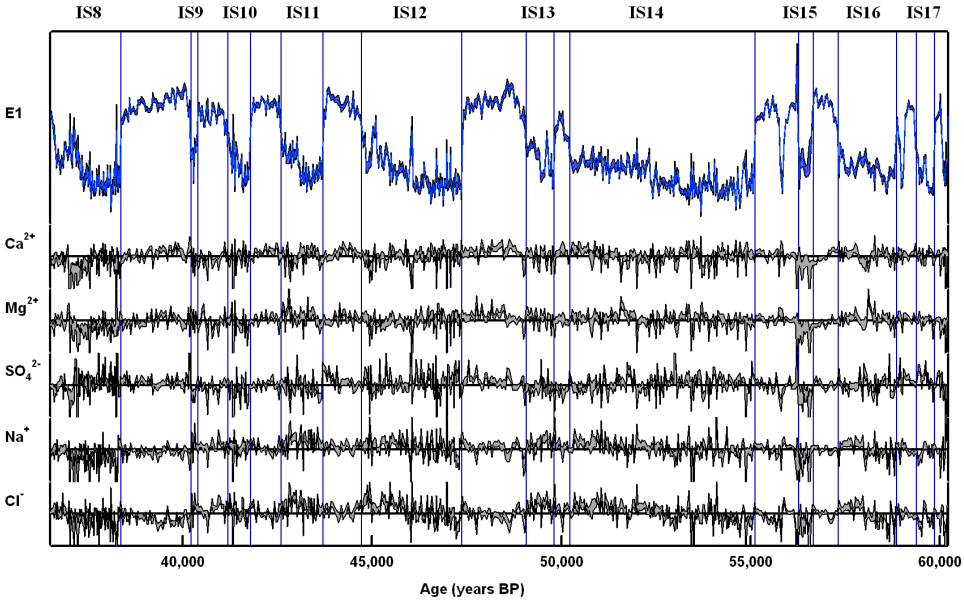

Figure 6.12.a: *The principal component series, $E_1(t)$ (top curve), and logarithmic residual series, c^R, for Ca^{2+}, Mg^{2+}, SO_4^{2-}, Na^+ and Cl^-, all with significance bands. Interstadials are indicated by numbers at the top. The major ions both from dust and sea salt show a negative compensation around the Z2 volcanic eruption at around 56 ka BP. The major dust components Ca^{2+}, Mg^{2+} and SO_4^{2-} show large residuals during stadials. This pattern is most prominent for Ca^{2+} where the residual during stadials accounts for up to 20% of the measured calcium concentrations (see Figure 6.13.a). The residual series for Na^+ and Cl^- show a tendency to a positive signal during the later part of interstadials.*

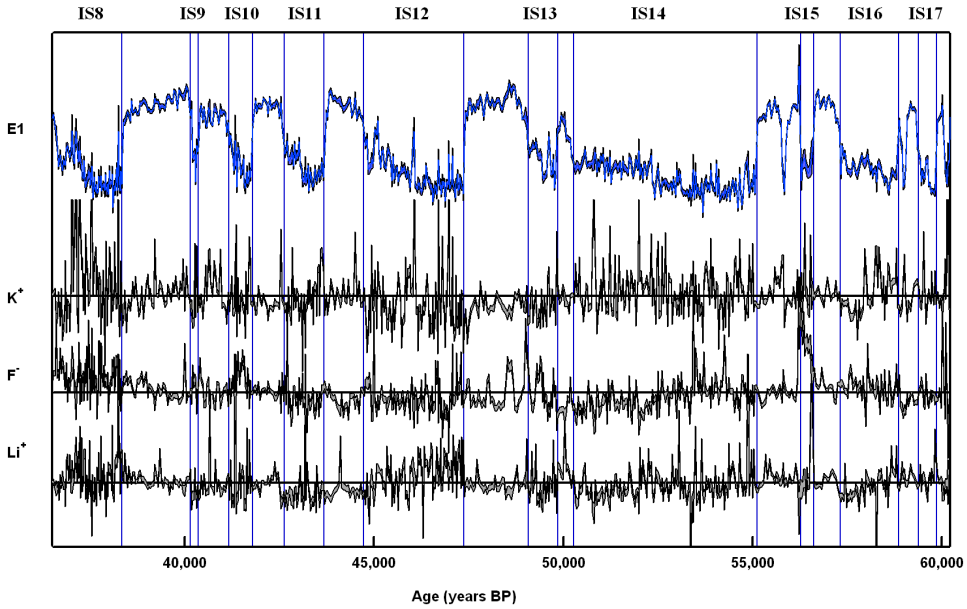

Figure 6.12.b: *The principal component series, $E_1(t)$ (top curve), and logarithmic residual series, c^R, for K^+, F^-, and Li^+. Interstadials are indicated by numbers at the top. The ions F^-, Li^+ and K^+ are dust derived, but show a pattern different from the major dust derived ions Ca^{2+}, Mg^{2+}, and SO_4^{2-}. The generally high residuals during interstadials could be an effect of using logarithmic concentrations.*

EOF analysis of the six dust components: The ion species that we analyse here represent two different types of aerosol, sea salt and mineral dust. We did an analysis only for the six dust components, leaving out Na^+ and Cl^-. This analysis showed no major differences in the residuals compared to the analysis including all eight ions. The residual concentrations, C^R, for Ca^{2+} in the two analyses, with and without sea salt species, showed a correlation coefficient of 0.92, which means that the systematic patterns of Ca^{2+} residuals is a feature within the dust species and not an effect of the relationship between mineral dust and sea salt aerosol. The invariance of residuals for dust species in the two analyses implies for the sea salt species (Na^+ and Cl^-) that their residuals represent features of the relationship between sea salt and mineral dust aerosol.

Robustness against the Z2 signature: We tested the robustness of the principal component series against the large contribution associated with the Z2 eruption by repeating the analysis without two data points around the Z2 eruption. The correlation coefficient between the residuals in concentrations, C^R, obtained by the analyses including and excluding these data points was better than 0.99 for all ions, which means that the chemical signature of the Z2 eruption had no impact on the

analysis even though it appears as an artefact in the climate series evaluated from the principal component.

Model concentrations: Measured ion concentrations, C^m, model concentrations, C^M, and residuals $C^R = C^m - C^M$, are shown for all eight ions in Figures 6.13.a-6.13.c. The residuals appears differently in the concentration series. The residual for Ca^{2+} concentrations show large positive deviations from the power law in the cold periods of stadials S-9, S-11, S-12 and S-13. These deviations correspond to up to 20% of Ca^{2+} concentrations. The Mg^{2+} residual show the same tendency, but to a lesser extent and not exactly synchronous with Ca^{2+}. The SO_4^{2-} series show a slightly larger residual in stadials S-12 and S-13.

The sea salt components $Na^+$and Cl^- show negative residuals in cold periods and positive residuals in the late part of the warm periods. These systematic patterns suggest an effect of minor differences in the large-scale transport patterns of the stadials and interstadials rather than a source effect.

The dust components K^+, F^-, and Li^+ show negative residuals during stadials, which could be a consequence of using logarithmic concentrations or an effect of possible different weathering mechanisms in the source area during cold and warm periods.

Investigation of influence from accumulation rates: To evaluate effects of changing accumulation rates we repeated the analysis including accumulation rates estimated on the basis of $\delta^{18}O$ values (Sigfus Johnson unpublished data). Inverse accumulation rates respond to climate changes very similarly to ion concentrations and will affect ion concentrations linearly. We included normalized logarithmic accumulation rates in the analysis. The principal component explained 80 % of the variance for this series, which is a relatively high covariance. However $\alpha_{\mathrm{acc,i}}$ was far below 1 for all ion species (e.g. $\alpha_{\mathrm{acc,Ca}} = 0.26$; $\alpha = 1$ indicates a linear relationship). This means that possible effects from deposition processes are of secondary importance only.

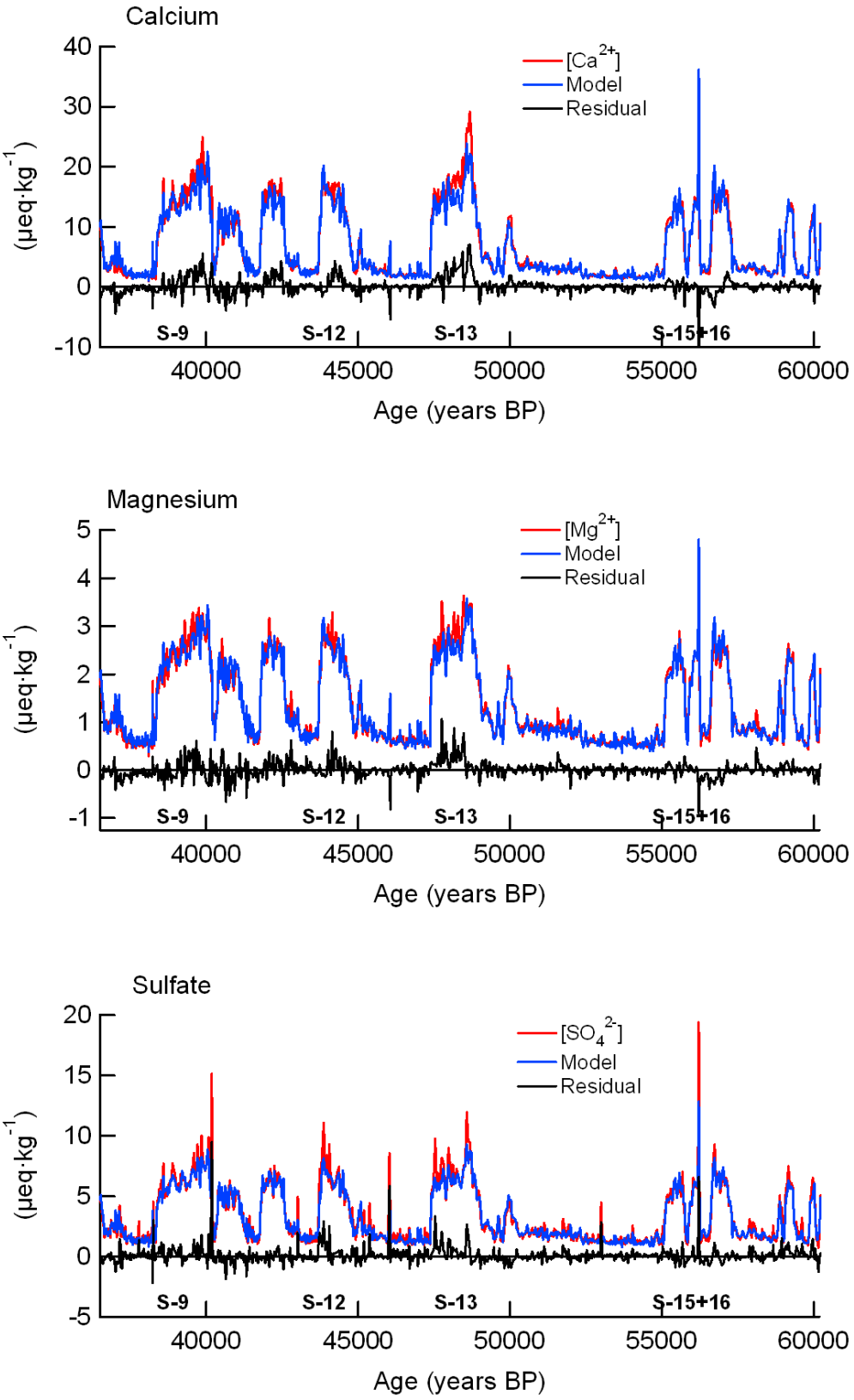
Calcium
[Ca2+]
Model
Residual
(µeq·kg-1)
40
30
20
10
0
-10
S-9
S-12
S-13
S-15+16
40000
45000
50000
55000
60000
Age (years BP)
Magnesium
[Mg2+]
Model
Residual
(µeq·kg-1)
5
4
3
2
1
0
-1
S-9
S-12
S-13
S-15+16
40000
45000
50000
55000
60000
Age (years BP)
Sulfate
[SO4 2-]
Model
Residual
(µeq·kg-1)
20
15
10
5
0
-5
S-9
S-12
S-13
S-15+16
40000
45000
50000
55000
60000
Age (years BP)

Figure 6.13.a: (Previous page) *Measured ion concentrations, model concentrations and residuals (measured - model) for the dust species Ca^{2+}, Mg^{2+}, SO_4^{2-}.*

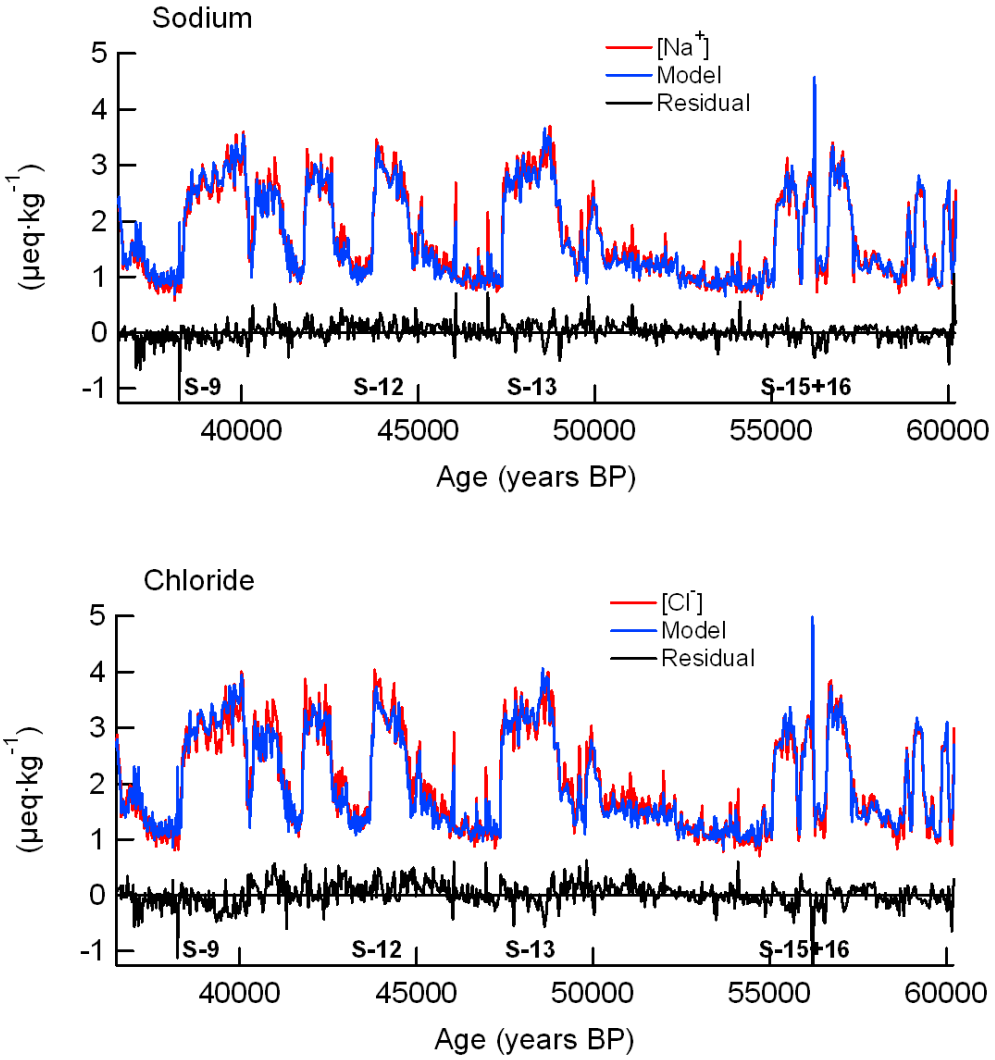

Figure 6.13.b: (Above) *Measured ion concentrations, model concentrations and residuals (measured - model) for the sea salt species Na^+ and Cl^-.*

Figure 6.13.c: (Next page) *Measured ion concentrations, model concentrations and residuals (measured - model) for K^+, F^-, and Li^+.*

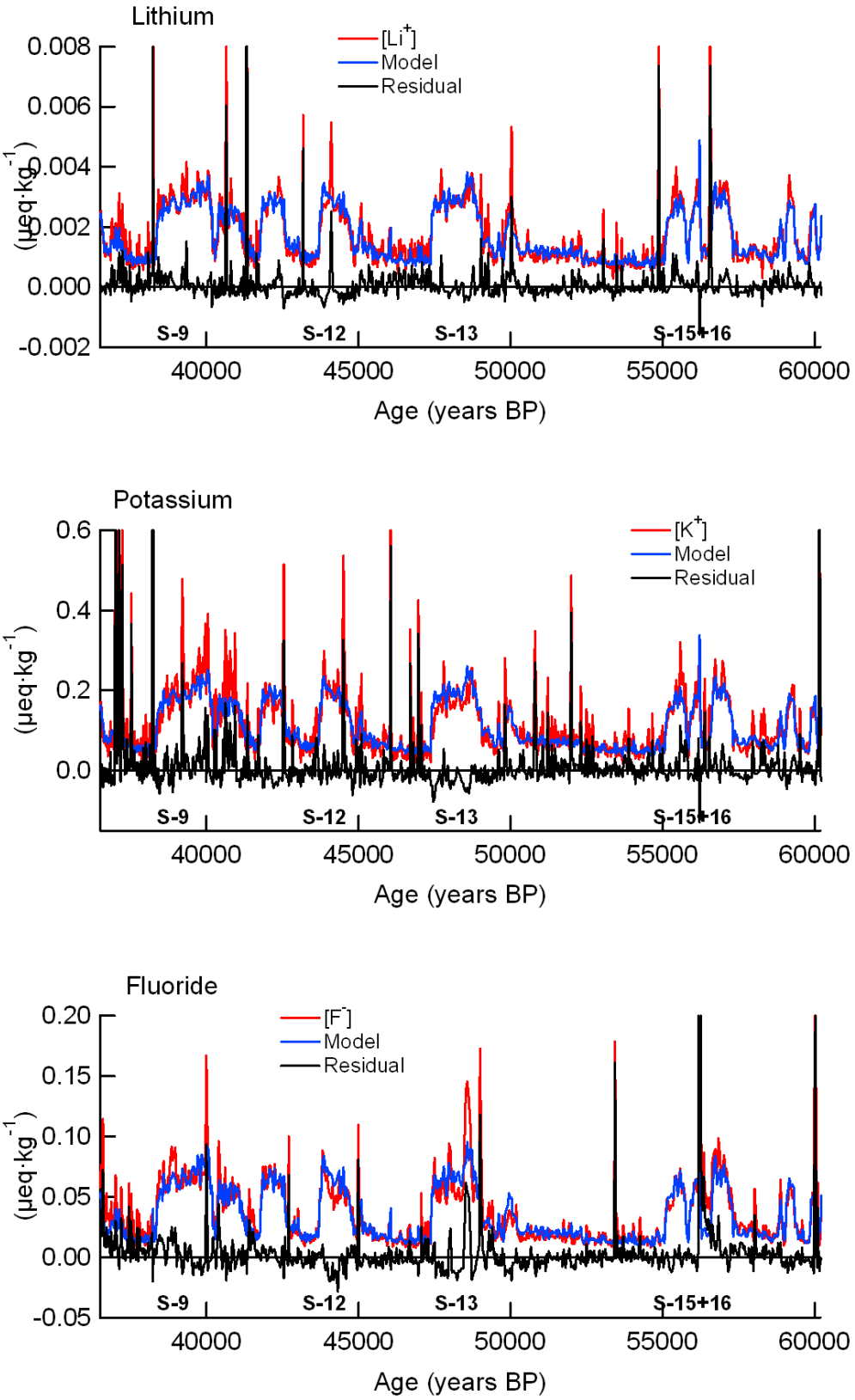
Lithium
[Li+]
Model
Residual
0.008
0.006
0.004
0.002
0.000
-0.002
(μeq·kg-1)
S-9
S-12
S-13
S-15+16
40000
45000
50000
55000
60000
Age (years BP)
Potassium
[K+]
Model
Residual
0.6
0.4
0.2
0.0
(μeq·kg-1)
S-9
S-12
S-13
S-15+16
40000
45000
50000
55000
60000
Age (years BP)
Fluoride
[F-]
Model
Residual
0.20
0.15
0.10
0.05
0.00
-0.05
(μeq·kg-1)
S-9
S-12
S-13
S-15+16
40000
45000
50000
55000
60000
Age (years BP)

6.6 Discussion

A main result of the analysis is the estimation of sensitivities, λ, for all investigated ions, where λ are found to be larger for the dust species than for the sea salt species. According to the simple transport model, applied in this analysis, λ is directly related to aerosol life time, τ, and transport path length L.

Dust: Chinese desert areas have been found to be the dominant source area for the dust in Greenland ice cores (Biscaye et al., 1997; Svensson et al., 2000). Therefore we can consider the transport path for different dust species to be identical, and the different λ among dust species must be explained by different aerosol lifetimes for the different species. We can range the life time for dust species as follows:

$$\tau_{\text{insoluble dust}} < \tau_{Ca^{2+}} < \tau_{SO_4^{2-}} < \tau_{F^-} < \tau_{Mg^{2+}} < \tau_{K^+} < \tau_{Li^+}.$$

where we also have included the range of life times for insoluble dust and Ca^{2+} determined from concentrations of insoluble dustmass and Ca^{2+} in the GRIP ice core. The different transport life times for the different ion species can be resulting from mineral fractionation during transport.

During long-range transport, dust particles are subject to various fractionation processes. Dry deposition and collision scavenging processes result in different kinds of size fractionation, whereas nucleation scavenging result in fractionation according to hygroscopic properties of the aerosols.

Clay minerals are considered more hygroscopic than other minerals and hence are more sensitive to nucleation scavenging. Therefore, if nucleation scavening is the the dominant fractionation process, ions derived from clay minerals would show a relatively shorter lifetime. Based on our observation of longer lifetimes for the clay derived dust species (Li^+ and K^+), we can exclude fractionation by nucleation scavenging as a major effect on ion characteristics. The different lifetimes for dust species must therefore be explained as an effect of different size characteristics for various mineral types.

Under dry conditions lifetimes depends inversely on the square of particle radius (gravitational settling). Particles of quarts and feldspars belong to the coarse particle fraction whereas clay particles are related to the very fine size fraction and have under dry conditions therefore a relatively longer lifetime (Arnold et al., 1998). Quartz and feldspars are insoluble minerals and our observation of the relatively shorter lifetime of the insoluble dust material is likely to be associated with those minerals. The soluble dust species of Ca^{2+}, Mg^{2+}, and SO_4^{2-} are mainly derived from carbonates and sulphates (limestone, dolomite and gypsum), that might have smaller particle sizes than quartz and feldspars. A fraction of the soluble Mg^{2+} is probably dissolved from clay minerals. F^-, K^+, and Li^+ are mainly derived from clay minerals. However, a large fraction of K^+ is from sea salt, which might have a influence of the estimated lifetime for K^+.

Collision scavenging has a larger effect on particles that are both larger and smaller than particles around 1 μm in diameter. The dust particle size mode observed in Greenland ice cores vary close to 1 μm in diameter. Therefore the dust material in Greenland ice cores can have been affected by collision scavenging.

We observed a factor of 1.7 in difference of the Mg^{2+}/Ca^{2+} ratio between stadials and interstadials in the NorthGRIP MIS3 ion record. For such a large change in ratios between ion concentrations to be a result of changes in particle size mode of only 10 %, as observed by Ruth et al. (2003), requires that the two species $Mg^{2+}$and Ca^{2+} are related to distinctly different particle size fractions, which would be the case if a relatively large fraction of Mg^{2+} is derived from clay minerals.

Sea salt: The sensitivities, λ, for sea salt species are smaller than for dust species. This we consider to be partly an effect of a shorter transport path length for sea salt; i.e.:

$$L_{\text{sea salt}} < L_{\text{dust}}$$

We assume that the source of sea salt is located at open ocean, more specificly where wind conditions for uplift and long-range transport are most favourable. This means that the location of the sea salt source is coupled to the patterns and strength of the jet stream (see Chapter 2.5). If the sea salt source during the last glacial was located in the North Pacific, the transport path to Greenland would be smaller for sea salt than for the dust, as inferred from the λ's.

Possible changes in the jet stream patterns could result in a change in location of the sea salt aerosol, which would affect the dust/sea salt relationship in Greenland ice cores. Therefore we will consider changes in the jet stream patterns as a possible explanation for non-linear patterns in the relationship between logarithmic dust and sea salt concentrations.

Non-linear properties: Non-linear properties of the relationship between logarithmic concentrations of soluble ions in Greenland ice cores include both systematic non-linearly patterns and long term trends, and reflect limitations in the simple transport model. Such limitations could be related to the source, to the trajectories and to the processes influencing the aerosol during transport. Concerning the source, the model would be invalid if the source areas differ significantly from a point source, or if the source has changed location or strength during the time period of the series analysed. Concerning the trajectories, the model would be invalid if there was significant changes in trajectory patterns, e.g. seasonal changes in trajectory patterns, or if different dust species were transported along different trajectories. Concerning the aerosol life time, the model would be invalid if the dominant fractionation process changes with changing climate.

Ion concentrations in Greenland ice cores show strong seasonality both for present and for the last glacial (Ruth et al., 2002; Steffensen, 1988). At present dust and sea salt in Greenland is mainly deposited during spring and winter, respectively (Steffensen, 1988) mainly due to more effective uplift and transport during this time of the year (see Chapter 2.9). Seasonal changes in the jet stream patterns and strength adds could be a limitation for the simple transport model that we used to explain the relationship between ion concentrations in Greenland ice cores.

A analysis including only six components: Li^+, K^+,Mg^{2+}, Ca^{2+}, F^-, and SO_4^{2-}, showed that the large residuals during stadials for Ca^{2+} is a feature of the dust it self rather than an effect of the relationship between dust and sea salt. To explain the non-linear features of Ca^{2+}, we therefore will look for effects acting on the dust

alone. Assuming that the dust source location remains constant during changing climate, one explaination for the large Ca^{2+} residual could be changes in mineral characteristics of the aerosol dust material. Another explanation could be related to trajectory patterns, which during the last glacial might have been affected by changes in temperatures, sea ice extent, and ice sheet topography. Furthermore, the season for dust storms during the last glacial might have been extended compared to present (Tegen et al., 2002) and therefore dust in Greenland during the last glacial could have been influenced by seasonal changes in trajectory patterns. However, if the dust source can be considered as a point source, changes in trajectory patterns for dust would affect the relationship between dust species, only, when combined with other effects acting on the aerosol lifetimes. An exsample could be seasonal changes in trajectories combined with seasonal changes in mineral characteristics in case of an extended dust season confined to only a part of the desert dust source areas.

A resent model simulation has shown a strong seasonality in the LGM jet stream patterns, with a split configuration over the Laurentide ice sheet and a strong northern branch during winter and a single branch south of the Laurentide during summer (Bromwich et al., 2004). In such a pronounced seasonality, an extended dust season would result in a very strong seasonal change in transport patterns for dust, most likely to be associated with seasonal effects both in the source areas and in the dominant fractionation process.

The small deviations in linear properties between sea salt and dust, as reflected in the large residuals for Na^+ and Cl^- during interstadials, could be an effect of small changes in the source location of the sea salt source. We would expect that the sea salt source, following the jet stream patterns, moved south during cold periods, but the large residuals at the end of interstadials suggest a larger λ for sea salt during these periods, which we can explain as a west ward movement of the sea salt source during the warm periods. However, we must also consider the possibility of a change in trajectories and eventually changes in seasonal patterns of trajectories.

6.7 Conclusions

We have developed a statistical method that provides characteristics of ice core ion records. On the basis of a simple transport model we infer physical meaningful parameters from these characteristics. We can interpret statistical parameters obtained from the NorthGRIP record of soluble ions in terms of large-scale transport patterns, aerosol life times, and source strength.

Our interpretation is partly motivated by the systematic relationship between the $\delta^{18}O$ record and logarithmic ion concentrations. The ion characteristics that we obtain from the statistical analysis are in principle just the mean and the amplitude (standard deviation or "sensitivity") of D/O variations in the different ion series. However stadials and interstadials represent two distinctly different climate regimes, and we therefore have to be concerned about systematic differences in ion characteristics for warm and cold periods. The results of our analysis of ion characteristics in the NorthGRIP ice core suggest that source strengts and large-scale transport patterns changed only little during the D/O events. Major changes in ion

concentrations can be explained as mainly an effect of changing transport efficiency. At present the seasonal variation in windspeeds results in a seasonal pattern of deposition of sea salt aerosol in Greenland. This leads us to suggest that windspeeds have had an important influence on aerosol transport during the last glacial period. Changes in transport patterns and source strength during the last glacial have had only a secondary influence on concentrations of dust and sea salt in Greenland ice cores. These seondary effects are reflected in the non-linear patterns represented by the EOF residual series.

Various sensitivities for dust species are explained in terms of different aerosol life times, and the relatively small sensitivities for sea salt species are explained in terms of a relatively shorter tranport path.

Interpretations of the parameters C^0, λ, and p could be further improved. C^0 might be determined in terms of an upper limit of ice core concentrations with respect to the prevailing source strength and transport patterns. This upper limit would depend on the high frequency variance in the jet stream patterns.

More detailed investigations of non-linear patterns in the ion records is needed in order understand the underlying physical processes. Comparisons with model simulations of jet stream patterns will help understand effects of source emission and trajectory patterns, and possible seasonal effects.

Comparisons of ion characteristics in Greenland ice cores from different locations (e.g. NorthGRIP and GISP2) could improve understanding large-scale transport patterns during the last glacial period and the relative importance of source effects and transport effects on non-linear properties in the ion record.

Acknowledgement: The NorthGRIP project is directed and organized by the Department of Geophysics at the Niels Bohr Institute for Astronomy, Physics and Geophysics, University of Copenhagen. It is being supported by funding agencies in Denmark, Belgium, France, Germany, Iceland, Japan, Sweden, Switzerland, and the United States of America.

6.8 References

Alley, R., R. C. Finkel, et al. (1995). "Changes in continental and sea-salt atmospheric loadings in central Greenland during the most recent deglaciation: Model-based estimates." Journal of Glaciology **41**(139): 503-514.

Andersen, K. K., A. Armengaud, et al. (1998). "Atmospheric dust under glacial and interglacial conditions." Geophysical Research Letters **25**(13): 2281-2284.

Arnold, E., J. Merrill, et al. (1998). "The effect of source area and atmospheric transport on mineral aerosol collected over the North Pacific Ocean." Global and Planetary Change **18**(3-4): 137-159.

Biscaye, P. E., F. E. Grousset, et al. (1997). "Asian provenance of glacial dust (stage 2) in the Greenland Ice Sheet Project 2 Ice Core, Summit, Greenland." Journal of Geophysical Research **102**(C12): 26765-26781.

Bromwich, D. H., E. R. Toracinta, et al. (2004). "Polar MM5 simulations of the winter climate of the Laurentide Ice Sheet at the LGM." Journal of Climate **17**: 3415-3433.

Dahl-Jensen, D., N. Gundestrup, et al. (2002). "The NorthGRIP deep drilling program." Annals of Glaciology **35**: 1-4.

Dansgaard, W., S. J. Johnsen, et al. (1993). "Evidence for general instability of past climate from a 250-kyr ice-core record." Nature **364**(6434): 218-220.

De Angelis, M., J. P. Steffensen, et al. (1997). "Primary aerosol (sea salt and soil dust) deposited in Greenland ice during the last climatic cycle: Comparison with east Antarctic records." Journal of Geophysical Research **102**(C12): 26681-26698.

Ditlevsen, P. D. and N. D. Marsh (1998). "New method for identification of sources for chemical time series and its application to the Greenland Ice Sheet Project ice core record." Journal of Geophysical Research **103**(D5): 5649-5660 .

Fuhrer, K. and M. Legrand (1997). "Continental Biogenic species in the Greenland Ice Core Project ice core: Tracing back the biomass history of the North American continent." Journal of Geophysical Research **102**(C12): 26735-26745.

Fuhrer, K., A. Neftel, et al. (1993). "Continuous measurements of hydrogen peroxide, formaldehyde, calcium and ammonium concentrations along the new GRIP ice core from Summit, central Greenland." Atmospheric Environment , Part A **27**(12): 1873-1880.

Fuhrer, K., A. Neftel, et al. (1996). "High-resolution ammonium ice core record covering a complete glacial-interglacial cycle." Journal of Geophysical Research **101**(D2): 4147-4164.

Fuhrer, K., E. W. Wolff, et al. (1999). "Timescales for dust variability in the Greenland Ice Core Project (GRIP) ice core in the last 100,000 years." Journal of Geophysical Research **104**(D24): 31043-31052.

Hammer, C., P. A. Mayewski, et al. (1997). "Preface." Journal of Geophysical Research **102**(C12): 26315-26316.

Holland, H. D. (1984). The Chemical Evolution of the Atmosphere and Oceans. Princeton, New Jersey, Princeton University Press.

JGR Special Issue (1997). "Greenland Summit Ice Cores, Greenland Ice Sheet Project 2 and Greenland Ice Core Project." Journal of Geophysical Research **102**(C12).

Johnsen, S. J., D. Dahl-Jensen, et al. (2001). "Oxygen isotope and palaeotemperature records from six Greenland ice-core stations: Camp Century, Dye-3, GRIP, GISP2, Renland and NorthGRIP." Journal of Quaternary Science **16**(4): 299-307.

Laj, P., G. Ghermandi, et al. (1996). "Coupling PIXE and SEM/EDAX for characterizing atmospheric aerosols in ice-cores." Nuclear Instruments and Methods in Physics Research Section B: Beam Interactions with Materials and Atoms **109-110**: 252-257.

Laj, P., G. Ghermandi, et al. (1997). "Distribution of CA, Fe, K, and S between soluble and insoluble material in the Greenland Ice Core Project ice core." Journal of Geophysical Research **102**(C12): 26615-26623.

Legrand, M., M. De Angelis, et al. (1993). "Field investigation of major and minor ions along Summit (Central Greenland) ice cores by ion chromatography." Journal of Chromatography **A, 640**: 251-258.

Legrand, M., C. Hammer, et al. (1997). "Sulfur-containing species (methanesulfonate and SO_4) over the last climatic cycle in the Greenland Ice Core Project (central Greenland) ice core." Journal of Geophysical Research **102**(C12): 26663-26679.

Maggi, V. (1997). "Mineralogy of atmospheric microparticles deposited along the Greenland Ice Core Project ice core." Journal of Geophysical Research **102**(C12): 26725-26734.

Mahowald, N., K. Kohfeld, et al. (1999). "Dust sources and deposition during the last glacial maximum and current climate: A comparison of model results with paleodata from ice cores and marine sediments." Journal of Geophysical Research **104**(D13): 15895-15916.

Marsh, N. D. and P. D. Ditlevsen (1997). "Climate during glaciation and deglaciation identified through chemical tracers in ice-cores." Geophysical Research Letters **24**(11): 1319-1322.

Mayewski, P. A., L. D. Meeker, et al. (1997). "Major features and forcing of high-latitude Northern Hemisphere atmospheric circulation using a 110,000-year-long glaciochemical series." Journal of Geophysical Research **102**(C12): 26345-26366.

Mayewski, P. A., L. D. Meeker, et al. (1994). "Changes in atmospheric circulation and ocean ice cover over the North Atlantic during the last 41,000 years." Science **263**: 1747-1751.

Meeker, L. D., P. A. Mayewski, et al. (1997). "A 110,000-year history of change in continental biogenic emissions and related atmospheric circulation inferred from the Greenland Ice Sheet Project Ice Core." Journal of Geophysical Research **102**(C12): 26489-26504.

North Greenland Ice-Core Project (NorthGRIP) Members (2004). "High resolution Climate Record of the Northern Hemisphere reaching into the last Glacial Interglacial Period." Nature **431**: 147-151.

O'Brien, S. R., P. A. Mayewski, et al. (1995). "Complexity of Holocene climate as reconstructed form a Greenland ice core." Science **270**: 1962-1964.

Reader, M. C. and N. McFarlane (2003). "Sea-salt aerosol distribution during the Last Glacial Maximum and its implications for mineral dust." Journal of Geophysical Research **108**(D8): 4253, doi:10.1029/2002JD002063.

Röthlisberger, R., M. Bigler, et al. (2000). "Technique for continuous high-resolution analysis of trace substances in firn and ice cores." Environmental Science & Technology **34**(2): 338-342.

Röthlisberger, R., M. A. Hutterli, et al. (2002). "Nitrate in Greenland and Antarctic ice core: A detailed description of post-depositional processes." Annals of Glaciology **35**: 209-216.

Ruth, U., D. Wagenbach, et al. (2002). "High resolution microparticle profiles at NGRIP: Case studies of calcium-dust relationship." Annals of Glaciology **35**: 237-242.

Ruth, U., D. Wagenbach, et al. (2003). "Continuous record of microparticle concentration and size distribution in the central Greenland NGRIP ice core during the last glacial period." Journal of Geophysical Research **108**(D3): 4098, doi:10.1029/2002JD002376.

Steffensen, J. P. (1988). "Analysis of the seasonal variation in dust, Cl^-, NO_3^-, and SO_4^{2-} in two Central Greenland firn cores." Annals of Glaciology **10**: 171-177.

Steffensen, J. P. (1997). "The size distribution of microparticles from selected segments of the Greenland Ice Core Project ice core representing different climatic periods." Journal of Geophysical Research **102**(C12): 26755-26763.

Svensson, A., P. E. Biscaye, et al. (2000). "Characterization of late glacial continental dust in the Greenland Ice Core Project ice core." Journal of Geophysical Research **105**(D4): 4637-4656.

Tegen, I. (2003). "Modeling the mineral dust aerosol cycle in the climate system." Quaternary Science Reviews **22**: 1821-1834.

Tegen, I., S. P. Harrison, et al. (2002). "The impact of vegetation and preferential source areas on global dust aerosol: Results from a model study." Journal of Geophysical Research **107**(D21): 4576, doi:10.1029/2001JD000963.

Wagenbach, D., F. Ducroz, et al. (1998). "Sea-salt aerosol in coastal Antarctic regions." Journal of Geophysical Research **103**(D9): 10961-10974.

Werner, M., I. Tegen, et al. (2002). "Seasonal and interannual variability of the mineral dust cycle under present and glacial climate conditions." Journal of Geophysical Research **107**(D24): 4744, doi:10.1029/2002JD002365.

Yiou, P., K. Fuhrer, et al. (1997). "Paleoclimatic variability inferred from the spectral analysis of Greenland and Antarctic ice-core data." Journal of Geophysical Research **102**(C12): 26441-26454.

High-resolution record of Northern Hemisphere climate extending into the last interglacial period

North Greenland Ice Core Project members*

**A full list of authors appears at the end of this paper*

Two deep ice cores from central Greenland, drilled in the 1990s, have played a key role in climate reconstructions of the Northern Hemisphere, but the oldest sections of the cores were disturbed in chronology owing to ice folding near the bedrock. Here we present an undisturbed climate record from a North Greenland ice core, which extends back to 123,000 years before the present, within the last interglacial period. The oxygen isotopes in the ice imply that climate was stable during the last interglacial period, with temperatures 5 °C warmer than today. We find unexpectedly large temperature differences between our new record from northern Greenland and the undisturbed sections of the cores from central Greenland, suggesting that the extent of ice in the Northern Hemisphere modulated the latitudinal temperature gradients in Greenland. This record shows a slow decline in temperatures that marked the initiation of the last glacial period. Our record reveals a hitherto unrecognized warm period initiated by an abrupt climate warming about 115,000 years ago, before glacial conditions were fully developed. This event does not appear to have an immediate Antarctic counterpart, suggesting that the climate see-saw between the hemispheres (which dominated the last glacial period) was not operating at this time.

The two deep ice cores drilled at the beginning of the 1990s in central Greenland (GRIP[1–3] and GISP2[4,5], respectively 3,027 m and 3,053 m long) have played a key role in documenting rapid climate changes during the last glacial period. However, it quickly became clear that the bottom 10% of at least one (and most probably both) of these ice cores[4,6–9] was disturbed owing to ice folding close to the bedrock. The Central Greenland ice core records are fully reliable climate archives back to 105,000 years before present (105 kyr BP), but the disturbances mean that no reliable Northern Hemisphere ice core record of the previous interglacial (the Eemian climatic period) was known to exist in the Northern Hemisphere.

This situation motivated the search for a new drilling site where undisturbed ice from the last interglacial period[10], and even from the previous glacial period, would be accessible[11]. The North Greenland Ice Core Project (NGRIP) site, located at 75.10 °N and 42.32 °W with an elevation of 2,917 m and an ice thickness of 3,085 m (Fig. 1), was selected on the basis of three criteria that, when satisfied together, should produce dateable ice older than that found in central Greenland: a position on a ridge to reduce deformation by ice flow, flat bedrock, and a lower precipitation rate. The present accumulation rate is 0.19 m ice equivalent yr^{-1}, the annual mean temperature is −31.5 °C, and the ice near the base originates 50 km upstream of the ice ridge in the direction of Summit[12]. The NGRIP drilling started in 1996, and bedrock was reached in July 2003.

Dating of the NGRIP climate record

The climate record of the oxygen isotopic composition of the ice ($\delta^{18}O$) from the NGRIP ice core is shown in Fig. 2 (and is available as Supplementary Information). In cold glaciers where the basal ice temperature is below freezing, the annual ice layers typically thin towards zero thickness close to bedrock, and flow induced disturbances can limit the usefulness of the deepest part of ice cores[13]. In contrast, at NGRIP high rates of basal ice melting, estimated to be 7 mm yr^{-1} (refs 12, 14), remove the bottom layers, greatly restricting the thinning of the layers and the possibility of ice disturbances. Whereas the present-day accumulation is 15% lower at NGRIP than at GRIP, NGRIP annual layer thicknesses at 105 kyr BP (depth 2,900 m) are of the order of 1.1 cm, twice that of GRIP ice of this age.

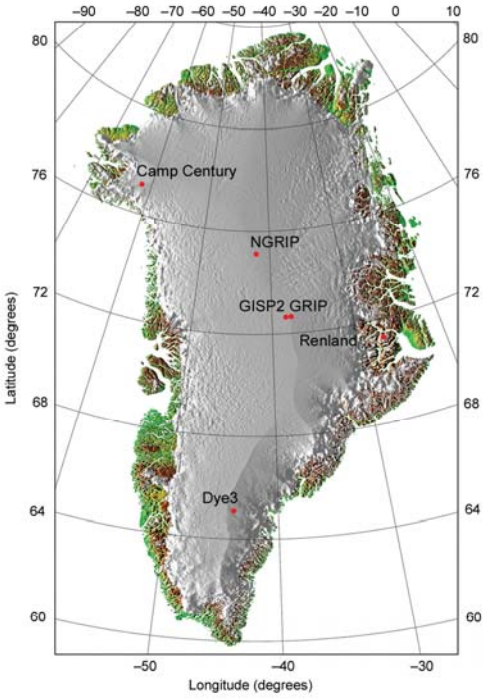

Figure 1 Map of Greenland, showing the locations of the deep ice core drilling sites. The sites GRIP (72.5 °N, 37.3 °W), GISP2 (72.5 °N, 38.3 °W), NGRIP (75.1 °N, 42.3 °W), Camp Century (77.2 °N, 61.1 °W), Dye3 (65.2 °N, 43.8 °W) and Renland (71.3 °N, 26.7 °W) are marked. The Greenland map was provided by S. Ekholm, Danish Cadastre.

The NGRIP isotopic record covers the Holocene, the entire last glacial period, and part of the Eemian period. The 24 abrupt and climatic warm Dansgaard–Oeschger (DO) events, or Greenland interstadials (GIS), initially numbered in the GRIP record[1,2] are very clearly identified (Fig. 2a, b), as are the climatic cold Greenland stadials (GS) that follow the DO events. The NGRIP core has been cross-dated to the GRIP core ss09sea chronology[15] down to 105 kyr BP using the high-resolution ice isotope profiles and volcanic events found in the ECM and DEP records[5,16]. Older ice is cross-dated to the Antarctic Vostok ice core records by using concentrations of methane and $\delta^{18}O$ of the entrapped air[9,17–22]. To determine if deep ice folding is a problem at NGRIP, we concentrate on the period corresponding to the marine isotope stage (MIS) 5d/5c transition dated around 105 kyr BP at Vostok (GT4 timescale). From methane and $\delta^{15}N$ air measurements, we confirm that this transition is the counterpart of the Northern Hemisphere stadial 25[18,21,23] that ends with the abrupt onset of DO 24 at the NGRIP depth of 2,940 m (Fig. 3). At this depth, methane concentrations in air exhibit a rapid increase from 450 to 650 p.p.b.v., a shift which is also observed in the Vostok data[24] (Fig. 3), and the $\delta^{15}N$ air signal, measured with a resolution of better than 100 yr, shows a rapid increase typical of DO events, resulting from thermal and gravitational fractionation processes. The increase in $\delta^{15}N$ and in methane concentration over the warming of DO 24 are both located 7 m deeper in the ice core than the corresponding $\delta^{18}O$ transition[25–27] (Fig. 3). This reflects the typical depth shift, or gas-age/ice-age difference, expected with normal firnification processes and later thinning through ice flow[28]. This supports our contention that the bottom ice is undisturbed by folding or ice mixing. We note that similar investigations on the GRIP core have confirmed that this record is indeed disturbed at the time of the 5d/5c transition[7,18], as in that core the isotope and gas transitions are located at the same depth.

Below DO 19 the NGRIP record is compared to the planktonic oxygen isotope record from marine core MD95-2045 drilled on the Iberian margin[29] (Fig. 4). On the basis of strong similarities between these two records and ice modelling as well as $\delta^{18}O$ air measurements on the deepest parts of the core compared with Vostok, the basal part of the NGRIP record is dated to 123 kyr BP. Owing to the basal melting, the annual layer thickness of the ice from 2,700 to 3,085 m (90 to 123 kyr BP) thins much less than in the case of no melting, further making dating straightforward. At these depths, the depth scale is almost linearly proportional to time. Thus, we feel confident in interpreting the ice isotopic record at NGRIP as the first Northern Hemisphere ice core record of a highly detailed, undisturbed climate record of the late Eemian and the inception of the last glacial period.

Climate record of the late Eemian period

We first examine the implications arising from the relatively high (warm) and stable Eemian ice isotopic values found in the bottom 85 m of the ice core. As noted above, the annual layers are unusually thick, 1.0 to 1.6 cm, through this period of glacial interception and the latter part of the Eemian period, allowing a very detailed look at this key climatic period. The maximum isotopic value of −32‰ found for the Eemian in the NGRIP core corresponds to the highest values found in the GRIP and GISP2 ice cores. Although these other cores have disturbed chronologies for ice older than 105 kyr BP, they do contain Eemian age ice[15,18], and the maximum isotopic values can be assumed to represent the warmest Eemian climate[30]. Because both the present interglacial isotopic values (−35‰) and the Eemian values are similar in the GRIP, GISP2, and NGRIP ice, we infer that the ice from the bottom of the NGRIP core has sampled the warmest part of Eemian climate. This maximum isotopic value is 3‰ higher than the present value, and if attributed solely to temperature, implies at least a 5 K warmer temperature in the Eemian than at present[30–33]. It is notable that the 3‰ isotopic value difference between the present and the Eemian period seen at NGRIP, GRIP and GISP2 is also found in northern Greenland ice

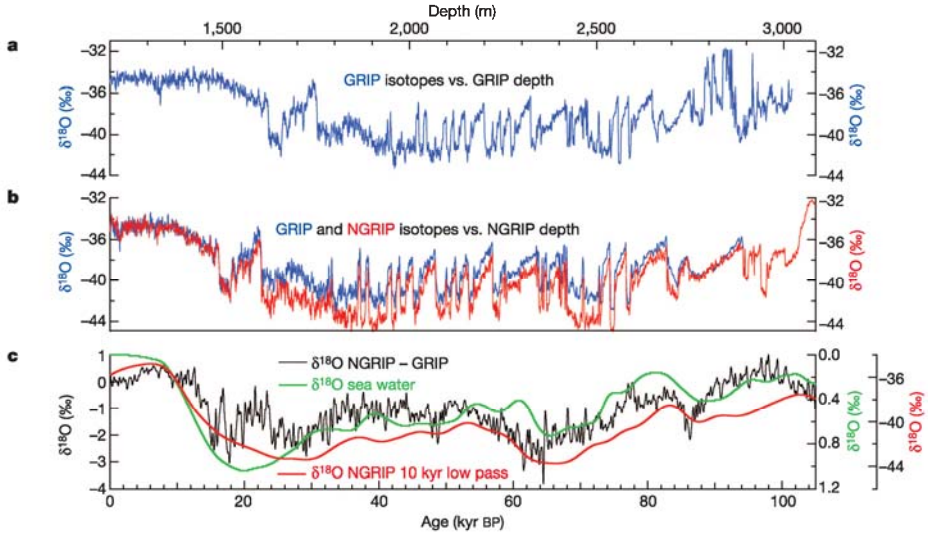

Figure 2 The NGRIP stable oxygen isotopic record compared to the GRIP record. **a**, The GRIP oxygen isotopic profile (blue) with respect to depth at GRIP. Isotopic values ($\delta^{18}O$) are expressed in ‰ with respect to Vienna Standard Mean Ocean Water (V-SMOW). The measurements have been performed on 55 cm samples with an accuracy of ±0.1‰. **b**, The NGRIP oxygen isotopic profile (red) with respect to depth at NGRIP. For comparison, the GRIP record (blue) has been plotted on the NGRIP depth scale using the rapid transitions as tie points. **c**, The difference between the NGRIP and GRIP oxygen isotopic profiles plotted above on the GRIP2001/ss09sea timescale[15] in 50 yr resolution (black). The record is compared to a record representing sea level changes[39] (green) and a 10-kyr smoothed oxygen isotope profile from NGRIP (red).

cores nearer the coast, such as Camp Century (77.2 °N, 61.1 °W) in the west[15], and Renland (71.3 °N, 26.7 °W) in the east[15]. We conclude that the relative elevation differences during the Eemian in northern Greenland are thus not large, and further, as the Renland ice cap only is 325 m thick and cannot change elevation by more than 100 m, the absolute elevation changes between the Eemian and the present can only be of the order of 100 m. In contrast, the Dye3 ice core in south Greenland (65.2 °N, 43.8 °W) has an isotope difference of 5‰ (ref. 15), suggesting as much as 500 m lower elevation there. The Eemian isotopic values reported here paint a picture of an Eemian ice sheet with northern and central ice thicknesses similar to the present, while the south Greenland ice thickness is substantially reduced. This provides a valuable constraint for both future glaciological models of the Greenland Eemian ice sheet as well as models of sea level changes[30,34–36].

Climate record of the glacial inception

This high resolution NGRIP record reveals a slow decline in temperatures from the warm Eemian isotopic values to cooler, intermediate values over 7,000 yr from 122 to 115 kyr BP. The end of the last interglacial thus does not appear to have started with an abrupt climate change, but with a long and gradual deterioration of climate. Before full glacial values are reached, however, the record does reveal an abrupt cooling, with a first $\delta^{18}O$ decrease at about 119 kyr BP, followed by relatively stable depleted $\delta^{18}O$ levels, which we name here the Greenland stadial 26. The stadial is followed by an abrupt increase at ~115 kyr BP, the onset of DO 25[37] (Fig. 4). NGRIP is the first ice core climate record to so clearly resolve these rapid and large fluctuations in climate right at the beginning of the full glacial period. It is remarkable how well the features of the record compare with the marine planktonic isotope record from the margin of the Iberian coast, a proxy for the sea surface temperatures here. The features are thus believed to be large-scale features typical of the North Atlantic region[38]. It is significant that DO 25, while weak (with an amplitude 25% of the following DO events), was similar in character to the following DO events, although it occurred at the time when the ice caps were first building up. Thus it seems difficult to call on melting ice or other large freshwater input to the North Atlantic to trigger this event, although clearly we need more information from this and future ice cores to fully understand this first abrupt climate change of the last glacial.

Regional climate differences in Greenland

We now focus on a detailed comparison of the NGRIP $\delta^{18}O$ ice profile with the GRIP ice isotopic record over their common part. Despite being only 325 km apart, these records have significant differences that illustrate the importance of regional variations in Greenland climate, even on quite long timescales. Figure 2b shows the NGRIP ice isotope profile. The GRIP record shown in Fig. 2a is plotted on the NGRIP depth scale using the DO events as references, so the two records can be compared. At first glance, the two records are very similar as expected, given the relative proximity of the cores. But closer inspection shows substantial differences between the records. Whereas NGRIP and GRIP have very similar $\delta^{18}O$ levels during the Holocene, glacial isotopic levels in the NGRIP record are systematically depleted by 1‰ to 2‰. The difference between these isotopic profiles (Fig. 2c) reaches maxima at about 15–20 kyr BP, 25–30 kyr BP and 60–70 kyr BP. The magnitude of the difference appears to be related to the Northern Hemisphere climate curve, as represented by a smoothed version of the NGRIP record, such that colder conditions have larger differences (Fig. 2c). The difference curve also compares relatively well to the global sea level curve[39], implying that the extent of the glacial continental ice sheets may help to explain the difference.

The difference curve only weakly traces the DO events, suggesting that the differences are not very well connected to processes operating on millennial timescales. A preliminary reconstruction of past temperatures based on the measured borehole temperatures

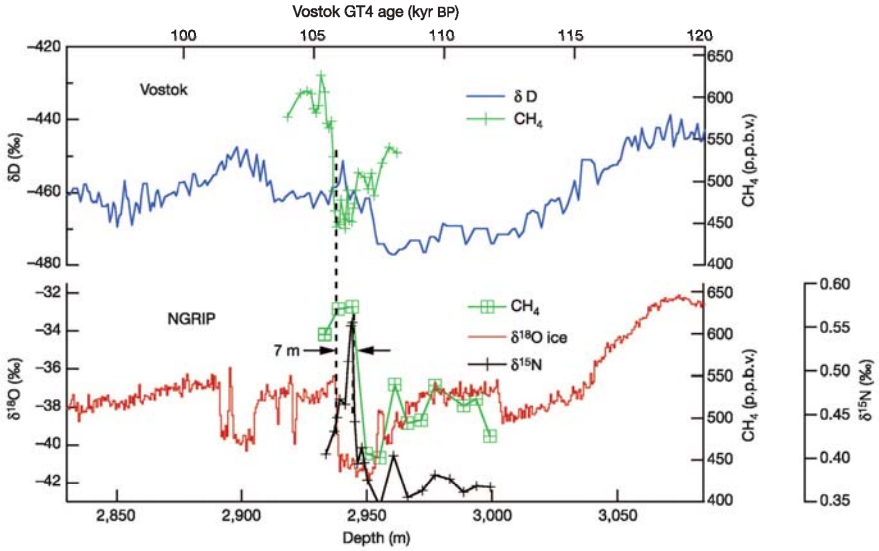

Figure 3 Comparison of ice core records from NGRIP and Vostok for NGRIP depths 2,830 to 3,085 m. The isotopic composition, δD, of the ice (blue) and of methane in the air (green) for Vostok are on the top, and the isotopic composition, $\delta^{18}O$, of the ice (red), methane (green) and $\delta^{15}N$ (black) of the air for NGRIP are on the bottom. A 50-kyr resolution NGRIP record is available as Supplementary Information. The detailed Vostok methane profile combines published data and recent measurements performed to examine the 5d/5c transition at Vostok[24]. The Vostok and NGRIP data are reported on their own scales, namely the GT4 timescale for Vostok (top axis) and the depth scale for NGRIP (bottom axis). These two independent scales have been simply shifted in order to match the sharp methane shift in Vostok with the sharp NGRIP warming at 2,940 m. Furthermore, matching of the two scales should result in the estimated mean 1.1 cm annual layer thickness for the NGRIP profile.

at NGRIP supports this finding. Temperatures reconstructed at NGRIP during the Last Glacial Maximum are several degrees colder than those at GRIP and GISP2. The observed isotopic differences are large, given the relatively small distance between the two sites, and our finding that the two sites are believed to have only undergone small relative elevation changes during the glacial period[34,40]. Whereas the isotopic records in the central parts of East Antarctica[41] are rather similar and thus do not reveal large and significant climatically driven differences, the Greenland sites, located just 325 km apart, reveal major differences. Now that we are beginning to have a spatial distribution of deep ice core records, this brings into play a new source of palaeoclimatic information for these deep ice cores, that is, changes in geographical gradients with time. Our best theory is to postulate that the air masses reaching the two sites during the glacial had different sources. In response to the extent of the Laurentide ice sheet, sea ice and the extensive North Atlantic ice shelves, NGRIP has become further from the ocean, and may have seen a higher fraction of air coming over the northern side of the Laurentide ice sheet, bringing with it colder and more isotopically depleted moisture than GRIP might have seen[42,43]. Taken as a whole, the findings here suggest that the atmospheric water cycle over Greenland is substantially different between modern and glacial worlds.

Basal water under the ice

When drilling was completed at NGRIP, basal water flooded the deepest 45 m of the bore hole. Although we knew from temperature profiles taken in 2001–02 that the base of the ice sheet was at or very near the pressure melting point, liquid water was not seen in radar profiles done during site selection. The melt rate at the base at NGRIP is 7 mm ice yr^{-1}, so the geothermal heat flow appears to be as high as 140 mW m^{-2} (70 mW m^{-2} from latent heat, and 70 mW m^{-2} conducted though the ice based on the measured bore temperature). This high geothermal heat flow value is atypical for Precambrian shields[44] believed to cover most of Greenland. The recent indications of bacterial life in and under Antarctic ice[45] have revealed that the Earth possibly contains a previously unrecognized cold biosphere that would be actively involved in biogeochemical processes. Thus Greenland, like Antarctica, is now known to have liquid water at its base in some locations, water that awaits further study for basal sediment composition and evidence of life in a truly extreme environment.

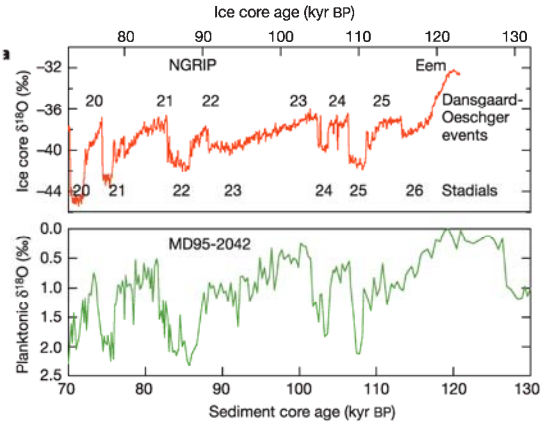

Figure 4 The NGRIP isotopic profile from the Supplementary Information (**a**) compared with the planktonic isotopes in the Iberian margin sediment core MD95-2024[29] (**b**). The Greenland Dansgaard–Oeschger events (interstadials) are numbered along with the associated stadials. The two age scales are independent and seem to match within a few kyr.

Implications for future palaeoclimatic studies

The first measurements available on the NGRIP core already provide a wealth of new and promising environmental information. Most importantly, the NGRIP core contains the first continuous record of the late Eemian and the interception of the last glacial period to be recorded in a deep Greenland ice core. The palaeoclimatic signal for Greenland now reaches 123,000 yr back in time, and reveals a stable and warm late Eemian period. The end of the Eemian is a slow decline to glacial, cooler, intermediate conditions, but the onset of abrupt climate changes, the DO events that mark the last glacial period, precedes full glacial conditions. The bottom ice at NGRIP is essentially undisturbed and annual ice layers are quite thick, a situation caused by basal melting which in turn results from an unexpectedly high geothermal heat flow in North Greenland. The additional knowledge that the central and northern ice sheet during the Eemian period was at the same elevation as present constrains modelled ice volumes and sea level changes during the Eemian and glacial period. This interpretation is only consistent with modelling studies of the ice sheet during the Eemian that, although predicting an overall smaller ice sheet in accord with higher observed sea levels during this time[34,35,46–48], allow for no large ice elevation change for the central Greenland ice. The next generation of models of the Greenland ice sheets should also include substantial melt under the northern part of the ice sheet as well as the northeast ice stream, important for the mass balance of the ice sheet[49,50].

The deepest ice should allow a detailed study of the last glacial inception, including greenhouse gases and atmospheric dust loading, and in future comparisons with Antarctic records we should be able to investigate in detail the sequence of climatic events and forcing between north and south during this key climatic period. We find that the 5d/5c Vostok time period is the counterpart of the Northern Hemisphere stadial 25 that ends with the abrupt onset of DO 24 at the NGRIP depth 2,940 m. The north–south teleconnection observed here is similar in behaviour to all the following events (DO events 1–23), and behaves as predicted by the simple thermodynamic see-saw model[23]. In contrast, the weak stadial 26 followed by the abrupt onset of DO 25 is not opposed by an Antarctic reversal. This could be due to dating uncertainties between the two cores, but it could also be information on the timing of the onset of the teleconnection during the building of the ice caps and the cooling of the climate. When did the north–south climate see-saw begin? Is there information waiting to be found that can tell us how glacial periods begin, and whether we are in danger of entering one in the near future? New and detailed measurements from the EPICA Antarctica ice cores are expected to clarify this observation. And finally, is there life at the base of the Greenland ice sheet? These are some of the many questions that await further study of the new NGRIP ice core. □

Received 5 March; accepted 30 June 2004; doi:10.1038/nature02805.

1. Johnsen, S. J. *et al.* Irregular glacial interstadials recorded in a new Greenland ice core. *Nature* **359,** 311–313 (1992).
2. Dansgaard, W. *et al.* Evidence for general instability of past climate from a 250-kyr ice-core record. *Nature* **364,** 218–220 (1993).
3. Greenland Ice-Core Project (GRIP) Members. Climate instability during the last interglacial period recorded in the GRIP ice core. *Nature* **364,** 203–208 (1993).
4. Grootes, P. M., Stuiver, M., White, J. W. C., Johnsen, S. J. & Jouzel, J. Comparison of oxygen isotope records from the GISP2 and GRIP Greenland ice cores. *Nature* **366,** 552–554 (1993).
5. Taylor, K. C. *et al.* Electrical conductivity measurements from the GISP2 and GRIP Greenland ice cores. *Nature* **366,** 549–552 (1993).
6. Bender, M. *et al.* Climate correlations between Greenland and Antarctica during the last 100,000 years. *Nature* **372,** 663–666 (1994).
7. Fuchs, A. & Leuenberger, M. $\delta^{18}O$ of atmospheric oxygen measured on the GRIP Ice Core document stratigraphic disturbances in the lowest 10% of the core. *Geophys. Res. Lett.* **23,** 1049–1052 (1996).
8. Johnsen, S. J. *et al.* The $\delta^{18}O$ record along the Greenland Ice Core Project deep ice core and the

problem of possible Eemian climatic instability. *J. Geophys. Res.* **102**, 26397–26410 (1997).
9. Chappellaz, J., Brook, E., Blunier, T. & Malaizé, B. CH_4 and $\delta^{18}O$ of O_2 records from Antarctic and Greenland ice: A clue for stratigraphic disturbance in the bottom part of the Greenland Ice Core Project and Greenland Ice Sheet Project 2 ice cores. *J. Geophys. Res.* **102**, 26547–26557 (1997).
10. Dahl-Jensen, D. *et al.* The NorthGRIP deep drilling program. *Ann. Glaciol.* **35**, 1–4 (2002).
11. Dahl-Jensen, D. *et al.* A search in north Greenland for a new ice-core drill site. *J. Glaciol.* **43**, 300–306 (1997).
12. Dahl-Jensen, D., Gundestrup, N., Gorgineni, P. & Miller, H. Basal melt at NorthGRIP modeled from borehole, ice-core and radio-echo sounder observations. *Ann. Glaciol.* **37**, 207–212 (2003).
13. Alley, R. B. *et al.* Comparison of deep ice cores. *Nature* **373**, 393–394 (1995).
14. Grinsted, A. & Dahl-Jensen, D. A Monte Carlo-tuned model of the flow in the NorthGRIP area. *Ann. Glaciol.* **35**, 527–530 (2002).
15. Johnsen, S. J. *et al.* Oxygen isotope and palaeotemperature records from six Greenland ice-core stations: Camp Century, Dye-3, GRIP, GISP2, Renland and NorthGRIP. *J. Quat. Sci.* **16**, 299–307 (2001).
16. Clausen, H. B. *et al.* A comparison of the volcanic records over the past 4000 years from the Greenland Ice Core Project and Dye3 Greenland ice cores. *J. Geophys. Res.* **102**, 26707–26723 (1997).
17. Blunier, T. *et al.* Asynchrony of Antarctic and Greenland climate change during the last glacial period. *Nature* **394**, 739–743 (1998).
18. Landais, A. *et al.* A tentative reconstruction of the last interglacial and glacial inception in Greenland based on new gas measurements in the Greenland Ice Core Project (GRIP) ice core. *J. Geophys. Res.* **108**, doi:10.1029/2002JD0003147 (2003).
19. Flückiger, J. *et al.* N_2O and CH_4 variations during the last glacial epoch: Insight into global processes. *Glob. Biogeochem. Cycles* **18**, doi:10.1029/2003GB002122 (2004).
20. Suwa, M., von Fischer, J. & Bender, M. Age reconstruction for the bottom part of the GISP2 ice core based on trapped methane and oxygen isotopes records. *Geophys. Res. Abstr.* **5**, 07811 (2003).
21. Caillon, N. *et al.* Estimation of temperature change and of gas age-ice age difference, 108 kyr BP, at Vostok, Antarctica. *J. Geophys. Res.* **106**, 31893–31901 (2001).
22. Petit, J. R. *et al.* Climate and atmospheric history of the past 420,000 years from the Vostok ice core, Antarctica. *Nature* **399**, 429–436 (1999).
23. Stocker, T. F. & Johnsen, S. J. A minimum thermodynamic model for the bipolar seesaw. *Paleoceanography* **18**, doi:10.1029/2003PA000920 (2003).
24. Caillon, N., Jouzel, J., Severinghaus, J. P., Chappellaz, J. & Blunier, T. A novel method to study the phase relationship between Antarctic and Greenland climate. *Geophys. Res. Lett.* **30**, doi:10.1029/2003GL017838 (2003).
25. Severinghaus, J. P., Sowers, T., Brook, E. J., Alley, R. B. & Bender, M. L. Timing of abrupt climate change at the end of the Young Dryas interval from thermally fractionated gases in polar ice. *Nature* **391**, 141–146 (1998).
26. Chappellaz, J. *et al.* Synchronous changes in atmospheric CH_4 and Greenland climate between 40 and 8 kyr BP. *Nature* **366**, 443–445 (1993).
27. Brook, E. J., Sowers, T. & Orchardo, J. Rapid variations in atmospheric methane concentration during the past 110,000 years. *Science* **273**, 1087–1091 (1996).
28. Schwander, J. *et al.* Age scale of the air in the Summit ice: Implication for glacial-interglacial temperature change. *J. Geophys. Res.* **102**, 19483–19493 (1997).
29. Shackleton, N. J., Hall, M. A. & Vincent, E. Phase relationships between millennial-scale events 64,000–24,000 years ago. *Paleoceanography* **15**, 565–569 (2000).
30. Cuffey, K. M. & Marshall, S. J. Substantial contribution to sea-level rise during the last interglacial from the Greenland ice sheet. *Nature* **404**, 591–594 (2000).
31. Johnsen, S., Dahl-Jensen, D., Dansgaard, W. & Gundestrup, N. Greenland palaeotemperatures derived from GRIP bore hole temperature and ice core isotope profiles. *Tellus B* **47**, 624–629 (1995).
32. Cuffey, K. M. *et al.* Large arctic temperature change at the Wisconsin-Holocene glacial transition. *Science* **270**, 455–458 (1995).
33. Bennike, O. & Boecher, J. Land biotas of the last interglacial/glacial cycle, Jameson Land, East Greenland. *Boreas* **23**, 479–488 (1994).
34. Marshall, S. J. & Cuffey, K. M. Peregrinations of the Greenland Ice Sheet divide in the last glacial cycle: Implications for central Greenland ice cores. *Earth Planet. Sci. Lett.* **179**, 73–90 (2000).
35. Huybrechts, P. Sea-level changes at the LGM from ice-dynamic reconstructions of the Greenland and Antarctic ice sheets during the glacial cycles. *Quat. Sci. Rev.* **21**, 203–231 (2002).
36. Gregory, J. M., Huybrechts, P. & Raper, S. C. B. Threatened loss of the Greenland ice-sheet. *Nature* **428**, 616 (2004).
37. McManus, J. F., Oppo, D. W., Keigwin, L. D., Cullen, J. L. & Bond, G. C. Thermohaline circulation and prolonged interglacial warmth in the North Atlantic. *Quat. Res.* **58**, 17–21 (2002).
38. Khodri, M. *et al.* Simulating the amplification of orbital forcing by ocean feedbacks in the last glaciation. *Nature* **410**, 570–573 (2001).
39. Waelbroeck, C. *et al.* Sea-level and deep water temperature changes derived from benthic foraminifera isotopic records. *Quat. Sci. Res.* **21**, 295–305 (2002).
40. Reeh, N., Oerter, H. & Thomsen, H. H. Comparison between Greenland ice-margin and ice-core oxygen-18 records. *Ann. Glaciol.* **35**, 136–144 (2002).
41. Watanabe, O. *et al.* Homogeneous climate variability across East Antarctica over the past three glacial cycles. *Nature* **422**, 509–512 (2003).
42. Charles, C. D., Rind, D., Jouzel, J., Koster, R. D. & Fairbanks, R. G. Seasonal precipitation timing and ice core records. *Science* **269**, 247–248 (1995).
43. Charles, C. D., Rind, D., Jouzel, J., Koster, R. D. & Fairbanks, R. G. Glacial-interglacial changes in moisture sources for Greenland: Influences on the ice core record of climate. *Science* **263**, 508–511 (1994).
44. Dawes, P. R. in *Geology of Greenland* (eds Escher, A. & Watt, W. S.) 248–303 (The Geological Survey of Greenland, Denmark, 1976).
45. Petit, J. R., Alekhina, I. & Bulat, S. A. in *Lessons for Exobiology* (ed. Gargaud, M.) (Springer, in the press).
46. Letréguilly, A., Huybrechts, P. & Reeh, N. Steady-state characteristics of the Greenland ice sheet under different climates. *J. Glaciol.* **37**, 149–157 (1991).
47. Letréguilly, A., Reeh, N. & Huybrechts, P. The Greenland ice sheet through the last glacial-interglacial cycle. *Palaeogeogr. Palaeoclimatol. Palaeoecol.* **90**, 385–394 (1991).
48. Kukla, G., McManus, J. F., Rousseau, D.-D. & Chuine, I. How long and how stable was the Last Interglacial? *Quat. Sci. Rev.* **16**, 605–612 (1997).
49. Fahnestock, M., Abdalati, W., Joughin, I., Brozena, J. & Gogineni, P. High geothermal heat flow basal melt, and the origin of rapid ice flow in central Greenland. *Science* **294**, 2338–2342 (2001).
50. Fahnestock, M. A. *et al.* Ice-stream-related patterns of ice flow in the interior of northeast Greenland. *J. Geophys. Res.* **106**, 34035–34045 (2001).

Supplementary Information accompanies the paper on **www.nature.com/nature**.

Acknowledgements NGRIP is directed and organized by the Department of Geophysics at the Niels Bohr Institute for Astronomy, Physics and Geophysics, University of Copenhagen. It is supported by funding agencies in Denmark (SNF), Belgium (FNRS-CFB), France (IPEV and INSU/CNRS), Germany (AWI), Iceland (RannIs), Japan (MEXT), Sweden (SPRS), Switzerland (SNF) and the USA (NSF, Office of Polar Programs).

Competing interests statement The authors declare that they have no competing financial interests.

Correspondence and requests for materials should be addressed to D.D.-J. (ddj@gfy.ku.dk) or S.J.J. (sigfus@gfy.ku.dk).

K. K. Andersen[1], N. Azuma[2], J.-M. Barnola[3], M. Bigler[4], P. Biscaye[5], N. Caillon[6], J. Chappellaz[3], H. B. Clausen[1], D. Dahl-Jensen[1], H. Fischer[7], J. Flückiger[4], D. Fritzsche[7], Y. Fujii[8], K. Goto-Azuma[8], K. Grønvold[9], N. S. Gundestrup[1]*, M. Hansson[10], C. Huber[4], C. S. Hvidberg[1], S. J. Johnsen[1], U. Jonsell[10], J. Jouzel[6], S. Kipfstuhl[7], A. Landais[6], M. Leuenberger[4], R. Lorrain[11], V. Masson-Delmotte[6], H. Miller[7], H. Motoyama[8], H. Narita[12], T. Popp[13], S. O. Rasmussen[1], D. Raynaud[3], R. Rothlisberger[4], U. Ruth[7], D. Samyn[11], J. Schwander[4], H. Shoji[14], M.-L. Siggard-Andersen[1], J. P. Steffensen[1], T. Stocker[4], A. E. Sveinbjörnsdóttir[15], A. Svensson[1], M. Takata[2], J.-L. Tison[11], Th. Thorsteinsson[16], O. Watanabe[8], F. Wilhelms[7] & J. W. C. White[13]

Affiliations for authors: 1, Niels Bohr Institute for Astronomy, Physics and Geophysics, University of Copenhagen, Juliane Maries Vej 30, DK-2100 Copenhagen OE, Denmark; 2, Nagaoka University of Technology, 1603-1 Kamitomioka-machi, Nagaoka 940-2188, Japan; 3, Laboratoire de Glaciologie et Géophysique de l'Environnement (CNRS), BP 96, 38402 St Martin d'Héres Cedex, France; 4, Climate and Environmental Physics, Physics Institute, University of Bern, Sidlerstrasse 5, CH-3012, Switzerland; 5, Lamont-Doherty Earth Observatory of Columbia University, Rte 9W - PO Box 1000, Palisades, New York 10964-8000, USA; 6, Institute Pierre Simon Laplace/ Laboratoire des Sciences du Climat et de l'Environnement, UMR CEA-CNRS, CE Saclay, Omme des Merisiers, 91191 Gir-Sur-Yvette, France; 7, Alfred-Wegener-Institute for Polar and Marine Research (AWI), Postfach 120161, D-27515 Bremerhaven, Germany; 8, National Institute of Polar Research, Kaga 1-9-10, Itabashi-ku, Tokyo 173-8515 Japan; 9, Nordic Volcanological Institute, Grensásvegur 50, 108 Reykjavik, Iceland; 10, Department of Physical Geography and Quaternary Geology, Stockholm University, S-106 91, Stockholm, Sweden; 11, Département des Sciences de la terre et de l'Environnement, Faculté des Sciences, CP 160/03, Université Libre de Bruxelles, 50 avenue FD Roosevelt, B1050 Brussels, Belgium; 12, Research Institute for Humanity and Nature, 335 Takashima-cho, Marutamachi-dori Kawaramachi nishi-iru, Kamigyo-ku, Kyoto 602-0878, Japan; 13, INSTAAR, Campus Box 450, University of Colorado, Boulder, Colorado 80309-0450, USA; 14, Kitami Institute of Technology, Koencho 165, Kitami, Hokkaido 090-8507 Japan; 15, Raunvísindastofnun Háskólans, Dunhagi 3, Iceland; 16, National Energy Authority, Grensásvegur 9, IS-108 Reykjavík, Iceland

*Deceased

8: Long term trends in the NorthGRIP records of mineral dust and sea salt

This chapter is based on a poster: "The North-GRIP record of sea-salt and mineral dust aerosols revealing new insight into long-range atmospheric transport properties during the last glacial period" presented at the Euresco conference in Polar regions and Quaternary climate, San Feliu de Guixols, Spain , 4-9 October 2003, by: [1]Marie-Louise Siggaard-Andersen, [1]Urs Ruth, [1]Hubertus Fischer, [2]Sigfus Johnsen, [3]Margareta Hansson, [2]Joergen Peder Steffensen, [4]Matthias Bigler, [5]Regine Röthlisberger, [6]Kumiko Goto-Azuma, and [1]Heinrich Miller

[1]Alfred Wegener Institute for Polar and Marine Research, Bremerhaven, Germany, [2]Niels Bohr Institute for Astronomy, Physics and Geophysics (NBI*f*AFG), Copenhagen, Denmark, [3]Department of Physical Geography and Quaternary Geology, Stockholm University, Sweden, [4]Department of Climate and Geophysics, Institute of Physics, University of Bern, Switzerland, [5]NCCR-Climate University of Bern, Switzerland, [6]National Institute of Polar Research, Tokyo, JAPAN

Abstract: The NorthGRIP ice core provides continuous records of sea salt and mineral dust aerosols from the last glacial period. A large number of soluble ions were analysed by ion chromatography and have opened up for new possibilities looking into details in the relationship between ion composition and climate conditions.
Changes in ion composition seem to be related to changes in particle size distribution as an effect of fractionation during long-range atmospheric transport.
Analysis of ion composition in the NorthGRIP ice core suggests that long-range atmospheric transport patterns were constant through most of the last glacial period and remained nearly unchanged during the Dansgaard/Oeschger (D/O) events.
However, in sections of the early part of the last glacial period, our analysis shows a markedly different pattern of ion composition. These differences are associated with differences in particle size distributions and suggest major differences in long-range atmospheric transport patterns during the early part of the last glacial period.

8.1 Background

The NorthGRIP ion record: Samples from the NorthGRIP ice core were collected continuously in 55 cm resolution from decontaminated ice core melt-water obtained from the Bern continuous flow analysis system. The ion species used in this analysis are Li^+, Na^+, K^+, Mg^{2+}, Ca^{2+}, F^-, Cl^-, and SO_4^{2-} that are mainly derived from sea salt and mineral dust aerosols.
In figure 8.3.A is shown the NorthGRIP $\delta^{18}O$ record (from NorthGRIP members, 2004). The record of soluble Ca^{2+} concentrations is shown in Figure 8.3.B.

Transport model: Concentrations of soluble ions from sea salt and mineral dust aerosols in central Greenland ice cores are strongly related to each other and follow very closely a power-law. To explain this relationship we apply a simple transport model to the ion concentrations, where ice core concentrations, C^{ice}, are expressed in terms of transport efficiency, p, and sensitivity, λ:

$$C^{ice}(t) = C^{ice,0} \cdot \exp(-\lambda \cdot p).$$

In a very simple approach, p is given by the inverse wind speed ($1/v$) and λ is given by transport path length divided by aerosol lifetime: $\lambda = L/\tau$. In a more general approach, $C^{ice,0}$ represents a regional term for source contribution, dependent both on source strength and on large scale transport patterns.
The transport model implies that ion concentrations, C_A and C_B, of two different ion species are related to each other by a power law where the power is given by the ratio $\alpha = \lambda_A / \lambda_B$ between the sensitivities for the two species, i.e.

$$C_A = K \cdot C_B^{\alpha}$$
$$\Rightarrow \ln C_A = \ln K + \alpha \ln C_B$$

We have illustrated the linear relationship between logarithmic concentrations of ions in Figure 8.2.C by matching together the curves of logarithmic concentrations from Li^+, Ca^{2+}, and Na^+, which are mainly derived respectively from clay minerals, carbonates, and sea salt aerosols. During Marine Isotope Stage 3 (MIS-3) the curves are perfectly matching.
The simple power law relationship between ion concentrations for both stadials and interstadials during this time period suggests that the large-scale transport patterns are nearly unchanged during the Dansgaard/Oeschger (D/O) events.

Method: The covariance resulting from the linear relationship of logarithmic ion concentrations is represented by the principal component series $E_1(t)$ of an Empirical Orthogonal Function analysis (EOF). The logarithmic ion concentrations $\ln C_i$ are proportional to $E_1(t)$, i.e.:

$$\ln C_i = avg(\ln C_i) + \lambda_i \cdot E_1(t).$$

For $E_1(t)$ normalized, the sensitivity λ_i indicate the standard deviation of logarithmic ion concentrations. Sensitivities for ion concentrations from a section within MIS-3, obtained from an EOF analysis, are shown in Table 8.1. We explain the smaller sensitivity for clay minerals (Li^+) than for carbonates (Ca^{2+}) as an effect of particle size fractionation during transport, and we explain the smaller sensitivity for sea salt

aerosols (Na^+ and Cl^-) than for mineral dust aerosols as an effect of a shorter transport distance for sea salt than for dust.

	%var	$\alpha=\lambda/\lambda_{Ca}$	
Li^+	73	0.6	±0.1
Na^+	93	0.54	±0.03
K^+	59	0.6	±0.2
Mg^{2+}	96	0.71	±0.03
Ca^{2+}	95	1	±0.03
F^-	74	0.7	±0.2
Cl^-	92	0.50	±0.05
SO_4^{2-}	92	0.78	±0.03

Table 8.1: *Relative sensitivities for ion species during MIS-3 obtained from an EOF analysis.*

8.2 Long term trends in the NorthGRIP ice core

In the NorthGRIP ice core record we have observed two different long term features. One feature in associated with the transition between MIS-5 and MIS-4 (70 – 75 ka BP) and could be linked to the major decrease in sea level and simultaneous increase of the Laurentide ice sheet that took place at that time (Siddall et al., 2003). The second feature is observed only within MIS-5 as alternations between two different characteristic patterns. These alternations take place on a different time scale than the D/O events.

Long term trends in ion composition: The curves representing logarithmic ion concentrations for Li^+, Na^+, and Ca^{2+} are mutually matching during MIS-3, but show different long term trends during MIS-4 and MIS-5 (see Figure 8.3.C). We consider these long term trends as mainly an effect of changing source strength due to changing emission and uplift in the source regions.
The record of Li^+ seems to have no trend while concentrations of Na^+ and Ca^{2+} are increasing by 35% during the transition between MIS-5 and MIS-4. In Figure 8.2.D we have reconstructed the increases in source contribution. Our reconstruction shows that the increases take place gradually over a relatively long time and occurs earlier for Ca^{2+} than for Na^+.

After subtracting trends from the Na^+ and Ca^{2+} records we can match the two curves together (see Figure 8.2.E) except for some time sections during MIS-5 that are indicated on the figure with grey bars. The matching on logarithmic scales indicate a power law relationship between ion concentrations and suggests that large scale transport patterns for sea salt and mineral dust aerosols were constant throughout most of the last glacial period. These patterns we refer to in the following as mode I.
In the sections marked with grey bars the relationship between concentrations of Na^+ and Ca^{2+} is markedly different from relationship in the rest of the records. We believe that these different patterns represent different large scale patterns for atmospheric long-range transport. In the following we refer to the patterns in the sections marked in grey

as mode II.

Identifying two modes of chemical composition: Ion concentrations from the sections marked in the figure with grey bars and ion concentrations from the rest of the record were analysed separately. In these analyses only the major ions Ca^{2+}, SO_4^{2-}, Mg^{2+}, Na^{+}, and Cl^{-} were considered. The two analyses showed a markedly different relationship between mineral dust and sea salt. The analyses are described in more detail in the Appendix (Section 8.6).
The ion composition in the marked sections (mode II) can be characterized by a relatively higher sensitivity for Na^{+} and Cl^{-} which could be an effect of weaker conditions for transport of sea salt aerosols during the corresponding time periods.

The two different modes of ion composition are illustrated in Figure 8.1 showing changes in logarithmic ion concentrations relative to changes in $\log[Ca^{2+}]$.

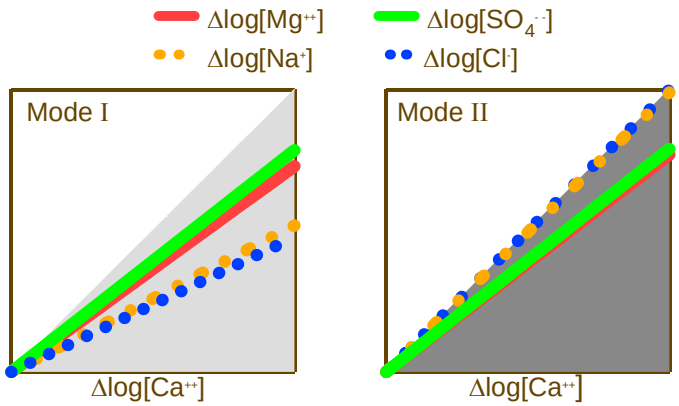

Figure 8.1: *The two different modes of ion composition observed in the NorthGRIP ice core. The dust species (Ca^{2+}, Mg^{2+}, and SO_4^{2-}) show nearly the same relationship in the two modes, but the sea salt (Na^{+} and Cl^{-}) and dust species show a markedly different relationship in the two modes.*

Dust particle characteristics: Ruth et al. (2003) observed a systematic relationship between particle sizes and climate in the NorthGRIP record of insoluble particles with larger particles during stadials than during interstadials. They explained the changes in particle sizes as an effect of enhanced wind transport during cold periods.
On longer terms, particle sizes changes around the transition between MIS-5 and MIS-4 (see Figure 8.2.F). This shift in particle sizes occurs simultaneously with the increasing trend seen in the Ca^{2+} curve. Therefore we consider this change in particle sizes as an effect of changed source characteristics associated with enhanced source load. This could be the case if the enhanced source load was resulting from an extension of the source areas.
In the time sections marked on Figure 8.2 with grey bars (mode I), we find significantly smaller particles in line with larger variation in particle size than in the rest of the record (mode II). Small particles would be a consequence of poor conditions for long-range wind transport e.g. long transport distance or weak transport winds.

The GRIP deuterium records: A comparison of the GRIP records of deuterium (**δD**) and excess deuterium (**d**) from Jouzel et al. (in preparation) with our observations on the

NorthGRIP records of mineral dust and sea salt aerosols strongly supports the idea of different large-scale transport patterns in time sections of MIS-5.
Excess deuterium is believed to reflect surface temperature and humidity in the moisture source area and thereby indicate latitude for the moisture source. In Figure 8.2.G we matched the two records of **δD** and **d,** where **δD** is reversed for comparison. During MIS-3 and MIS-4 the two curves show strong similarities indicating that the moisture source is located at more southern latitudes during cold periods than during warm periods due to the shifting polar front. During the periods of mode II the relationship between the two curves is different, suggesting a different moisture source during these periods.
The comparison of the records of aerosols and water isotopes indicates that conditions for transport of aerosols and moisture are strongly coupled.

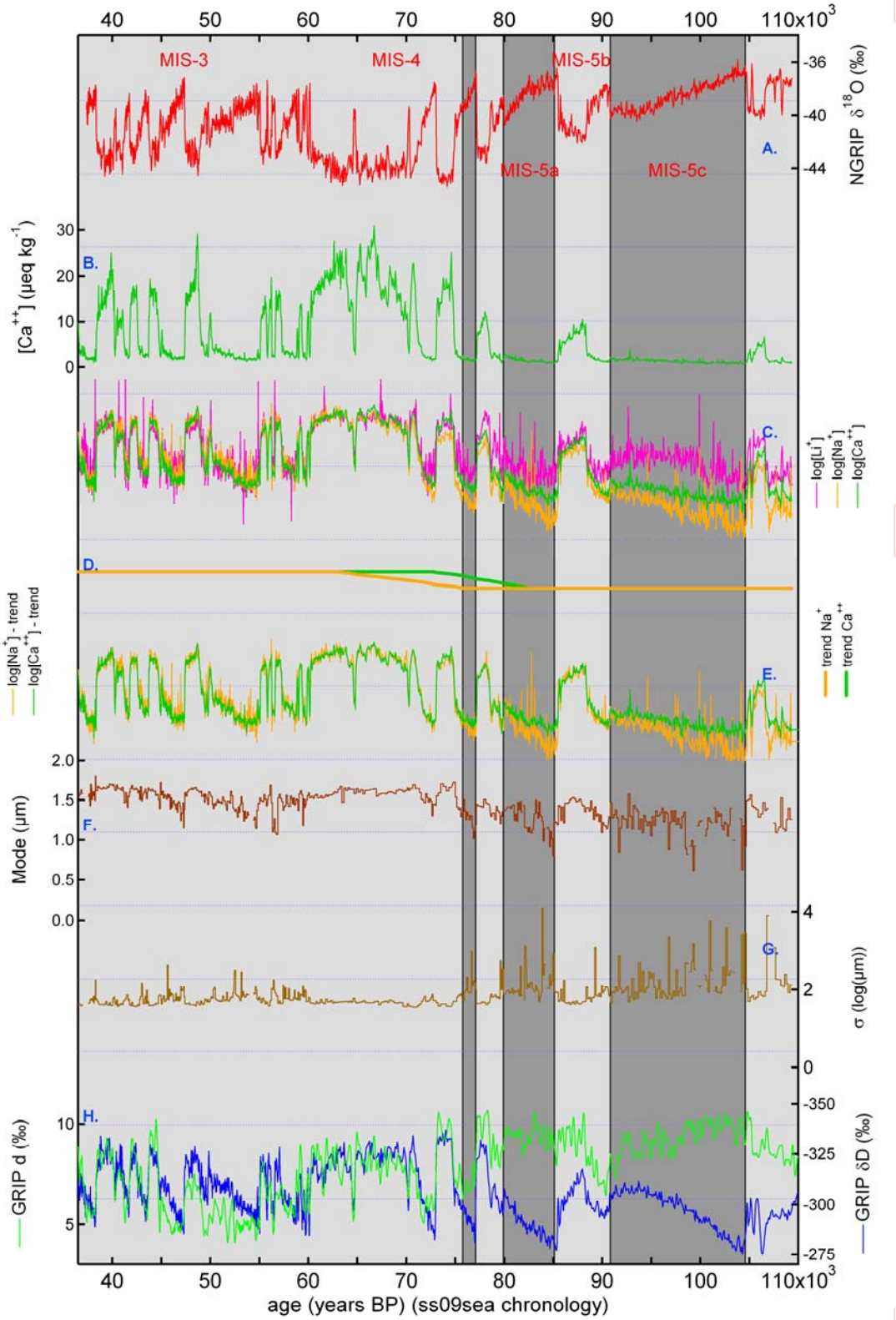

Figure 8.2: *Long term trends in the NorthGRIP ice core record (see text).*

8.3 Discussion

Investigations of the mineral dust in Greenland ice cores have shown that Chinese desert areas are the most likely source areas both for present (Bory et al., 2003) and for the last glacial period (Biscaye et al., 1997; Svensson et al., 2000).

The increase in Ca^{2+} concentrations between MIS-5 and MIS-4 in the NorthGRIP ice core can be explained by an extension of dust source areas.
At present dust deposition in Greenland is associated with dust storms generated mainly in the Taklamakan desert located in Western China (Bory et al., 2003). During the last glacial period Chinese deserts covered a larger area than today (Sun et al., 1998) and conditions for generation of dust storms were better (Ono and Irino, 2004). Dust from desert areas located e.g. in Inner Mongolia could have contributed to dust deposited in Greenland during the last glacial period.

Large-scale transport patterns in the northern hemisphere are associated with the patterns of the jet stream. At present dust aerosol from Asian desert areas and possibly sea salt from the North Pacific is long-range transported by the westerlies over North America. The high variability of the jet stream patterns in the North Atlantic region result in transport of aerosol to Greenland from lower latitudes (see Chapter 2.4).

The increase in Na^{+} concentrations during the transition between MIS-5 and MIS-4 would be resulting from a larger emission of sea salt aerosol over the North Pacific during this time.

A Resent simulation of the Last Glacial Maximum (LGM) jet stream pattern using a mesoscale model with GCM output as boundary conditions showed a strong seasonality in the jet stream patterns during LGM (Bromwich et al., 2004). This simulation suggests a split jet stream configuration during winter, with a strong branch north of the Laurentide ice sheet as a consequence of a strong anti-cyclone located over the ice sheet. The simulated summer configuration shows a single branch south of the Laurentide ice sheet that had shifted northwards compared to the southern winter branch.

A winter jet stream configuration as simulated by Bromwich et al. (2004) could have transported dust and sea salt from Asian and North Pacific source regions north of the Laurentide ice sheet.
During MIS-5, the Laurentide ice sheet had not reached its full size, and therefore probably had less influence on the jet stream pattern, which therefore was more likely to be following a path south of the Laurentide ice sheet. The two modes that we have observed in the NorthGRIP record can be explained by a northern and a southern transport path respectively. These two configurations are illustrated in the Figure 8.3.

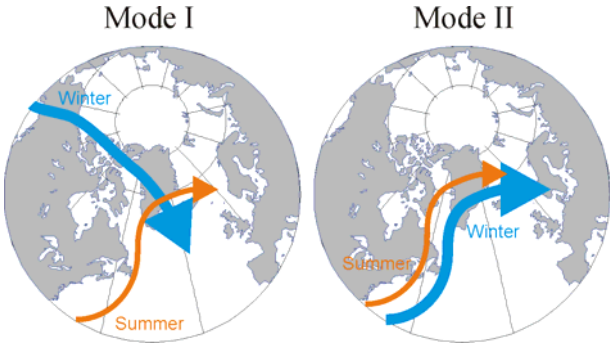

Figure 8.3: *Large scale transport patterns for dust and sea salt suggested for the two modes I and II observed in the NorthGRIP ice core record. Mode I is based on resent simulations of Bromwich et al. (2004).*

The records of particle size distributions shows generally smaller particle sizes for mode II suggesting a longer transport path length for the dust during these periods than during periods of mode I. This support the idea of a transport path north of the Laurentide ice sheet for mode I and south of the Laurentide ice sheet for mode II.

Deuterium excess shows different patterns for the two modes suggesting that the two modes are associated with different moisture source regions. In mode I a northern winter branch of the jet stream could be associated with transport of moisture from the North Pacific to Greenland during winter and from the North Atlantic during summer. In mode II the moisture source area would be located in the North Atlantic both during winter and during summer.

The changes in ice sheet volume, and corresponding sea level, are reflected in deep sea sediment records of benthic foraminifera. In Figure 8.4 is shown a record of reconstructed mean ocean water $\delta^{18}O$ (from Waelbroeck et al., 2002) indicating sea level changes. The periods of mode II are characterized by relatively high sea levels, which suggest that the Laurentide ice sheet has been relatively small during these periods.

Heinrich events during MIS-4,-3 and -2, have resulted in abrupt decreases in the size of the Laurentide ice sheet, and a corresponding increase in sea level. During MIS-5, there have been no large Heinrich events, but possible smaller events of ice berg discharge during this period could have resulted in a significant change in the size of the Laurentide ice sheet around a certain threshold leading to a major reorganization of atmospheric circulation patterns.

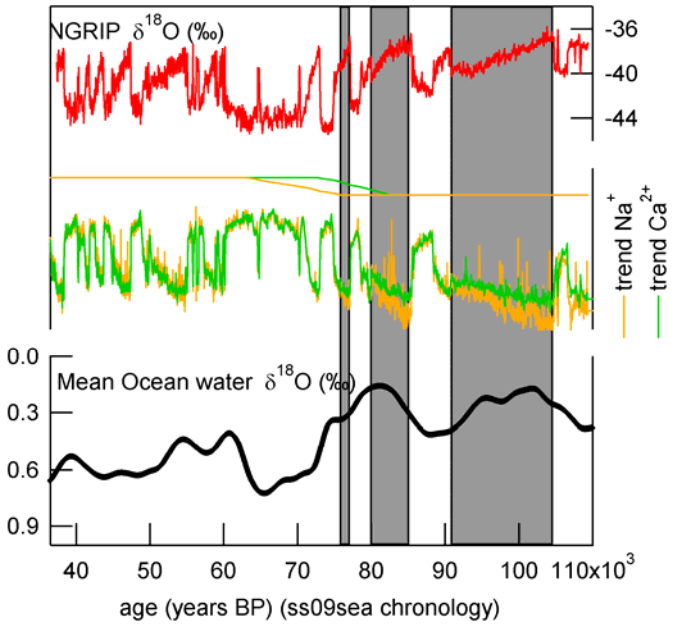

Figure 8.4: *Changing sea level represented by a reconstructed deep sea record of benthic foraminifera (difference from present) from Waelbroeck et al. (2002).*

8.4 Conclusions

A detailed investigation of the NorthGRIP chemical record has identified two different modes, I and II, in ion composition where mode I is characteristic for most of the glacial period during MIS-3 and MIS-4. During MIS-5, ion composition alternates between the two different modes I and II. The two modes can be explained by two different large-scale atmospheric transport patterns. Mode II is characterized by relatively small dust particles, suggesting a longer transport path for mode II than for mode I. We can explain the two different transport patterns by a path north of the Laurentide ice sheet for most of the last glacial period and a path south of the Laurentide ice sheet for time intervals during the early part of the last glacial period, where the Laurentide ice sheet had not reached its full size.

Acknowledgement: The NorthGRIP project is directed and organized by the Department of Geophysics at the Niels Bohr Institute for Astronomy, Physics and Geophysics, University of Copenhagen. It is being supported by funding agencies in Denmark, Belgium, France, Germany, Iceland, Japan, Sweden, Switzerland, and the United States of America.

8.5 References

Biscaye, P. E., F. E. Grousset, et al. (1997). "Asian provenance of glacial dust (stage 2) in the Greenland Ice Sheet Project 2 Ice Core, Summit, Greenland." Journal of Geophysical Research **102**(C12): 26765-26781.

Bory, A. J.-M., P. E. Biscaye, et al. (2003). "Two distinct seasonal Asian source regions for mineral dust deposited in Greenland (NorthGRIP)." Geophysical Research Letters **30**(4): doi:10.1029/2002GL016446.

Bromwich, D. H., E. R. Toracinta, et al. (2004). "Polar MM5 simulations of the winter climate of the Laurentide Ice Sheet at the LGM." Journal of Climate **17**(17): 3415-3433.

Dahl-Jensen, D., N. Gundestrup, et al. (2002). "The NorthGRIP deep drilling program." Annals of Glaciology **35**: 1-4.

GRIP deuterium record: Jouzel J., and others. *(In preparation).*

Johnsen, S. J., D. Dahl-Jensen, et al. (2001). "Oxygen isotope and palaeotemperature records from six Greenland ice-core stations: Camp Century, Dye-3, GRIP, GISP2, Renland and NorthGRIP." Journal of Quaternary Science **16**(4): 299-307.

North Greenland Ice-Core Project (NorthGRIP) Members (2004). "High resolution Climate Record of the Northern Hemisphere reaching into the last Glacial Interglacial Period." Nature **431**: 147-151.

Ono, Y. and T. Irino (2004). "Southern migration of westerlies in the Northern Hemisphere PEP II transect during the Last Glacial Maximum." Quaternary International **118-119**: 13-22.

Ruth, U., D. Wagenbach, et al. (2003). "Continuous record of microparticle concentration and size distribution in the central Greenland NGRIP ice core during the last glacial period." Journal of Geophysical Research **108**(D3): 4098, doi:10.1029/2002JD002376.

Siddall, M., E. J. Rohling, et al. (2003). "Sea-level fluctuations during the last glacial cycle." Nature **423**: 853-858.

Sun, J., Z. Ding, et al. (1998). "Desert distribution during the glacial maximum and climatic optimum: Example of China." Episodes **21**(1): 28-31.

Svensson, A., P. E. Biscaye, et al. (2000). "Characterization of late glacial continental dust in the Greenland Ice Core Project ice core." Journal of Geophysical Research **105**(D4): 4637-4656.

Waelbroeck, C., L. Labeyrie, et al. (2002). "Sea-level and deep water temperature changes derived from benthic foraminifera isotopic records." Quaternary Science Reviews **21**: 295-305.

8.6 Appendix

Sections of different ion composition characteristics were identified in the NorthGRIP ice core ion record using a running linear regression analysis along the ice core record. The sections characteristic for mode I was each subtracted by their average before they were all normalized combined and EOF analysed. The same was done with the sections characteristic for mode II. The powers α, obtained from these analyses are show in Table 8.2.

	$\alpha=\lambda/\lambda_{Ca}$ Mode1	$\alpha=\lambda/\lambda_{Ca}$ Mode2
Na^{+}	0.52	1.02
Mg^{2+}	0.73	0.79
Ca^{2+}	1	1.00
Cl^{-}	0.48	1.01
SO_4^{2-}	0.79	0.87

Table 8.2: *Powers that characterize ion composition in the two modes I and II obtained from EOF analyses.*

In Figure 8.5 is shown the sections used for analysis of mode I and in Figure 8.6 is shown the intermediate sections. Only the sections of MIS5 (and MIS4) were used in the analysis of mode II. The sections from MIS3 were used in neither of the two analyses. Ion characteristics in these sections are different from both of the modes I and II, but could be associated with a transport pattern similar to mode II. However, these sections of MIS3 (see Figure 8.6) are not suitable for a statistical analysis since the ion concentrations only vary little in these sections.

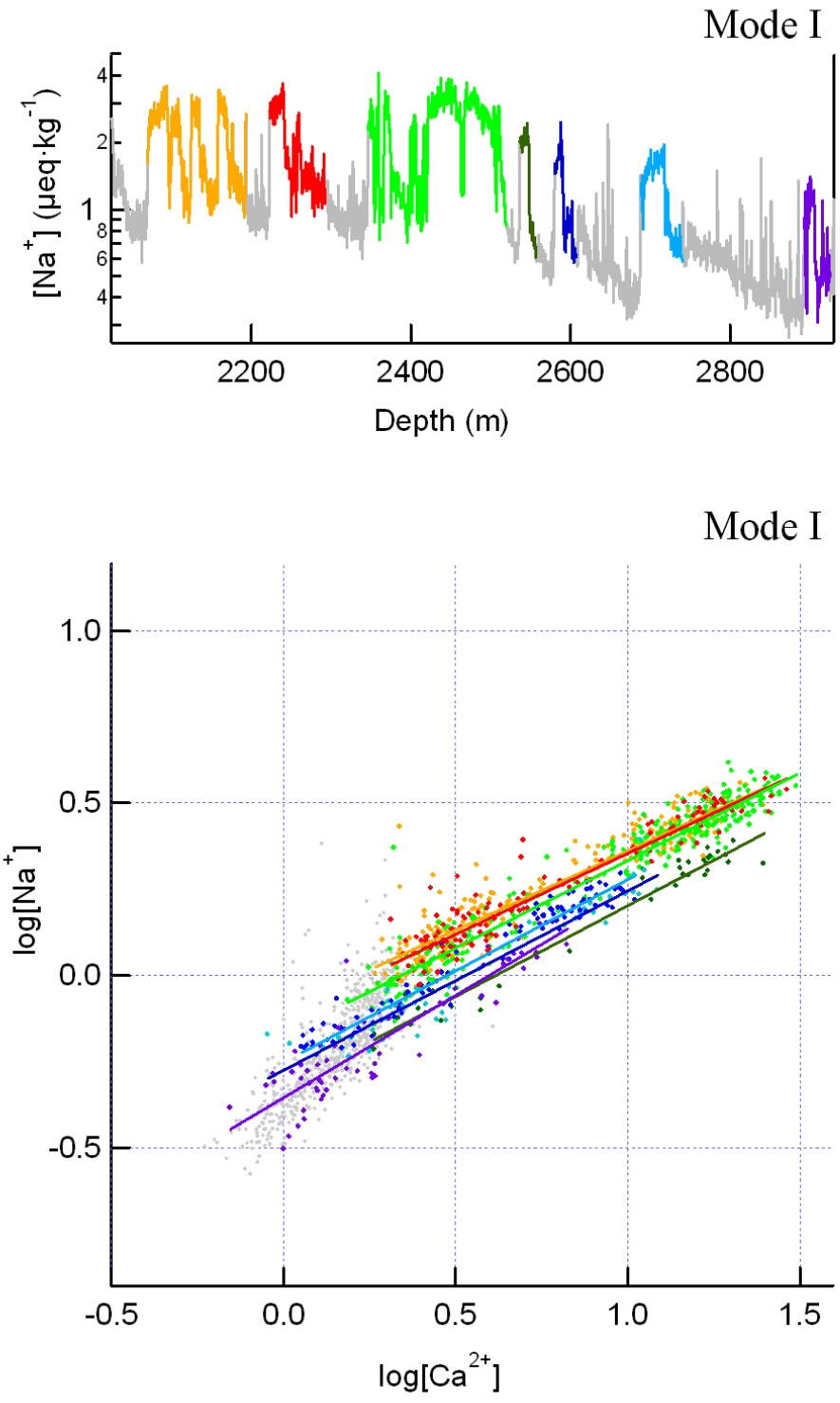

Figure 8.5: *Sections characterized by ion composition of mode I. The colors in the top Figure correspond to the dots and linear fits in the bottom Figure. The scale in the top plot refers to bag numbers (55 cm each).*

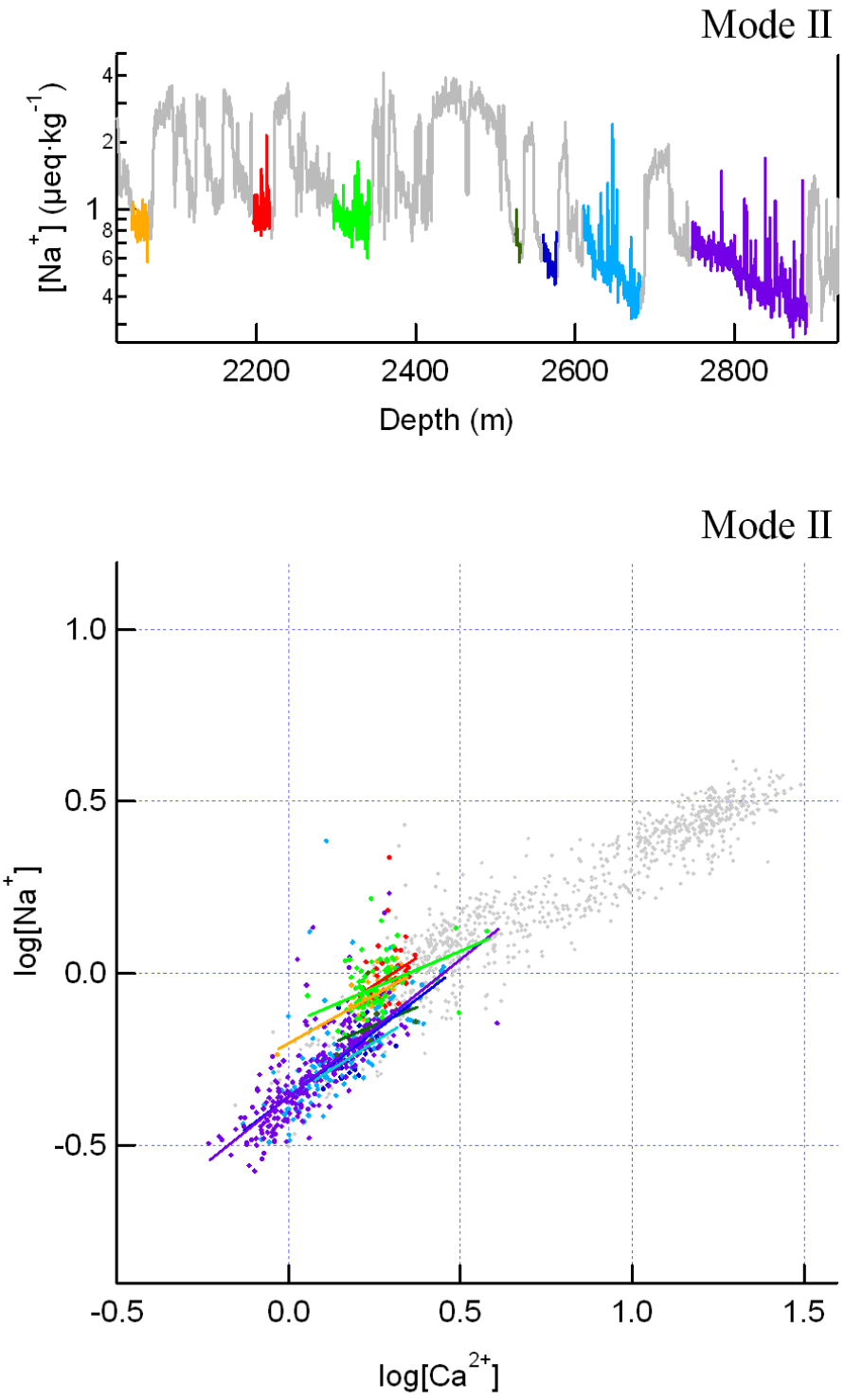

Figure 8.6: *Sections of different characteristics than mode I. The sections in MIS5 (violet, blue and dark green colors) are identified as mode II. The sections from MIS3 are very warm interstadials. Their characteristics are different from both mode I and Mode II.*

9: Ion chromatographic method and data validation

9.1 Principle of ion chromatography

Ion chromatography is a liquid chromatography method used for identification and quantitation of soluble ionic species in a mixed solution.
The basic principle in ion chromatography is a liquid flow-line separation of the soluble ions before quantitation. The separation takes place in a column filled with a porous material (resin) and is controlled by the pH value of the eluding liquid that is constantly pumped through the system. The separation is an effect of different affinities for chemical binding to the column material that cause the sample species to move through the column with different speeds. An injection valve controls the instantaneous injection of the sample. The retention time, which is the time between the injection and peak detection, is used to identify various ionic species. A scheme of the principle of an ion chromatograph is shown in Figure 9.1:

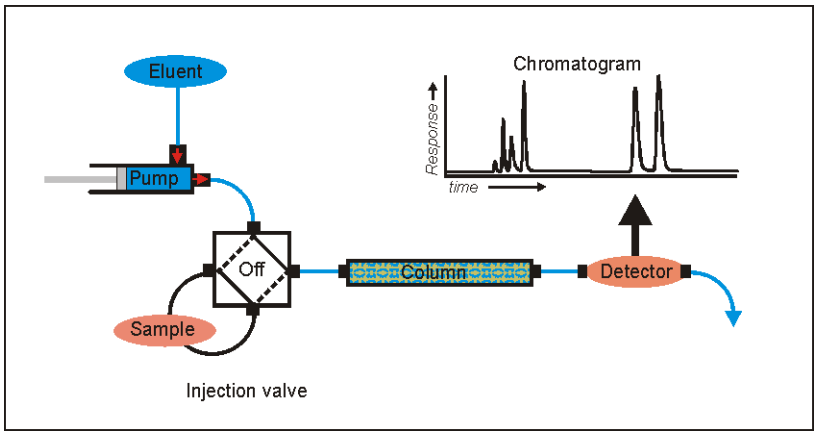

Figure 9.1: *Schematic illustration of the principle of an ion chromatograph.*

Ion chromatography is often used for routine measurements of a large number of samples where the injection valve is connected to an auto-sampler that successively loads samples into the sample-loop.
While the injection valve is “off”, the sample loop is disconnected from the eluent flow and sample can be loaded into the sample loop. When the injection valve is “on” (in inject mode) the eluent flows through the sample loop injecting the sample into the system.

9.2 Setup

Data presented in this work are measured at Department of Geophysics, Niels Bohr Institute for Physics, Astronomy, and Geophysics. In the following a detailed description of setup and procedures in this laboratory is given.

The ion chromatograph used is a Dionex 500 IC with a special two channel setup for simultaneous measurements of anions and cations, where portions from each sample are injected from a single sample-vial into the two channels. The injection is controlled by timings of the auto-sampler, a system-switch and the two injection-valves. The valve system for this setup is scheduled in Figure 9.2:

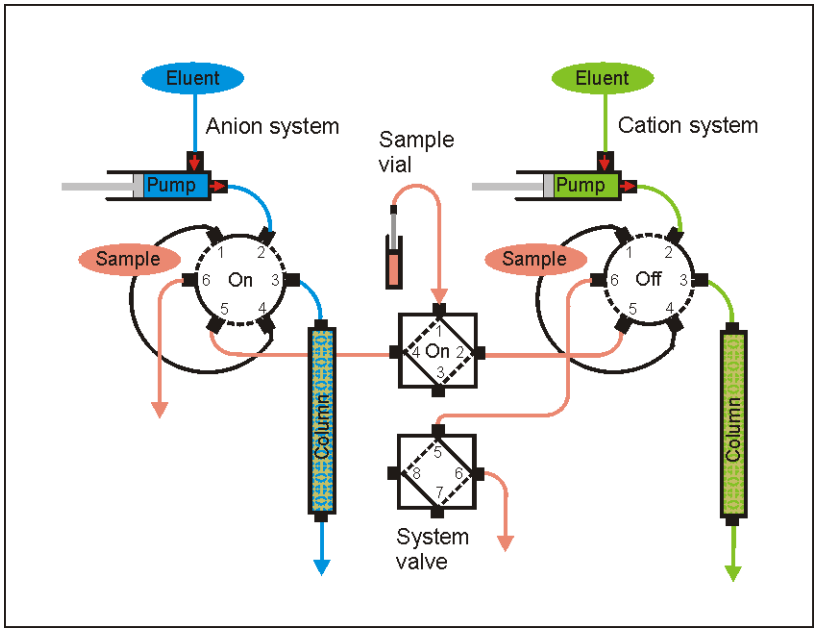

Figure 9.2: *Valve system successively injecting sample portions into two channels for simultaneous measurement of anions and cations.*

The valves are pneumatically operated with compressed nitrogen. The system-switch and the anion injection valve are connected to the same nitrogen pressure-line and therefore they shift simultaneously.
In an initial state all three valves are in “off”-position and sample has been loaded into both sample loops. At the time of sample-injection all three valves are simultaneously switched “on”. In this mode the system-switch is open toward the cation system. Subsequently, when the sample is flushed out of the sample loops, the cation injection-valve is switched off and a portion of the next sample is loaded in to the cation sample-loop. Then the anion injection valve and the system switch are switched off and another portion of the sample is loaded into the anion sample-loop. The valve system is now again in the initial state - ready to inject the next sample. This will happen when the measurement of the first sample has ended.
In this setup, concern has been taken to avoid system cross-talk and sample-to-sample cross-talk. Firstly the tubing system is secured against siphon effects and secondly the tubing from the auto-sampler to the sample loop is rinsed with the first 1.5 ml of the sample volume while both systems are still in injecting mode.

To improve the detection limit, pre-concentration columns were installed in the sample-loops, whereby a larger volume from each sample could be injected within the same

time. Pre-concentration columns capture ions in the sample environment. When the eluent later is flushed through the columns in the opposite direction the ions are released from the columns and injected into the system. Use of pre-concentrator columns has another advantage of minimizing effects from the sample matrix on the first peak in the chromatograms.

The amounts of ions were determined using conductivity detectors. Suppressors eliminating the contribution to conductivity from the eluent solution were installed in the flow-line immediately before the detectors. The suppressors were installed in self-regenerating recycle mode where the detectors out-flow is connected to the suppressor as the regenerant. For high eluent flow-rates this configuration shows high stability of the detected base-line.

The highest stability of the flow-system and the detection base-line was obtained by the high flow rates of 0.6 $ml \cdot min^{-1}$ and 0.5 $ml \cdot min^{-1}$ respectively for the anion and the cation systems.

Eluent solutions: Eluent solutions were made manually using chemicals of highest purity and super quality (SQ) water, obtained using an Elgastat Ultra High Purity unit from Elga.
For the cation system was used Methane Sulfonic Acid, puriss, from FLUKA, and for the anion system was used Sodium Tetraborate, suprapur, from Merck. The eluent solutions were flushed with pure helium gas in order to remove CO_2 from the liquids.

Standard solutions: A stock standard solution was made from salts of highest purity and stored in a refrigerator. Before use is was diluted 1:1000, to obtain concentrations in the range of the measured samples. The standard solution was tested against a commercial standard solution (Six Cation-II Standard and Five Anion Standard from Dionex). The results from these tests are shown in Tables 9.1 and 9.2. Concentrations for all ions in the external standard except ammonium were determined within an accuracy of 3 %.

Cations	*Standard ($mg \cdot L^{-1}$)*	*Diluted 1/10,000 ($\mu equiv \cdot kg^{-1}$)*	*Measured*	*Diff%*
Lithium	53.3	0.768	0.75	-2
Sodium	201	0.874	0.86	-2
Ammonium	249	1.38	1.16	-16
Potassium	507	1.3	1.26	-3
Magnesia	269	2.21	2.22	0
Calcium	534	2.67	2.60	-2

Table 9.1: *Test of the standard solution against a commercial cation standard, Six Cation-II Standard from Dionex. The commercial standard was diluted 1:10000 to obtain concentrations comparable to the standard solution used for calibrations.*

Anions	*Standard ($mg \cdot L^{-1}$)*	*Dilution 1/1000 ($\mu equiv \cdot kg^{-1}$)*	*Measured*	*Diff%*
Fluoride	19.4	1.02	1.01	-1
Chloride	29.3	0.87	0.85	-3
Nitrate	98	1.58	1.63	3
Phosphate	147	1.86		
Sulphate	155	3.22	3.17	-1

Table 9.2: *Test of a commercial anion standard, Five Anion Standard from Dionex. The commercial standard was diluted 1:1000 to obtain concentrations comparable to the standard solution.*

9.3 IC-method

Cations: Generally cations are eluded iso-cratic i.e. with a constant strength of the eluent solution. However in the IC-method used here cations were gradient-eluded. Low eluent strengths in the beginning of the measurement helped a better separation of ammonium and potassium. Cations were separated on Ionpac CS12 columns, and gradient eluded with 20mM Methane Sulfonic Acid (MSA) beginning with 45 % eluent and 55 % SQ water and ending with 80 % eluent and 20 % SQ water (see Figure 9.4).
Peak broadening from diffusion can be seen in the chromatograms. Therefore peak-area was used for quantitations for run with a high variability in concentrations.
For cations there is almost no effect from the sample matrix. This is essential for detection of lithium which is present in ice core samples in amounts just beyond the detection limit.

Anions: Fluoride is very rapidly eluded out of the column and therefore sensitive to the water-dip, which is caused by the sample matrix. A good separation from the water-dip can be obtained using an eluent with low ion strength. Sulphate on the other hand is only eluded out of the column using an eluent with high ion strength. For simultaneous measurement of fluoride and sulphate it is therefore necessary to elude the anions with gradually increasing ion strength. Anions were separated on Ionpac AS14 columns with 35mM $Na_2B_4O_7$ beginning with 12 % eluent and 88 % super quality water and ending with 100 % eluent (see Figure 9.4). With this IC method and use of pre-concentrator column the water-dip from the sample matrix has no effect on the fluoride peak. However the response from MSA (Methane Sulfonic Acid) is very low and the peak is not well separated from chloride. Use of Ionpac AS14 columns is therefore not optimal for measuring MSA.
The Ionpac AS14 column separates anions so well so that no peak broadening from diffusion is seen in the chromatograms. Therefore peak-height, which is more reproducible than peak-area, was used for quantitations. A better separation of nitrogen and hydrogen carbonate could be obtained by installation of an anion trap column to the eluent pump outlet.

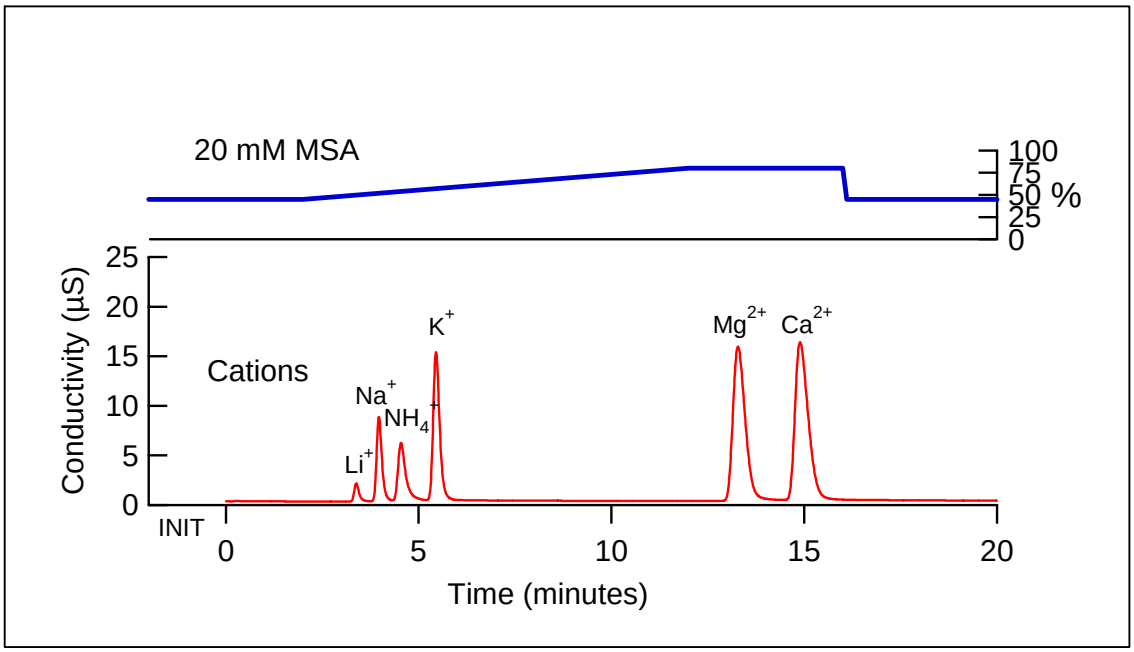

Figure 9.3: *Cation-chromatogram representing cations in the standard solution. Cations were gradient eluded with 20 mM MSA beginning with 45 % eluent and 55 % SQ water and ending with 80 % eluent and 20 % SQ water*

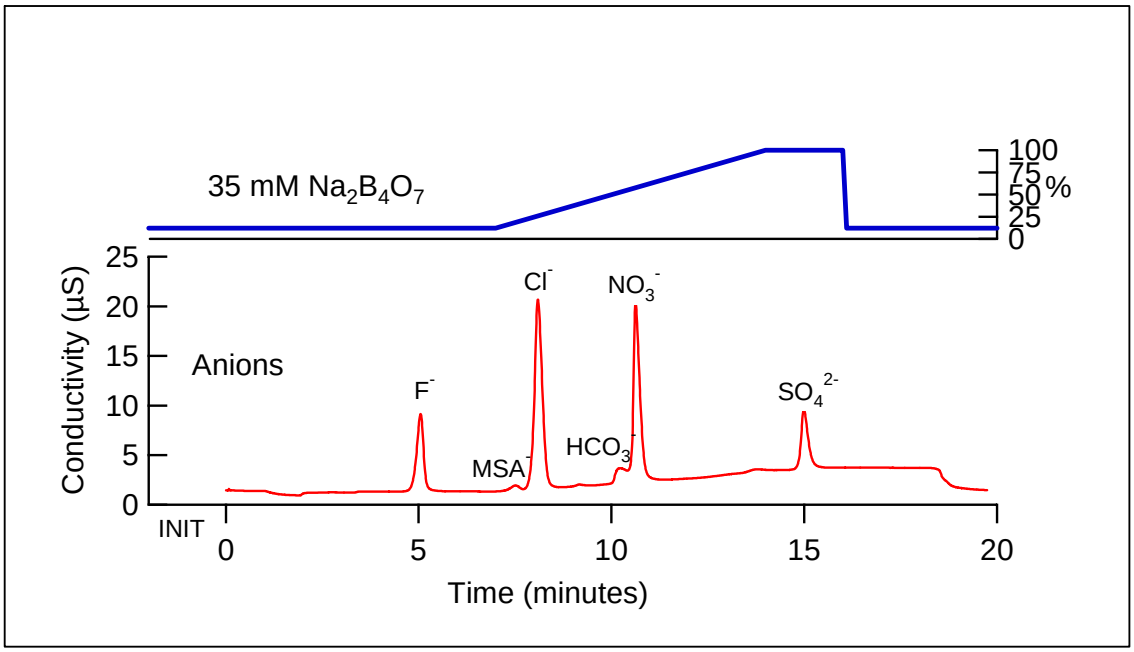

Figure 9.4: *Anion-chromatogram representing the anions in the standard solution. Anions were gradient-eluded with 35 mM $Na_2B_4O_7$ beginning with 12 % eluent and 88 % SQ water and ending with 100 % eluent.*

Procedures: During the normal procedure, samples were measured continuously over several days, refilling the auto-sampler with new samples every day. The samples were melted in the Coulter Accuvettes used for the frozen sample storage. In a clean air laminar flow bench they were decanted into 5 ml sample vials and placed in the auto sampler. For every 22 samples two standards and two blanks were inserted. One standard measurement was used for calibration of the whole run. Typically standard no. 3 was chosen. For quantitation a linear response was assumed. If different types of samples were measured in one run, or if the ion chromatograph had to be restarted within a run, the run was divided into sub-series that were processed separately.

9.4 Data validation

Accuracy: Based on linearity tests, ranges for accurate quantitation was determined. These ranges are only guide lines since linearity have only been checked using a few different dilutions of the standard solution. The results are listed in Table 9.3, where the first column shows the lowest limit of quantitation (L.O.Q) (detection limit), and the next two columns show lower and upper limits (L.L and U.L) of the ranges within which accuracies better than 10 % are obtained. Some upper limits for accuracies better than 15 % are listed in the last column. For low concentrations accuracy is limited by: a short durability of the diluted standard (nitrate), a curving trend in the calibration (MSA, magnesium), effects of contaminants in standards (ammonium, sodium, and potassium), and high variation in response (chloride, sulphate, calcium). For high concentrations accuracy is mainly limited by curving trends in the calibrations. The test curves are shown at the end of this chapter.

	L.O.Q	*L.L 10 % acc*	*U.L. 10 % acc*	*U.L. 15 % acc*
Lithium	0.0002	0.0002	0.8	
Sodium	0.01	0.1	>7	
Potassium	0.02	0.2	>15	
Magnesium	0.04	0.1	8	16
Calcium	0.04	0.1	>33	
Fluoride	0.02	0.04	5	
MSA	0.006	0.03	0.3	0.6
Chloride	0.05	0.1	20	40
Nitrate	0.1	0.4	-	
Sulphate	0.02	0.2	7	15

Table 9.3: *Limit of quantitation (L.O.Q), lower and upper limit for better than 10 % accuracy, and upper limit for better than 15 % accuracy.*

Routine performance: Detection limits and reproducibility are dependent on day-to-day performance of the ion chromatograph. Here performances during two different runs, 00-08-14 and 00-11-20, are shown.
In Tables 9.4 and 9.5 are listed for the two runs the concentrations of the standard solution, average measured concentrations of standards, difference between the two in %, standard deviations, and standard deviations in % of concentrations. Below that is listed average blank concentrations for all blanks and for second blanks, and there

concentrations in % of standard concentration. Blank values are affected by sample to sample cross-talk. Second blank values are therefore lower than average blank values.
Heights and areas of a noise generated peak are evaluated. In practice detection limits are determined by the area-reject limit set in the integration program. In the chromatograms one height unit corresponds to 10^{-4} µS.

Ammonium show high blank values. This is due to a contribution from the air in the laboratory while the samples are placed in the auto-sampler. For potassium, fluoride, and MSA, however, data are above the limit of quantitation but low concentrations are not within the range of better than 10 % accuracy.

Run 00-08-11: Run 00-08-14 was unusually long. 358 samples, 27 standards, and 30 blanks were measured. The samples were all refrozen bag-samples from NorthGRIP 2000. At that time of measurements the nitrate peak was not well separated from the hydrogen-carbonate peak. Therefore nitrate was not quantified for that run.
For cations the area reject limit was set to 100. A noise-generated peak had a height of 17 and area of 82.
The high standard deviation of standards for sodium and potassium is possibly due to a contamination of four of the standards during decanting of a standard portion. Blanks and standards have a higher risk of being contaminated than samples since they are subject to handlings outside the laminar flow bench. It is not suitable, however, to do these handlings in the laminar flow together with the samples.

		Lithium	*Sodium*	*Ammonium*	*Potassium*	*Magnesium*	*Calcium*
Standards	Conc ($\mu eq \cdot kg^{-1}$)	0.206	0.886	2.045	1.852	4.221	4.131
N=27	Avg	0.206	0.923	2.299	1.938	4.197	4.143
	Diff.(%)	0	4	12	5	-1	0
	Std	0.007	0.074	0.172	0.111	0.089	0.193
	Std (%)	4	8	7	6	2	5
Blanks	Avg	0.0001	0.009	0.38	0.02	0.06	0.10
N=30	% of standard	0.0	1.0	16.7	1.0	1.4	2.4
2. blanks	Avg	0.0000	0.01	0.37	0.01	0.02	0.05
N=14	% of standard	0.0	0.8	16.0	0.7	0.5	1.3
Samples	Avg	0.0022	1.81	0.78	0.15	1.81	9.50
N=359	Std	0.0013	0.98	0.53	0.12	1.25	7.98
	Min	0.0003	0.42	0.03	0.02	0.34	1.06
	Max	0.0093	4.12	3.29	1.44	4.36	30.94
Detect. limit		0.0001	0.0001	0.0002	0.0001	0.0001	0.0001

Table 9.4a: *Statistical parameters for cations in run 00-08-14.*

For anions the area reject limit was set to 500. A noise-generated peak had a height of 64 and area of 262. For sulphate some extreme sample values are higher than the range of better than 10 % accuracy.

		Fluoride	*M.S.A.*	*Chloride*	*Nitrate*	*Sulphate*
Standards	Conc ($\mu eq \cdot kg^{-1}$)	2.251	0.302	5.017		1.852
N=27	Avg	2.268	0.321	5.056		1.840
	Diff.(%)	1	6	1		-1
	Std	0.03	0.02	0.10		0.03
	Std (%)	1	7	2		2
Blanks	Avg	0.011	0.003	0.009		0.00
N=30	% of standard	0.5	0.9	0.2		0.0
Second blanks	Avg	0.008	0.002	0.003		0.00
N=14	% of standard	0.3	0.7	0.1		0.0
Samples	Avg	0.054	0.035	2.02		4.18
N=359	Std	0.1276	0.014	1.03		3.06
	Min	0.008	0.002	0.53		0.71
	Max	2.383	0.075	4.28		19.42
Detect limit		0.001	0.001	0.001		0.001

Table 9.4b: *Statistical parameters for anions in run 00-08-14.*

In Figure 9.5 is shown sulphate and magnesium standard measurements for the run 00-08-14. For anions standard no. 3 was chosen whereas standard no. 24 was chosen for cations. The variation from standard to standard is of the same magnitude as the variation of the whole run of standards.

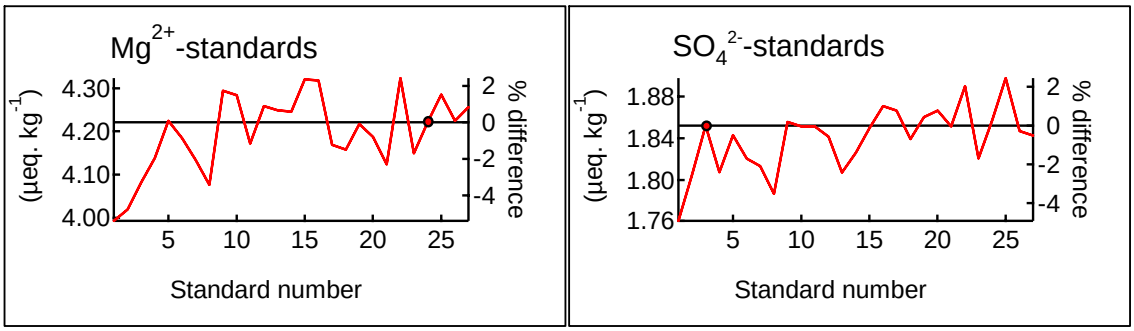

Figure 9.5: *Standard measurements of sulphate and magnesium for run 00-08-14. Standard no. 3 was chosen for calibration of anions and standard no. 24 was chosen for calibration of cations. On the left side in shown measured concentrations. On the right hand side is shown deviations in % from the chosen standard.*

Run 00-11-20: In the 00-11-20 run 49 refrozen samples from NorthGRIP-2000 (samples-I) and 64 refrozen samples from DomeC (samples-II) were measured.
For cations the area reject limit was chosen to 50 and the base-line variation was much less than 0.001 µS that corresponds to around 0.0001 µeq · kg^{-1}.

		Lithium	*Sodium*	*Ammonium*	*Potassium*	*Magnesium*	*Calcium*
Standards	Conc ($\mu eq \cdot kg^{-1}$)	0.206	0.886	2.045	1.852	4.221	4.131
N=14	Avg	0.204	0.885	2.109	1.839	4.236	4.154
	Diff.(%)	-1	0	3	-1	0	1
	Std	0.01	0.03	0.15	0.10	0.06	0.10
	Std (%)	3	4	7	6	1	2
Blanks	Avg	0.0001	0.013	0.30	0.02	0.07	0.12
N=14	%	0.0	1.5	14.5	1.3	1.7	2.8
Samples I	Avg	0.0012	0.78	1.58	0.04	0.63	2.55
N=49	Std	0.0006	0.39	0.48	0.02	0.34	1.78
	Min	0.0003	0.31	0.00	0.02	0.24	0.61
	Max	0.0028	1.71	2.95	0.12	1.56	6.70
Samples II	Avg	0.0018	3.55	0.10	0.13	1.37	1.89
N=64	Std	0.0006	0.74	0.14	0.04	0.33	0.53
	Min	0.0009	1.12	0.00	0.05	0.40	0.50
	Max	0.0035	7.16	0.80	0.26	2.54	3.18
Detect. limit		0.0001	0.0001	0.0001	0.0001	0.0001	0.0001

Table 9.5a: *Statistical parameters for cations in run 00-11-20.*

For anions a noise generated peak had a height of 33 and area 250. The area reject limit was set to 500.

		Fluoride	*M.S.A.*	*Chloride*	*Nitrate*	*Sulphate*
Standards	Conc($\mu eq \cdot kg^{-1}$)	2.251	0.302	5.017	4.221	1.852
N=14	Avg	2.267	0.309	5.064	4.100	1.869
	Diff.(%)	1	2	1	-3	1
	Std	0.026	0.011	0.094	0.229	0.034
	Std (%)	1	4	2	6	2
Blanks	Avg	0.012	0.000	0.008	0.012	0.008
N=14	% of standard	0.5	0.0	0.2	0.3	0.5
Samples I	Avg	0.021	0.011	0.90	1.44	1.68
N=48	Std	0.012	0.009	0.48	0.32	0.94
	Min	0.006	0.000	0.26	0.55	0.44
	Max	0.066	0.029	2.17	2.37	5.37
Samples II	Avg	0.078	0.181	4.11	0.54	4.34
N=64	Std	0.048	0.033	0.96	0.27	1.97
	Min	0.014	0.062	0.19	0.17	2.01
	Max	0.208	0.241	5.65	1.41	15.9
Detect. limit		0.001	0.002	0.001	0.001	0.001

Table 9.5b: *Statistical parameters for anions in run 00-11-20*

Process blanks: To investigate the possible influence from manual sample cutting on measured sample concentrations a rod of artificial blank ice was made by filling a clean plastic tube with super quality water and let it freeze. 22 samples were manually cut from the ice rod and measured one after the other.
In general the process blank values seem lower than normal blank values that are affected by sample-to-sample cross-talk with standard measurements (see Table 9.6). Nitrate and sulphate were not detected in the process blanks. However there is more lithium in the process blanks than in normal blanks. Whether this lithium is coming from the preparation of the artificial ice rod or whether it is a contamination from the manual sample cutting is not obvious, but the concentrations are very similar in all the process blanks and with similar Li/Ca ratios. Therefore it is likely that lithium is derived from the preparation of the ice rod.

	Lithium	*Sodium*	*Potassium*	*Magnesium*	*Calcium*
Avg	0.0002	0.032	0.016	0.012	0.043
Std	0.0001	0.027	0.013	0.005	0.026
% of standard	0.1	3.3	0.8	0.3	1.0

	Fluoride	*M.S.A.*	*Chloride*	*Nitrate*	*Sulphate*
Avg	0.010	0.001	0.007	0.000	0.000
Std	0.002	0.001	0.010	0.000	0.000
% of standard	0.4	0.4	0.1	0.0	0.0

Table 9.6: *Blank samples were cut from frozen SQ water and measured in order to test the sampling procedure.*

Linearity test – low concentrations: A test of linearity at low concentrations was made. Below is shown the logarithmic response versus concentration (markers) and the calibration curve (line). For MSA and nitrate the assumption of linearity do not hold. For sodium and potassium the deviation from linearity for small concentrations could be an effect of contaminations of the low concentration standard solutions rather than a non-linear response.
Lithium shows high linearity for very low concentrations while in general measured values show higher variation for low concentrations, therefore a higher reproducibility is obtained by choosing a standard of higher concentration for quantitations in the low concentration range (see Figure 9.6).

Linearity test – high concentrations: A linearity-test for high concentrations was made. 10 % error bars are inserted in the calibration curve. Within the range of measured concentrations only ammonium shows a deviation from linearity (see Figure 9.7). The test was made at a time where the nitrate peak was not separated from the hydrogen-carbonate peak.

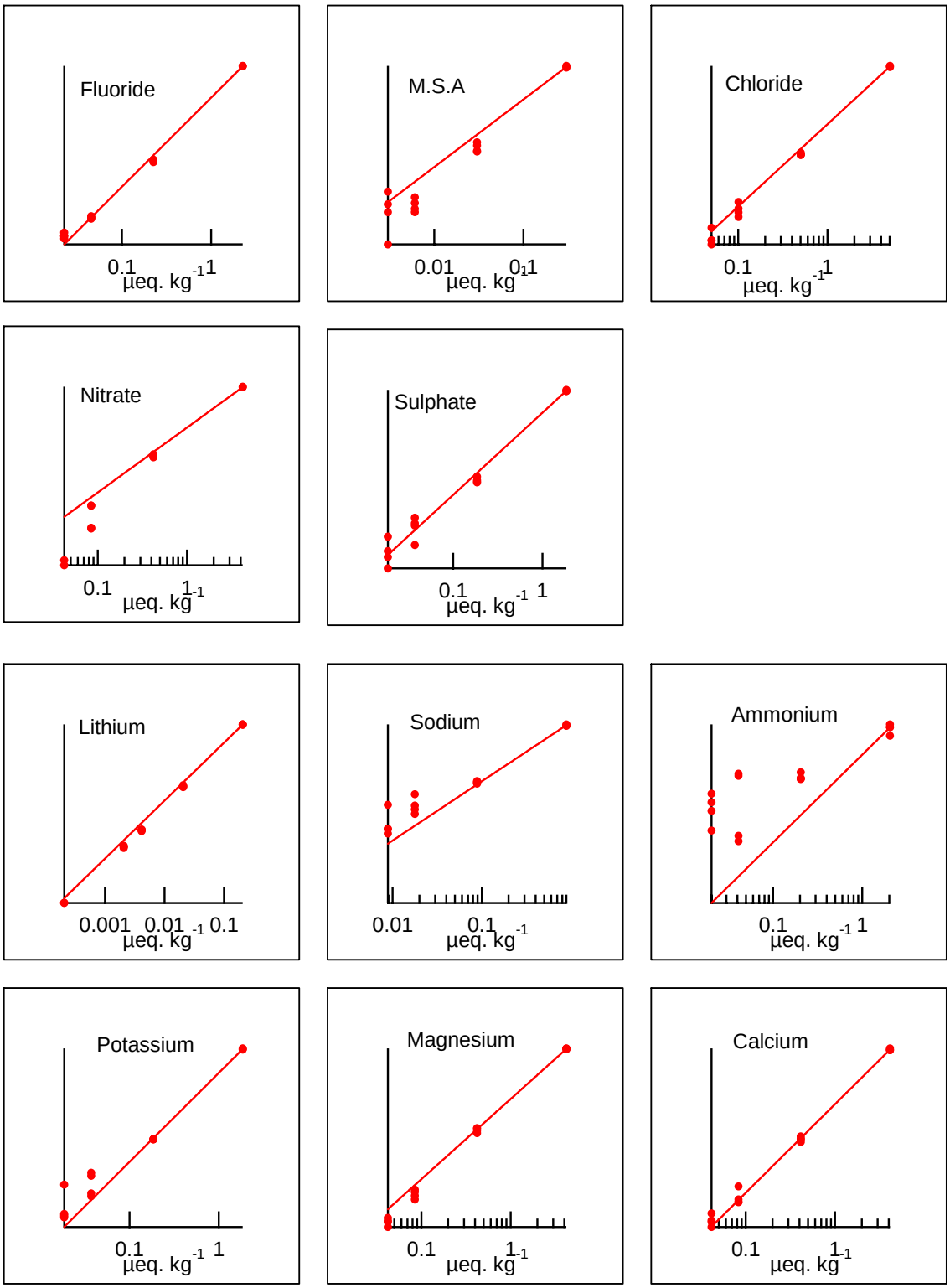

Figure 9.6: *Linearity test for low concentrations.*

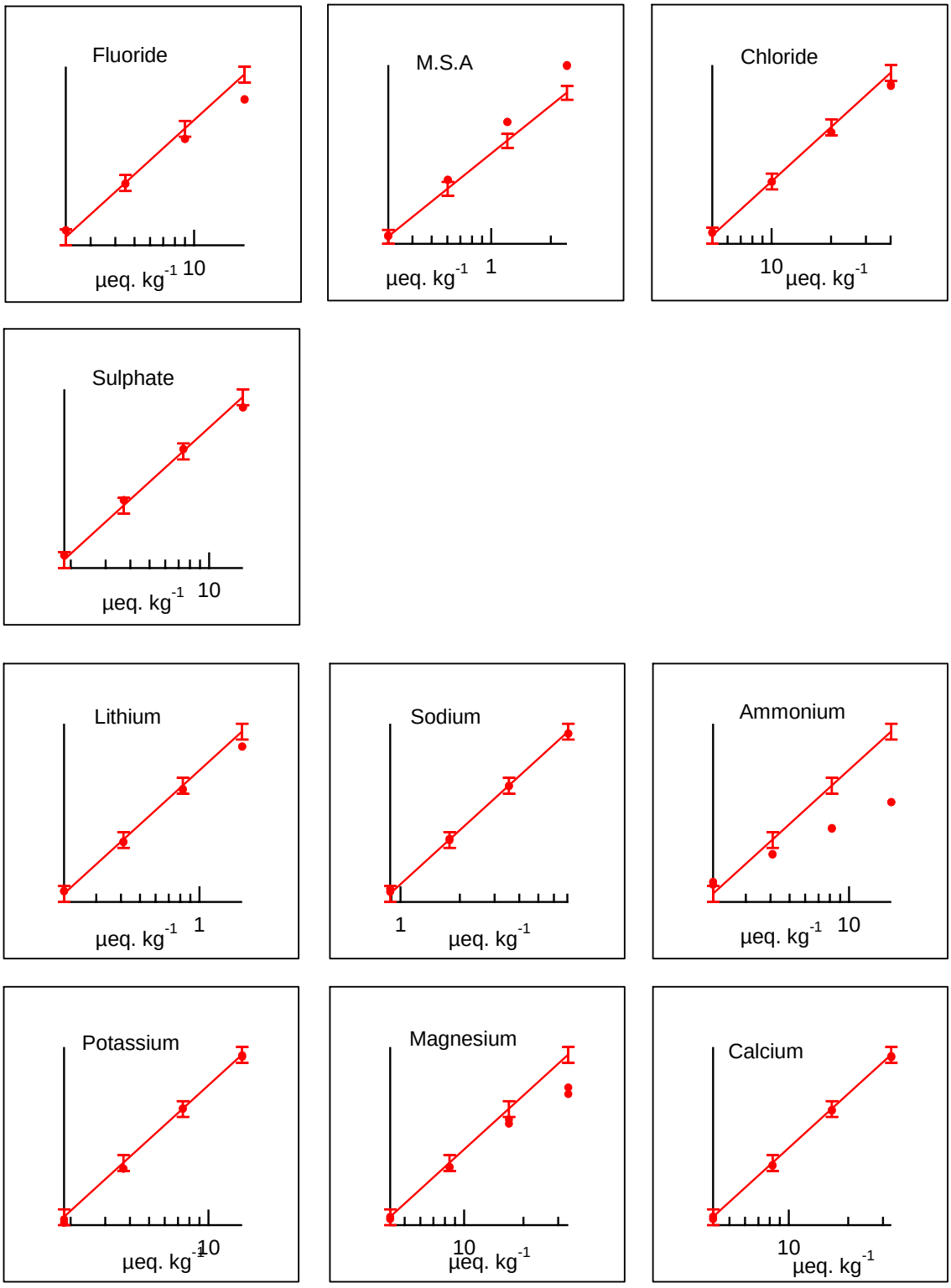

Figure 9.7: *Linearity test for high concentrations.*

10: Summary and Outlook

Ion chromatography (IC) is a conventional method frequently applied in ice core analyses because of its high quality in simultaneous analysis of multiple components and in accurate quantification of trace contents of soluble ions. In this work a continuous record of ion chemistry in the NorthGRIP ice core obtained using ion chromatography is presented (Chapter 6).

Soluble lithium was introduced as a new species to be analysed in polar ice cores (Chapter 3). Ice core contents of soluble lithium are three orders of magnitudes lower than contents of major soluble ions. However, ice core concentrations of soluble lithium can be quantified using an optimized IC technique.
Sea salt contribution to ice core contents of lithium is negligible compared to contributions from mineral dust. Therefore ion chromatographic ice core analysis of lithium in line with calcium, which is often used as an indicator for contents of mineral dust, has a potential of providing details in chemistry and mineralogy of ice core dust material.

A detailed investigation of a lithium anomaly observed in the NorthGRIP ice core around the Holocene cold event 8.2 ka BP concluded that this particular lithium anomaly is related to the transformation of the Qarhan salt lake (in the Qaidam basin, north of the Tibetan plateau) into a playa (Chapter 4). This coincidence between the 8.2 ka BP event and environmental changes in Western China indicates a strong influence of the North Atlantic climate on the Asian monsoon circulation. Furthermore, the rapidity at which lithium concentrations increases in the NorthGRIP ice core during this event shows that the changes of the Qarhan lake occurred abruptly. An open question raised here is whether the drought period associated with the 8.2 ka BP event could have caused permanent environmental changes in the Chinese desert areas, eventually initiating conditions for higher evaporation and thereby irreversibly affecting the water balance in the area.
Further measurements of soluble lithium in Greenland ice cores for the last 30,000 years can show if the lithium anomaly around the 8.2 ka BP event is an isolated event in the ice core, or if Greenland ice core records contain important information about changes in lake status in Western China. Such a record would provide an ice core chronology of monsoon induced environmental changes in the dust source area.

A detailed analysis of lithium chemistry in the DomeC ice core comparing soluble lithium concentrations, measured using IC, with total (soluble and insoluble) contents of lithium, measured using inductively coupled plasma mass spectrometry, suggested that the source location of the dust changed during the last transition (Chapter 5). The Holocene dust material shows characteristics that differ markedly from the characteristics of the glacial dust material. In the glacial dust material lithium seems to be related to clay minerals whereas in the Holocene dust material lithium seems to be related to evaporites. These results are new findings and can significantly contribute to the discussion about changes in the South American dust source areas and changes in large-scale transport patterns for dust in East Antarctica during the last transition.

Processes that are important for the cycles of dust and sea salt were discussed in order to provide an understanding of the climatic influences on contents of dust and sea salt in Greenland ice cores (Chapter 2). Assuming that transport is of only secondary importance in the global dust cycle, dust models mainly focus on climate induced surface conditions in the dust source areas in order to quantify dust emission. The discussion in Chapter 2 led to the conclusion that the surface conditions in the source areas for dust in Greenland ice cores is not affected significantly by climate changes, and therefore Greenland dust is not reflecting the global dust cycle. Another conclusion from this chapter was that contents of dust and sea salt are resulting from the large variability of upper level wind patterns in the northern hemisphere, and therefore mainly response to changing strength of north hemispheric upper-level winds. At present the most likely transport path for dust from Chinese dust sources to Greenland is over the North Pacific and North America and then northward in the North Atlantic.

During the last glacial, conditions were markedly different from present. Large ice sheets, low sea level, and extended sea ice cover during the last glacial most likely have resulted in a reorganization of the atmospheric circulation compared to the present.

The development of a statistical method for analysing ion composition in the NorthGRIP ice core record was partly based on the observation that the relationship between concentrations of different ion species may be approximated well by a power law (Chapter 6). The method has shown its potential for providing characterizing parameters of ice core ion records, and for interpretations of statistical properties in terms of large-scale transport patterns and strength, when applying a simple transport model. This is a completely new approach in ice core analysis and will undoubtedly contribute to discussions about atmospheric circulation during the last glacial and dynamical processes in the climate system.
The analysis of the NorthGRIP ion records of Marine Isotope Stage 3 (MIS-3) suggests that large-scale transport patterns changed only little between stadials and interstadials. These small changes might reflect changes in the upper level wind patterns associated with changed extent of sea ice. In order to fully understand second order patterns in the ion records, interpretations of the ion characteristics must be improved. Seasonality could play an important role for the atmospheric transport patterns. Therefore a better understanding of the large-scale transport patterns during the last glacial and possible seasonal effects is needed.

An investigation of long term trends in ion characteristics in the NorthGRIP ice core has shown markedly different ion characteristics for time sections during MIS-5, indicating that although large-scale transport patterns are relatively resistant towards the climatic changes of the Dansgaard/Oeschger events, they are able to reorganize rapidly (Chapter 8). Reorganization of atmospheric circulation patterns could be related to the size of the Laurentide ice sheet. During MIS-5 the Laurentide had not reached its full size, and the size could have been varying around a certain threshold for the influences on the atmospheric patterns. The observations of alternating atmospheric patterns during MIS-5 is a new finding and will contribute to a better understanding of the influences from the Laurentide ice sheet on atmospheric circulation patterns.

Also during very warm time periods of MIS-3, ion compositions may show different characteristics (Chapter 8.6; Appendix). However, in these time periods, variations in ion concentrations are small, and therefore they are not detected during the statistical analysis of MIS-3 performed in Chapter 6. These very warm periods are succeeding Heinrich events H4 and H5. Wind patterns could have changed during a Heinrich event, as a response to the changed size of the Laurentide ice sheet, and then within the succeeding interstadial, have reorganized into the general glacial configuration. This topic could be interesting to follow and could contribute to the discussion about atmospheric and other dynamical processes during Heinrich and Dansgaard/Oeschger events.

The isotope record from the NorthGRIP ice core was recently presented by NorthGRIP members (Chapter 7). One of the main results from that paper was the finding of a regional effect in Greenland moisture sources during the last glacial with a possible northern transport path for moisture to Northern Greenland. The paper further concluded that circulation patterns during the last glacial were significantly different from the present.

Below is shown a comparison between the NorthGRIP and the GISP2 ice core records of soluble chloride and calcium (the GISP2 record has been synchronized to the ss09sea chronology for comparison). While chloride concentrations are generally higher in the NorthGRIP ice core than in the GISP2 ice core, calcium concentrations show regional effects in variations.

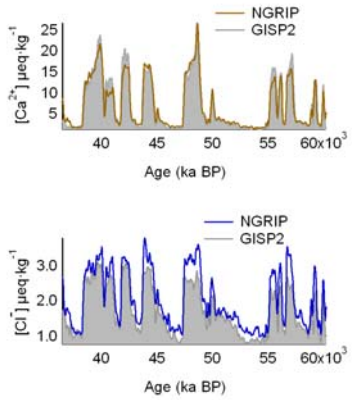

Dust and sea salt aerosol are likely to be transported along the same pathways as the moisture. Therefore further studies of regional effects in Greenland isotope records and in ion chemistry combined can provide a deeper understanding of the atmospheric system during the last glacial period. A detailed investigation of regional effects in Greenland using high resolution ice core chemical records might help understanding the importance of seasonality.

All in all, this work has introduced new applications to ice core ion records, and raised new questions related to large-scale transport patterns in the northern and southern hemispheres. The results from this work have demonstrated the importance of ice core records of ion chemistry in understanding atmospheric dynamical processes.